CAVERN DEVELOPMENT

IN

THE DIMENSIONS OF LENGTH AND BREADTH

By

©

RALPH O. EWERS, B.S, M.S.

A Thesis

Submitted to the School of Graduate Studies

in Partial Fulfillment of the Requirements

for the degree

Doctor of Philosophy

McMaster University

June 1982

CAVERN DEVELOPMENT IN THE DIMENSIONS OF LENGTH & BREADTH

DOCTOR OF PHILOSOPHY (1975)
(Geography)

McMaster University
Hamilton, Ontario

TITLE: Cavern Development in the Dimensions of Length and Breadth

AUTHOR: Ralph Owen Ewers, B.S. (University of Cincinnati)
M.S. (University of Cincinnati)

SUPERVISOR: Professor Derek C. Ford

NUMBER OF PAGES: i-xxii; 1-398.

ABSTRACT

Three conceptual models are proposed for the integration of the large systems of conduits responsible for groundwater flow in soluble rocks. These models are supported by laboratory experiments with scaled solution models, flow-field analogues, and evidence from existing caves.

The three models reflect different boundary conditions imposed by geologic structure and stratigraphy. They have three characteristics in common. First, the smaller elements of the larger systems propagate separately from points of groundwater input toward points of discharge as distributary networks. Second, the integration of the smaller networks proceeds headward from the resurgence, in a stepwise fashion. Third, the result of the integration process in each case is a tributary system with many inputs discharging through a single discharge point.

The potential for growth of each of the smaller networks, within a common pressure field, is related to its distance from the discharge boundary and the distribution of other inputs. The first input to establish a low-resistance link to the discharge boundary will effect a localized depression within the potential field, thus attracting the flow and redirecting the growth of nearby networks until they eventually link with it. As additional orders of links develop, the system takes on a tributary pattern.

The first model applies to steeply dipping rocks. Inputs occur where bedding planes are truncated by erosion, and discharge takes place to the strike. Conduits in this case evolve as a roughly rectangular grid of strike and dip oriented elements. Dip elements are the initial form, with subsequent integration along the strike. The type example is the Holloch in Switzerland.

The second model applies to flat-lying rocks. Inputs occur over a broad area, and discharge takes place along a linear boundary. Conduits in this case evolve in a trellised array with elements normal to the discharge boundary predating those parallel to it. These latter conduits integrate the flow. The type example is the Mammoth Cave Region, Kentucky.

The third model applies to simple systems which occur beneath an impermeable cap rock. Inputs occur where erosion has breached the capping beds. The type example is Cave Creek, Kentucky.

ACKNOWLEDGEMENTS

It is a pleasure to acknowledge the support and assistance of many persons in the completion of this thesis and the program of study of which it is the culmination. Without the urging, support, and personal sacrifice of my wife, Lynda Miriam Ewers, I would never have embarked upon such a project. She has been not only a companion but a scientific and literary critic of no mean qualification.

Professor Dereck C. Ford has provided the advice and critical comment expected of a thesis advisor, but more importantly, he created an atmosphere of good scholarship, intellectual curiosity, and excitement about karst which made study at McMaster a very special experience.

Fellow graduate students at McMaster, especially John J. Drake, Russel S. Harmon, Johnnie E. Fish, Julian Coward, Stuart E. Waterman, and Alan Jackson provided camaraderie, helpful discussion, and an environment for research which was of great importance.

Dr. James F. Quinlan, Professor Alfred Bogli, and Mr. Noel J. Christopher have shared, without reservation, their time and their special knowledge of the Karst regions discussed in Chapter Nine. Without their help and guidence in the field, and their discussions late into the night many of the ideas presented here could not have been formulated.

Prof. T. M. L. Wigley, Prof. William James, and Prof. Hoc Woo engaged in many helpful discussions. Their provocative criticisms and suggestions helped to crystalize many of the principal elements of this thesis.

The technical expertese of Mrs. Lorelle Schenkel, typist; Mr. Robert Bignall photographer; Mr Larry Simpson and Mr. Michael Johnson, cave enthusiasts are Also greatfully acknowledged.

TABLE OF CONTENTS

TABLE OF CONTENTS: Page

TABLE OF CONTENTS: Page

TABLE OF CONTENTS: Page

TABLE OF CONTENTS: Page

TABLE OF CONTENTS: Page

TABLE OF CONTENTS: Page

LIST OF FIGURES

LIST OF FIGURES: Page

LIST OF FIGURES: Page

LIST OF FIGURES: Page

LIST OF FIGURES: Page

LIST OF FIGURES: Page

LIST OF FIGURES: Page

LIST OF FIGURES: Page

LIST OF FIGURES: Page

LIST OF FIGURES: Page

CHAPTER 1

INTRODUCTION

1.1 AN HISTORICAL PERSPECTIVE

The evolution of groundwater conduit systems in carbonate rocks has commanded the attention of earth scientists for more than six decades. Katzer (1909), Sawicki (1909), Grund (1914), Cvijic (1918), and Martel (1921) are numbered among the early workers in the field. Reviews of the history of this research are to be found in Halliday (1960), Cullingford (1962), Jennings (1971), Sweeting (1972) and Bleahu (1974). It is generally agreed (Ford and Ewers, 1978) that the early 1940s marked the end of a period of formulation of general speleogenesis theories that began with these early authors. By this time, three conflicting points of view had been expressed. Martel (1921) in Europe and Malott (1937) in North America, among many others, held that development in the vadose zone (above the water table) by the subsurface capture of surface streams was of primary importance. They argued strongly in favor of mechanical corrasion in a turbulent regime as the principal formative process. Davis (1930) and his preeminent supporter Bretz (1942), concluded that the majority of conduits formed in the phreatic zone, beneath the water table. They called upon the process of dissolution in a laminar regime of sufficient slowness that Darcy's Law was applicable. They asserted that turbulent flow and corrasion were of importance only in the most mature developmental phases. Swinnerton (1932) proposed that groundwater flow and rock dissolution should be maximum proximal to the developing water table. He argued that this route was shortest and would win in any route competition for access to the discharge. Supporters of these general theories have persisted, in declining numbers, to this day.

Many authors have drawn attention to the wide divergence of opinion expressed in these generalizations. In the words of Halliday (1960), "...each appears to have drawn reasonable conclusions from the evidence observed in specific geographic areas ...". White and Longyear (1962) have suggested that "...the multitudinous theories are neither correct nor incorrect in the general case, they are irrelevant". Howard (1963) stated that it is not possible to discover "...a universally applicable origin of caves unless one speaks in the vaguest and most inconsequential terms." Given this state of controversy, it is not surprising that subsequent research efforts have focused upon site specific studies and upon studies of specific physical-chemical processes, geological controls, and environments which influence the propagation and enlargement of these conduits.

On at least one point there is general agreement: paleozoic limestones, as well as many of younger age, function initially as fracture aquifers (Ford and Ewers, 1978). This is to say that, before solution modification, the permeability of these rocks is to be found chiefly as secondary porosity, in joints, faults and bedding planes. It follows then, that in the most fundamental sense solution conduits owe their origin to a host of depositional, tectono-structural, and erosional processes such as sequential deposition, synerisis, folding, faulting, and unloading. These processes determine the type orientation and density of the microporosity upon which the presence and circulation of groundwaters almost wholly depends in carbonate rocks. The origin of these conduits further depends upon the hydraulic effectiveness of the various fracture porosities and their spatial relation to the hydraulic parameters and boundary conditions imposed by the evolution of the surface topography, prior to the onset and during the early stages of groundwater circulation. Conduits must originate as groundwater circulation interacts with the fracture porosity and dissolution of the rock commences. Except in those rare situations where the primary porosity is so great that the bulk of the available precipitation can be accommodated by such voids, it is difficult to see how conditions other than those of a phreatic type can exist initially. The term, phreatic, is used here to describe a condition in which all connected joints and bedding planes are water filled. Thus, most conduits can be considered to have a phreatic origin and enlarging processes will inherit a phreatic framework of secondary openings in which to work. Enlarging processes are here defined as those which act principally to incease the diameter of the solution network elements, as opposed to increasing their number or length. The concept of solution conduit origin is frequently misconstrued in the literature. It is often equated with the concept of conduit enlargement. The distinction between origin and enlargement is not merely semantical. To be sure, the primitive secondary voids are enlarged to form initial solution conduits, but only a minor proportion of existing joint and bedding plane surface is so modified. The present work will attempt to show that selection of the route of enlargement is frequently a dynamic, partly stochastic process, not the simple enlargement of a pre-existing best route.

1.2 THE DIRECTION OF THE THESIS

The research reported in this thesis focuses upon the evolution of solution porosity within a single type of structural discontinuity, the bedding plane. It attempts to relate that evolution to the hydraulic potential fields, and limestone dissolution chemistry within these partings to boundary conditions imposed by three common sets of geologic parameters. The analysis deals principally with processes by which solution voids propagate through the partings and integrate to form subsurface conduit systems composed of many input points and a small number of discharge points. It is concerned with the horizontal dimensions of the problem rather than the classical vertical section embodied in the work of the authors mentioned above. The purpose of the research is to provide a conceptual framework within which the planimetry of conduit systems, in a wide variety of settings, may be analized and understood. It is not a general theory in the sense of the classical theorists but, like the work of Ford and Ewers (1978), it describes end member models in a continuum of possibilities.

Chapter Two reviews the pertinent chemical considerations and their significance to speleogenesis. Chapter Three reviews past experimental work and describes the methods used in the present research. Chapter Four describes the network growth model, which forms the basis of this research. This model was developed by the author over the period of 1966 to 1972 and was formally set forth in the form of an M.S. thesis (Ewers, 1972). Chapters Five and Six explore the hydraulic interactions of networks in the framework of the network propogation model. Chapter Seven verifies these interactions in laboratory solution experiments with simulated bedding planes. Chapter Eight sets forth the end member models for the evolution of multiple input systems of conduits. Finally, Chapters Nine and Ten relate these end member models to natural prototypes and to recognized speleogenetic problems.

CHAPTER 2

KARST SOLUTION

2.1 THE SOLUTION OF CARBONATES

The solution of carbonate rocks is complex. In this regard they differ from sulphate and halide rocks, the other significant karst rocks. In terms of the mineral species, calcite, limestone solution may be considered as:

$$CaCO_3 \Leftrightarrow Ca^{2+} + CO_3^{2-} \qquad (2\text{-}1).$$

However, in the range of pH 6 to pH 9 which includes most natural waters (Stumm & Morgan, 1970, p69), the bicarbonate ion is the stable carbonate species (Buch, 1930). In that pH range the solution process may be considered as:

$$H_2O \Leftrightarrow H^+ + OH^- \qquad (2\text{-}2)$$

and $$CaCO_3 + H^+ \Leftrightarrow Ca^{2+} + HCO_3^- \qquad (2\text{-}3)$$

This reaction accounts for a maximum of 12.7 mg/l dissolved calcite at 20 C (Hutchinson, 1957), well below observed values in karst aquifers which commonly range from 50 to 400 mg/l (Davis and DeWiest, 1966 p. 107). Acids are generally present in natural waters which dissociate to form additional H+ ions, permitting the formation of additional bicarbonate ions and the attainment of higher concentrations of dissolved carbonate mineral. These include carbonic acid from the absorption of atmospheric carbon dioxide:

$$CO_2(g) \overset{HOH}{\Longleftrightarrow} CO_2(aq). \qquad (2\text{-}4)$$

$$CO_2(aq) + H_2O \Longleftrightarrow H_2CO_3 \Longleftrightarrow H^+ + HCO_3^- \qquad (2\text{-}5);$$

and sulphuric acid from the oxidation of sulphides such as pyrite by organic or inorganic means:

$$4FeS_2 + 15O_2 + 14H_2O \Longleftrightarrow 8H_2SO_4 + 4Fe(OH)_3 \qquad (2\text{-}6)$$

$$H_2SO_4 \Longleftrightarrow 2H^+ + SO_4^{2-}. \qquad (2\text{-}7)$$

Equation 2-6 may be important in localized situations where sulfides are abundant. Morehouse (1968) cites evidence which indicates caves in the Galena formation near the Dubuque, Iowa, sulfide mining district may be primarily formed through this agency. In the great majority of cases, however, the solution of limestone is considered to occur primarily as a result of the reactions in equations 2-4 and 2-5. All carefully conducted field investigations (ie. with field measurement of pH) in limestone regions may be said to point to this conclusion.

We may generalize the steps in the solution of carbonates through the agency of carbon dioxide as follows:

1. The absorption of carbon dioxide:

$$CO_2(g) \overset{HOH}{<=>} CO_2(aq) \qquad (2\text{-}8)$$

2. The formation of carbonic acid:

$$CO_2(aq) + H_2O <=> H_2CO_3 \qquad (2\text{-}9)$$

3. The dissociation of carbonic acid:

$$H_2CO_3 <=> H^+ + HCO_3^- \qquad (2\text{-}10)$$

4. The dissociation of water:

$$H_2O <=> H^+ + OH^- \qquad (2\text{-}11)$$

5. The dissociation of the carbonate mineral:

$$CaCO_3 <=> Ca^{2+} + CO_3^{2-} \qquad (2\text{-}12)$$

6. The formation of the bicarbonate ion:

$$CO_3^{2-} + H^+ <=> HCO_3^- \qquad (2\text{-}13)$$

Roques (1969) represents these reactions diagramatically as shown in Figure 2.1.

2.2 THE GEOMORPHIC AND HYDROLOGIC SIGNIFICANCE OF CARBONATE SOLUTION CHEMISTRY

The significance of these chemical reactions with regard to karst geomorphic and hydrologic problems lies in

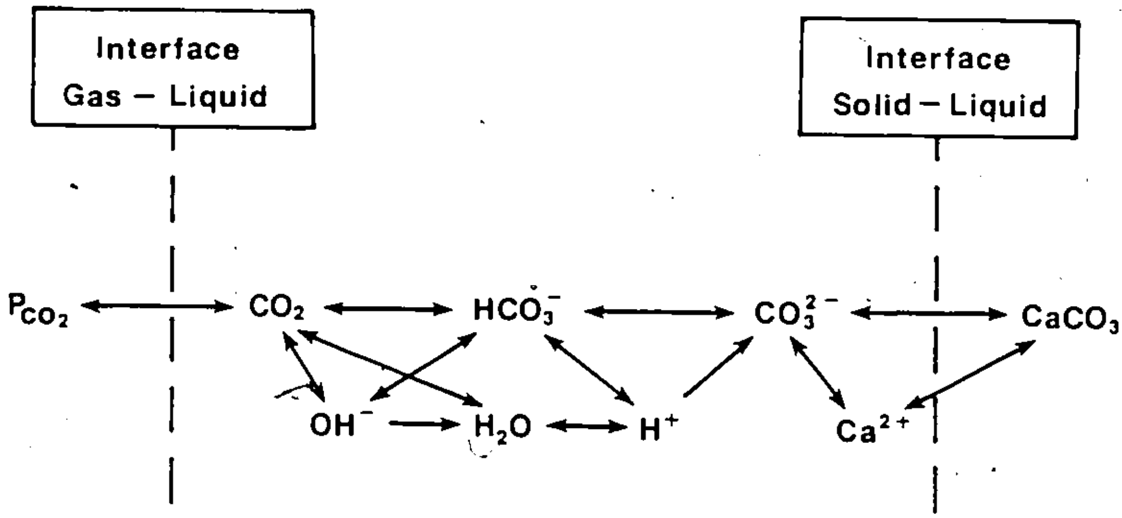

Figure 2.1
The relationship between solid, liquid, and gas phases and the various ions in the dissolution of calcite; after Roques (1969).

their control by environmental factors which ultimately affect the saturation of natural waters. These factors include temperature, carbon dioxide partial pressure, closed and open system conditions, and the effects of other ions. The kinetics of the reactions also have relevance to karst problems, and these are influenced by the additional factors of flow rate, flow path geometry and turbulence.

2.2.1 TEMPERATURE EFFECTS.

The temperature at which dissolution in any chemical system occurs influences not only the reaction rate but the equilibrium state as well. In most two phase solid-liquid systems this influence is a direct relationship; in most three phase gas-liquid-solid systems it is inversely related. The three phase carbonate solution system is controlled by the temperature dependence of the gas-liquid subsystem represented by equation 2-8.

Figure 2.2 shows the inverse relationship between carbon dioxide solubility and temperature. This curve is based upon the work of Bohr (1899), which has been substantially confirmed by later workers (Hutchinson, 1957). The equilibrium concentration of calcite which is dependent on carbon dioxide concentration is also shown as an inverse function of temperature in Figure 2.3. This data is based on the work of Frear and Johnson (1929) and is likewise in substantial agreement with later workers (Hutchinson, 1957).

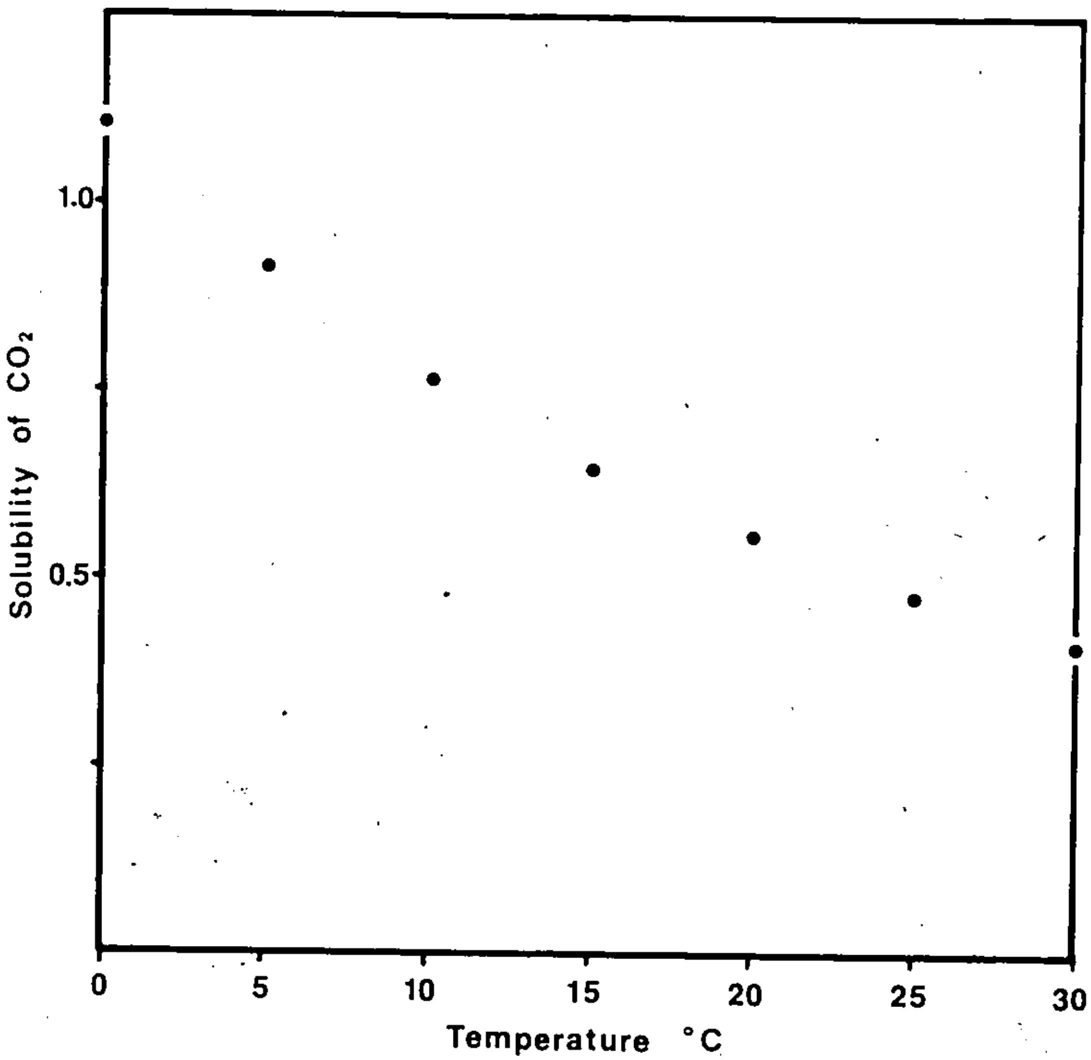

Figure 2.2
The relationship between solubility of carbon dioxide and temperature; from the data of Bohr (1899).

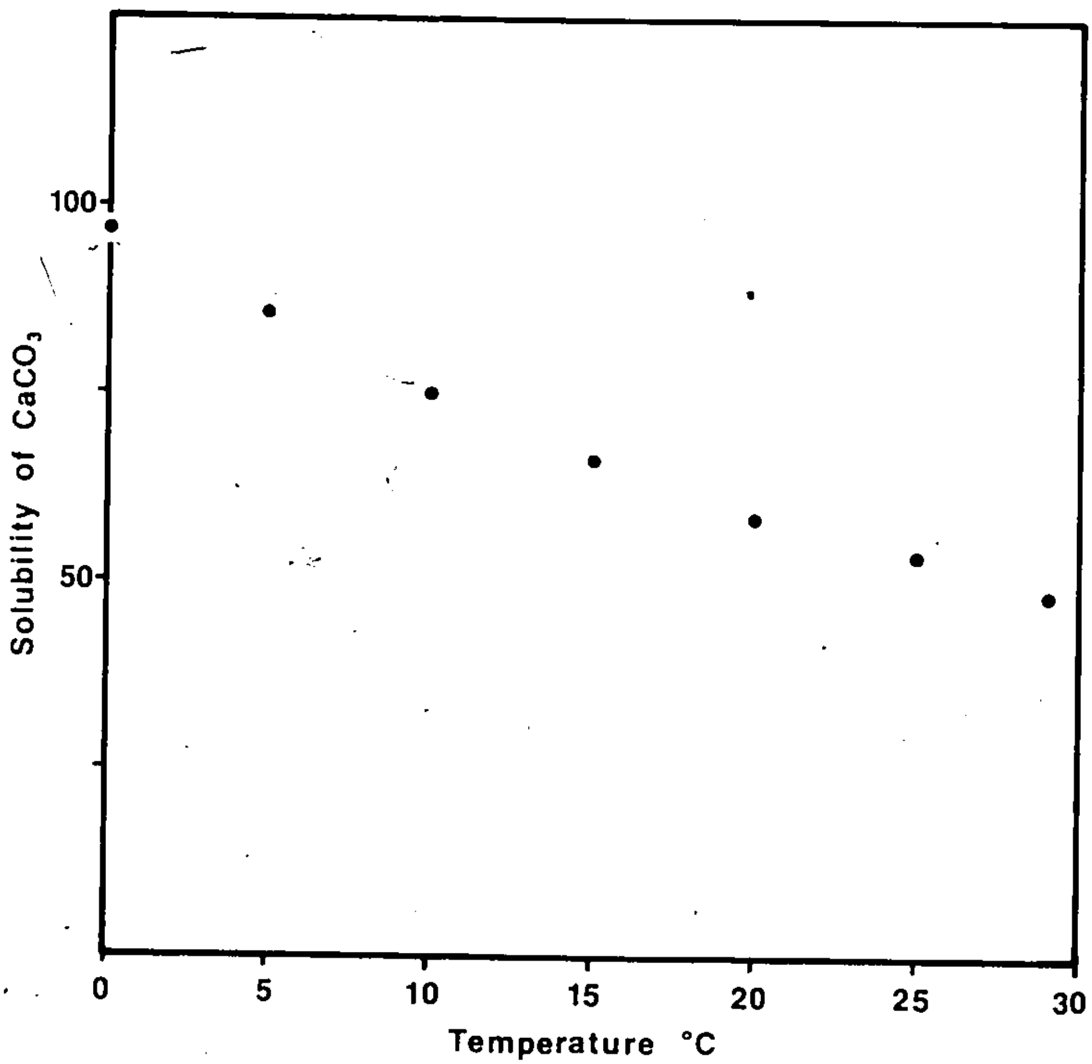

Figure 2.3
The relationship between solubility of calcite and temperature; from the data of Frear and Johnson (1929).

The inverse relationship of the carbonate mineral dissolution is clearly demonstrated.

The negative temperature dependence of carbonate mineral solubility was discussed by Tillmans (1932) and further quantified by Trombe (1952), Picknet (1964), and Garrels and Christ (1965). Trombe's work led Corbel (1959) to conclude that karstification should proceed most rapidly in regions of low temperature. Citing Patterson (1972), Pitty (1966), Pulina (1971), and Harmon et al., (1972); Drake (1974) pointed out that a number of studies show karstification rates to be a positive function of temperature, and he argued that "temperature is not the overriding factor Corbel considered it to be".

2.2.2 THE EFFECT OF CARBON DIOXIDE PARTIAL PRESSURE.

The advent of computer methods has made possible the computation of the carbon dioxide partial pressure with which a given water sample would be in equilibrium, assuming an equilibrium state. This value is obtained using analyses for ions of calcium, magnesium, bicarbonate, hydrogen, and sulphate, as well as temperature, with programs such as those developed by Langmuir (1971) and Wigley (1971). These analyses confirm the arguments of Adams and Swinnerton (1937) and Sweeting (1966) that the increased carbon dioxide concentrations of the soil atmosphere, through which most groundwater must pass, accounts for the high hardness of such waters. These authors further contended that the variation in carbon dioxide partial pressure, with which the waters could be in contact, is more important than the thermal factor in determining water hardness.

Ford's (1971a) water analysis data from alpine environments of western Canada support these contentions as well as any (Fig. 2.4). The calculated carbon dioxide partial pressure values for these samples spanned four orders of magnitude about the global mean of 10E-3.52 atmospheres (0.03% by volume). Ford attributed this variation to the nature of the biotic activity associated with each sample. He found a correlation between the type and thickness of the soil zone through which the water percolated and the calculated carbon dioxide partial pressure value. Glacier and snow melt water typically had carbon dioxide partial pressure values one to two orders of magnitude less than the global mean atmosphere. Tundra waters and turbid glacial waters had carbon dioxide partial pressure values which ranged from the global mean to one order of magnitude less. Samples obtained below the tree line gave carbon dioxide partial pressure values which ranged from global atmospheric mean to two orders of magnitude greater.

The "snow and glacial meltwaters" represented waters previously depleted in carbon dioxide by the freezing process, which had not completed their equilibration with

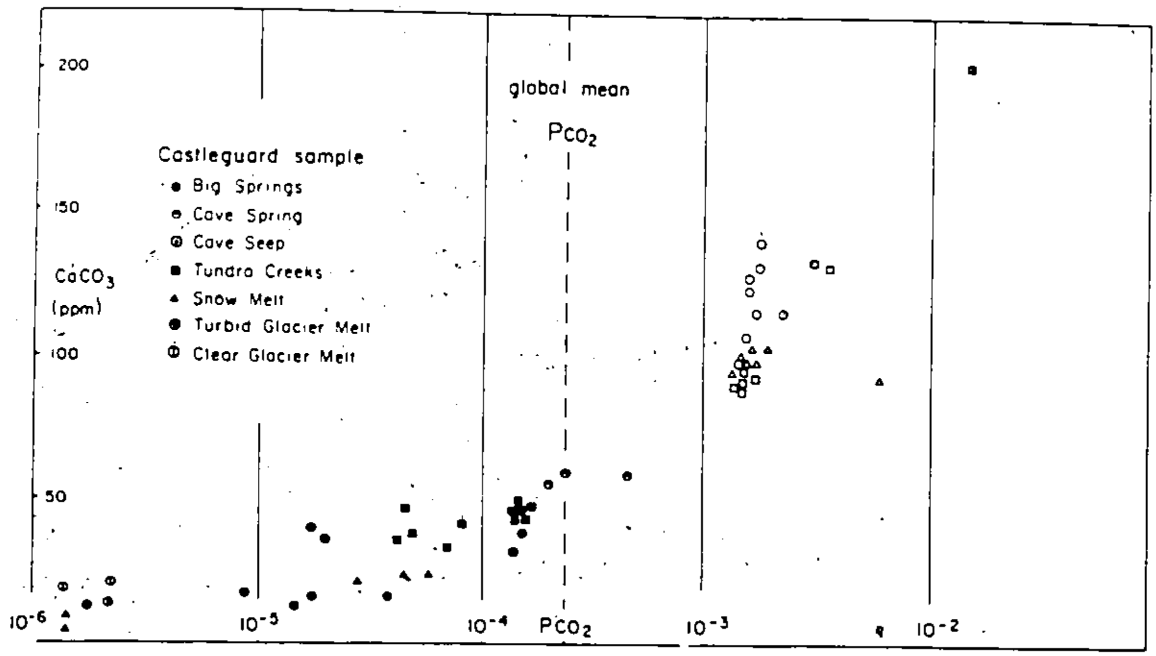

Figure 2.4

The relationship between dissolved carbonate mineral, reported as calcite, and the calculated atmospheric partial pressure of the atmosphere with which each water sample would be in equilibrium. Seven environments of origin are represented among these data from Crowsnest Pass and Mt. Castleguard, Alberta-British Columbia. Adapted from Ford, (1971).

atmospheric carbon dioxide and were without contact with biological activity. The "tundra waters" represented meltwater, which had intermittent and incomplete contact with the meager biological activity of a discontinuous tundra environment. The third group contained water which had traversed the alpine forest environment, where vigorous biological activity contributed large amounts of carbon dioxide.

Direct measurements of soil carbon dioxide have been made by many workers, including Miotke (1974), who used a modified Drager apparatus (Dragerwerk Lubeck, W-Germany). His measurements from karst terrains (table 2.1) show concentrations well in excess of atmospheric values.

Much indirect evidence exists to show that biological activity in the soil effects carbonate dissolution. White and Stellmack (1968) and Groom and Williams (1965) reported distinctly greater hardness of karst waters in summer than in winter for Virginia and Wales respectively. Gams (1968) reported a 35% fluctuation in water hardness of drip waters between autumn and spring in areas of Postojna Cave (Yugoslavia) situated beneath forest cover. He recorded a smaller fluctuation (10%) for drip waters in areas of the cave beneath grasslands.

2.2.3 CLOSED AND OPEN SYSTEMS.

Garrels (1960) recognized two environments for

Table 2.1

CARBON DIOXIDE CONCENTRATIONS IN SOIL ATMOSPHERES

Location	Volume %
PUERTO RICO (Feb. 1969)	
Mogotes Slopes	0.08 - 1.2
Cockpit Soil, clay	1.5 - 7.0
FLORIDA (April/May 1972)	
Key Largo, stony soil	0.2 - 0.4
Everglades, grass	0.7 - 2.2
Cape Kennedy, woods	0.3 - 0.5
ROCKY MOUNTAINS, SOUTHERN CANADA (July/Aug. 1971)	
Atmosphere	0.018
Perennial snow	0.1 - 0.14
Rock Debris	0.04 - 0.1
Alpine Tundra	0.04 - 0.38
Alpine Meadow	0.1 - 0.4
Woods, coniferous	0.1 - 0.5
MAMMOTH CAVE, KENTUCKY (Oct. 1971/June 1972)	
Ridges & Slopes, Clay	0.1 - 0.9
River Terrace, Echo River	0.3 - 5.0
Sinkhole Plain, clay, winter	0.1 - 1.75
" " " summer	0.5 - 4.0

After Miotke, (1974)

carbonate solution which are applicable to subsurface karst erosion. These involved the presence or absence of a gas phase of a fixed carbon dioxide partial pressure during the dissolution of the carbonate. If the gas phase is absent, the process will be limited by the reaction involving the production of bicarbonate ion from the hydrogen and carbonate ions (Equation 2-9). If the gas phase is present, the removal of hydrogen ions will drive Equation 2-8 to the right allowing additional carbon dioxide to be dissolved. This results in the solution of significant amounts of additional carbonate mineral. Figure 2.5, adapted from Holland et al. (1964), shows that, for water equilibrated with a carbon dioxide partial pressure of 10E-2 atmospheres, final solute concentration, for systems with and without a gas phase, differed by a factor of five.

Sweeting (1972) referred to the work of Smith and Mead (1962) in which this effect was called aerobic and anaerobic solubility. Holland et al. (1964) and Thrailkill (1968) referred to it without name. More recent authors (Langmuir, 1971; Harmon, 1973; and Harmon et al., 1973) used Garrels and Christ's (1965) open and closed system solution terminology. While it is possible that open system solution will produce greater geomorphic effects, it need not be so. Few caves with air filled connections to the surface have atmospheric carbon dioxide partial pressures in the range of 10E-2.5, a common figure for soil air. They range from near

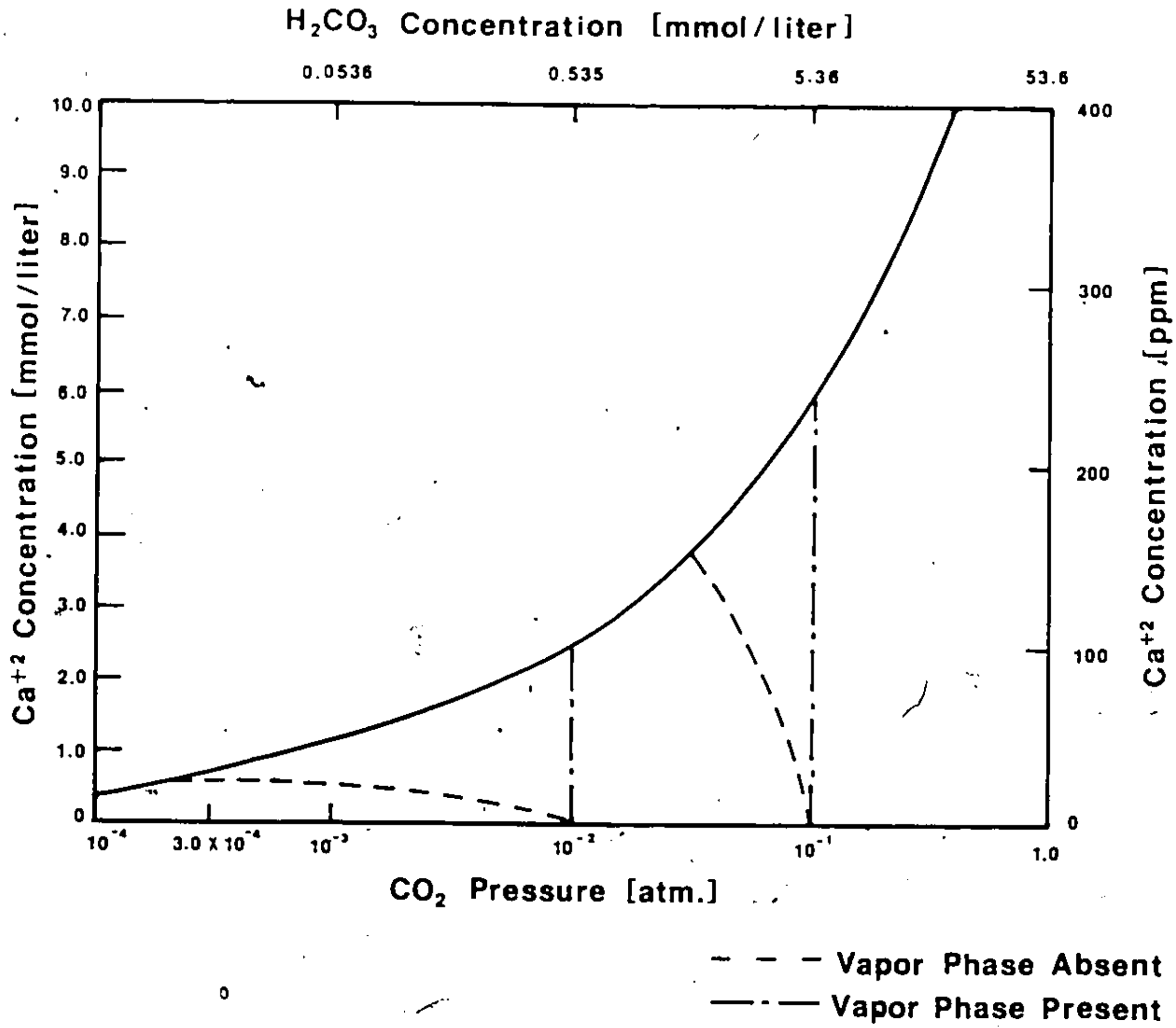

Figure 2.5
Open and closed system equilibria for calcite for waters equilibrated with partial pressures of 1ØE-1 and 1ØE-2 atmospheres of carbon dioxide; after Holland et al., (1964).

atmospheric (about 10E-3.5) in Mammoth Cave (Quinlan, personal communication) to higher values (10E-2.85, Grotte de Moulis, Roques, 1969; 10E-2.4, Carlsbad Caverns, Thrailkill, 1968). Water in equilibrium with high carbon dioxide values, which comes into contact with cave air of lower carbon dioxide concentration, will de-gas, driving equations 2-8, 2-9, 2-10, 2-11, 2-12, and 2-13 in reverse. In most cases, this will limit the equilibrium concentration to a value less than its initial closed system potential, a point noted by Moore (1964).

2.2.4 THE EFFECT OF OTHER IONS.

A variety of metal ions have been shown to affect the dissolution of calcite, the principal constituent of limestone. Among these is magnesium, a major component of the double carbonate, dolomite, and a minor component of most limestones. The importance of magnesium carbonate in this regard is not clear. Pure magnesium carbonate, magnesite, appears more soluble than calcium carbonate, while the double carbonate is less soluble than calcite or magnesite [see Schoeller, Chilingar, ~~Gersten~~, Lauer and Pfeiffer, and Preisnitz, as reported in Sweeting, (1972); also Langmuir, (1971)]. Rauch and White (1970), in a Pennsylvania study, maintained that limestones with two to five mole percent magnesium are most conducive to cavern development, based upon the fact that they contain a greater measured volume of solution voids. Plummer (1972), on the other hand, suggested that the solubility of magnesium calcite reaches a maximum at 24 mole percent magnesium. This contradiction would be resolved if it could be demonstrated that the kinetics of the solution of magnesium calcite in the two to five mole percent range was slower, leading to enhanced solution at depth rather than at the surface. Otherwise, it seems likely that geologic factors may be at work. Rauch and White suggested that the lesser solubility of the magnesium limestones in their study was due to the occurence of these rocks in proximity to argillaceous formations which may be effective aquicludes.

King and Lieu (1933) demonstrated that traces of ferric and chromic ion could inhibit the rate of carbonate solution. Erga and Terjesen (1956) demonstrated a similar effect for copper ions in very low concentrations. Subsequently, other metal ions including lead, lanthanum, yttrium, scandium, cadmium, gold, zinc, germanium, manganese, nickel, barium, and cobalt were also shown to inhibit the solution of calcite in trace concentrations (Fig. 2.6) (Terjesen, 1961; Nestas and Terjesen, 1969; Pesret, 1972). Morse and Berner (1972) demonstrated an inhibiting effect for phosphate ions, which has subsequently been verified by Morse (1974). There is strong evidence that phosphate ions may be responsible for long term undersaturation of limestone waters in Florida (Plummer &

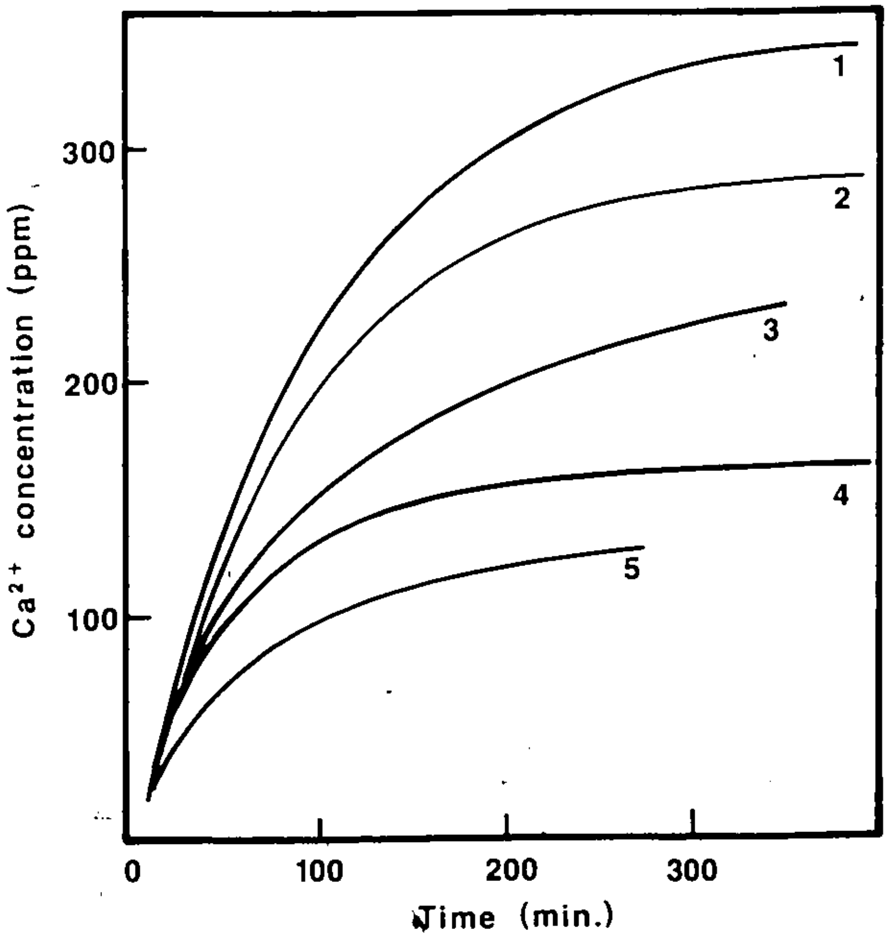

Figure 2.6
Calcium ion concentration as a function of time for solutions dissolving pure calcium carbonate and for solutions dissolving calcium carbonate in the presence of the following ions:

1. None
2. Sc 1ØE-6 M/l
3. Cu 1ØE-4 "
4. Sc 1ØE-5 "
5. Cu 1ØE-3 "

These experiments were conducted under a carbon dioxide pressure of 1 atmosphere. After Terjesen et al., (1961).

Wigley, 1976). Unfortunately, these studies for the most part were carried out at one atmosphere carbon dioxide and are not directly applicable to the situations under consideration. The extent to which these ions effect carbonate equilibria and rates of equilibration in the range of natural systems remains to be demonstrated.

2.2.5 LITHOLOGIC CONTROLS.

In their exhaustive study of lithologic controls in the solution of central Pennsylvania carbonates, Rauch and White (1970) concluded:

> Cavity development is enhanced by purity of the bulk rock, small grain size (micrite), and possibly by silty streaks.
>
> Cave development is inhibited by high concentrations of [quartz, aluminum oxides] dolomite, sparite and impurities, or by very low dolomite concentrations. (p. 1191)

They concurred with Bretz (1942) that insolubles probably create a shield against further solution, not only by armouring upward facing surfaces, as Bretz had suggested, but by creating a porous barrier to mass transfer on all dissolving surfaces. The contentions of Rauch and White were supported by the observations of Sweeting (1972 p. 39).

2.2.6 REACTION KINETICS.

In order to predict the rates of propogation and, as will be shown later, the form of subsurface karst drainage networks, it is important to determine the rate at which a moving groundwater mass approaches saturation. It would be useful to know this for a variety of natural conditions. The rate of dissolution of any mineral is dependent upon: (1) the rate of tranport of reactants and products between the mineral surface and the bulk solution and (2) the reaction rates at the mineral surface or within the bulk solution. If either the reaction rates or the transport rates are very slow relative to the other we may say that the process is reaction or transport limited. Depending upon the hydrodynamic and chemical characteristics of a particular environment, we may reasonably expect different reaction or transport factors to be limiting.

King and Liu (1933), Gortikov (1937), and Tominaga, et al. (1939) studied the effects of solvent motion on calcite and marble dissolution rates in dilute acids. They found these rates to be a direct function of solvent velocity and concluded that the process was limited by diffusion of hydrogen ions to the liquid solid interface.

Kay (1957), in a series of simple qualitative experiments with dilute (10%) hydrocholoric acid on calcite crystals and small limestone blocks, concluded that solvent velocity was an important positive rate controlling factor in carbonate dissolution. This effect was assumed to be a function of the reduction of the saturated laminar sublayer in contact with the solute, across which solute and solvent ions must migrate.

Using crude quantitative measures and theoretical considerations derived from heat transfer theory, Weyl (1958) produced equations for the reaction kinetics of calcite. The equations relate mean solvent velocity (v), fracture width (d) or capillary radius (a), and the diffusion constant for the solute species (D), to the penetration distance (L).

$$L = 0.572va^2/D \tag{2-15}$$

$$L = 0.304vd^2/D \tag{2-16}$$

Penetration distance is defined by Weyl (1958) as the distance a solvent must travel through a solute bounded space to satisfy 90% of the saturation deficit. These equations assume that calcite solution is diffusion limited. Weyl supported this contention with experimental evidence showing a nearly linear relationship between velocity and dissolution rate. His work considered only dissolution in the laminar regimes.

Wigley (1971) reformulated Weyl's work in terms of relaxation length and extended the theoretical considerations to include the turbulent regime. Following engineering practice, relaxation length was defined as the distance a solvent must travel through a solute bounded space to satisfy 1/e of the saturation deficit. These equations also assume a simple diffusion limited reaction.

Erga and Terjesen (1956), Terjesen, et al. (1961), Plummer (1972), Berner and Morse (1974), and Wigley and Plummer (1976) presented experimental data which suggest that solution rate is relatively independent of solvent velocity. This is in contrast to Weyl's findings and those of the earlier workers.

Curl (1968) attempted to resolve this apparent conflict. He suggested that at low solvent velocities dissolution rate is determined by transfer of calcium and bicarbonate ions from the surface and at very high velocities by transfer of carbonic acid to the surface. In both of these cases, dissolution rate would be proportional to velocity. Over a wide transition region he proposed that the dissolution rate is nearly independent of velocity but dependent upon carbon dioxide hydration rate in the boundary layer. He suggested that experiments like those by Gortikov (1937), and Erga and Terjesen (1956) fall in this region.

Curl cautioned that this hypothesis is a preliminary and much simplified step in the analysis of the limestone dissolution process and involves certain simplifying assumptions. He drew specific attention to the assumption of a simple simultaneous reaction diffusion model, a simple "film theory" in turbulent flow, and the lack of consideration of equilibrium effects in the boundary layer and activity effects.

The experiments of Berner and Morse (1974), although primarily done in an oceanographic context, have broad applicability to the geochemistry of carbonate dissolution. Their method achieves a steady state determination of transfer rate of calcium carbonate into solution, a technique in which a solution of constant carbon dioxide partial pressure and pH is allowed to react with calcite.

Figure 2.7 shows their dissolution rate experiment plotted as functions of the the deviation of pH from its equilibrium value. The plot can be readily divided into three regions covering five orders of magnitude. Each of these regions has a characteristic rate of change in the solution rate. Of particular interest here is the dramatic drop in the dissolution rate in region 3. This suggests that aggressive (undersaturated) water might penetrate to great distances but the rate at which it accomplishes geomorphic work may be quite small.

White (1977) reviewed the Berner and Morse (1974) results in a karst context. He pointed out that for karst waters the break in slope occurs at about 90% saturation, which corresponds to the region 3A - 3B boundary. He then calculated the travel distance required to reach 90% saturation for a range of capillary openings and ground water flow gradients (Fig. 2.8). For this, he used both the Plummer-Wigley rate equations, which suggest a second order surface reaction control, and the Weyl diffusion control model. He selected carbon dioxide partial pressure values of 10E-2.5 and 10E-1 for the reaction limited calculations.

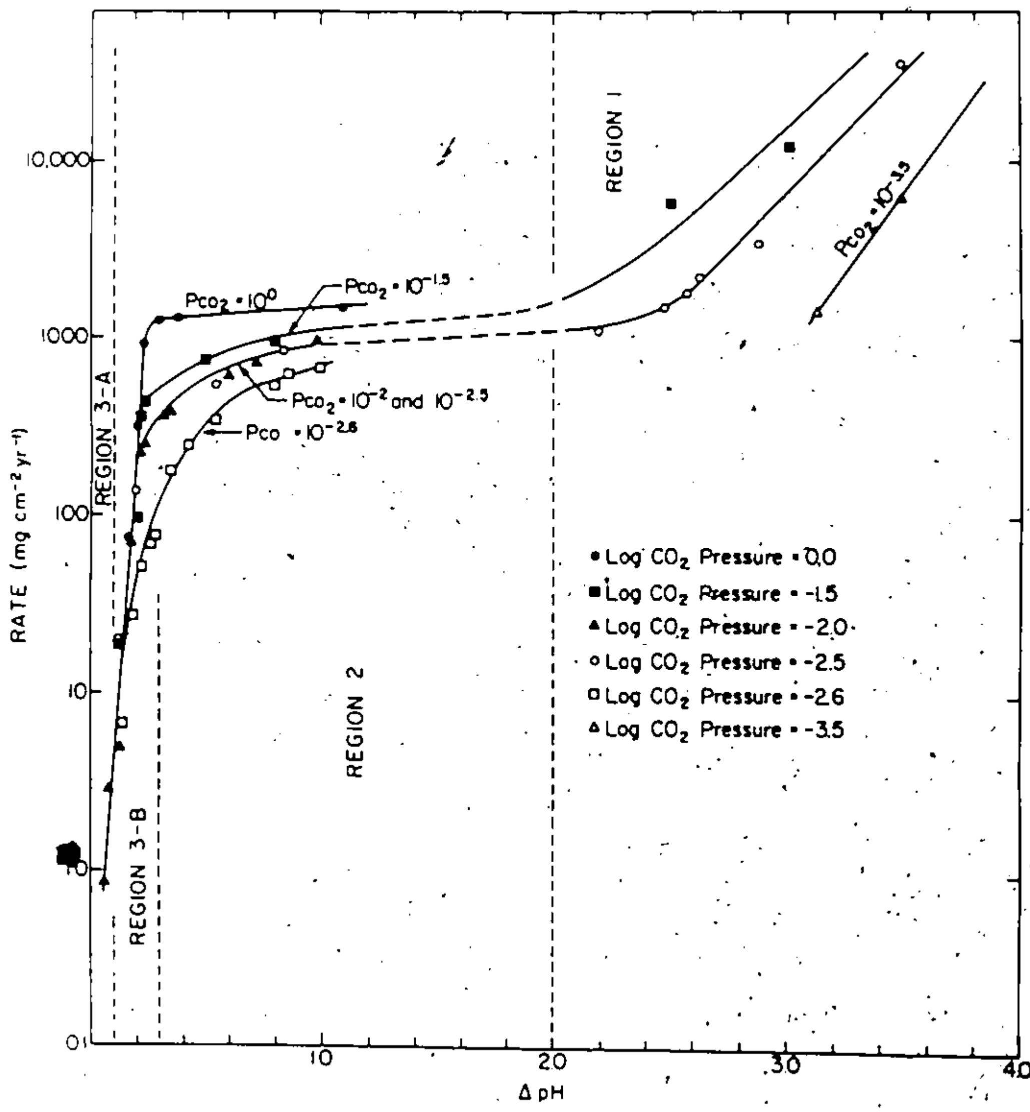

Figure 2.7

Solution rate experiment data of Berner and Morse (1974) plotted as functions of the deviation of pH from its equilibrium value at the given carbon dioxide partial pressure; From White, (1977).

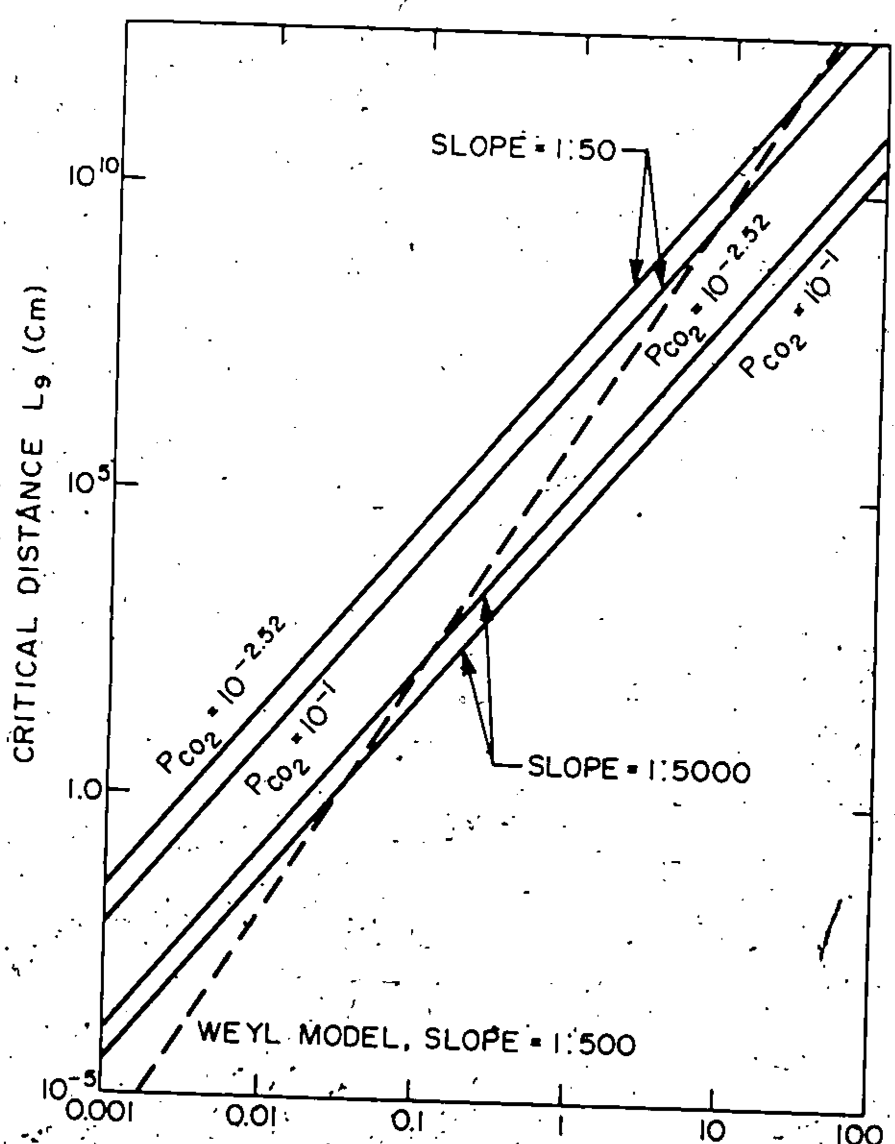

Figure 2.8

Distance to 90% saturation with respect to calcite as a function of conduit diameter. Hydraulic potential surface slopes of 1:50 and 1:5000 are shown, calculated with the Plummer and Wigley rate equations. A slope of 1:500 is also calculated using the Weyl model. Carbon dioxide partial pressures of 10E-2.52 and 10E-1 are used, reflecting values typical of spring waters and soil waters, respectively. Adapted from White, 1977.

These values correspond to typical carbonate spring values and typical soil water values for carbon dioxide concentrations, respectively. These plots cover the full range of pertinent, published, experimental data and theoretical arguements. As White pointed out, they are in substantial agreement that for small capillaries and fractures representative of virgin pore space of tectonic, diagenetic, and sedimentary origin in limestone, the bulk of the geomorphic work accomplished by the dissolution process takes place within a few meters or tens of meters of the point where it gains access to the limestone.

In a more recent series of calcite dissolution experiments, Plummer, Wigley, and Parkhurst (1978) have extended the pH, carbon dioxide partial pressure, and temperature range of previous experiments. They propose a mechanistic model that describes their observations. Their results in general corroborate the results of Berner and Morse (1974).

These laboratory investigations are supported by several types of field observations. Bogli (1966) and Cogley (1972) have demonstrated that thin films of water from rain and snowmelt traversing exposed limestone surfaces quickly saturate to levels appropriate for open system waters in contact with atmospheric concentrations of carbon dioxide.

In the subsurface, large numbers of "soda straw" stalactites form from seeps along cavern ceilings. Frequently, these cavities are only a few meters beneath the surface. These deposits form by crystallization at the perimeter of successive drops of seepage water supplied through a central canal (Fig. 2.9). Typically, soda straws are a few decimeters in length but range to one meter or more. The shallowness of some of these cavities makes it probable that the drip waters have not travelled far from their initial contact with limestone, yet they have achieved a degree of saturation which not only makes stalactite growth possible but precludes the re-solution of its base from the inside in these slender forms. Finally, White (1977) pointed out that springs in the Appalachians are typically undersaturated at the critical 90% level. This corresponds to the dramatic decline in the mass transfer rate in region 3 of the Berner and Morse experiments.

2.2.7 MISCHUNGSKORROSION

The degree of saturation of a carbonate groundwater may also be influenced by the mixing of waters from different environments. Bogli (1964) showed that waters in equilibrium with an atmosphere of high carbon dioxide partial pressure, such as those derived from soil percolation, when mixed with waters in equilibrium with a low carbon dioxide partial pressure, such as water derived from direct runoff, yields a solution of lower saturation.

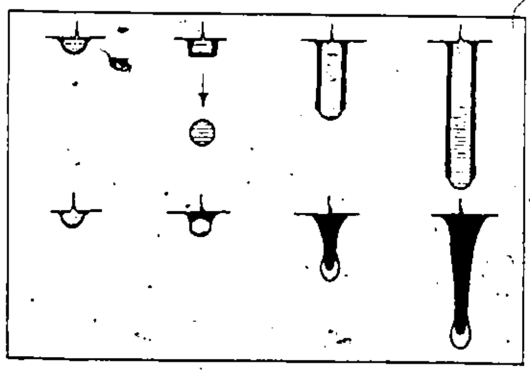

Figure 2.9
Typical hollow "soda straw" stalactites compared to normal stalactites; From Ford, (197x).

This is true even in the case where the two original waters are at saturation. By this means, it should be possible to regenerate undersaturation within the aquifer and produce dissolution in regions more distal to the groundwater input points than would otherwise be the case. Figure 2.10 shows that this effect is strongly influenced by the proportions of the mixing and the degree to which the waters differ in their carbon dioxide content. The absolute dissolution effect is also directly related to the quantity of water mixed.

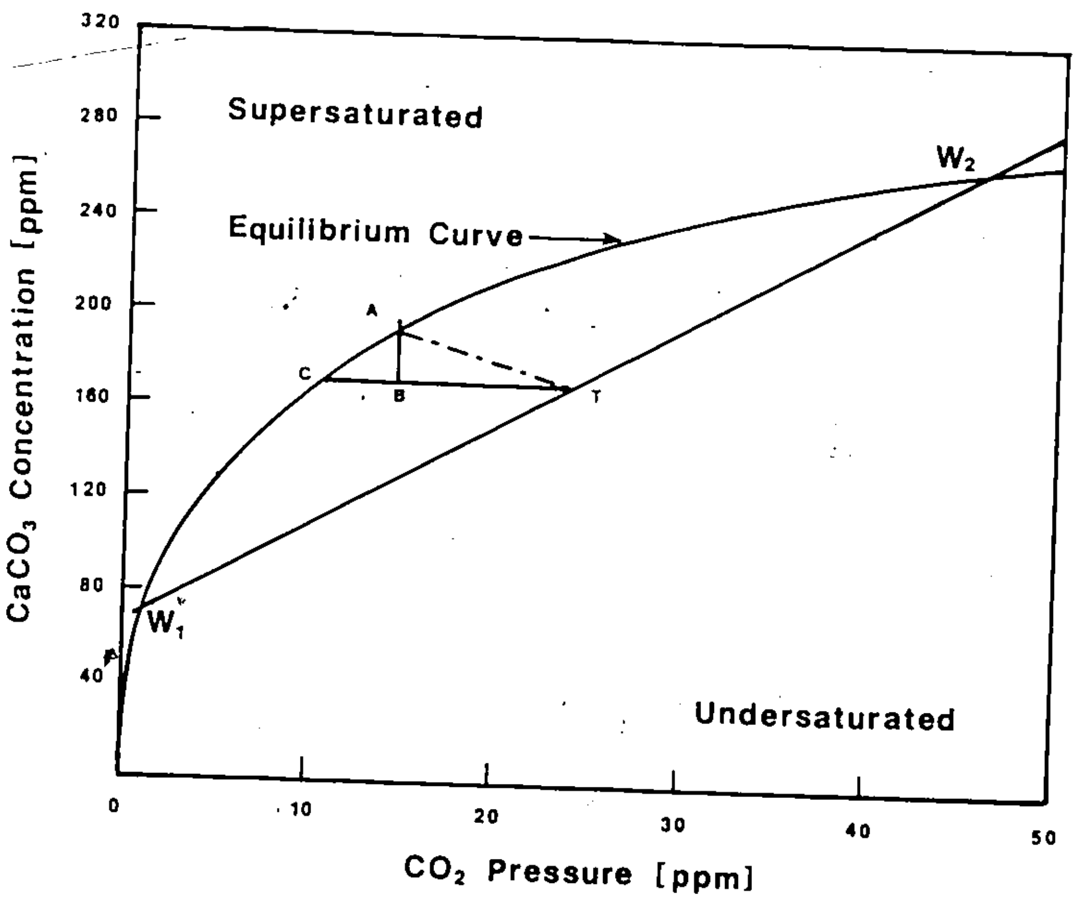

Figure 2.1Ø

An example of the mischungskorrosion effect after Bogli (1964). Water 1 [W1] and water 2 [W2] mix in a 1:1 ratio to form a solution of composition T. The saturation deficit of this solution is equal to A-B.

CHAPTER 3

RESEARCH METHODS

3.1 THE EXPERIMENTAL APPROACH

The early processes leading to cavern genesis are all but impossible to observe directly in the field. The portions of these tube networks where the first significant enlargement, beyond the initial fracture and bedding plane porosity, occurs are inaccessible to all presently available means of direct study because of their small size. Furthermore, the nature of limestone solution chemistry coupled with the hydraulic characteristics of its primitive fractures produce reaction rates which cause the evolution of the system to proceed very slowly. The period of time required for the development of a modest network of small tubes may be orders of magnitude longer than the lifespan of the investigator. The author intends to demonstrate that an understanding of these processes is, nonetheless, of paramount importance because they determine, in large measure, the course of subsequent solutional and hydraulic history of the limestone.

The products of these initial processes of development, which are preserved in accessible caverns, are also, in large measure, unexplorable because of their size, and are frequently further obscured by sediment fillings. Those which can be studied are fragmentary at best and are commonly so modified by subsequent events that few irrefutable conclusions can be gained concerning the earliest formative processes.

This study attempts to overcome these difficulties by evaluating the processes of phreatic solution and groundwater flow integration by means of experiments with laboratory models. These include solution experiments, flow envelope experiments, and electric analogue experiments.

3.1.1 MODEL STUDIES

Model studies fall into three fundamental classes: conceptual models, involving thought experiments; mathematical models, frequently involving computer simulation; and physical models, involving laboratory experiment. Although their methods differ, the three classes have similar objectives in geologic research. They contrive to understand the operation and predict the outcome of situations where several processes and variables arepresumed to interact but in an unknown way. These techniques have two important advantages over direct observation. They readily permit the manipulation of variables so that they may be studied for their individual effects, and they render amenable to research situations in which the size of the elements or the rate of the process precludes direct observation, as noted.

3.1.2 PHYSICAL MODELS IN KARST RESEARCH

Physical models, in the sense of simulations of natural processes with laboratory hardware, have a long history in earth science generally and in geomorphology particularly. The tectonic deformation studies of Cloos (1930) and the drainage network studies of Schumm and Khan (1972) come readily to mind. A selection of the early work in this area has been summarized by Hubbert (1937), and more recent works in geomorphology are reviewed by Morgan (1967). Karplus (1958), Todd (1960), and Yalin (1971) have done likewise for hydrogeology.

3.1.3 CHEMICAL MODELS

The bulk of the laboratory experiments directed toward karst problems have been for the purpose of testing conceptual models of carbonate solubility and solution kinetics. Weyl (1958) directed jets of carbon dioxide charged water on Iceland spar crystals to observe the effects of solvent velocity on dissolution rate which formed the basis for his diffusion controlled model of carbonate solution kinetics. Howard (1967) circulated carbon dioxide charged water between carefully fitted limestone blocks in an unsuccessful attempt to obtain an experimental verification of Weyl's diffusion limited model. Rauch and

White (1970) passed carbon dioxide charged water through holes bored in limestone blocks, primarily to obtain experimental verification for a model of limestone solubilities based upon field studies. Plummer and Wigley (1976) stirred pure calcite crystals in reaction vessels with water and carbon dioxide, under very carefully controlled conditions, to determine mass transfer rates. Pioneer work of this nature was undertaken by King (1928), Gortikov (1937), and Tominaga, et al. (1939), Erga and Terjesen (1956) and Berner and Morse (1974) among others.

3.1.4 MODELS INVOLVING DETAILED MORPHOLOGY

Although the chemical experiments contributed to our understanding of karst, they are not simulations in the sense of reproducing specific patterns and shapes of naturally occurring solution voids directly by experiment. To this end, Lange (1960) and Mowat (1962) subjected variously shaped pieces of salt and limestone to dissolving fluids to verify Lange's earlier theoretical conclusions on the changing geometry of cavern structures. Their experiments showed that exterior angles preserve their sharpness with negative uniform mass transfer, while interior angles, under the same conditions, are rounded.

Goodchild and Ford (1971) and Blumburg and Curl (1974) successfully simulated the formation of eddy induced scallops on plaster of Paris in a flume. The ability to observe their formation and manipulate variables was an important factor in refining their initial conceptual models to produce a fairly complete understanding of these useful fluid flow direction and velocity indicators.

Glew (1976) reproduced rillenkarren, a type of solution feature found on inclined, epigean limestone surfaces. The experiments were carried out on plaster of Paris beneath a rain simulator. Once again, the ability to reproduce the features in a reduced time span, together with the ability to manipulate the variables, provided new and valuable insights which materially aided the research (Glew and Ford, 1980).

Kay (1957) conducted experiments with dilute hydrochloric acid on limestone blocks to show that "differential solution commensurate with velocity takes place, causing preferential conduit enlargement" and, thereby, caverns.

Meuner (1899) and Reams (1965) conducted experiments with dilute hydrochloric acid and limestone in an effort to gain insights into the processes leading to the development of domepits. The difficulty of scaling turbulent vadose processes in these simulations places their conclusions in some doubt. Later work, in actively eroding domepits, has proven more useful (Brucker, Hess, and White 1972).

3.1.5 GENERAL SPELEOGENESIS MODELS

Several model studies have been directed toward elucidating the processes which control the patterns of cave systems in a general sense. Thrailkill (1968) produced, mathematically, a series of pipe models, in an effort to understand what processes could localize the development of subsurface drainage trunks in proximity to pre-existing peizometric surfaces. He demonstrated that there was no hydrologic reason for the flow in shallow conduits to be significantly greater than deeper ones (Fig. 3.1). This was shown to be true in laminar and turbulent flow cases, given that the lateral extent of the aquifer is great relative to its thickness, which is almost invariably the case.

Ewers (1964, 1966, 1972, 1974, 1976, 1977) and Waterman (1975) experimented with laboratory models in salt and plaster of Paris to gain insights into the processes by which tube networks could propagate across bedding planes. The conclusions of these experiments are summarized in Chapter 4 and form the starting point for the research reported here.

Bedinger (1966) employed a rectangular array of electrical resistance elements to simulate flow paths along vertical joints and horizontal bedding planes (Fig. 3.2). By assuming flow in the prototype, to be within the range of applicability of Darcy's Law, he could validly assume that current flow in the resistance elements was analogous to

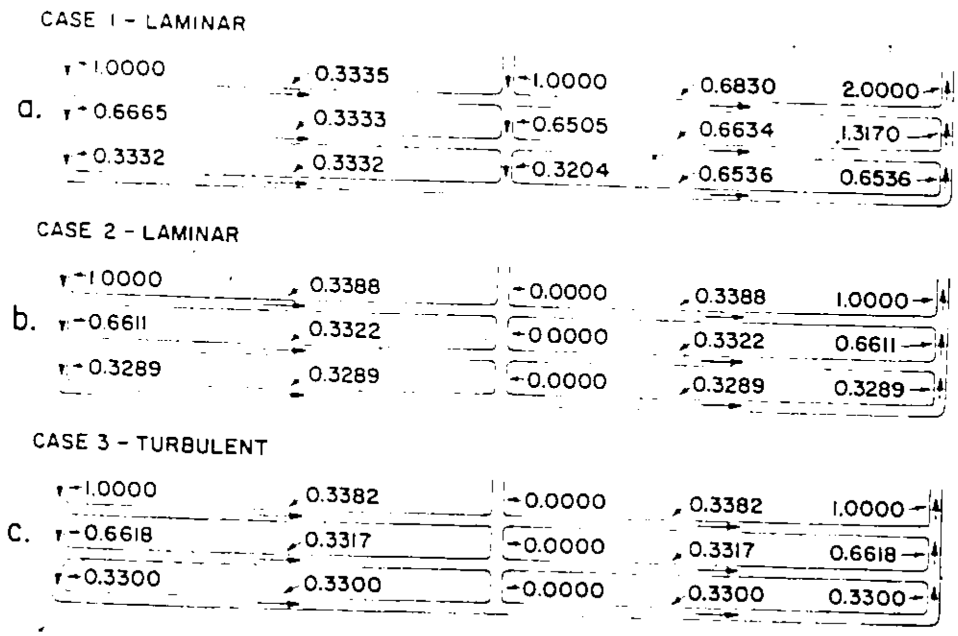

Figure 3.1

Pipe networks from Thrailkill (1968). Figures indicate flow volume when horizontal segments are 100x vertical segments (note 10x vertical exaggeration).

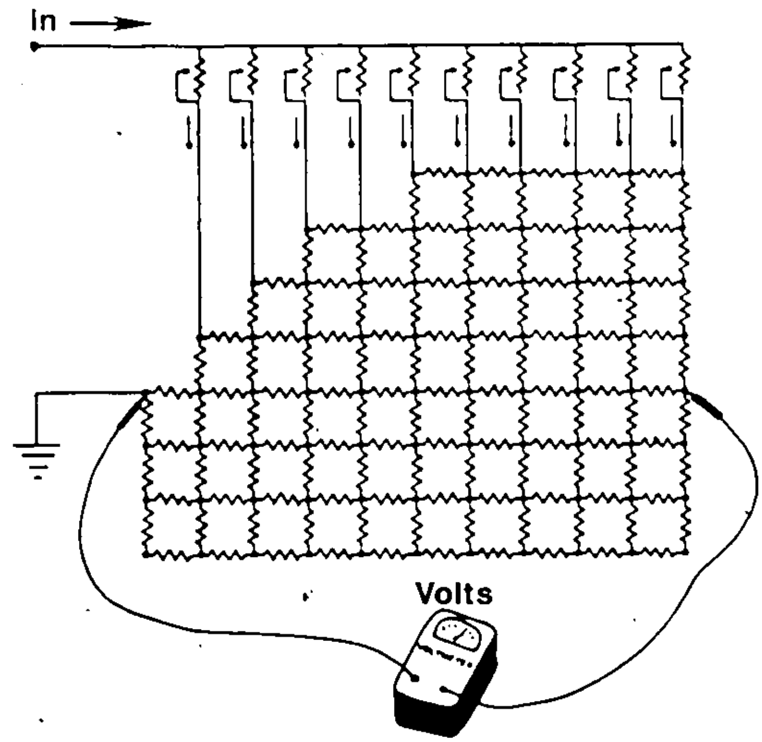

Figure 3.2
Resistance networks for simulation of groundwater flow in limestone; from Bedinger, (1966).

water flow in the prototype, provided that the individual electrical resistances were proportional to one another in the same way as the fluid resistances in the prototype. Similarly, the voltages at the resistor node points are analogous to fluid potential (head), which permits a potential field to be mapped (Fig. 3.3). By measuring the potential loss across each resistor, Bedinger could calculate the current flow in that element. By assigning a factor for enlargement by dissolution which was related to current flow, he could reduce the resistance of individual elements, which was analogous to an increase in the fissure size in the prototype (Fig. 3.4). Bedenger interpreted his model results as supporting the Swinnerton (1932) water table theory of cavern genesis. Though an elegant scheme, it possessed several flaws. Ford (1971) noted that the ratio of bedding plane to joint elements in the experiments was 1:1 and that, in his field experience, such ratios commonly equal 100:1 in nature. Bedinger made another error of geometry in supposing that the limestone unit was nearly as thick as its lateral extent. Only in isolated knobs, areas of imbricate thrusting, or in reef limestones (which are often quite devoid of bedding planes) do such proportions obtain. Thrailkill (1968) suggested that in horizontal limestone sequences (the type modeled by Bedinger) lateral extent to thickness ratios are commonly 100:1 or 1000:1. The most important oversight in the

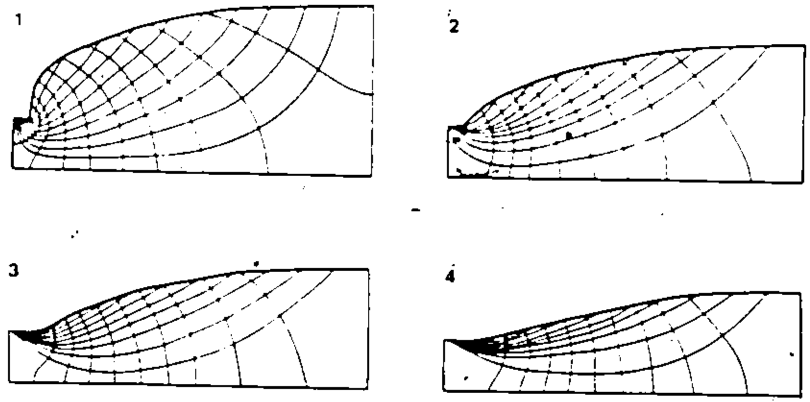

Figure 3.3
Progressive development of flow fields in limestone; from Bedinger, (1966).

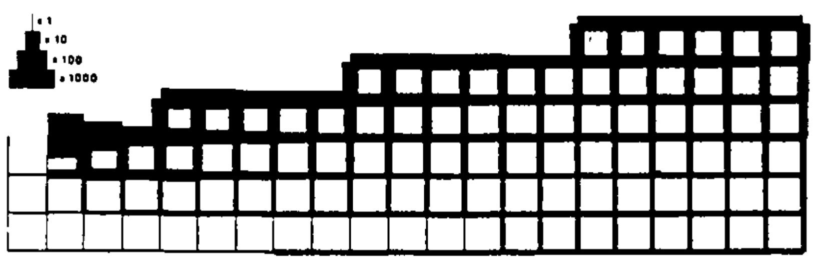

Figure 3.4
Progressive development of porosity in limestone; from Bedinger, (1966).

Bedinger models, however, is the assumption that dissolution is proportional to the solvent throughput at all points in the model. This ignores the important fact that the solvent efficiency, especially in primitive fractures, is rapidly diminished with distance. As will be demonstrated subsequently, the enlargement is exactly the reverse of that predicted by these models. This error has been compounded by most other students of cavern development. They have erroneously assumed that a more or less uniform and continuous enlargement over the entire length of a clearly established path has occurred since the inception of the speleogenetic process. The present research presents a much less deterministic view. Finally, the Bedinger models were evolved to a state which, almost certainly, would have carried them well beyond the Darcy flow regime, where the equivalence between Ohm's Law and Darcy's Law no longer holds.

Ewers (1972) used liquid medium electrical analogues to map hydraulic potential fields in bedding planes. More specifically, the experiments delineated the changes in the flow fields engendered by the growth of tertiary porosity (dissolution porosity) and the reasons for the pattern of that growth. They took full account of the solution kinetics, as they were understood at that time. Similar experiments form part of the present research and will be described in detail subsequently.

3.2 LABORATORY MODELS AND THE PROBLEM OF SCALE

Two types of laboratory models can be recognized among these studies and in model studies generally. The first type are direct simulations which deal with processes identical to those occurring in nature. The second involves an analogue in which a functionally similar, but physically different, process or medium is employed. In the first case, the scale is frequently unity. The chemical experiments of Howard (1968) or Plummer and Wigley (1976) qualify as this type of model. The second case usually involves the manipulation of specific parameters to accommodate a size or rate change. The eddy scallop studies of Goodchild and Ford (1971) or the bedding plane dissolution experiments of Ewers (1972) exemplify this type of model. These clearly involve parametric scale changes which are, at once, the most desirable and most troublesome characteristics of this model type.

Hubbert (1937) laid the foundation for the scaling of geological model studies, and Yalin (1971) has applied these concepts to hydraulic models specifically. These authors have pointed out that among the scale considerations such a model may be required to meet are geometric, kinematic and dynamic similarity.

3.2.1 GEOMETRIC SIMILARITY

Two bodies are said to be geometrically similar when all corresponding lengths are proportional. If Lp is a length in the prototype and Lm is the corresponding length in the model then:

$$Lp/Lm = Lr \tag{3-1}$$

where Lr is the dimensionless scale factor of length in the two bodies. Similarly, where Ap and Am are correspondingly areas Ar is the area scale factor:

$$Ap/Am = Ar \tag{3-2}$$

Volumes are related by Vr:

$$Vp/Vm = Vr \tag{3-3}$$

where Vp and Vm are corresponding volumes.

3.2.2 KINEMATIC SIMILARITY

If two geometrically similar bodies undergo geometrically similar changes of shape or position or both, the two bodies are kinematically similar, provided the times required for all such transformations are related as:

$$Tp/Tm = Tr \tag{3-4}$$

where Tp and Tm are the transformation periods, and Tr is the model ratio of time. Kinematically similar bodies must also exhibit proportional velocities and accelerations at corresponding points:

$$vp/vm = vr \tag{3-5}$$

$$ap/am = ar \tag{3-6}$$

where vr and ar are the model ratios for these quantities.

3.2.3 DYNAMIC SIMILARITIES

Dynamic similarity deals with the forces which are a result of the mass of the prototype and model bodies, in response to acceleration by gravity or otherwise. Four dimensionless parameters describe these forces in fluid systems:

1. Reynolds number (NR) = Inertial force/Viscous force
2. Froude number (NF) = Inertial force/Gravitational force
3. Mach number (NM) = Inertial force/Elastic force
4. Webber number (NW) = Inertial force/Surface energy force.

Dynamic similarity requires that the model and prototype exhibit identical values for these parameters. Because groundwater flow velocities are customarily quite low, viscous forces are relatively important, within an order of magnitude of the inertial forces. Therefore, only the Reynolds number is considered important.

3.2.4 OTHER FACTORS

Model situations frequently arise in which there are factors affecting the performance of a model, for which no scaling principles have been developed. In these cases, empirically derived adjustments are made, until the model performs in a way which can be verified by comparison to a range of prototype conditions actually observed. This technique is commonly used in the weighting of factors in computer simulations such as watershed models and in engineering practice.

3.2.5 SIMILARITY OF PROCESS APPROACH

In geological settings involving processes extending over long time spans, model verification schemes may be impractical or impossible. In these situations, if detailed quantitative results of great accuracy are not needed, a "similarity of process" approach (Hooke, 1968) may be used. In this type of study, the model is recognized as a separate system rather than a scaled replica of the prototype. Hook pointed out that this is an adequate technique in discerning general characteristics of the processes. He proposed three basic conditions which must be satisfied for such simulations of geomorphic processes:

1. General scaling relationships must be met.
2. The model must reproduce a morphological characteristic of the prototype.
3. The processes producing this characteristic in the model can logically be assumed to operate in the prototype.

Hook employed this type of model to gain insights into the processes forming alluvial fans. The laboratory models suggested explanations for specific field observations which could be reasonably assumed to be operating in the natural system.

Models, even poorly scaled, become tools to extend the perception of the investigator, tools which provide insights and a means to recognize overlooked factors, which frequently no other method can provide. When carefully constructed and cautiously applied, they are not mere "museum pieces" or contrivances to lend credibility to ill-conceived hypotheses, as some of their detractors have charged (Watson, 1965). Johnson (1970), in his lengthy treatise on physical processes in geology, recognized experimentation with physical models, whether accurately scaled or not, as the third of four principal facets of an approach to the solution of problems in physical geology first employed by G. K. Gilbert.

> "Experimentation is useful in at least three ways: It can check predictions based upon theory; it is helpful in an investigation of processes in more complex systems than those that can be treated readily by mathematical manipulation; and it stimulates the imagination of the investigator." (p. 8)

The other three aspects of this method are: 1. thorough field analysis, 2. the formulation of thought experiments based upon sound physical principles, and 4. investigation of specific processes to unify experimental and field observations. This is the approach employed in this research.

3.3 ELECTRIC ANALOGUES

The Laplace equation, in addition to providing the basic differential equation governing the steady state flow of groundwater, also describes steady state flow of heat and electricity and certain aspects of elastic theory. The reason for the broad applicability of the Laplace equation is evident from the correspondence between it and Darcy's Law for hydraulic flow, Fourier's Law for heat conduction, Ohm's Law for current flow, Maxwell's Law for electrostatics, and Hooke's Law for elastic stress. This has prompted investigators to pursue general and specific potential field studies with convenient laboratory analogues. Adams (1875) initiated the use of electrolytic field models, and Pavlovsky (1918) first proposed the use of the electrical model as an analogue method for analysis of confined hydraulic flow in granular aquifers. Electrical analogues of fluid flow in granular media have subsequently found wide use by hydrologists, civil engineers, and petroleum engineering (Todd, 1959). These analogues are particularly applicable to situations having the boundary conditions of confined aquifers. The technique is also applicable to the study of very thin aquifers, such as the bedding planes and fracture planes (Ewers, 1972) which are the subject of this study.

The symmetry of electrical and hydraulic phenomena have been discussed by many authors (Karplus, 1958; Todd, 1959). Figure 3.5, adapted from Yalin (1971), outlines these relationships. This symmetry establishes the validity of the common practice of interchanging one for the other for the purpose of demonstration or experimentation. Thus, a correspondence exists between hydraulic gradient and voltage gradient, lines of hydraulic and electric current flow, piezometric surface contours and electrical equipotential lines.

3.3.1 POTENTIAL FIELD MAPPING

The potential field mapping required for this research was achieved by means of a liquid medium, electrical analogue, consisting of a polyster resin coated wooden trough 1.2 meters square, containing a thin but uniform layer of dilute (Ø.ØlN) copper sulfate solution as a resistance element. Similar liquid media have been employed for mapping hydraulic flow fields by Vreedenburg and Stephens (1936) and, more recently, by Bear (1964). Copper electrodes were introduced into the liquid to simulate input points or networks of low resistance input tubes and to provide for the resurgence geometry. The liquid conductive medium served as the analogue of the bedding plane. Appropriate lines of constant potential were traced with the aid of a very high impedance voltmeter (one megaohm) and a

HYDRAULIC	ELECTRICAL
Energy Height H Filtration Coefficient k	Electrical Potential V Specific Conductivity c
Filtration Velocity v Darcy's Law:	Current Density i Ohm's Law:
v=-k x grad. H	i=-c x grad. V
Laplace eqn. for energy height:	Laplace eqn. for electrical pot.
$\frac{\partial^2 H}{\partial x^2} + \frac{\partial^2 H}{\partial y^2} + \frac{\partial^2 H}{\partial z^2} = 0$	$\frac{\partial^2 V}{\partial x^2} + \frac{\partial^2 V}{\partial y^2} + \frac{\partial^2 V}{\partial z^2} = 0$
Boundary Conditions: 1. Impermeable surface	Boundary Conditions: 1. Non-conductive surface
$\frac{dH}{dn} = 0$	$\frac{dV}{dn} = 0$
where n-normal to surface 2. Equi H-surface	where n-normal to surface 2. Equi V-surface
$H = f(x,y,z) = \text{const.}$	$V = f(x,y,z) = \text{const.}$
$Q = \frac{dH}{dl} \times k$ = Flow rate	$I = \frac{dV}{dl} \times c$ = Current
where l = length	where l = length

Figure 3.5
Comparison of hydraulic and electrical flow, after Yalin (1971).

copper probe. The details of construction and the electrical schematic are show n in Figure 3.6.

Alternating current was used in these models, as is customary in experiments of this kind. The use of direct current over the period of the potential field mapping leads to deterioration of the positive electrode and the plating of a copper sludge at the negative electrode. The RMS value of the potential used in the experiments was customarily 10 volts, except in situations where excessive current flow would cause heating of the electrolyte.

3.3.2 DISCHARGE DETERMINATIONS

The liquid medium electric analogue was primarily used in this study to assess the values of hydraulic throughput for individual inputs to a hydraulically conductive bedding plane. Copper electrodes in various arrays were used to simulate hydraulic inputs and resurgences of several types. The current flow through one or more of the electrodes was measured at a standard potential of 10 volts provided by a regulated power supply. This measured current flow is the analogue of hydraulic throughput. Because the duration of electrical readings from the analogue were short, and precision DC current measuring equipment readily available and less troublesome than AC equipment, direct current was used in these models.

The current meters used in these analogues operate

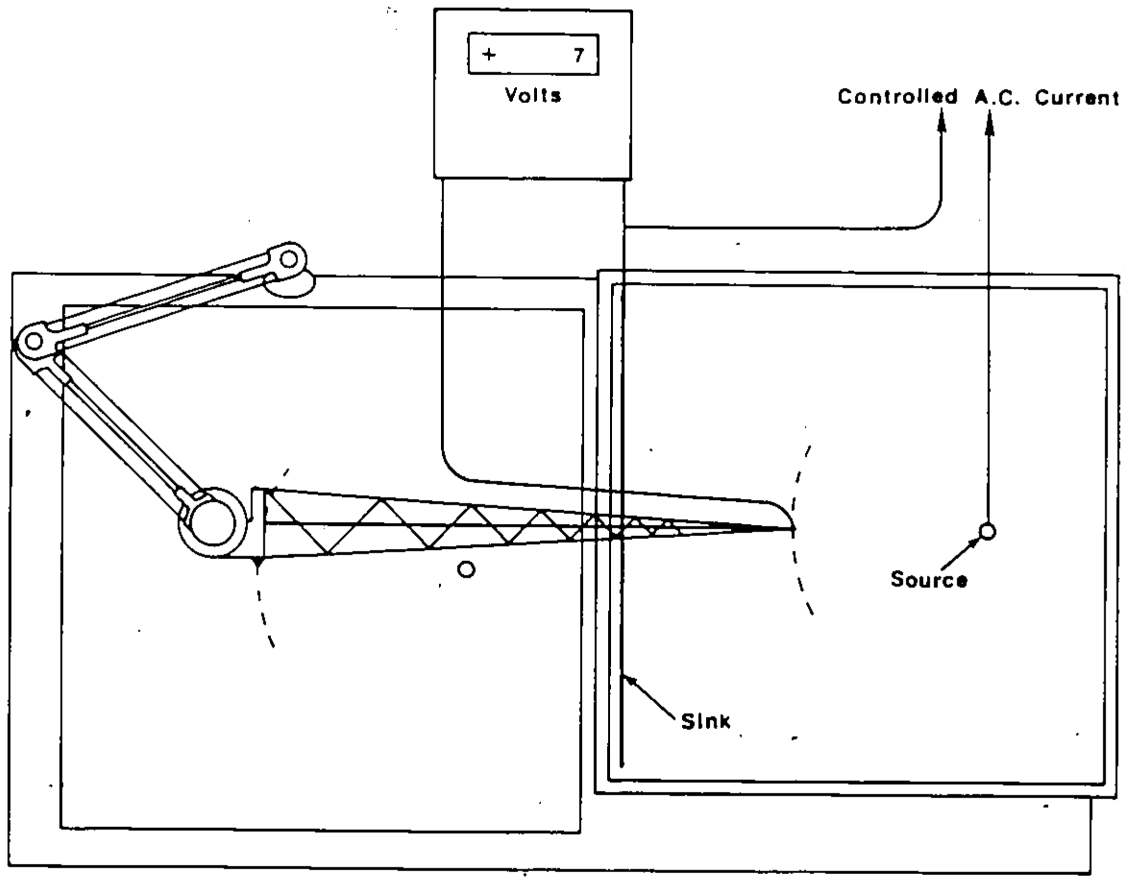

Figure 3.6
Liquid medium electric analogue for potential field mapping, constructed by the author.

by measuring the voltage drop across a fixed internal shunt resistance. They me asure the actual current flow in the meter circuit. The circuit may be considered as shown in Figure 3.7. Re, the effective resistance of the experiment medium, is a function of input position relative to the sink. The combination of the fixed meter resistance, Rm, and the variable, Re, causes a variable error in the current measurement. Re can be calculated from the measured current value, Im, the measured voltage, E, and the known value of Rm, using Ohm's Law:

$$Re = E/Im - Rm \qquad (3\text{-}6).$$

By substituting Re in the Ohm's Law equation, the actual current value (Ia) at 10 volts potential, without instrument error, can be calculated:

$$Ia = E/Re. \qquad (3\text{-}7).$$

These corrected current values were used in the data analysis.

An additional source of error derives from the introduction of the meter resistance when multiple inputs are measured. This resistance decreases the current value for the measured electrode and increases this value for the remainder of the inputs. To reduce this error, a precision resistor equivalent in value to the instrument resistance was placed in series with each electrode, except for the one being measured.

During the measurement process, the current was

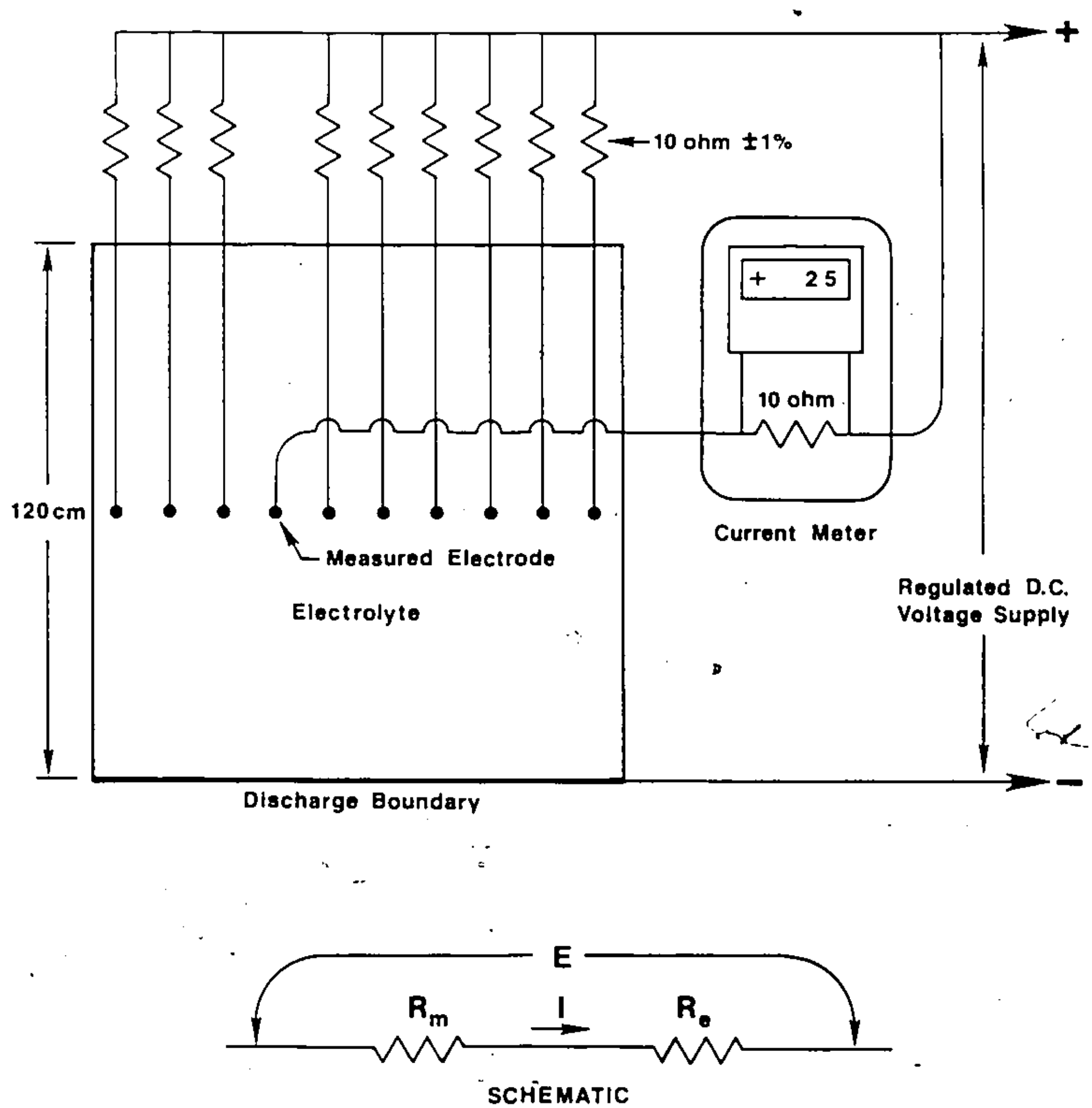

Figure 3.7
Liquid medium electric analog for discharge measurements, constructed by the author.

permitted to flow in the analogue for the shortest possible period consistent with the response time for the measuring instrument. Extended periods of measurement induce significant drift due to polarization effects (the accumulation of hydrogen and other substances at the electrode surface), and thermal drift resulting from heating of the electrolyte by passage of the current.

Care was taken to insure that the electrolyte temperature was maintained at 25 c ± 0.5 degrees. Repeated measurements of maximum and minimum values were made to further insure against drift. Electrodes were wiped clean between setups, and great care was taken to avoid contamination of electrodes with oils from all sources including fingers.

3.3.3 SCALING

No reliable values for the hydraulic transmissivity of primitive bedding plane partings and fractures in limestones are known to the author. For this reason, it is not possible to scale the discharge experiments in terms of absolute hydraulic throughput. Therefore, the geometrical relationships of the two dimensions which describe the areal extent of the bedding or fracture plane and the position of the inputs and resurgences within them are the only factors which are scaled. The model analogue of hydraulic transmissivity is the conductivity of the electrolyte which, in turn, is related to its ionic species, ionic concentration, depth, and temperature. The model analogue of the hydraulic potential is voltage. All of these model parameters are under the control of the investigator and could be scaled in such a way as to achieve a quantitative relationship between the model dependent variable, I (current flow), and absolute hydraulic throughput in the prototype, provided that the hydraulic transmissivity were known. Therefore, only relative values for hydraulic throughput dependent upon the type density and position of the inputs and resurgences were analysed.

The potential field mapping experiments do not involve estimations of the hydraulic throughput. Therefore, they do not require scaling of the conductivity. To the extent that a bedding plane or fracture possesses two dimensional, homogenous and isotropic transmissivity, the piezometric contours on the potential field maps in Chapters 4 and 8 can be regarded as the proportion of any applied head.

Dynamic similarity requires that the prototypes for all electric analogues be of such a nature that their hydraulic characteristics place them in the lower portion of the laminar regime. This zone is defined by values of the Reynolds number below about 4 (Lindquist, 1935). For Reynolds numbers above this value, there is increasing departure from the linear relationship between hydraulic throughput, hydrostatic pressure, and transmissivity. Weyl (1958) showed that, for any realistic assumptions regarding their porosity, bedding planes should exhibit flow which obeys the Darcy relationship.

3.4 FLOW ENVELOPE EXPERIMENTS

3.4.1 DESCRIPTION

These experiments were undertaken to delineate the flow domains associated with the individual inputs of a multi-input flow system contained within a single bedding plane. The experiments were conducted in an apparatus adapted from conventional hydraulic filtration models (Yalin, 1971, Chapter 4; Bear, 1972, Chapter 11). The bedding plane, assumed as before to be equivalent to a very thin porous medium, was represented in the models by a tabular body of sand 60 by 60 by 0.5 cm. The sand medium was enclosed in a rigid water-tight container of transparent acrylic plastic, fitted with orifices for the conduction of water (Fig. 3.8). The flow domains were rendered visible by the use of dye. A fully saturated, uniform packing, with hydraulically homogenous and isotropic characteristics is necessary for experiments of this type. To insure isotropy, the sand was sieved to correspond to a Wentworth medium sand, 0.5-0.25mm, and then thoroughly mixed. This procedure reduced the tendency for grain sorting by size while the container was being filled.

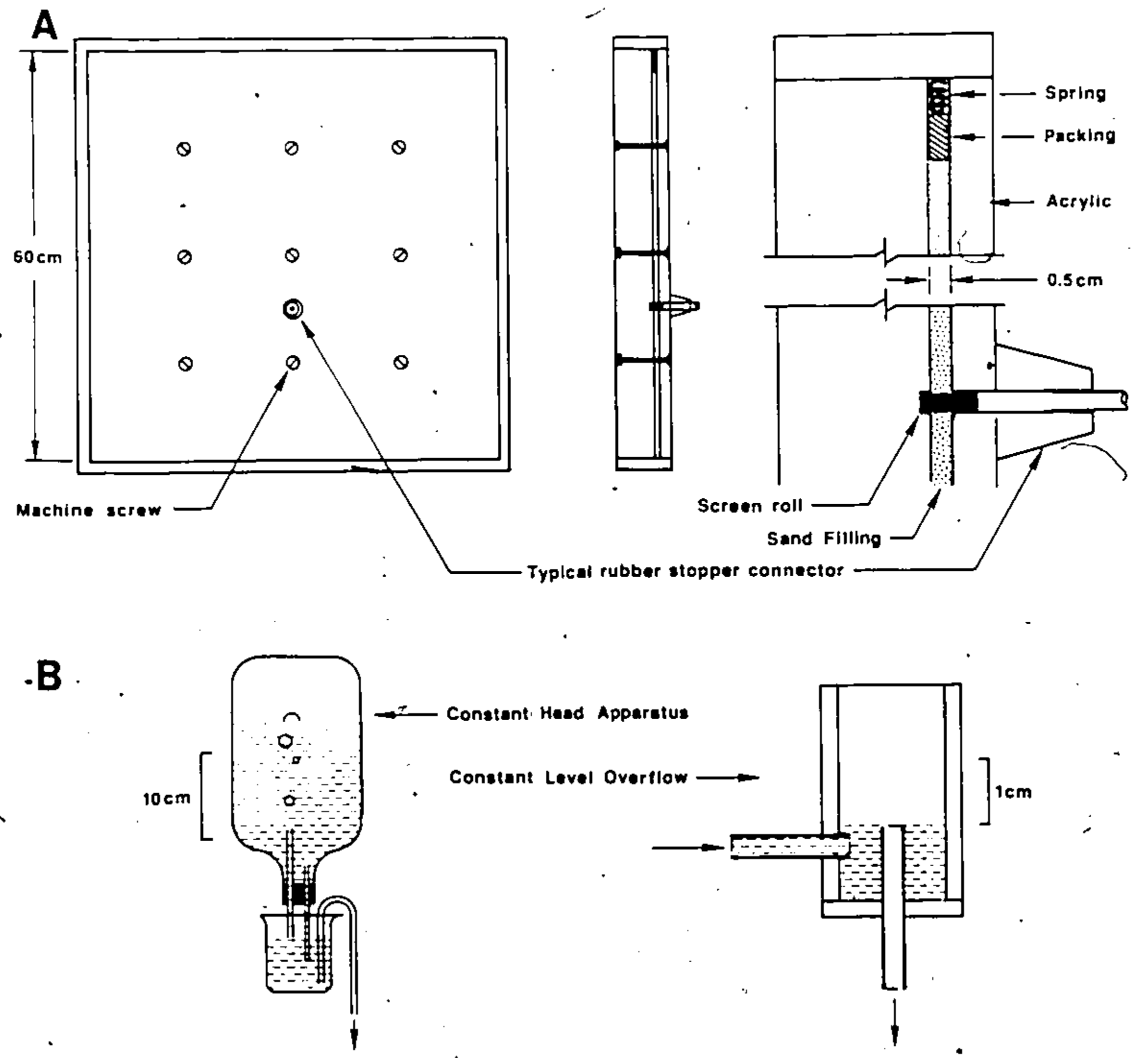

Figure 3.8
Filtration model for determination of flow envelopes, constructed by the author.

To insure optimal packing, the container was vibrated during filling. T o avoid entrapped air and achieve full saturation, the container was given a partial filling of water into which the sand was poured, while maintaining a depth of a few centimeters of water above the sand already in place. Recently distilled water was used in the experiments to avoid introducing air bubbles into the medium. Before sealing the container, a spring loaded packing was placed in the open end to insure that the optimum packing would be preserved when hydraulic pressure was applied to the medium during the experiments.

Water containing appropriate dyes was admitted to the apparatus through a constant head apparatus (Fig. 3.8a). The headloss between the inputs and outputs was controlled by a constant level overflow device (Fig. 3.8b).

3.4.2 SCALE

Because this apparatus takes the form of a reduced scale representation of a natural flow domain, both involving hydraulic flow through porous media, it is unnessary to demonstrate an analogy between the model and prototype. The geometrical scale of the models was adjusted to conform to the electric analogue models, which they directly augment. The scaling of these models is greatly simplified by the nature of the experiments performed with them. They are designed to show the region through which a particular input would discharge to a specific output geometry in the absence of diffusion. No rate data were taken, therefore, scaling of the particle size was unnecessary. The prototypes are assumed to operate within the region of Darcy flow, and the models have been shown by experiment to obey the linear Darcy relationship in the range of head differentials used in the experiments. Thus, we may assume the scaling to be appropriate.

3.5 LABORATORY SOLUTION MODELS

Seven types of solution experiments, related to seven types of boundary conditions, were carried out on blocks prepared from reagent grade plaster of Paris. The substance of these blocks is hereinafter referred to as plaster, in thre sense of the doubly hydrated form of Calcium sulfate. The purpose of the experiments was to simulate groundwater solution activity on a limestone bedding plane and, by so doing, to elucidate the factors which govern the geometrical properties of solution tube networks. More specifically, they show the response of the solution process to the continuous changes of the pressure field which are produced by that process. This was accomplished by creating a parting of known transmissivity between the soluble plaster block and a transparent lower boundary. This scheme provided a means for continuous observation of changes in the soluble medium produced by the circulation of the solvent. Similar experiments have been reported by Ewers (1964, 1966, 1972, 1974, 1976, 1977) and by Waterman (1975).

The requirements for the experiment medium are fairly stringent. First, it must possess sufficient solubility that with readily available solvents, solution features may be generated in reasonable time periods. With a diffusion constant of Ø.78 x 1Ø-3/cm2 sec-1 and a saturation value of 2.4 gm/l at 25 degrees C., plaster fills this requirement well.

Second, it must have a bulk permeability sufficiently low that the solvent will primarily follow the simulated bedding planes. Plaster blocks prepared by the method described below, prove sufficient in this regard.

Third, the medium must be isotropic with respect to solubility characteristics. The fine grain structure of plaster and the ability to produce a block from a single, well homogenized, pour assures that the individual blocks will possess isotropic solubility. The ability to prepare all of the blocks for a series of experiments, by standard methods, from a single batch of reagent grade plaster, low in insoluble residue, also assures uniform solubility characteristics from one experiment to the next.

Fourth, the soluble medium must be prepared with reaction surfaces of predetermined and reproducible hydraulic characteristics. Further, they must be produced readily in sizes appropriate to the experiments. These final requirements are especially well filled by plaster. It can be molded to quite large size without fracturing on curing. It is capable, because of its fine crystal structure, of retaining very detailed textures from molds.

3.5.1 MOLD PREPARATION

In order to establish a parting of appropriate transmissivity, a surface of known and replicable roughness and random characteristics must be imparted to the plaster. A positive impression surface was prepared by cementing a sheet of 100 grit abrasive paper 28.5cm x 41cm to a flat wood substrate of larger dimensions. The abrasive paper was evenly and repeatedly coated with a small quantity of catalized polyester resin. This had the effect of eliminating undercuts beneath the abrasive grains (Fig. 3.9a), securely adhering them to the paper, and waterproofing the paper for production of the mold. A smooth polyester resin surface was prepared adjacent to the abrasive surface for the purpose of effecting a hydraulic seal at the perimeter of the high transmissivity surface (Fig. 3.9b). Great care was taken to achieve a smooth transition between these rough and smooth surfaces to insure that this boundary did not contain a region of increased transmissivity. Such a region could affect the potential field in the simulated bedding plane. This preparation was

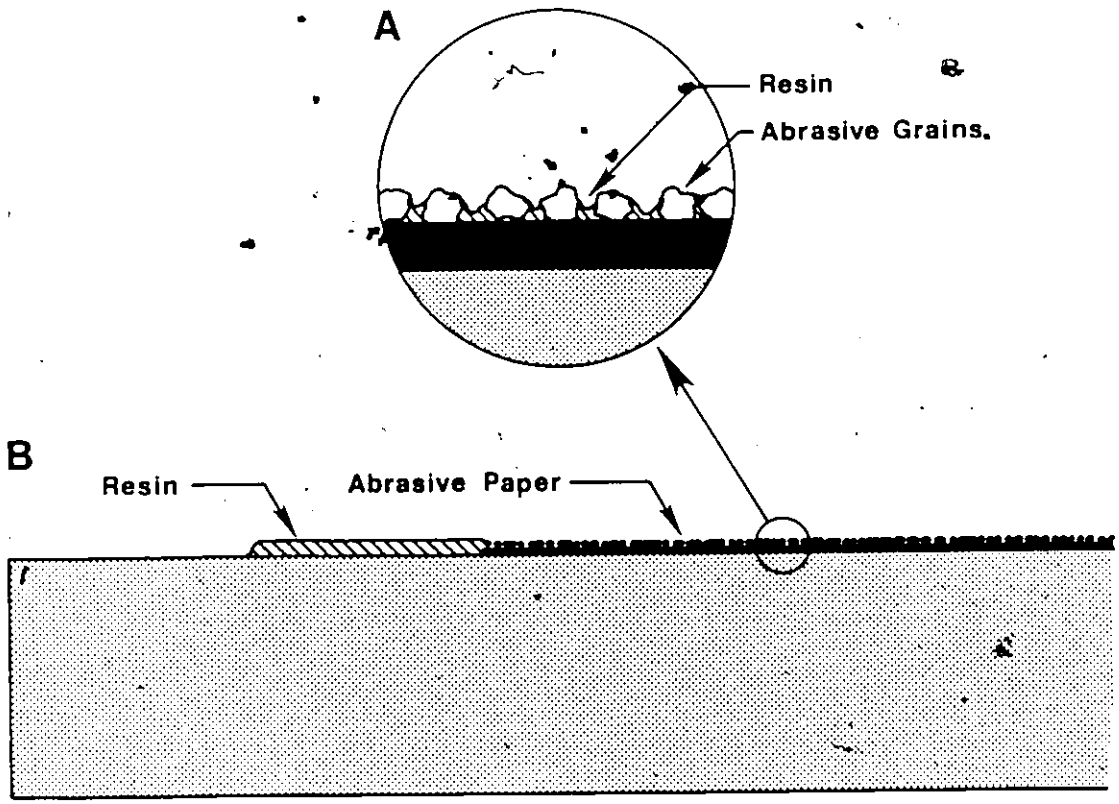

Figure 3.9
Cross-section of prepared surface for the construction of rubber molds used in the casting of solution experiment blocks.

designated surface "A" (Fig. 3.10).

A second surface was prepared with low transmissivity regions distributed by means of random numbers. The regions were produced by depositing drops of thinned and catalized polyester resin of known volumes on the Type A impression surface. Three drop volumes were used; their frequency of occurrence was inversely and geometrically related to their size. This preparation was designated surface "B" (Fig. 3.11).

The mold was prepared by applying several layers of latex mold compound to the impression surface. Before the final coats were applied, a sheet of 1 mm mesh fiberglass screen cloth was incorporated into the mold for dimensional stability.

3.5.2 PLASTER BLOCK PREPARATION

3.5.2.1 Casting

The reagent grade plaster was mixed with water in a ratio of 1:0.814 and placed briefly under a vacuum to remove air bubbles, insuring a uniformly void free cast. The liquid plaster was scraped across the moistened mold with a rubber blade to insure that its texture would be accurately reproduced. The filled mold was then vibrated to release any bubbles produced in the pouring process. During this procedure, the mold was held flat against a leveled vacuum board.

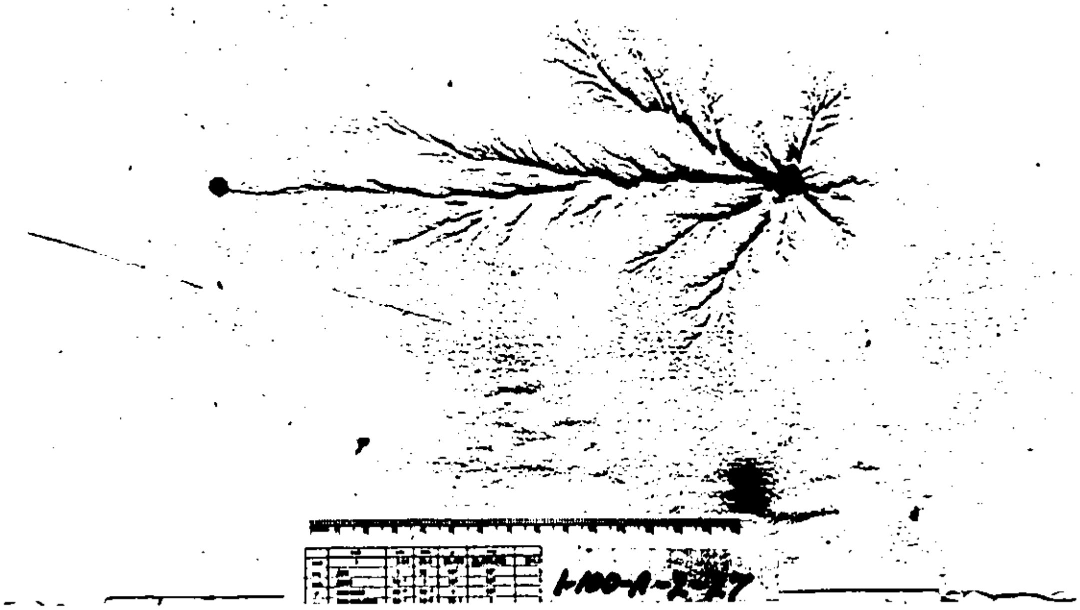

Figure 3.1∅

Type A surface on a plaster block after completion of a solution experiment.

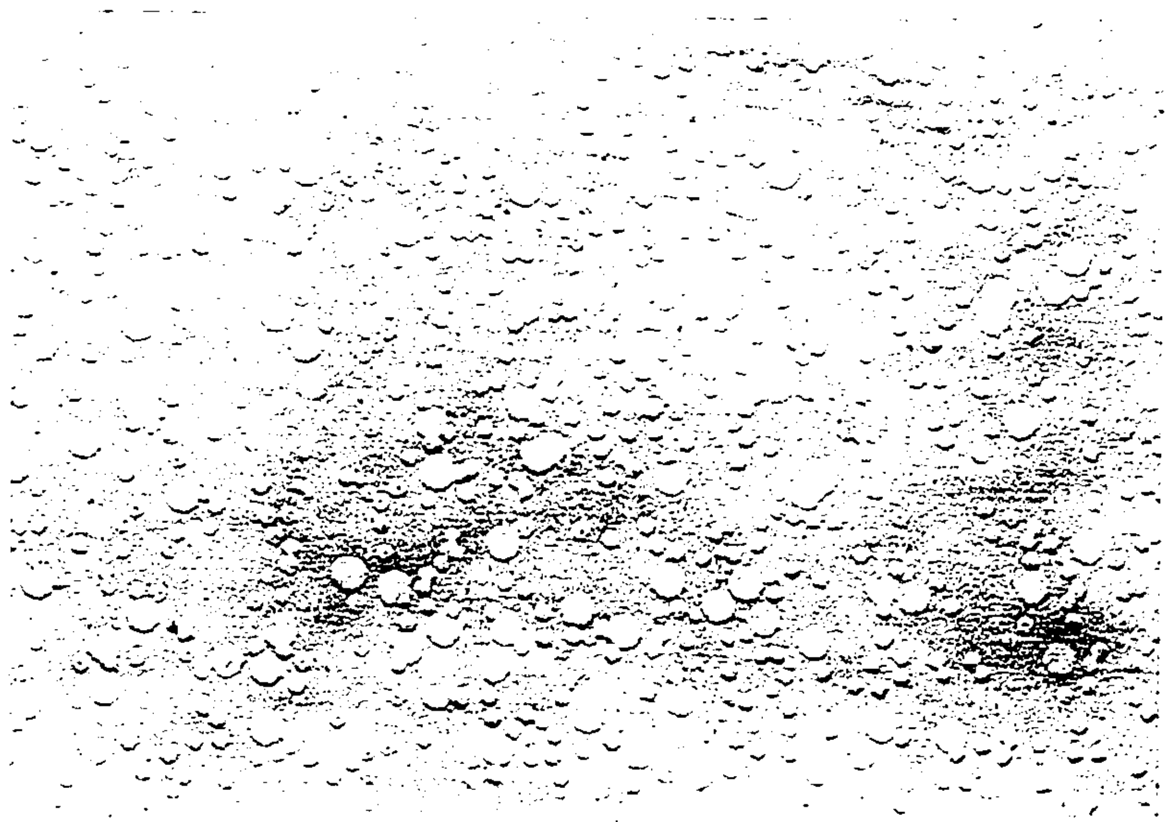

Figure 3.11
Type B surface on a plaster block ready for use in a solution experiment [Note the large, randomly distributed, low permeability zones].

Following a 12 hour period of curing, the plaster block was removed from the mold and oven dried at 65 C, well below the temperature of 128 C at which cured plaster, doubly hydrated calcium sulfate, converts to the half hydrate. Following insertion of input and output connections appropriate to the experiment, the thoroughly dried blocks were impregnated and sealed with hot paraffin on five sides.

Early experiments showed a tendency for air bubbles to accumulate on the reaction surface, and at times, this accumulation was so great as to completely block the flow of the solvent. The air bubbles had two sources, dissolved air in the solvent solution and air trapped in the plaster. The first source was eliminated through the use of distilled water. The second was virtually eliminated through the use of a specially prepared vacuum chamber. With this device, the blocks could be evacuated to a pressure of 2 cm-Hg and simultaneously immersed in a saturated calcium sulfate solution. This proved to be the only reliable means of saturating the blocks.

Once saturated, a block was transferred to the apparatus where the experiment was conducted. Here, it was submerged in a saturated calcium sulfate solution, and its edges sealed to a water filled vinyl plastic pillow with vacuum grease (Fig. 3.12). The upper surface of the pillow formed the lower boundary of the simulated bedding plane void, and because of its pliablility, the vinyl conformed uniformly to the reaction surface of the block. The turgidity of the pillow was held constant by pressurization at 65cm from an attached water reservoir.

During the course of an experiment, distilled water containing dyes was delivered to the input by a metering pump through a constant head overflow device (Fig. 3.12). The fresh water displaced the initial filling of saturated water through the outlet opening. From that point, the discharge was aspirated to a collection vessel for quantitative and qualitative measurement. The progress of the experiment was monitored visually and with still and time lapse photography through the transparent pillow and its glass support.

3.5.2.2 Special Precautions

Several early experiments were unsuccessful due to the growth of slime bacteria along the reaction surface. This type of failure was characterized by a sudden drop in hydraulic throughput to near zero. Upon disassembly, the reaction surface was seen to be covered with a gelatinous layer. Subsequently, all solutions which came in contact with the plaster after the casting process contained 0.5 percent of 40 percent formaldehyde solution. This precaution appeared to be completely successful.

The vinyl plastic in contact with the reaction

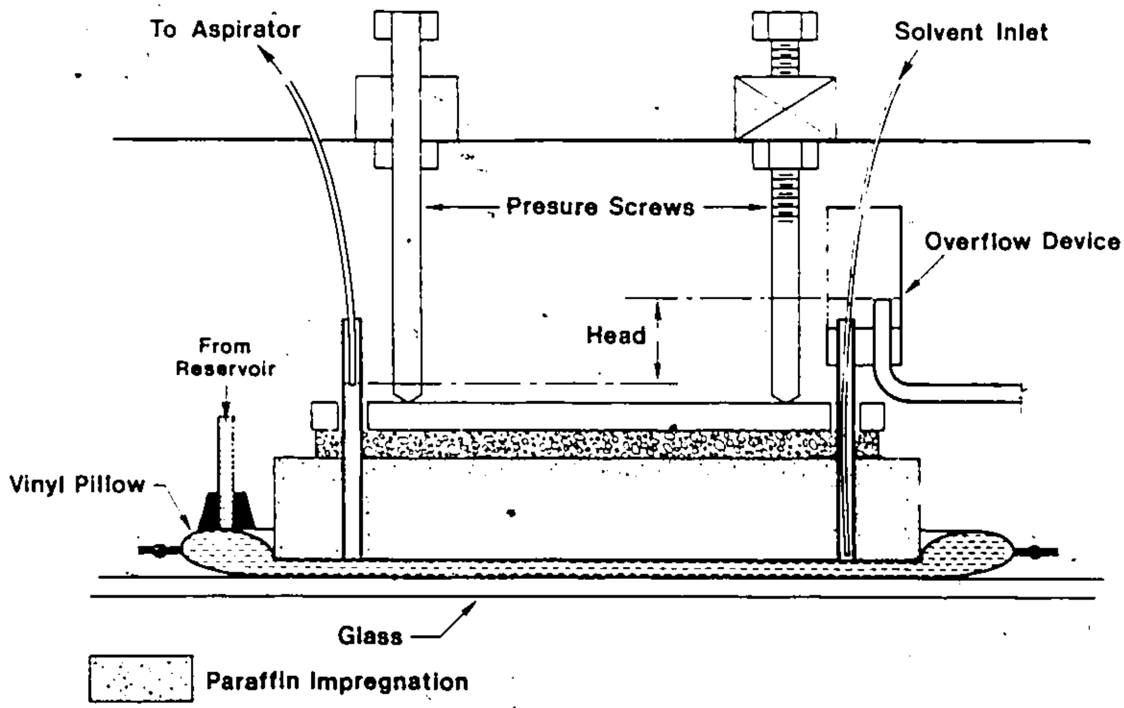

Figure 3.12
Cross-section of apparatus for conducting solution experiments.

surface of the plaster tended to retain an imprint of the characteristics of tha t surface, including the solution features. This imprint, if not removed, could affect the shape of solution features in subsequent experiments. By raising the temperature of the vinyl and the water filling to 7Ø C for several minutes, the imprint could be visibly erased and showed no tendency to return.

3.5.3 SCALE

To fully compare these experiments to their natural bedding plane parting prototypes, it would be necessary to scale them in the following ways. First, the gross geometry must be scaled in terms of the parting length and breadth with its associated boundaries. The location of the inputs and resurgences must also be scaled in these two dimensions. For the generalized cases with which this research deals, this is a fairly simple matter. Of greater difficulty is the geometrical scaling in the vertical dimension. It involves the vertical dimension of the hydraulic driving potential at the input relative to the output (headloss) and the vertical dimension of the parting itself. The headloss determines, with the other geometrical characteristics, the distribution of fluid potential throughout the parting. For all non-zero headloss values, however, a relative fluid potential distribution can be determined on the basis of the other geometrical properties alone. This was discussed earlier in the treatment of electrical analogues. The vertical dimension of the parting determines the flow rates, given the headloss and the area dimensions of the parting. For the reasons stated earlier in this chapter, the prototype dimensions of the parting are unknown and, therefore, the scaling of this element of the models is not presently possible. Scaling of the headloss is possible, of course, but it is of questionable importance lacking the parting values.

The time relationship between the model and prototype is influenced by the relative solubilities, the relative solution rates, and the relative flow rates between the model and prototype. The solubilities in both cases are well known, and the solution kinetics are probably known to an order of magnitude. However, in the absence of prototype flow rates, an assessment of the time scale is beyond our grasp.

Of much greater practical importance than the time scale is the geometry of the solution features, the principal object of this research. These features are governed by a special scale consideration, the relative relaxation lengths. If this dimension is greater than the entire flow path through the soluble medium by an order of magnitude or more, then the growth of primitive tubes would progress essentially equally along their entire length. If, on the other hand, the relaxation length is several orders of magnitude smaller than the total flow path, the growth of primitive tubes will be initially confined to the region surrounding the input. This has two important implications for the geometry of the developing tube network.

1. In the first case, a large number of primitive voids over much of the surface of the parting link the input and output from the onset of solvent flow. Each enlarges almost uniformly over its entire length. Curl (1974) concludes that such conduits would be covergently competitive, which is to say that initial differences in diameter would be lost as solution enlargement proceeds. The rate of convergence would be dependent on conduit length and proceeds most rapidly in the laminar regime. The end result (Fig. 3.13a) would be a large number of subparallel tubes following very closely the initial flow vectors. The gradual enlargement of the tubes produces a concomitant lowering of the hydraulic potential at the input as their combined carrying capacity approaches the solvent supply.

In the second case, the primitive voids enlarge as tapered tubes because of the rapidly diminished dissolution efficiency. A small number of tubes, as few as one, achieve a low resistance connection to the output (Fig. 3.13b). In contrast to the first case, these few favored tubes are responsible for diminished head at the input. This head loss is likely to be abrupt because of the existence, prior to breakthrough, of a large low resistance solution tube in

Figure 3.13
Enlargement of solution conduits under conditions where relaxation length of the dissolution process is long [A] and short [B], relative to the total flow path.

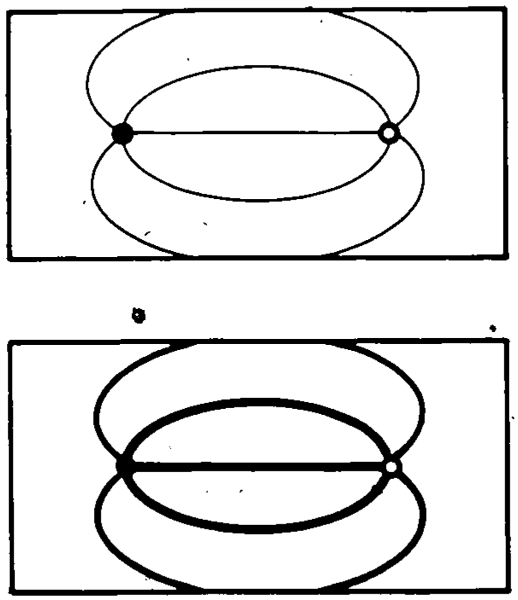

A

Case 1
Uniform Enlargement

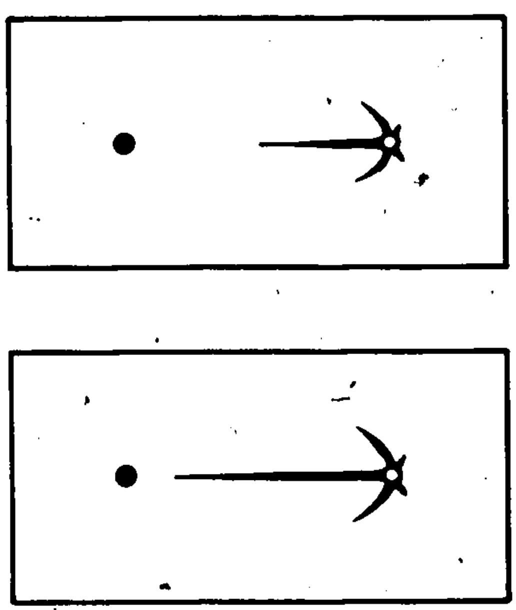

B

Case 2
Non–uniform Enlargement

series with a small high resistance element of virgin parting. The end result will be a large number of tubes incompletely linked to the output and one or a small number of tubes competent to conduct the available solvent supply. The conditions of reduced head and disparate size may prolong the time to convergence between the diameters of the incomplete tubes and the larger ones to very great periods.

2. The pressure fields in the two cases evolve differently. In the first case, changes in the gross pressure field are very slight. The head for any point (hp) along a conduit in the lower region of the laminar regime can be calculated from the following relationship, derived from electrical series resistance formulae:

$$hp = ht \times Rp/ Rt \quad (3\text{-}8)$$

where ht is the total head loss across the tube, Rp is the tube resistance between point p and the input, and Rt equals the total pipe resistance.

From this relationship, it can be seen that the headloss along tubes A and B (Fig. 3.13a) is continuous and similar (ie. 50% at the midpoint, 75% at a point 0.75% of the distance from the input, etc.). Figure 3.14a shows that no matter what changes in diameter occur, the piezometric slope along the tube length will be constant. This is true so long as the diameter changes are equal over the length of an individual tube and the input head relative to the

Figure 3.14
Gradients for the flow paths in Figure 3.13.

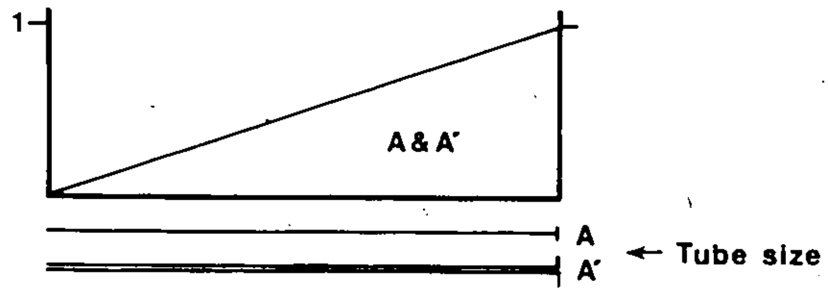
1
A & A'
A
A'
Tube size

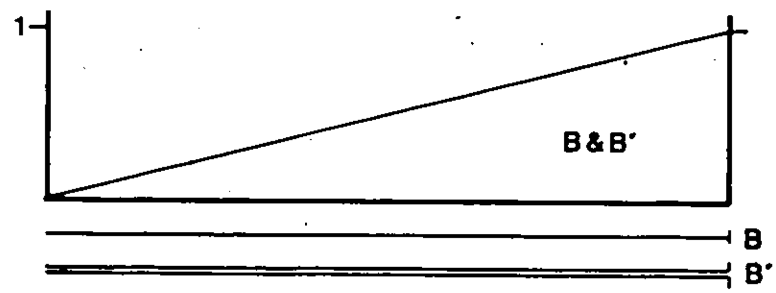
1
B & B'
B
B'

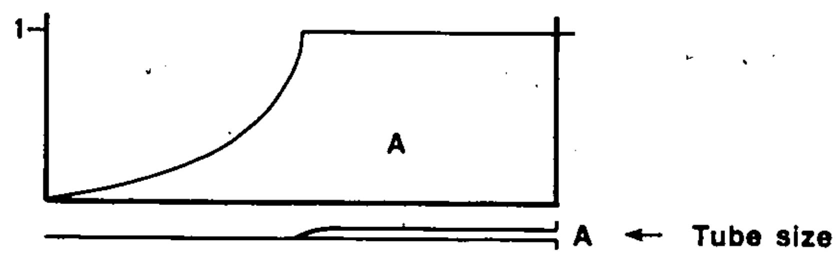
1
A
A
Tube size

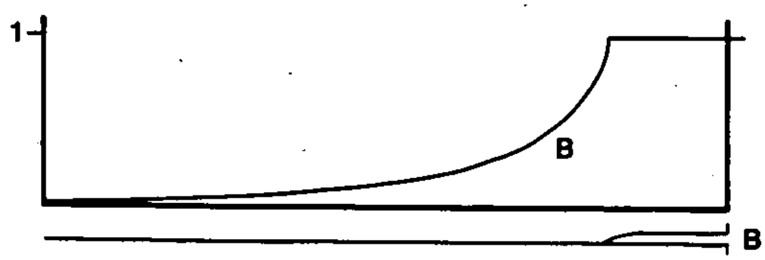
1
B
B

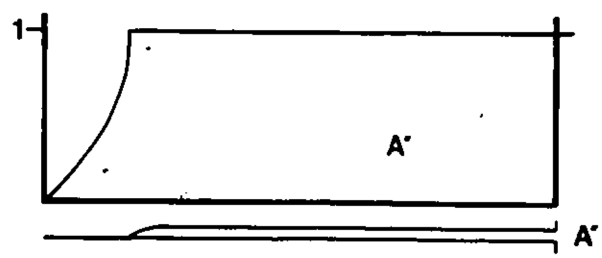
1
A'
A'

discharge point remains constant. Different diametrical growth rates in separat e tubes will, therefore, not affect the pressure field.

In the second case, the pressure field undergoes considerable change. The tapered tube section (Fig. 3.14b) represents a low resistance element in series with the virgin bedding plane, a high resistance element. The pressure loss in such a system is confined primarily to the region of the unaltered parting. This produces a considerable distortion of the pressure field (Fig. 3.15) and is responsible for the divergent length competition between parallel tubes observed in earlier experiments (Ewers, 1972, 1974, 1976). Using Weyl's diffusion limited formula (2-16),

$$L = 0.304\ vd^{2}/D \qquad (3\text{-}9)$$

and values for a typical experiment (1-100-A-2-27) at a distance of 2 cm from the input:

$$L = 0.304 \times 0.663 \times 0.02^{2} / 0.78 \times 10^{-3} \qquad (3\text{-}10)$$

the value for the penetration distance to 90% saturation (lp) is

$$L = 0.103\ \text{cm}. \qquad (3\text{-}11)$$

Given the shortest input to output distance of 20 cm, the penetration distance is two to three orders of magnitude shorter. This value is in agreement with the prototype values assumed by White (1977). He suggested typical flow

Figure 3.15
Pressure fields surrounding the conduits in Figure 3.13.

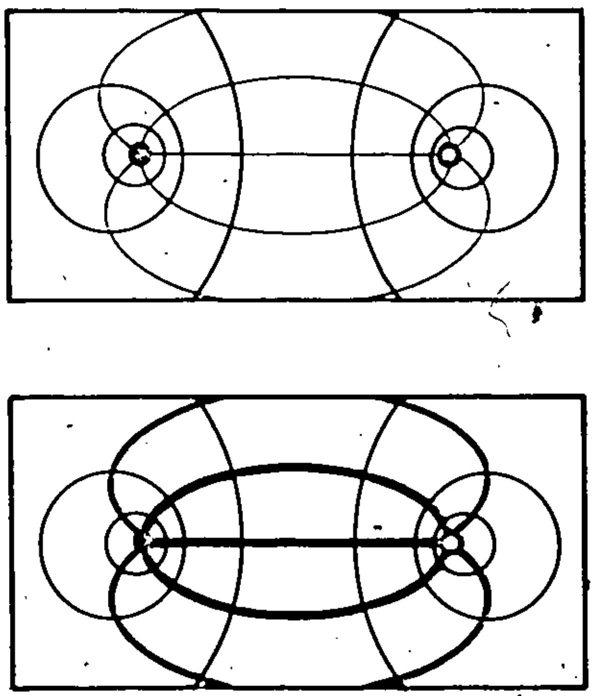

A

Case 1

Uniform Enlargement

No Pressure Field Change

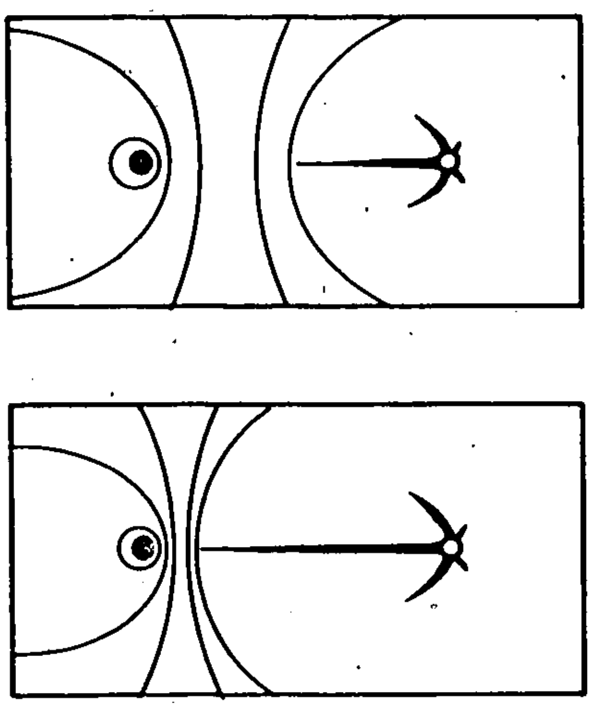

B

Case 2

Non–uniform Enlargement

Great Pressure Field Change

path distance of one kilometer and 9Ø% saturation within one to ten meters. Thi s places the differences in these values at two to three orders of magnitude. This also places the model and prototype in the conditions of Case 2 above.

Kinematic similarity requires that the solution models exhibit Reynolds numbers in the range of validity of the Darcy relationship, in order to be consistent with the prototypes and the electric analogue and flow envelope models. As previously stated, the upper limits for Darcy flow is about NR = 4. A typical solution experiment has a NR value of two or less.

These scale considerations are far from ideal, and many practical quantitative questions could be addressed with improved knowledge of these factors. However, important ordinal and ratio statements can be made with the scaling that is presently possible, using the similarity of process approach.

Provided that extrapolations from the models to nature are not too rigidly made and that such comparisons are largely of a qualitative geometrical nature, solution experiments of this type provide valuable insights into phenomena which are otherwise inaccessible to study.

CHAPTER 4

THE NETWORK GROWTH MODEL

4.1 INTRODUCTION

A series of laboratory solution experiments in a salt medium, conducted by the author, produced tube networks in simulated bedding planes which closely resemble natural networks found in carbonate rocks (Ewers, 1972). The growth of the laboratory networks has been studied by direct observation and by flow field analysis using electrical analogue techniques. The solution experiments and the electric analogues were similar to those described in Chapter 3. These experiments and the conceptual model derived from them form the foundation upon which the present work is based.

4.2 THE MODEL ASSUMPTIONS

The model derived from these experiments and from field observations assumes that a bedding plane functions as a thin, tabular, resistance element containing a great number of randomly spaced high and low resistance regions of sedimentological and diagenetic origin. The size of these regions ranges through several orders of magnitude, both larger and smaller than the cross-section of tubes of explorable dimension. It further assumes that solvents entering such a plane become saturated after moving a distance one to several orders of magnitude shorter than the length of a typical tube of explorable dimensions, except where the dissolving process has already produced large openings.

4.3 THE MODEL DESCRIPTION

The model is comprised of two discrete phases. The first describes a means by which solution-induced macroporosity may be initiated along bedding planes by through-flowing groundwater under laminar flow conditions. The second phase is one of selective enlargement of the network in a mixed laminar and turbulent flow regime. The model is here described in terms of the laboratory experiments.

4.3.1 PHASE I

4.3.1.1 Channelization Of The Flow

A pressure head of unsaturated water was applied at a point to a water-filled simulated bedding plane having the characteristics assumed above. The pressure field thus established bore the relationship to the discharge region and other boundary conditions depicted in Figure 4.1a. The pressure head induced solvent flow within the bedding plane,

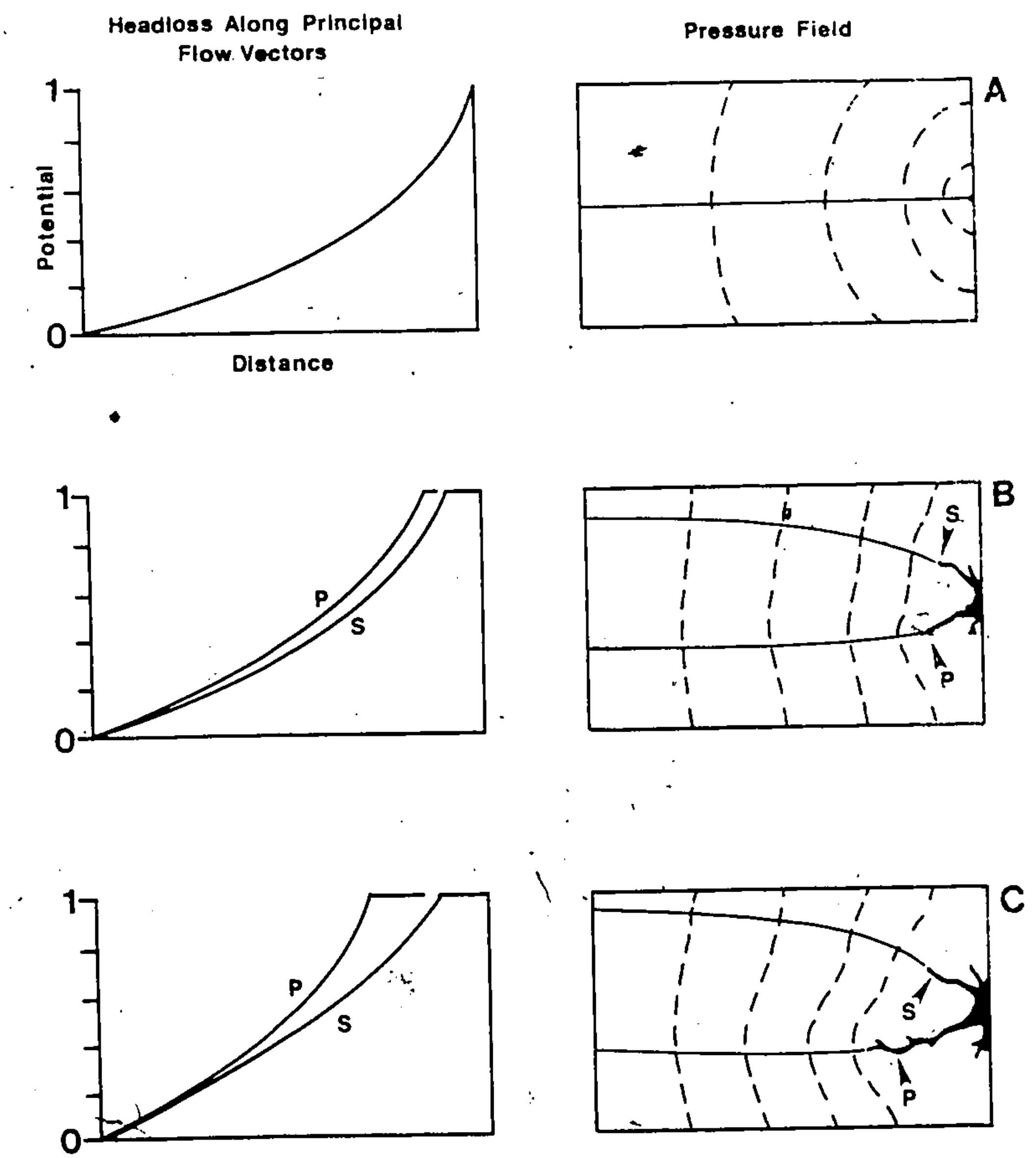

Figure 4.1
Flow conditions surrounding developing principal [P] and secondary [S] tubes in a solution experiment.

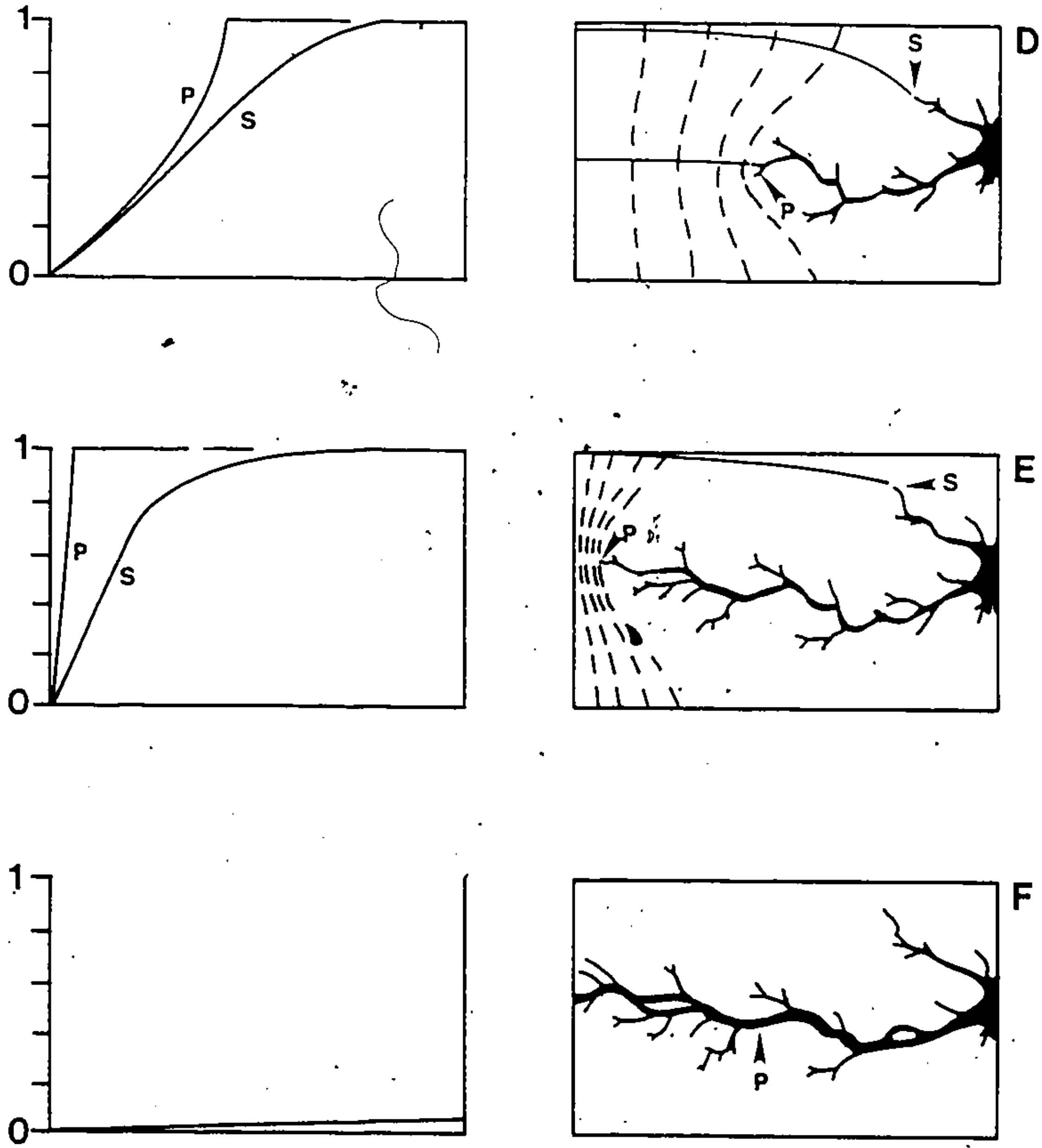
1
0
P
S
D
1
0
P
S
E
1
0
F
P

which quickly became channelled into a set of radial distributary tubes by the inhomogeneities of the bedding surface and the solvent action of the through-flowing water (Fig. 4.2a). The regions of higher permeability quickly developed larger openings due to their higher flow rates, which extended the penetration distance of the solvent before saturation occurred. Undersaturated waters could thus be delivered by these higher permeability zones to similar low resistance areas further downstream. The length and diameter of these early tubes were in direct relation to the piezometric slope along their discharge vectors. Continuous repetition of this process maintained channelized flow at all times during the experiments.

The solvent moving along the virgin parting a short distance beyond the tube extremities was assumed, for all practical purposes, to be saturated, since no detectable solution occurred there. These brines were conducted to the output by the parting, where they emerged as a measurably saturated solution.

4.3.1.2 The Principal Tube

After the initial channelization had occurred in the laboratory experiments, the tube leading by the shortest available path in the direction of discharge grew most rapidly and at a slowly increasing rate (Fig. 4.2b). Such a path leads in the direction of steepest piezometric slope,

Figure 4.2
Photographs of successive stages in the solution experiment shown in Figure 4.1.

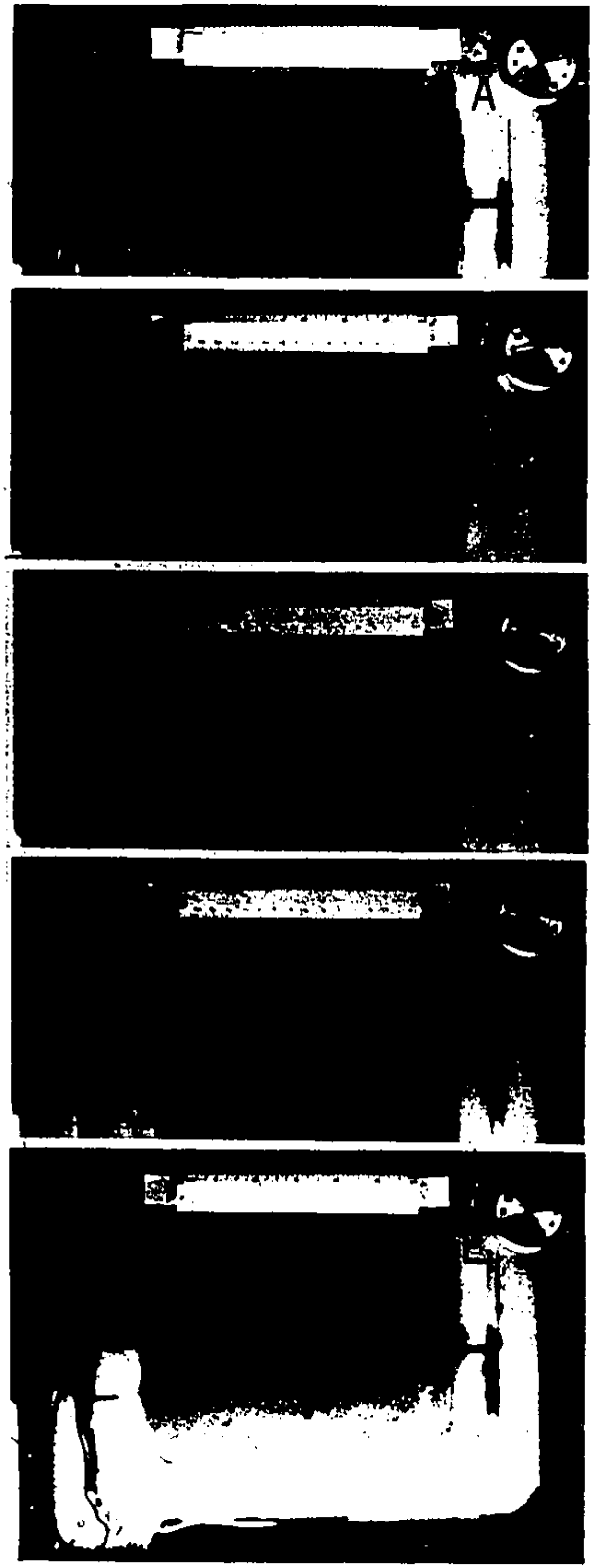
A

as shown by electric analogue (Fig. 4.1b). This path is seldom a straight course because of the irregular distribution of permeability within the plane. Darcy's Law predicts that the greatest solvent flow follows this course. The increasing rate of elongation which this tube exhibits is due to two factors related to the length change. First, its increasing length reduces the resistance of the entire flow path from input to resurgence because the proportion of virgin parting becomes progressively less. Second, the tube's increasing length steepens the piezometric gradient in the virgin parting. Both of these factors increase the flow rate along this vector, which increases the rate of propogation of this tube. The succession of piezometric gradients in Figure 4.1 show this phenomenon. For the purpose of this discussion, the tube following this course will be called the principal tube.

4.3.1.3 Secondary Tubes

The remaining or secondary tubes (Fig. 4.2b) show lower initial rates of development due to their longer or more impeded discharge routes and proportionally higher discharge resistance. The growth of the principal tube distorts the flow field in such a way as to decrease the gradient and increase the flow path length of the secondary tubes. The flow field distortion is due to the contrast in potential loss across the parting compared to the potential loss across the principal tube. The potential loss in these elements can be evaluated in the following way:

1. The mean flow velocity in the parting is given by,

$$v = d^2 \, Dh/12u\,L \qquad (4\text{-}1)$$

where d is the parting thickness, u is the dynamic viscosity of water, Dh is the headloss across the element, and L is the element length (Lamb, 1945, p.581). Substituting a value of 0.01cm. for the width of the bedding plane parting would hardly underestimate its size. Substituting values of 10E3 cm. for Dh, and 10E4 cm. for L, yield a gradient of 0.1. This would be in the upper range of values commonly quoted for karst regions (Ford, 1971; Thrailkill, 1968). Therefore,

$$v = 0.01^2 \times 10^3 / 12 \times 0.01 \times 10^4 = 8.33 \times 10^{-5} \text{ cm/sec.} \qquad (4\text{-}2)$$

2. The quantity of flow in the fracture is given by,

$$Q = d\,w\,v, \qquad (4\text{-}3)$$

where w is the width of the parting. Using an arbitrary value of 10E3 cm.,

$$Q = 0.01 \times 10^3 \times 8.33 \times 10^{-5} = 8.33 \times 10^{-4} \text{ cm}^3\text{/sec.} \qquad (4\text{-}4)$$

3. The velocity of flow in a tube of radius, r, is expressed by:

$$v = r^2 \, Dh/8u\,L \qquad (4\text{-}5)$$

(Lamb, 1945, p. 585). Multiplying by the area yields the expression for quantity of flow:

$$Q = pi\ r^4\ Dh/8u\ L \qquad (4\text{-}6)$$

Solving for Dh yields:

$$Dh = 8u\ L\ Q/pi\ r^4. \qquad (4\text{-}7)$$

Assuming that the fracture, analized above, is supplied by a tube of 1 cm diameter, 1ØE4 cm. long (Fig. 4.3a),

$$Dh = (8x0.01x10^4 x8.3x10^{-4})/(3.14159x0.5^4)$$

$$= 3.395\ cm. \qquad (4\text{-}8)$$

Thus, the pressure loss across the tube is very small, on the order of Ø.3 percent, in spite of the conservatively chosen parameters of the analysis. A decrease in the gradient or the fracture width from the high values used would decrease the amount of head loss in the tube section. Therefore, nearly the entire input pressure is delivered to the tube network extremities, providing the pressure distribution changes to effect the gradient along the discharge path of the secondaries. As a result of this reduced gradient and concomitant reduced discharge capability, the growth rate of these tubes is reduced. Each increment of growth of the principal tube, including its subsidiary branches, further reduces the discharge potential of the secondary tubes, leading eventually to their stagnation (Fig. 4.2).

Subsidiary branches which occur along the principal tube take on the character of secondary tubes, and by the process outlined above, they too eventually stagnate.

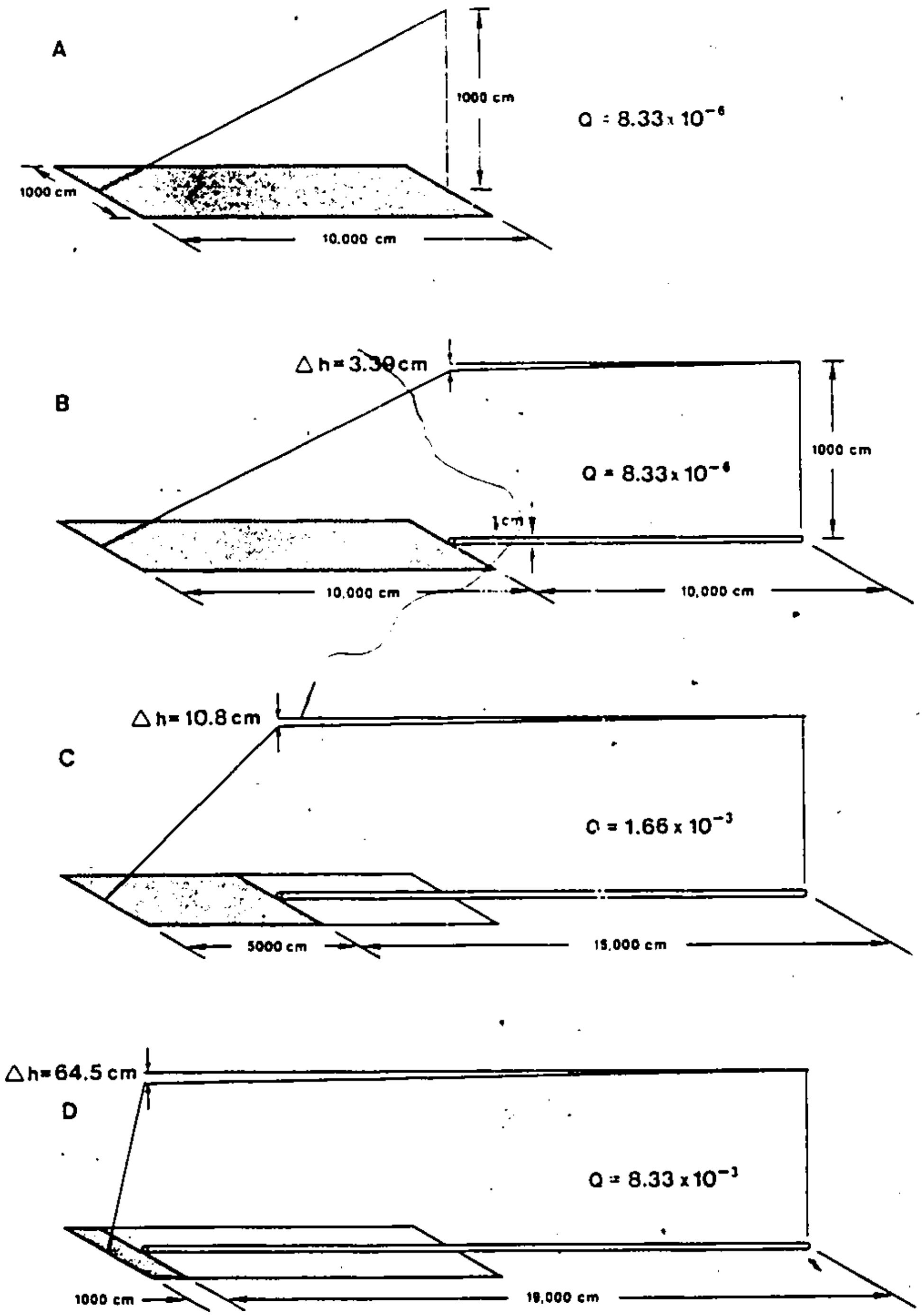

Figure 4.3
Pressure loss across a bedding plane, compared to a solution tube in series with it. The flow of the tube is considered to be applied to the full width of the bedding plane.

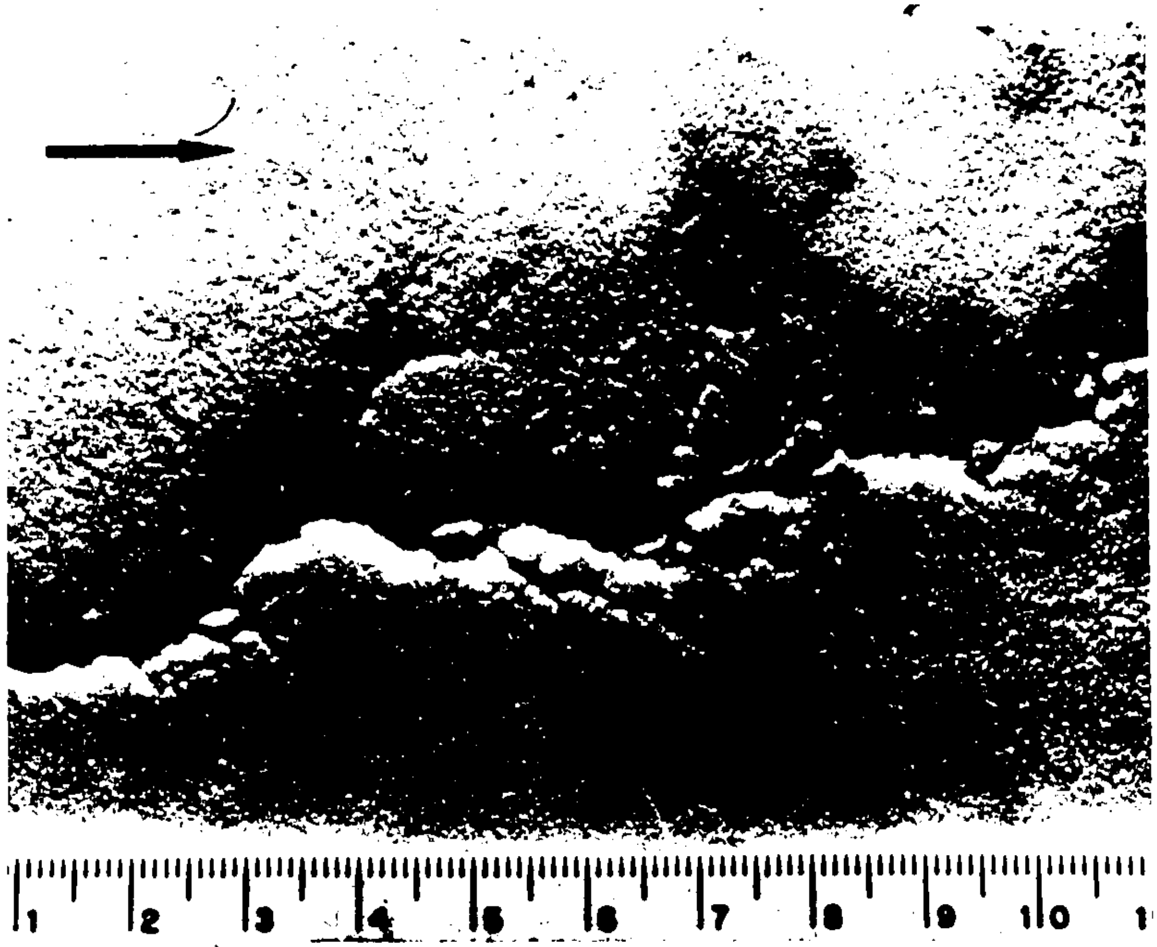

Figure 4.4
A network of tubes produced in laboratory solution experiments, from Ewers (1972). [scale in cm]

Interconnections between the inactive secondary tubes which provide paths parallel to the principal path may enlarge however, as their role shifts from one of lateral development of the network to one of parallel supply routes for the developing frontiers of the network downstream (Fig. 4.2e). This change in function modifies the dendritic aspects of the network and increases its anastomose character. The enlargement of the principal tube, and the tubes parallel to it, is the beginning of a process of gradual engulfment of the secondaries. This process can become nearly complete during the second phase of development.

In this way, the tube network is propagated across the bedding plane in a narrow, nearly straight band, closely following the dip of the original piezometric slope. Deviations from a straight course occur only in response to factors affecting the pressure field. The final result is a network closely resembling the "anastomotic bands" described by Ford (1971)(Fig. 4.4):

4.3.2 PHASE I HYDRAULIC CONDITIONS AND THEIR IMPLICATIONS

Because a portion of the original bedding plane remains essentially unmodified and in series with the developing tube network, the resistance of the phase I subsurface flow system remains high. As a consequence of this, the following conditions can be expected:

1. The flow regime will be laminar. Weyl (1958) demonstrated that laminar flow conditions should exist in fractures and bedding planes in limestone. The much larger tubes supplying these partings should also have laminar flow regimes because their large cross-sections require lower flow velocities.
2. The ratio of available recharge to the network's carrying capacity will be large in humid environments.
3. With more water available than the subsurface network can conduct, the network will be developing under phreatic conditions.
4. Because the bulk of the rainfall is carried away as surface runoff, surface karst phenomena which depend upon subsurface drainage will not be evident.
5. Physical differences between individual tubes within a single network will have virtually no effect upon the amount of groundwater the tubes conduct or the rate at which they grow. All of these physical variations, such as length, cross-section, sinuosity, angularity, and roughness, are expressed hydraulically in terms of resistance. Although differences in resistance between two tubes in a network could conceivably differ by an order of magnitude, their effect will be insignificant within the total system. This is due to the fact that neither resistance is likely to be more than a fraction

of a percent of the resistance of the entire flow path so long as any part of the path consists of an interstratal parting unmodified by solution. This contention is readily confirmed by the analysis in Figure 4.3. When the tube length is increased to 0.95 of the total flow path length, the head loss is of the order of 0.06 of the total. Therefore, the hydraulic pressure at every point in the low resistance tube network is substantially the same. Consequently, all tubes in the network will enlarge irrespective of their internal characteristics, their development being controlled only by the flow characteristics of the surrounding virgin bedding plane. Those which are able to discharge through this parting, grow; those which cannot, stagnate.

4.3.3 PHASE II

The second phase of development is initiated when the bedding plane is breached by the tube network. This removes the last of the high resistance parting from the principal tube flow path and abruptly establishes a low resistance path from the source to the resurgence. This reduced resistance will reduce the pressure head at the input when the solvent supply is less than the increased capacity of the network.

4.3.3.1 The Principal Tube

During a short space of time following the initial breaching, rapid enlargement of the principal tube occurs in its lower reaches (Fig. 4.2e). This enlargement is in response to the greatly increased discharge capacity of the system as a whole and the higher solvent velocities and turbulence in the narrower tubes of the younger portion of the network. This quickly brings the cross-section of this part of the tube into equilibrium with the solvent supply or the capacity of the upper reaches of the network, whichever is smaller. The rapid throughput time, probable turbulent flow regime, and the increasing cross-section of the tube decreases the saturation deficit over the length of the tube. This, in turn, increases the solute removal and causes further diameter change in the principal tube.

4.3.3.2 The Secondary Tubes

The discharge resistance of the secondary tubes remains high due to the presence of segments of unmodified parting along their discharge paths. This high resistance, coupled with the decrease in head which accompanies Phase II, attenuates the flow in these tubes to the point where growth becomes imperceptible in the laboratory models.

4.3.4 PHASE II HYDRAULIC CONDITIONS AND THEIR IMPLICATIONS

As a consequence of the greatly reduced network flow resistance in Phase II, the following conditions can be expected.

1. With greatly increased tube diameters, the flow regime will quickly become turbulent.
2. Since a very minor fraction of the available runoff was diverted into the subsurface during PHASE I, significant surface karst phenomena, large sinks in particular, were unlikely to form. Without such well developed sinks, the runoff and superficial groundwater that will be available for diversion into the new, low resistance, subsurface routes should, in most instances, be small. Throughout most of the second phase, the amount of water available to the tube net will frequently be less than its carrying capacity.
3. When the network capacity exceeds the supply, the head at the input will drop, and the fluid potential gradient along the tube will be low.
4. As a consequence of this reordering of hydrologic conditions, further development of the subsurface drainage will be much more akin to surface stream evolution. Specifically, such processes as downcutting, lateral cutting, meandering, corrasion, and sediment transport which depend upon strong, selective, highly directional, inertial forces will obtain.
5. Depending upon the elevation of the tube network, it may be epiphreatic in nature. This condition is

defined as one in which the network is partly air filled, at least during low flow conditions.

6. Karst topography will begin to be manifest during this phase.
7. Initially, enlargement of the principal tube diameter will be in equilibrium with the development of surface catchments and the quantity and quality of the throughput. This should continue until sink development pervades 100% of the basin. Thereafter, enlargement will continue at a rate determined by the hydraulic throughput and its chemical characteristics. Enlargement will cease only when and if the water is diverted through another conduit.

CHAPTER 5

THE ELECTRIC ANALOGUE EXPERIMENTS

5.1 INTRODUCTION

5.1.1 PRACTICAL EXPERIMENTS

The electrical analogue experiments, undertaken as a part of this research, had as their purpose the evaluation of groundwater flow within a single bedding plane as a consequence of input and output configurations with geological and geomorphic relevance to the problems specified in Chapter 1. The bedding plane being evaluated is assumed to function as a uniform, planar, granular aquifer. The experiments isolate specific factors of input density and distribution, as they relate to resurgence geometry, in an attempt to evaluate their individual effects. They address specific speleogenetic problems in clearly defined geologic settings. They do not address general groundwater flow theory. The theoretical basis for groundwater flow in prous media is already well understood and generally known. M. King Hubbert summarized these flow-field concepts in a geological context in 1940 (Hubbert, 1940).

No attempt has been made to achieve the infinite plane conditions of Hubbert's work for the conductive medium used in these experiments. There are obvious mechanical difficulties in establishing these conditions which preclude their use. Moreover these conditions are probably rarely, if ever, approached in nature and experiments based upon them would have little relevance to real-world considerations. The boundaries in the experiments are analogous to real flow boundaries, such as truncations of the bedding plane, or to interfaces with other flow systems, of similar order and scale (Fig. 5.1). These adjacent flow systems derive from inputs similar in order and distribution to the flow system under consideration. Evidence presented later, in the discussion of flow envelope experiments (Chapter 6), will testify to the reality of these interface boundaries.

5.1.2 SIMILITUDE

The fundamental similitude arguments relating electrical analogues and ground water flow have already been presented in Chapter 3. The experiments have been designed to achieve geometrical similitude with natural groundwater systems of two general types: those existing in nearly horizontally bedded carbonates, and those in steeply dipping soluble rocks. Accordingly, the experiments are divided into two general types which differ in their output geometry, linear resurgence, and point resurgence types.

Figure 5.1
Hypothetical boundaries in bedding plane flow systems.

Truncation Boundaries

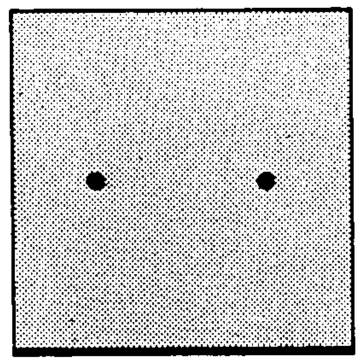

Interface Boundaries

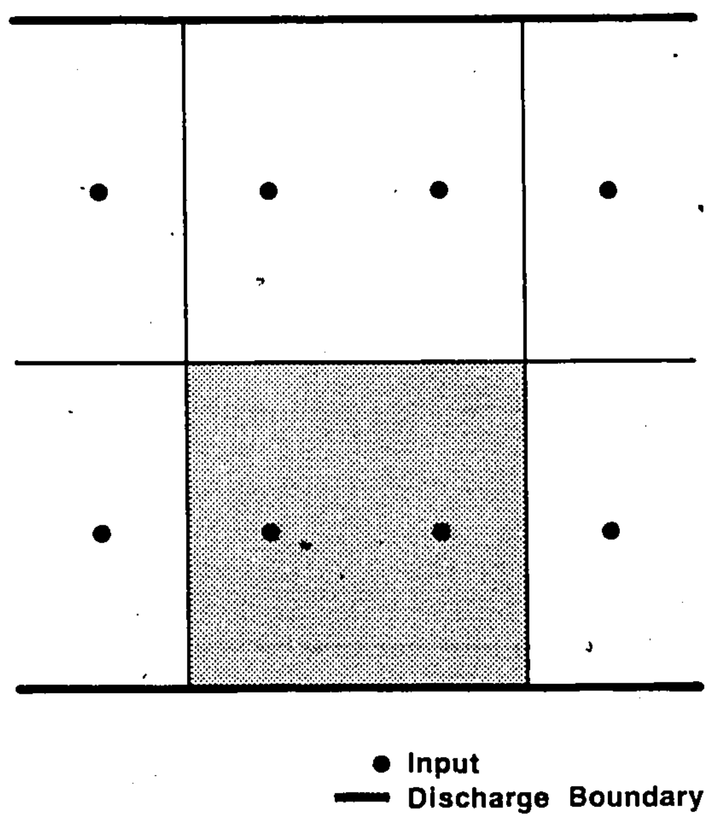

The linear resurgence experiments reflect a situation in which a uniformly conductive bedding plane is truncated in a roughly linear fashion, as by a stream of high Horton order. Such a stream provides a stable regional hydraulic sink and, subject to geological structure, one of comparatively uniform piezometric potential relative to the inputs.

The stream need not actually truncate the bedding plane. It is necessary only that it provide for the free discharge of waters entrained by the bedding plane at a large number of points along its course. Such discharge might be accomplished in a vertical sense via minor joints. Where such discharge points are of a density greater than the density of inputs, the author does not consider the condition of linear resurgence to be violated. This type of geometry is most frequently associated with regions of near horizontal strata.

Point resurgence experiments reflect those situations where a relatively horizontally eroding stream intersects a conductive bedding plane at a point, providing a highly localized discharge. This geometry is most frequently associated with regions of steeply dipping strata. As in the case of linear resurgences, the discharge point may be associated with local joints.

Both in the point and linear resurgence cases, these experiments are representative of initial conditions, which is to say, a state prior to the evolution of solution voids within the bedding plane and prior to the development of springs which localize resurgence flow. These "initial condition" experiments are, to a degree, inconsistent with modern time independent approaches to geomorphic processes. This inconsistency will be dealt with in Chapter 10.

5.2 LINEAR RESURGENCE ELECTRIC ANALOGUE EXPERIMENTS

These experiments evaluate initial conditions of flow through inputs to a unit square, rectangular bedding plane segment discharging uniformly on one boundary. A variety of input patterns, densities, and spacings were evaluated in terms of flow rate (Q) at the input, given a constant head. In analogue terms, input electrode current flow (I) was measured at a constant potential (e).

5.2.1 SINGLE RANK DENSITY EXPERIMENTS

5.2.1.1 Purpose

These experiments determine the variation in throughput (Q) for individual inputs as a function of input density. They apply specifically to two dimensional flowfields of square geometry having a linear output boundary (Fig. 5.2).

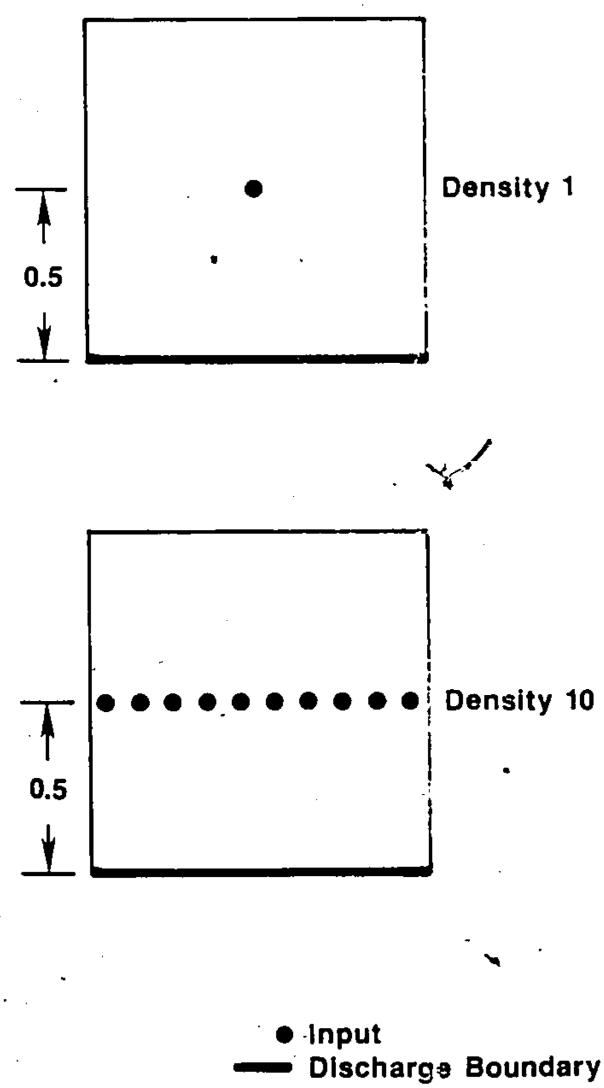

Figure 5.2
Input arrays for electric analogue density experiments.

5.2.1.2 Description

Successively 1,2,4,6, and 1Ø input electrodes were introduced along a line parallel to the discharge boundary of the unit square planar analogue medium. The line was spaced Ø.5 units from the discharge boundary and the input electrodes were arranged symmetrically and evenly spaced as shown in Table 5.1. All input electrodes were held at a potential of 1Ø volts relative to the sink electrode. Individual currents were measured and corrected for the internal resistance of the measuring instrument.

5.2.1.3 Expected Results

In the case of the single input experiment the entire area of the conductive medium is available for transmission of the current to the entire output boundary. This planar conductive medium can be considered as a large number of individual resistances or flow lines acting in parallel (Fig. 5.3A).

In the case of a larger number of inputs, the conductive medium plus the output boundary is divided among the several inputs. Each input can be considered to discharge through a smaller number of parallel resistances (Fig. 5.3B). Therefore, we expect that as input density increases, individual input Q will decrease.

Figure 5.3 shows that the average flow path length over the entire flow field is shorter in the multiple input

Table 5.1

RANK 1 INPUT POSITIONS

Density :	Input Positions					
1	Ø.5					
2	Ø.25	Ø.75				
4	Ø.125	Ø.375	Ø.625	Ø.875		
8	Ø.Ø625	Ø.1875	Ø.3125	Ø.4375	Ø.5625	Ø.6875
	Ø.8125	Ø.9375				
1Ø	Ø.Ø5	Ø.15	Ø.25	Ø.35	Ø.45	Ø.55
	Ø.65	Ø.75	Ø.85	Ø.95		

RANK 2 INPUT POSITIONS

Density :	Input Positions					
1	Ø.Ø	1.Ø				
2	Ø.Ø	Ø.5	1.Ø			
4	Ø.Ø	Ø.25	Ø.5	Ø.75	1.Ø	
8	Ø.Ø	Ø.125	Ø.25	Ø.375	Ø.5	Ø.625
	Ø.75	Ø.875	1.Ø			
1Ø	Ø.Ø	Ø.1	Ø.2	Ø.3	Ø.4	Ø.5
	Ø.6	Ø.7	Ø.8	Ø.9	1.Ø	

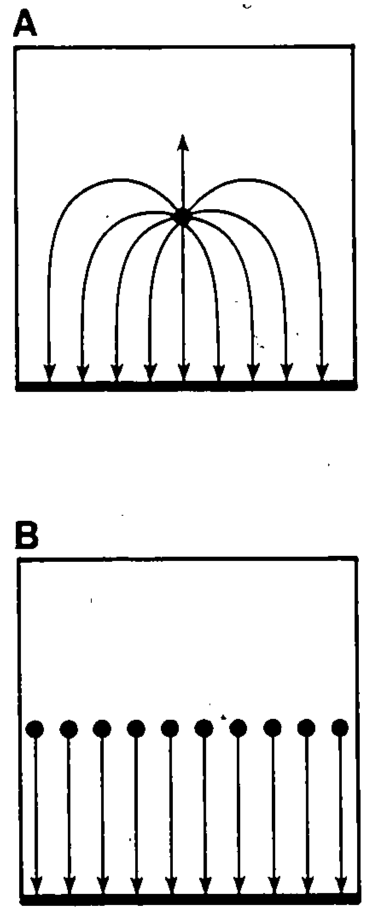

Figure 5.3
Flow vectors for arrays of high [A] and low [B] density.

case relative to the single input example. Because path length is related to resistance and resistance is inversely related to Q, we expect that the total output from the discharge boundary will increase with increasing input density.

The reader is reminded that the absolute relationship between the electrical analogue and the natural system is not important, so long as the natural system is in the range of applicability of the Darcy relationship. Both the head and hydraulic conductivity, which are unscaled in these experiments, affect the experiment in a way which does not perturb the ratio relationships between the elements of a single experiment or between experiments of different types, so long as the electrical conductivity of the experiment medium and the electromotive forces are constant throughout.

5.2.1.4 Measured Results

The data derived from these experiments are presented in Table 5.2 and Figure 5.4. They show Q to be an inverse function of input density. Within the defined limits of the experiments, the data closely approximate a logarithmic curve of the form

$$y = a + b \ln x. \qquad (5\text{-}1)$$

The least squares r2 value for the equation

$$y = 42.02 - 15.56 \ln x \quad (5\text{-}2)$$

Table 5.2

SINGLE RANK INPUT Q (mA)

Distance	Density				
	1	2	4	6	1Ø
Ø.5	43	31	19	13	8

Single electrode current values for single rank experiments - Rank position is Ø.5 units from the discharge boundary, input density varies from 1 to 1Ø.

Figure 5.4

Comparison of throughputs for individual inputs and entire input arrays, as a function of density.

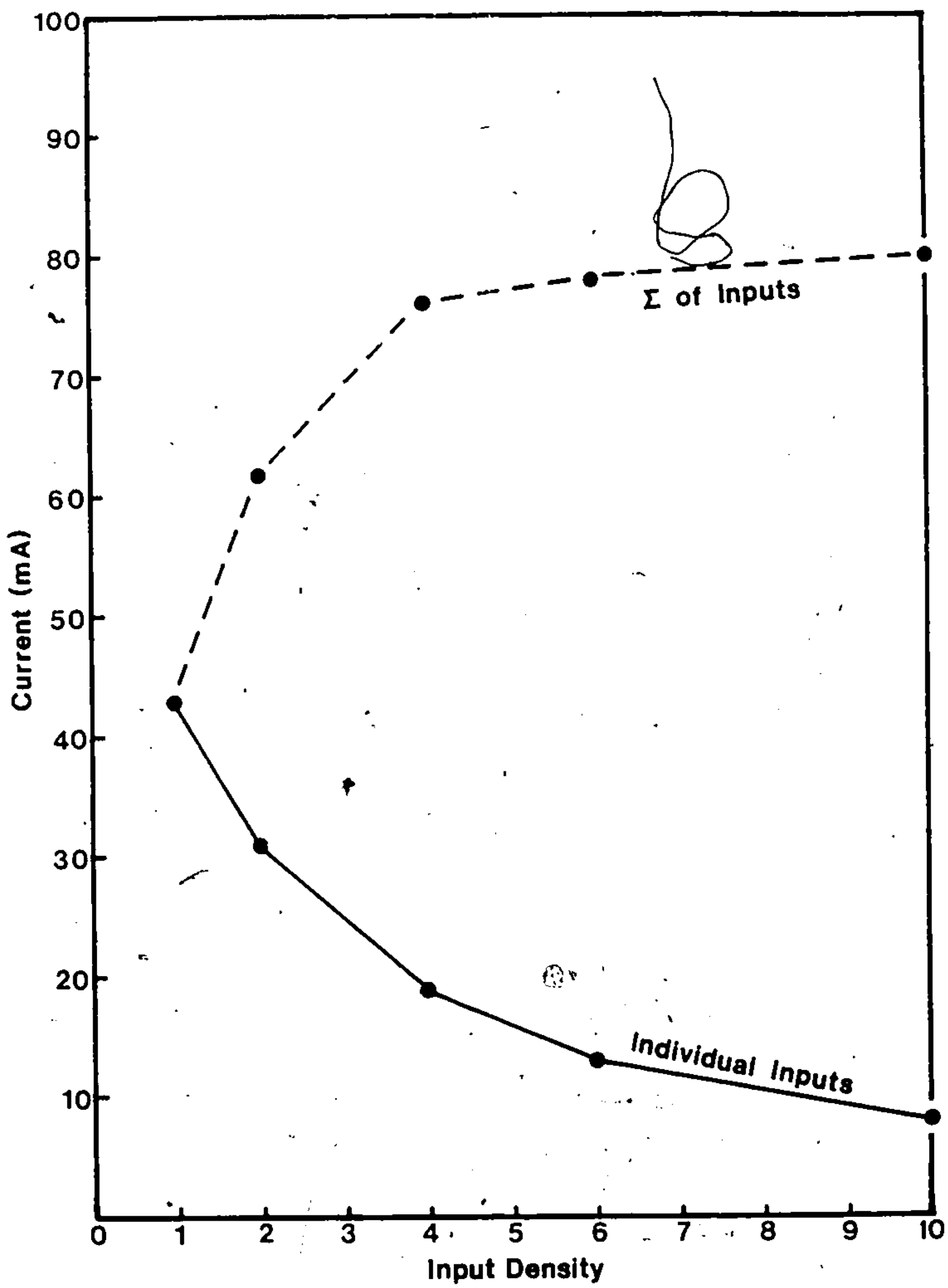
100
90
80
70
60
50
40
30
20
10
Current (mA)
Σ of Inputs
Individual Inputs
0
1
2
3
4
5
6
7
8
9
10
Input Density

fitted to the data is Ø.99Ø, indicating a very good fit.

5.2.1.5 The Simple Density Rule

In hydrologic terms, these experiments indicate that the throughput at any groundwater input to a planar parting is reduced by the existence of other inputs. In terms of karst hydrology, they indicate that to the extent that the propagation rate of solution voids along a bedding plane or fracture plane is controlled by flow rate, that rate will be reduced as input density increases.

It should be noted, however, that the sum of the throughput from all inputs increases with increasing input density (Fig. 5.4). Therefore, in karst situations the total soluble rock removed along the parting is increased as input density increases.

5.2.2 SINGLE RANK DISTANCE EXPERIMENTS

5.2.2.1 Purpose

These experiments quantify the variation in throughput (Q) for individual inputs as a function of distance from the discharge boundary. They apply specifically to two dimensional flow fields of square geometry having a linear output boundary. These experiments also extend the scope of the preceding experiments by quantifying the combined variation in Q with distance and density.

5.2.2.2 Description

Successively 1, 2, 4, 6, and 10 input electrodes were introduced along a line parallel to the discharge boundary of the unit square analogue medium. Each of these linear input arrays was in turn spaced at distances varying from 0.025 to 1 units from the discharge boundary. Electrode spacing within the arrays was determined by the formula given in Table 5.1 above. Electrode potential was 10 volts relative to the sink electrode in all cases. All measurements were corrected for instrument error.

5.2.2.3 Expected Results

5.2.2.3.1 Limiting Case One

Two limiting cases can be identified within the framework of the single rank distance experiments. The first and most easily visualized is the infinite density case. Here the inputs become a line source of unit length parallel to the unit length discharge boundary and varying in distance from it. Under these conditions, all flow lines are parallel, and potential loss is uniform per unit of length along any flow line. In such cases, distance may be equated with resistance provided that a proportionality constant is included which reflects the characteristics of the conducting medium.

Darcy's Law and Ohm's Law equations were derived from similar experiments, where unit area cross sections were used and flow lines were also parallel. In these instances, the equations are expressed with the length substitution:

OHM'S LAW	DARCY'S LAW
$I = \frac{E}{R}$	$Q = \frac{h}{R}$
$I = \frac{E}{L} \times C$	$Q = \frac{h}{L} \times C$

When appropriate units are chosen, a plot of Q versus length for the general equation covering these two laws yields a symmetrical rectangular hyperbola (Fig. 5.5). These curves are defined by the formula:

$$y = N/x \tag{5-3}$$

These equations show that as the length approaches zero, Q approaches infinity; as Q approaches zero, length approaches infinity.

In the infinite density experiments the current flow is confined to a region of constant cross section and can be considered identical to the Darcy Experiment where L is arbitrarily confined to values less than one unit. We, therefore, may assume that the infinite density experiment will yield a rectangular hyperbola for plots of Q versus L, where L = Input electrode to discharge boundary distance. The observed values for Q in these experiments are in agreement with this expectation.

Figure 5.5
Plot of Q verses length for the general equation covering electrical and fluid flow.

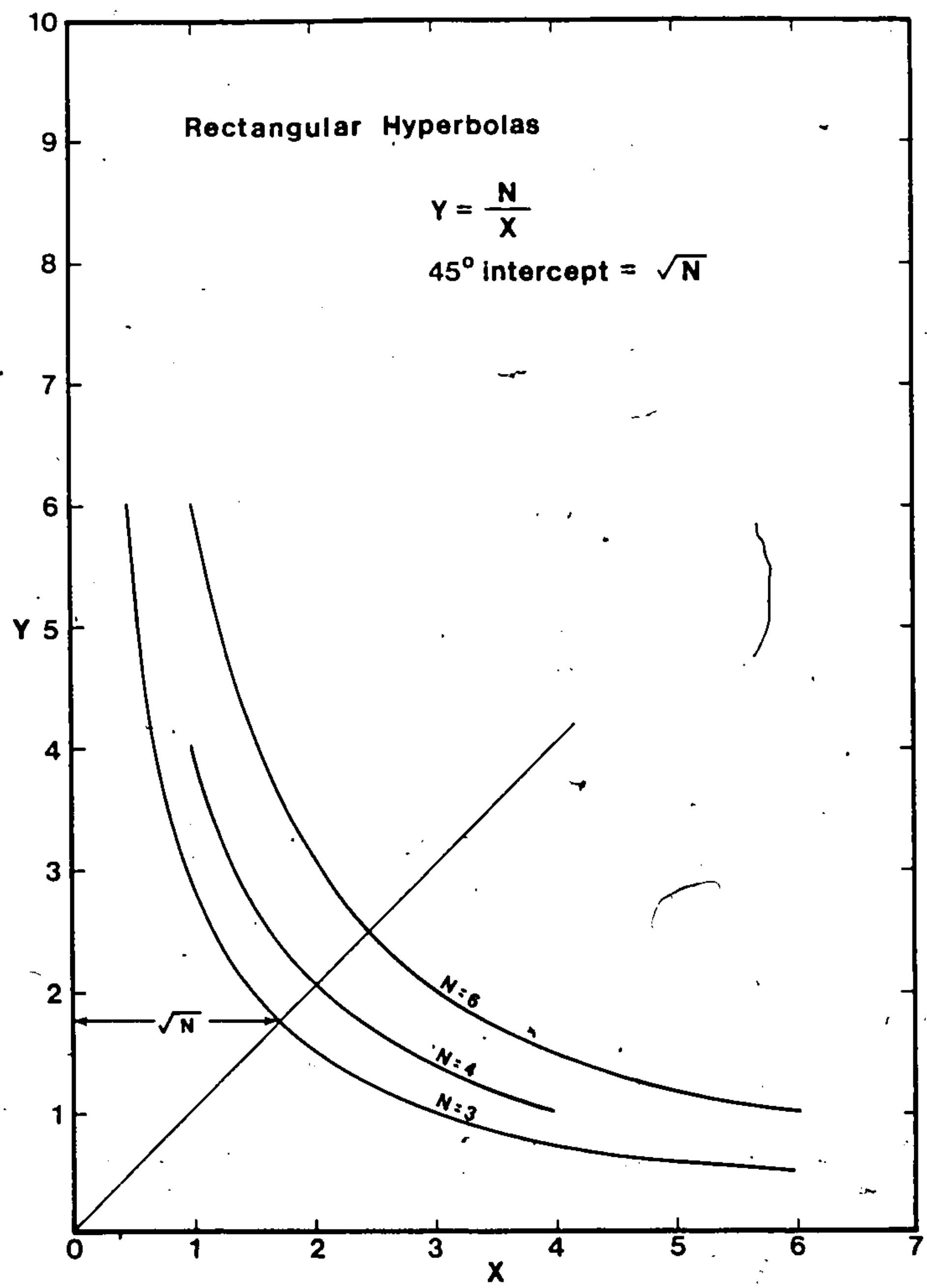
Rectangular Hyperbolas
$Y = \frac{N}{X}$
45° intercept = $\sqrt{N}$
$\sqrt{N}$
N=6
N=4
N=3
Y
X
0
1
2
3
4
5
6
7
8
9
10

It is not possible to isolate one of the infinite number of inputs and assess its contribution to the total current flow. Presumably, it is infinitely small. This observation, however, supports the finding of the density experiments discussed above, that the Q measured for each individual input is inversely related to the input number.

5.2.2.3.2 Limiting Case Two

The second limiting case involves a single input with varying distance from the unit length discharge boundary. This is the minimum number of inputs for a unit square bedding plane. In this case, the flow lines are divergent. Therefore, potential loss per unit length along separate flow lines is not equal, and potential loss along an individual flowline is non-linear.

As the input approaches the output boundary, Q should, as in the first case, increase without limit. Values for Q at intermediate distances should be higher than in the first case. This is due to the availability of flow paths in addition to the single shortest route path associated with each of the infinite number of input points in the first case. Thus, the expected curve should have the general form of a rectangular hyperbola.

As the input approaches the boundary opposite the discharge boundary, its local discharge area is compressed (Fig. 5.6). The resistance of that region is thus

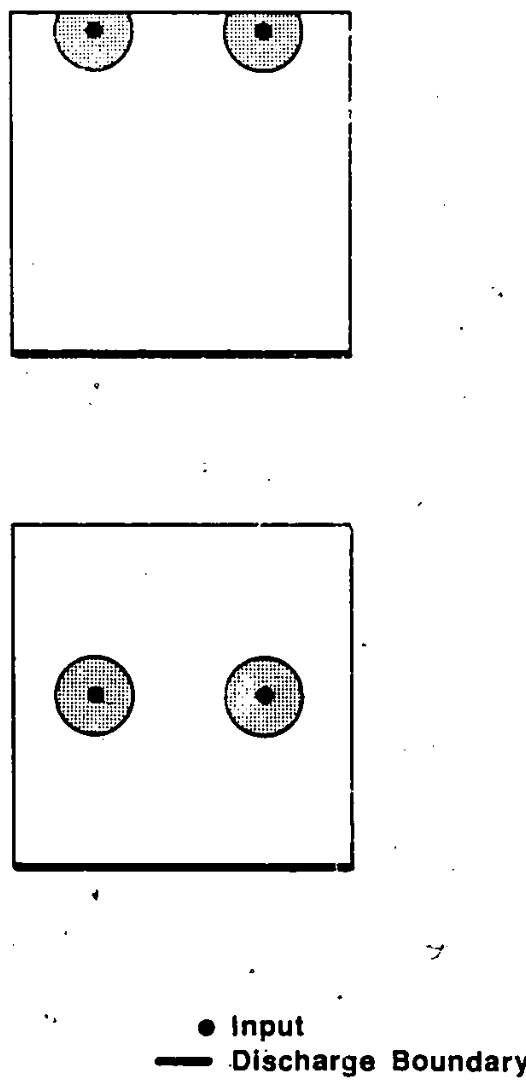

Figure 5.6
Restriction of an arbitrary flow domain as an input approaches the general flow domain boundary.

increased, and the current traversing it will be less. Therefore, we expect a boundary effect as the input-sink distance approaches maximum. In the infinite density case, however, the discharge is unidirectional, and no boundary effect would be expected. Following this reasoning, the strength of the boundary effect should be inversely proportional to the input density.

In summary, individual input Q should be inversely proportional to distance from the output boundary for all densities. Plots of Q vs. distance should approximate rectangular hyperbolas, with their N values inversely proportional to the density.

5.2.2.4 Measured Results

The data derived from these experiments are presented in Table 5.3 and Figure 5.7. In the case of the ten electrode experiment series, the data show Q to be an inverse function of distance, with a plot closely approximating the curve obtained for the infinite density experiment.

Experiments with progressively lower input density show increasing Q for individual inputs at all distances and an increasing boundary effect at the maximum distance of one unit. Thus, a regular progression of curves of Q versus distance exists between the limiting cases outlined above. Moreover, their measured values, including the N values, are

Table 5.3

SINGLE RANK INPUT Q (mA)

Distance	Density				
	1	2	4	6	1Ø
1.Ø	22	15	9	6	3
Ø.95	28	18	1Ø	6	3
Ø.9	3Ø	19	11	7	3
Ø.8	33	21	12	8	4
Ø.7	36	24	14	9	5
Ø.6	4Ø	27	16	11	6
Ø.5	43	31	19	13	8
Ø.4	47	35	22	16	1Ø
Ø.3	53	42	29	21	13
Ø.2	59	52	38	3Ø	19
Ø.1	72	66	58	48	35
Ø.Ø5	85	78	76	68	54
Ø.Ø25	1ØØ	98	94	86	68

Figure 5.7

Individual input Q for ranks of inputs varying in density from 1 to 10, and in distances of 0.05 to 1.0 units from a linear discharge boundary.

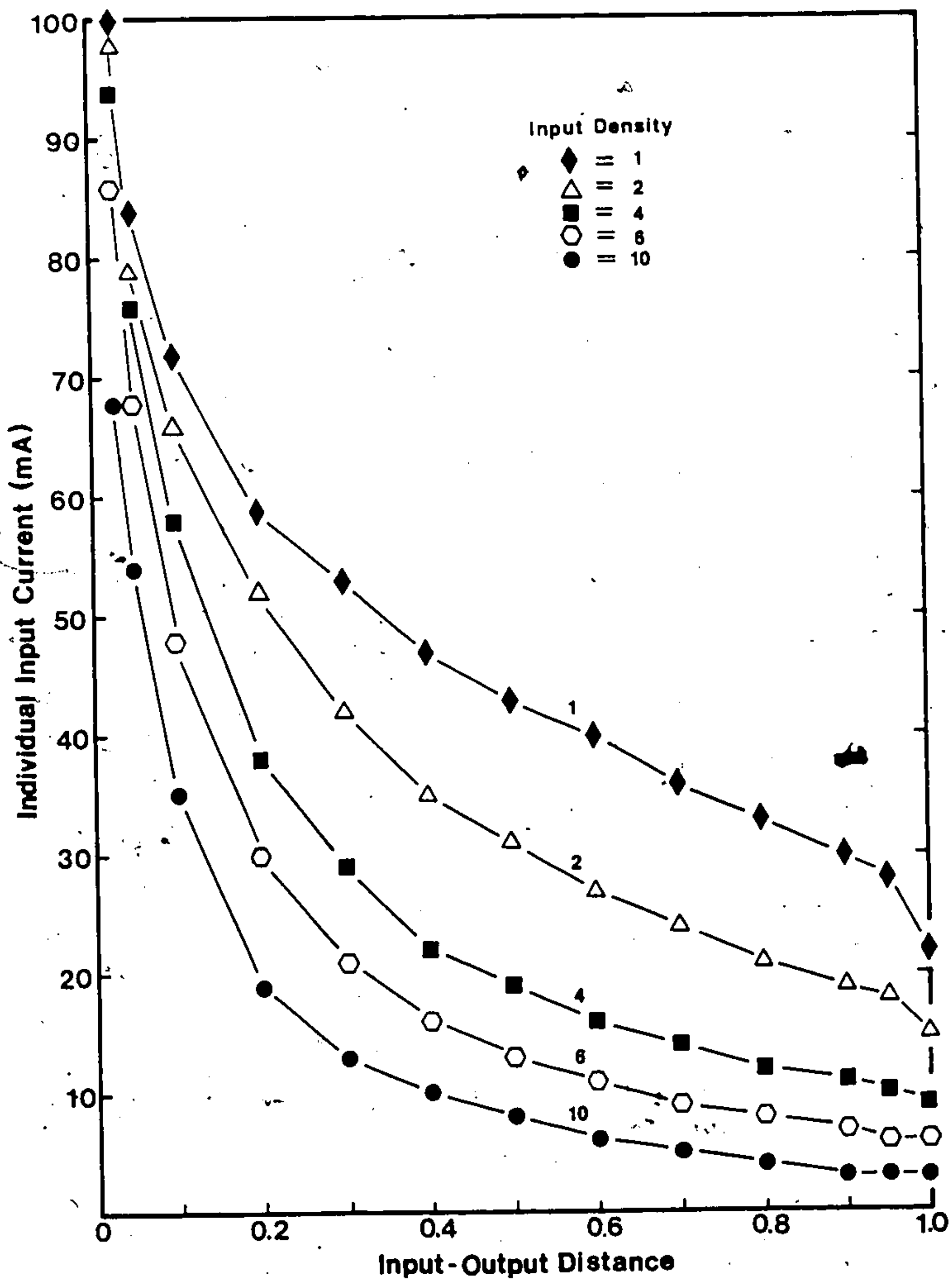
Input Density
= 1
= 2
= 4
= 6
= 10
Individual Input Current (mA)
Input-Output Distance
100
90
80
70
60
50
40
30
20
10
0
0.2
0.4
0.6
0.8
1.0
1
2
4
6
10

in agreement with the theoretical arguments. This experimental data is summarized in Figure 5.8. The family of curves s hown in this figure can be represented by an equation of the form:

$$Q = a - (bx) - (cy) + (dxE2) - (exy) + (fyE2) - (gxE3) + (hxE2y) + (ixyE2) - (jyE3) + (kxE4) - (lxE3y) - (mxE2yE2) - (nxyE3) + (oyE4),$$

with coefficients of determination and correlation in excess of Ø.99. Constants for this equation are listed in Table 5.4.

5.2.2.5 The Simple Distance Rule

In hydrologic terms, these experiments indicate that the throughput at any groundwater input to a planar parting is inversely proportional to the distance from the output boundary. In terms of karst hydrology, they indicate that to the extent that the propagation rate of solution voids along bedding planes and fracture planes is controlled by flow rate, they will be reduced as the distance from input to discharge boundary increases.

It should be noted that the sum of the throughput from all inputs increases with the input density, a direct relationship, and increases with proximity to the discharge boundary, an inverse relationship. In the first instance,

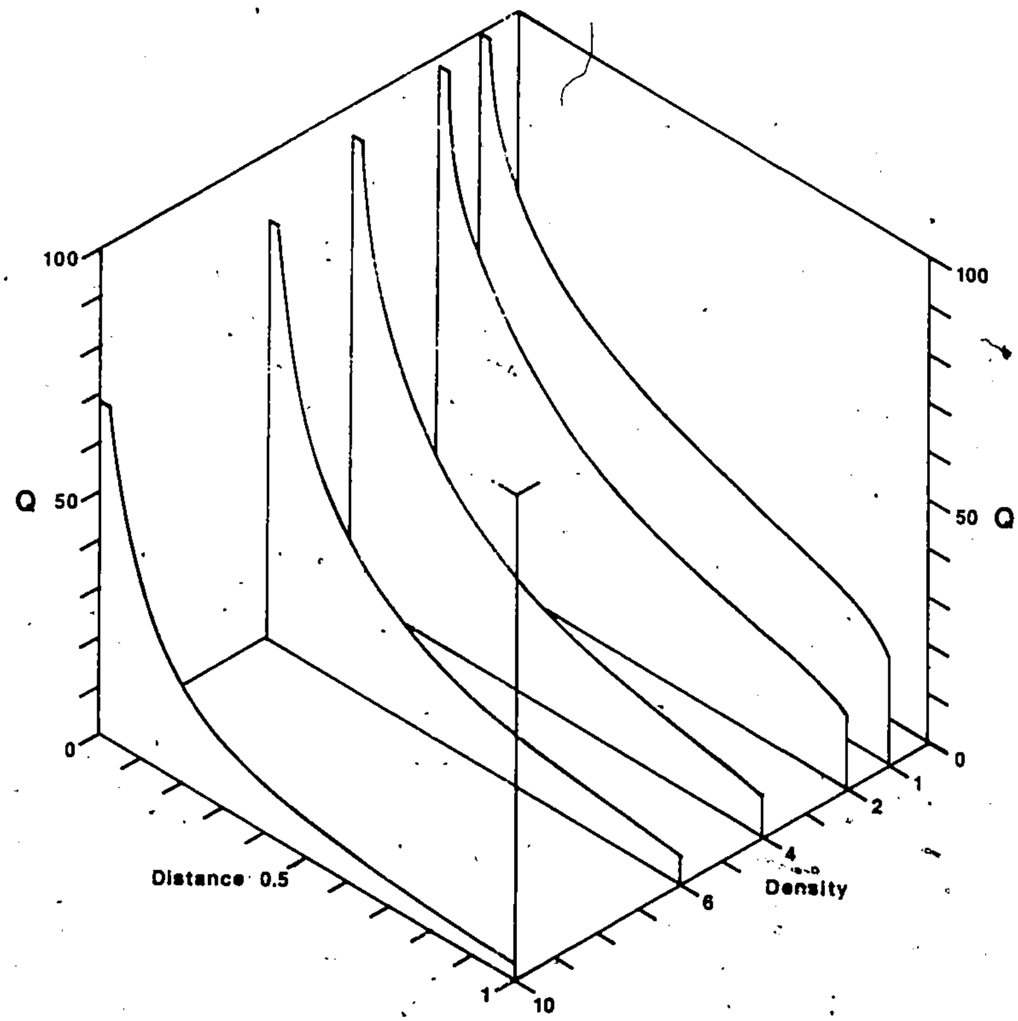

Figure 5.8
Individual input Q for ranks of inputs varying in density from 1 to 1Ø, and in distances of Ø.Ø5 to 1.Ø units from a linear discharge boundary.

Table 5.4

a	=	Ø.1154	x	1ØE 3
b	=	Ø.1135	x	1ØE 3
c	=	Ø.2828	x	1ØE 3
d	=	Ø.3635	x	1ØE 3
e	=	Ø.4Ø73	x	1ØE 3
f	=	Ø.1Ø44	x	1ØE 3
g	=	Ø.5539	x	1ØE 3
h	=	Ø.398Ø	x	1ØE 3
i	=	Ø.3738	x	1ØE 3
j	=	Ø.1226	x	1ØE 3
k	=	Ø.2646	x	1ØE 3
l	=	Ø.877Ø	x	1ØE 3
j	=	Ø.2Ø72	x	1ØE 3
n	=	Ø.7Ø14	x	1ØE 3
o	=	Ø.4914	x	1ØE 3

Constants for equation 5-4.

the combined flow from all inputs behaves in a way opposite to the individual input flows; in the case of distance, they behave similarly.

5.2.3 TWO RANK SPACING EXPERIMENTS

5.2.3.1 Purpose

These experiments are designed to quantify the effect of spacing between two or more similar ranks of inputs upon their relative Q values.

5.2.3.2 Description

Two similar ranks of input electrodes were introduced along lines parallel to the discharge boundary of the unit square analogue medium. Electrode densities of 2, 4, 6, and 10 were used. Electrode spacing within rank 1, the rank nearest the discharge boundary, was determined by the formula given in Table 5.1 above. Rank 2 consists of a number of inputs equal to the first rank +1. The electrodes within Rank 2 were spaced at intervals equal to Rank 1 but offset by 1/2 space (Fig. 5.9). This was done to permit closing the ranks to the same line (rank spacing = 0) in order to verify that their current flows converge to identical values. This scheme places two of the second rank electrodes on the lateral boundaries of the conductive medium. Because the flow lines originating from these two points are identical to one symmetrical half of the flow

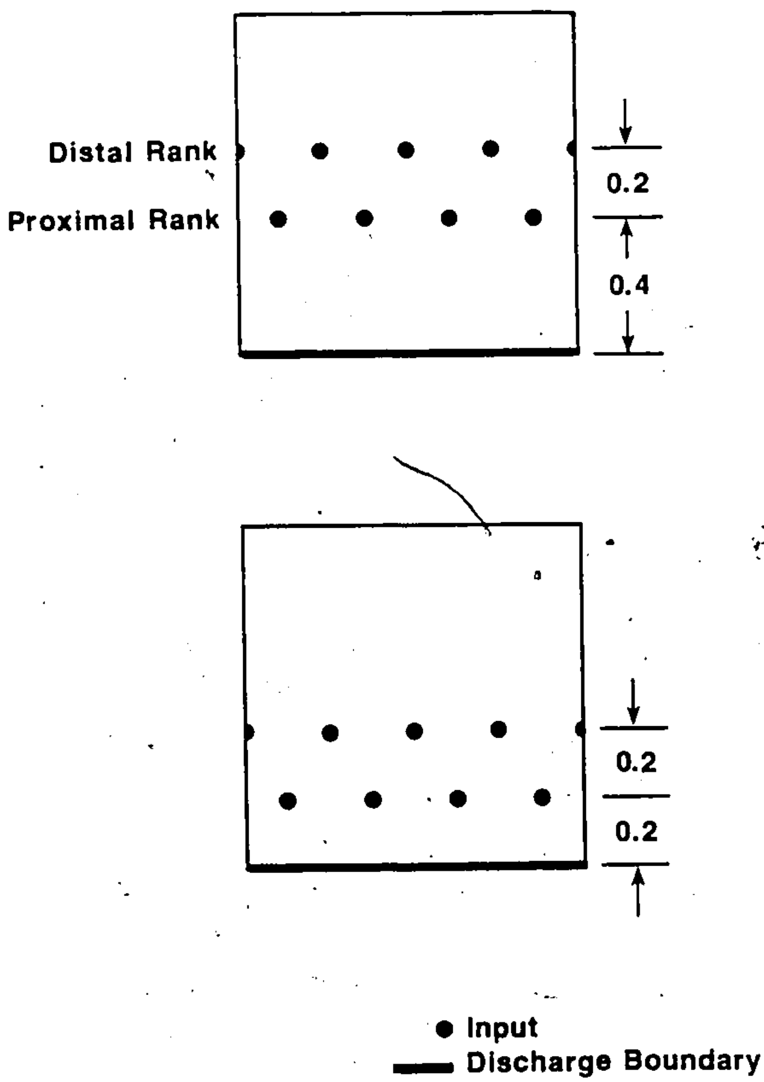

Figure 5.9
Input arrays for electric analogue two rank spacing experiments.

lines surrounding an evenly spaced electrode in a non-boundary position, they may be considered one half inputs, so that the input density remains unaltered. Figure 5.10 depicts the experimental verification of this assumption.

The two ranks of electrodes were placed at all unordered combinations of position between 0.1 and 1 units from the discharge boundary. At each of these positions, the current flowing through an individual electrode in the proximal and distal ranks was measured. The current flow was mathematically corrected for instrument error, and the ratio of proximal to distal electrode current was calculated. The experiment was repeated for density values of 1, 2, 4, 6, and 10 inputs per rank. The data are listed in Table 5.5.

5.2.3.3 Results

The data provided by these experiments can be analysed in a variety of ways. The three which are most useful to subsequent discussions are presented here.

1. Constant Between Rank Spacing

In this analysis, the data are selected to represent two input ranks of similar density separated by a constant space. The ranks were chosen for an initial separation for the output boundary of 0.1 units and advanced by 0.1 unit

FIGURE. 5.10 A

BOUNDARY INPUT Q
DENSITY =4 DISTANCE =0.5 UNITS
INPUTS 1 AND 4 ARE ON LATERAL BOUNDARIES

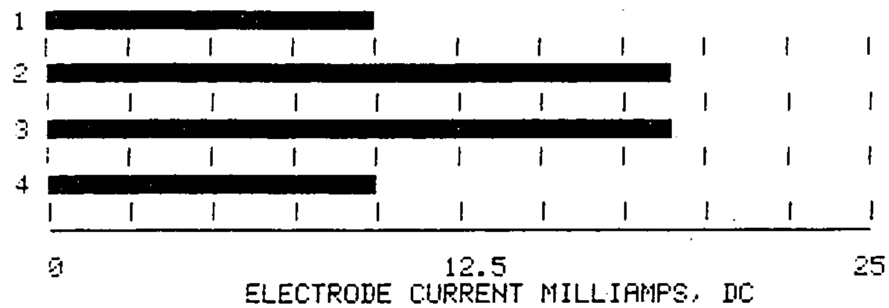

FIGURE. 5.10 B

BOUNDARY INPUT Q
DENSITY =10 DISTANCE =0.5 UNITS
INPUTS 1 AND 10 ARE ON LATERAL BOUNDARIES

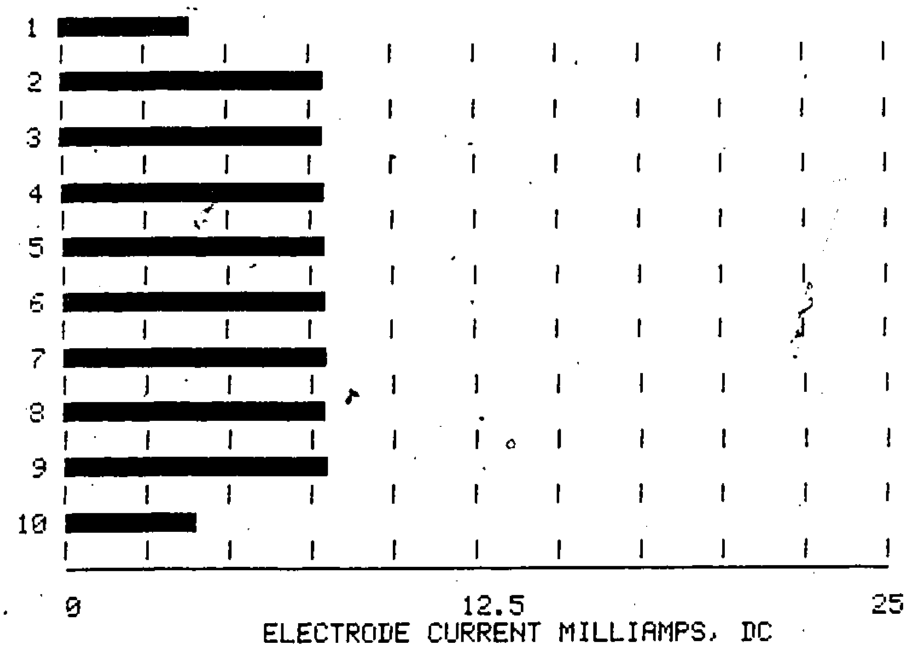

Table 5.5 A - DENSITY 2

DISTAL RANK POSITION	PROXIMAL RANK POSITION									
	Ø.1	Ø.2	Ø.3	Ø.4	Ø.5	Ø.6	Ø.7	Ø.8	Ø.9	1
Ø.1										
Ø.2	53 38									
Ø.3	55 3Ø	36 27								
Ø.4	56 25	38 21	3Ø 22							
Ø.5	57 2Ø	4Ø 17	32 18	25 18						
Ø.6	58 18	41 15	34 15	26 14	2Ø 15					
Ø.7	59 16	42 13	35 12	28 12	21 12	17 12				
Ø.8	6Ø 14	43 11	36 11	29 1Ø	24 1Ø	18 1Ø	15 11			
Ø.9	6Ø 12	45 1Ø	37 9	3Ø 9	25 8	2Ø 8	17 9	14 9		
1.Ø	62 1Ø	48 9	38 7	31 7	26 6	22 6	19 6	16 6	13 7	

Single electrode current values for two rank experiments - upper values are for a typical <u>proximal</u> rank input, lower values are for a typical <u>distal</u> rank input. Positions of the ranks vary from Ø.1 to 1 units from the linear discharge boundary.

Table 5.5 B - DENSITY 4

DISTAL RANK POSITION	PROXIMAL RANK POSITION									
	Ø.1	Ø.2	Ø.3	Ø.4	Ø.5	Ø.6	Ø.7	Ø.8	Ø.9	1
Ø.1										
Ø.2	47 22									
Ø.3	48 15	3Ø 15								
Ø.4	5Ø 11	33 1Ø	21 1Ø							
Ø.5	52 9	34 8	24 7	16 8						
Ø.6	54 8	36 6	26 5	18 5	13 6					
Ø.7	54 6	36 5	27 4	19 4	15 4	11 5				
Ø.8	55 5	37 4	27 3	2Ø 3	16 3	12 3	9 4			
Ø.9	56 4	37 3	28 3	21 2	16 2	13 2	11 3	8 3		
1.Ø	57 4	38 3	28 2	21 1	17 1	14 1	12 1	9 2	7 2	

Single electrode current values for two rank experiments - upper values are for a typical proximal rank input, lower values are for a typical distal rank input. Positions of the ranks vary from Ø.1 to 1 units from the linear discharge boundary.

Table 5.5 C - DENSITY 6

DISTAL RANK POSITION	PROXIMAL RANK POSITION									
	0.1	0.2	0.3	0.4	0.5	0.6	0.7	0.8	0.9	1
0.1										
0.2	43 15									
0.3	46 9	24 8								
0.4	47 6	27 5	16 5							
0.5	47 4	28 3	18 3	12 4						
0.6	49 4	29 2	19 2	14 2	10 3					
0.7	50 3	29 2	20 1	14 1	11 1	8 2				
0.8	50 2	30 1	20 0	15 0	12 0	9 0	7 1			
0.9	52 2	30 0	20 0	15 0	12 0	10 0	8 0	6 1		
1.0	52 1	30 0	21 0	16 0	12 00	10 0	8 0	6 0	5 0	

Single electrode current values for two rank experiments - upper values are for a typical <u>proximal</u> rank input, lower values are for a typical <u>distal</u> rank input. Positions of the ranks vary from 0.1 to 1 units from the linear discharge boundary.

Table 5.5 D - DENSITY 1Ø

DISTAL RANK POSITION	PROXIMAL RANK POSITION Ø.1	Ø.2	Ø.3	Ø.4	Ø.5	Ø.6	Ø.7	Ø.8	Ø.9	1
Ø.1										
Ø.2	33 6									
Ø.3	35 3	16 3								
Ø.4	36 2	18 Ø	11 1							
Ø.5	37 Ø	19 Ø	12 Ø	8 Ø						
Ø.6	37 Ø	19 Ø	13 Ø	9 Ø	6 Ø					
Ø.7	37 Ø	19 Ø	13 Ø	9 Ø	7 Ø	5 Ø				
Ø.8	37 Ø	19 Ø	13 Ø	9 Ø	7 Ø	6 Ø	4 Ø			
Ø.9	37 Ø	19 Ø	13 Ø	1Ø Ø	7 Ø	6 Ø	5 Ø	3 Ø		
1.Ø	38 Ø	2Ø Ø	13 Ø	1Ø Ø	7 Ø	6 Ø	5 Ø	4 Ø	3 Ø	

Single electrode current values for two rank experiments - upper values are for a typical <u>proximal</u> rank input, lower values are for a typical <u>distal</u> rank input. Positions of the ranks vary from Ø.1 to 1 units from the linear discharge boundary.

intervals to the maximum permitted by the unit square bedding plane. Input densities of 2, 4, 6, and 10 were chosen, with separation between ranks of 0.1, 0.2, and 0.3 units. Histograms of these data form Figures 5.11, 5.12, and 5.13.

These experiments show that the proximal input Q's always exceed those of the distal inputs, but the ratios of these quantities vary with density and rank spacing. Figure 5.14 shows that these ratios increase as the rank spacing increases, but they increase more rapidly with higher densities.

2. Rank 1 Constant: Rank 2 Variable.

The data selected for this analysis represent two ranks of inputs of similar density. The proximal rank is fixed at a distance of 0.1 units from the output boundary while the distal rank was varied from 0.2 to 1 units from this boundary. The analysis was repeated for input densities of 2, 4, 6, and 10. This data is plotted in Figure 5.15, A, B, C, and D. Under these conditions, the disparity in Q values between the proximal and distal ranks increases rapidly with spacing and distance.

3. Rank 1 Variable. Rank 2 Constant

This analysis covers situations which are the reverse of analysis 2 above. The distal rank remains at a

FIGURE. 5.11 A

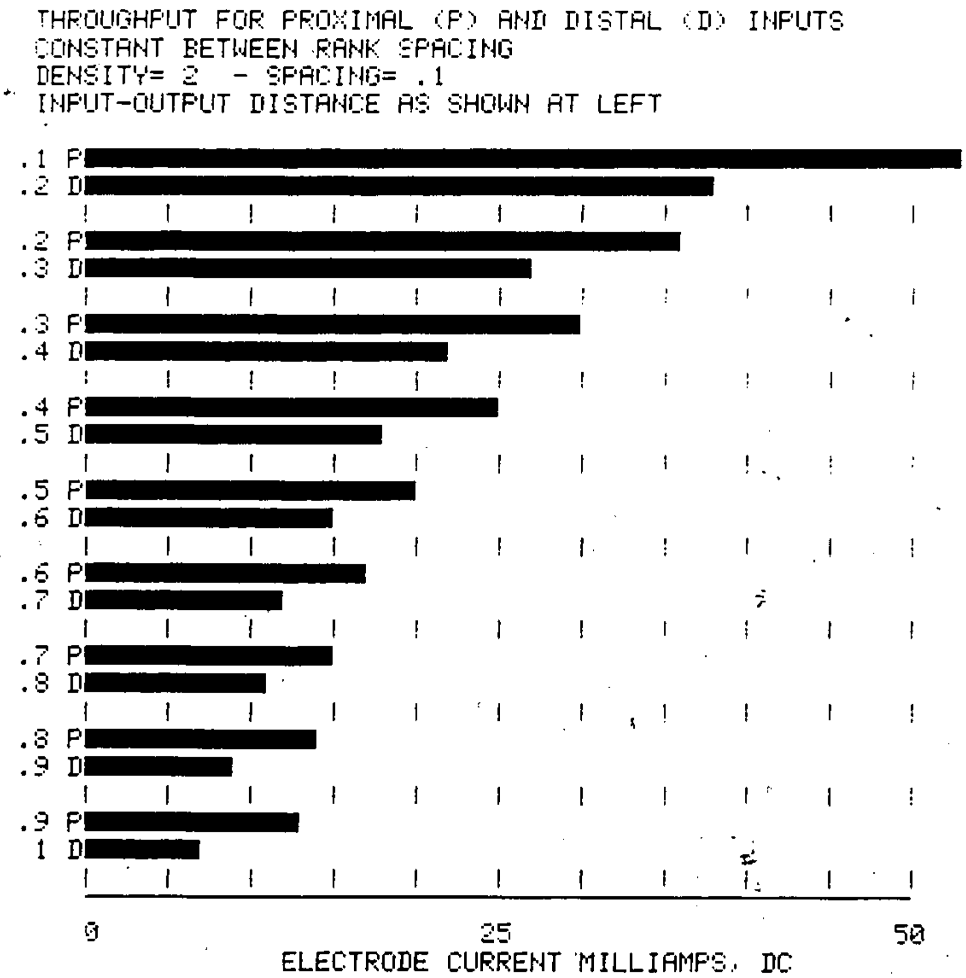
THROUGHPUT FOR PROXIMAL (P) AND DISTAL (D) INPUTS
CONSTANT BETWEEN RANK SPACING
DENSITY= 2 - SPACING= .1
INPUT-OUTPUT DISTANCE AS SHOWN AT LEFT
.1 P
.2 D
.2 P
.3 D
.3 P
.4 D
.4 P
.5 D
.5 P
.6 D
.6 P
.7 D
.7 P
.8 D
.8 P
.9 D
.9 P
1 D
0
25
50
ELECTRODE CURRENT MILLIAMPS, DC

FIGURE. 5.11 B:

THROUGHPUT FOR PROXIMAL (P) AND DISTAL (D) INPUTS
CONSTANT BETWEEN RANK SPACING
DENSITY= 4 - SPACING= .1
INPUT-OUTPUT DISTANCE AS SHOWN AT LEFT

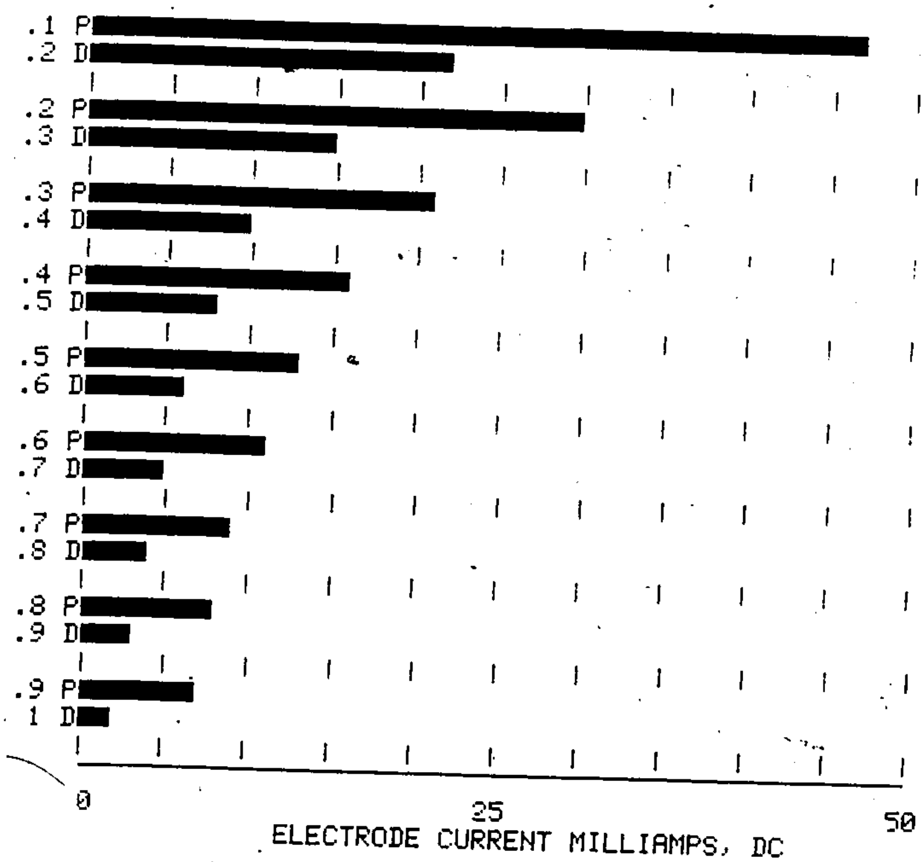

FIGURE. 5.11 C

THROUGHPUT FOR PROXIMAL (P) AND DISTAL (D) INPUTS
CONSTANT BETWEEN RANK SPACING
DENSITY= 6 - SPACING= .1
INPUT-OUTPUT DISTANCE AS SHOWN AT LEFT

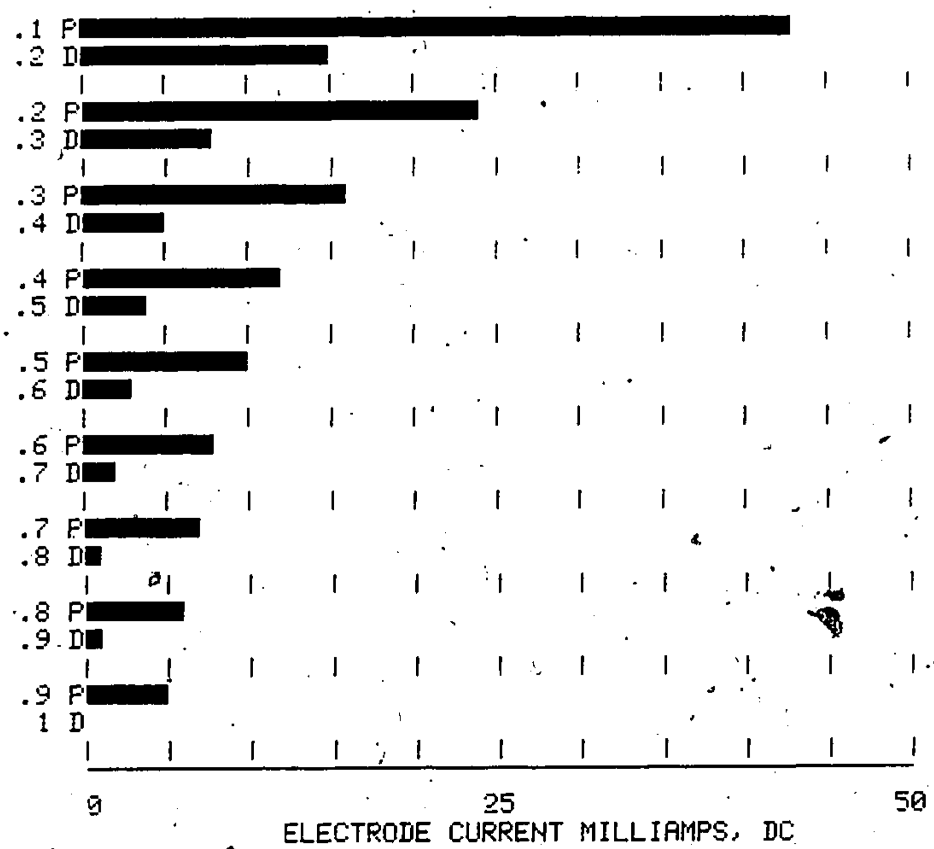

FIGURE. 5.11 D

THROUGHPUT FOR PROXIMAL (P) AND DISTAL (D) INPUTS
CONSTANT BETWEEN RANK SPACING.
DENSITY= 10 - SPACING=..1
INPUT-OUTPUT DISTANCE AS SHOWN AT LEFT

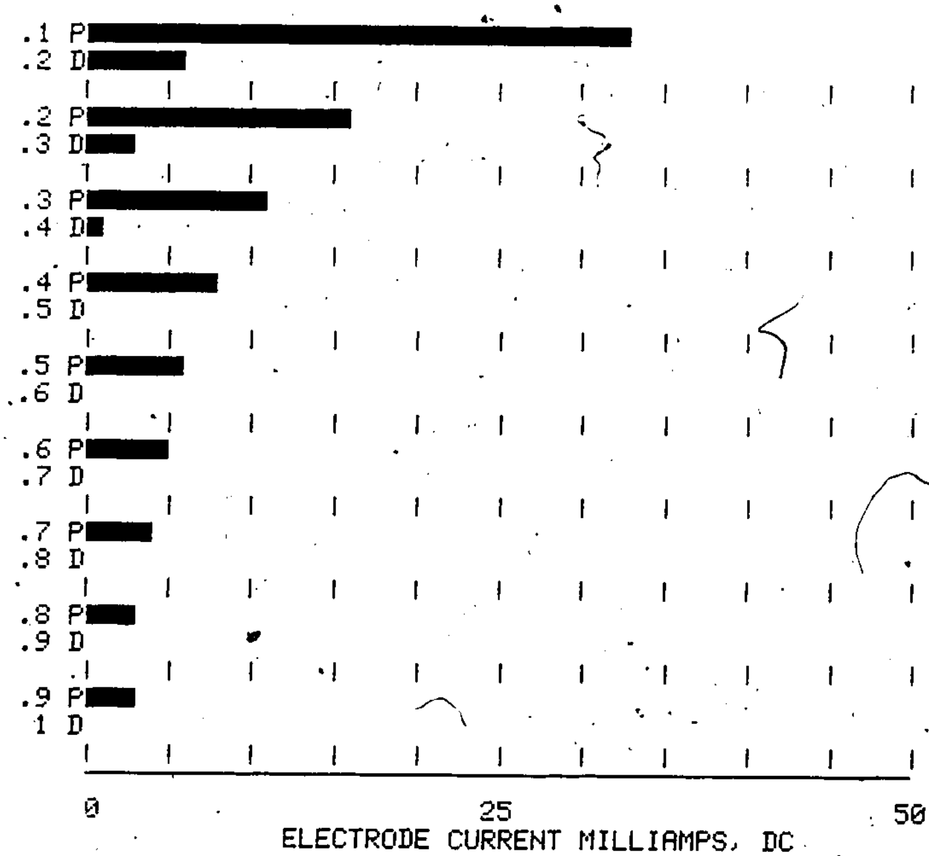

FIGURE. 5.12 A

THROUGHPUT FOR PROXIMAL (P) AND DISTAL (D) INPUTS
CONSTANT BETWEEN RANK SPACING
DENSITY= 2 - SPACING= .2
INPUT-OUTPUT DISTANCE AS SHOWN AT LEFT

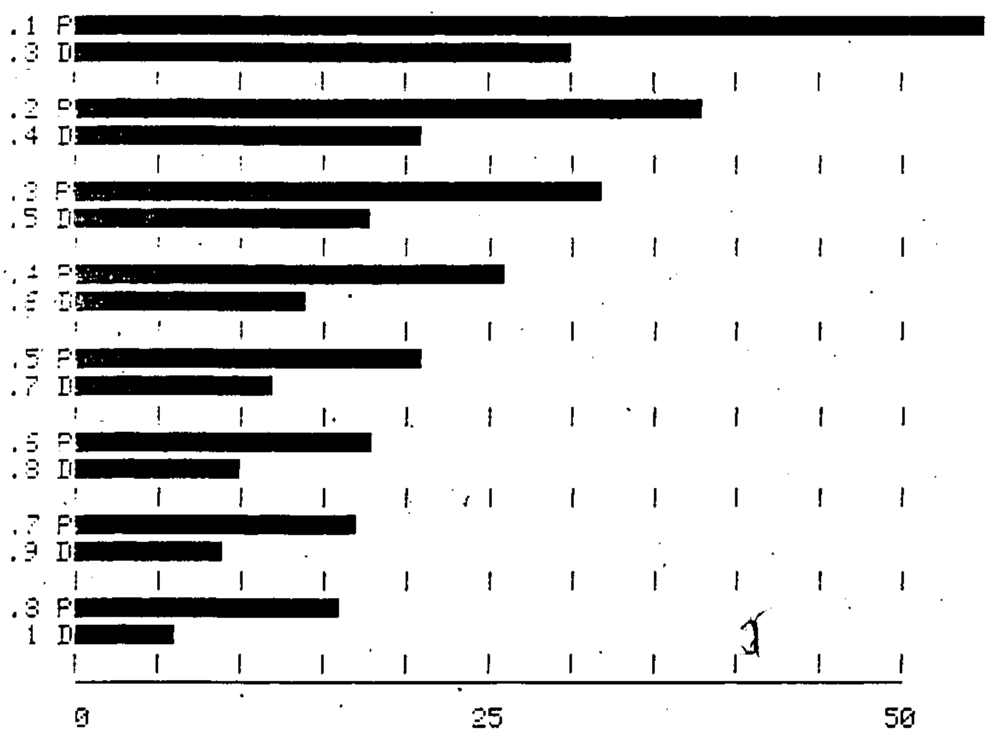

FIGURE. 5.12 B

FIGURE. 5.12 B

THROUGHPUT FOR PROXIMAL (P) AND DISTAL (D) INPUTS
CONSTANT BETWEEN RANK SPACING
DENSITY= 4 - SPACING= .2
INPUT-OUTPUT DISTANCE AS SHOWN AT LEFT

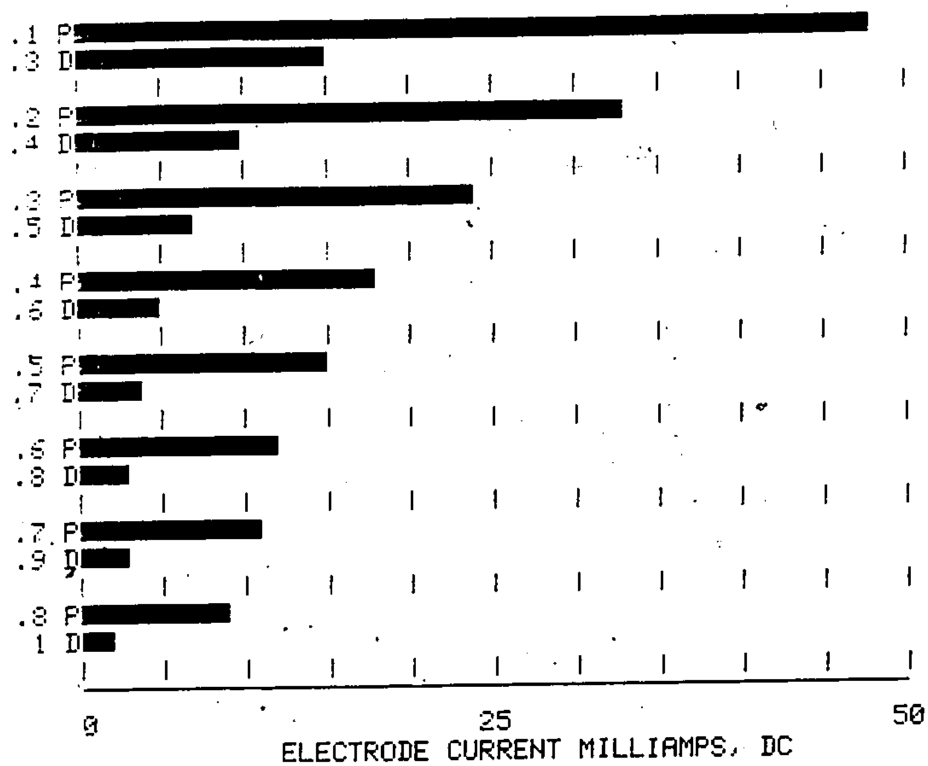

FIGURE. 5.12 C.

THROUGHPUT FOR PROXIMAL (P) AND DISTAL (D) INPUTS
CONSTANT BETWEEN RANK SPACING
DENSITY= 6 - SPACING= .2
INPUT-OUTPUT DISTANCE AS SHOWN AT LEFT

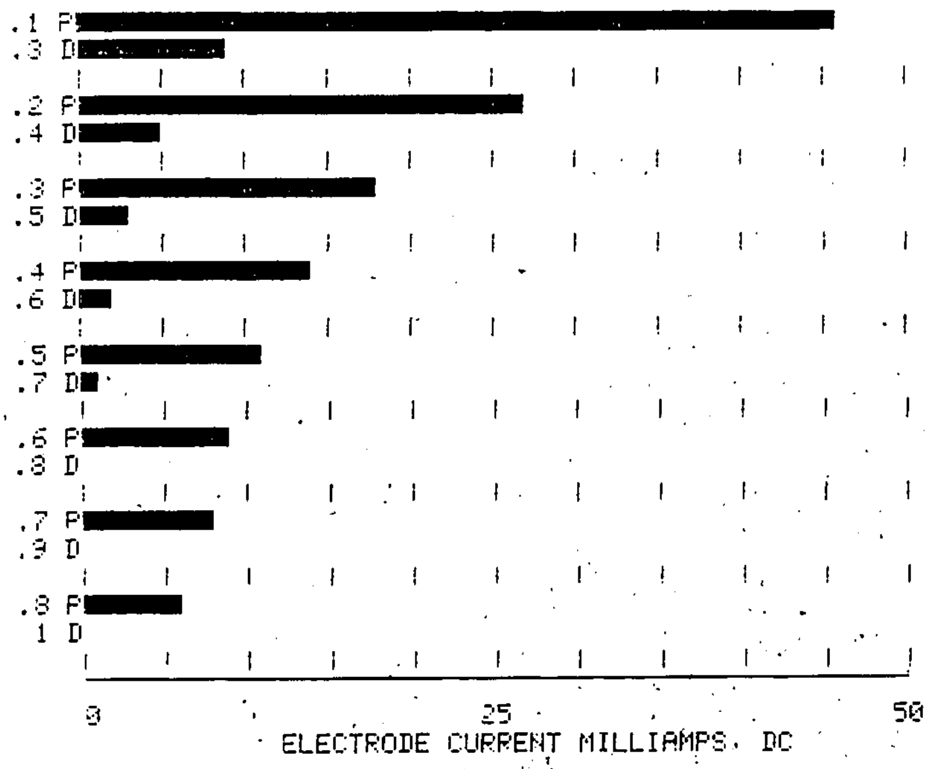

FIGURE. 5.12 D

THROUGHPUT FOR PROXIMAL (P) AND DISTAL (D) INPUTS
CONSTANT BETWEEN RANK SPACING
DENSITY= 10 - SPACING= .2
INPUT-OUTPUT DISTANCE AS SHOWN AT LEFT

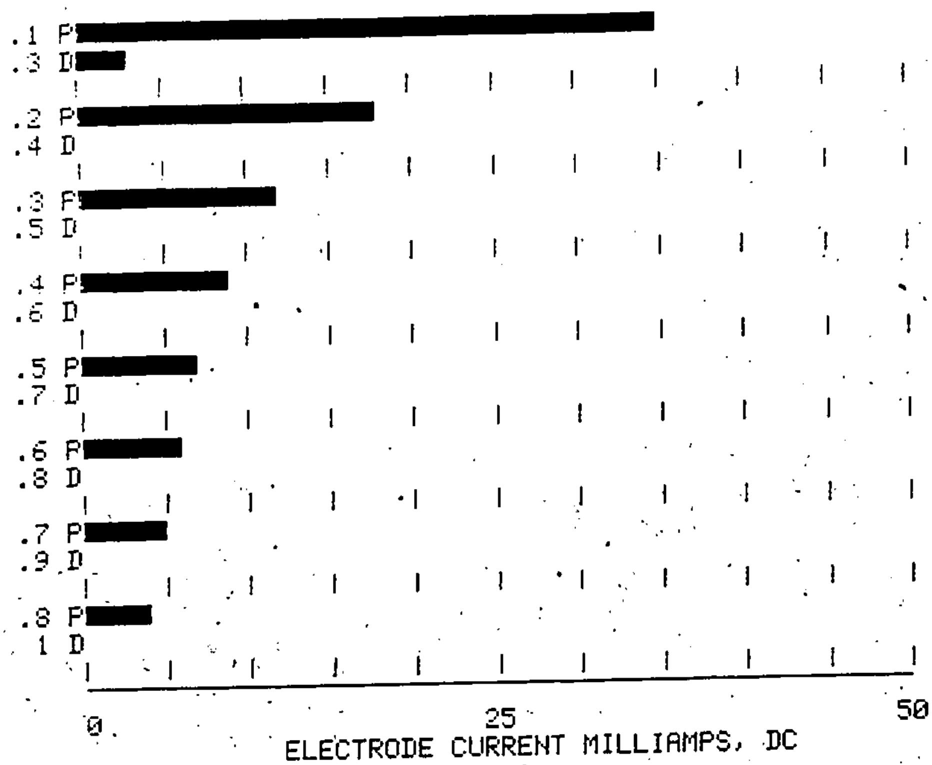

FIGURE. 5.13 A

THROUGHPUT FOR PROXIMAL (P) AND DISTAL (D) INPUTS
CONSTANT BETWEEN RANK SPACING
DENSITY= 2 - SPACING= .3
INPUT-OUTPUT DISTANCE AS SHOWN AT LEFT

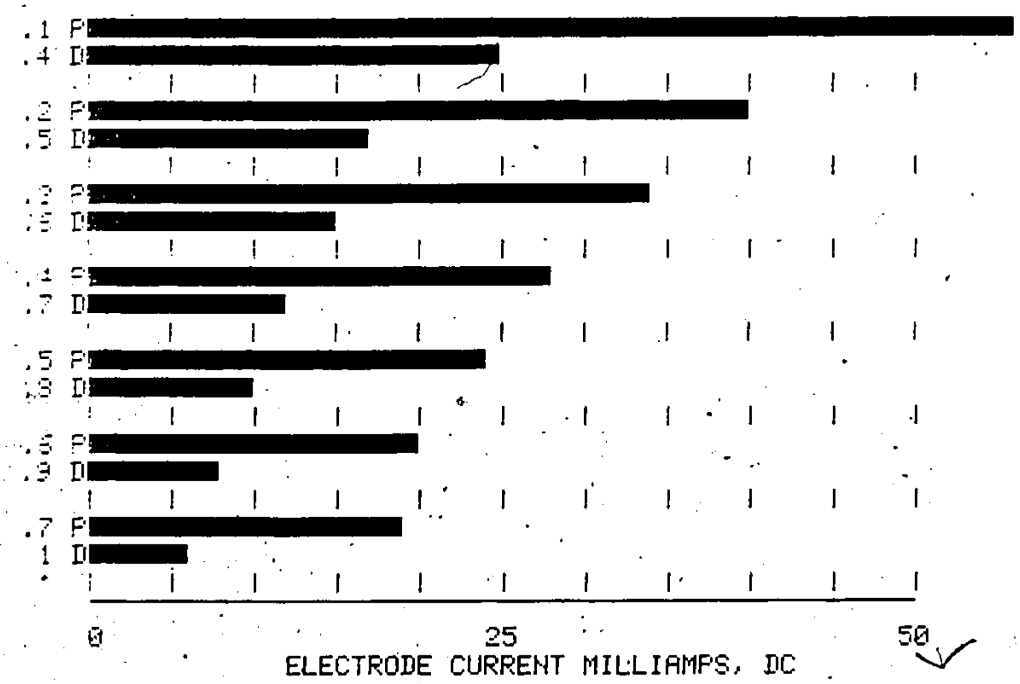

FIGURE. 5.13 B

THROUGHPUT FOR PROXIMAL (P) AND DISTAL (D) INPUTS
CONSTANT BETWEEN RANK SPACING
DENSITY= 4 - SPACING= .3
INPUT-OUTPUT DISTANCE AS SHOWN AT LEFT

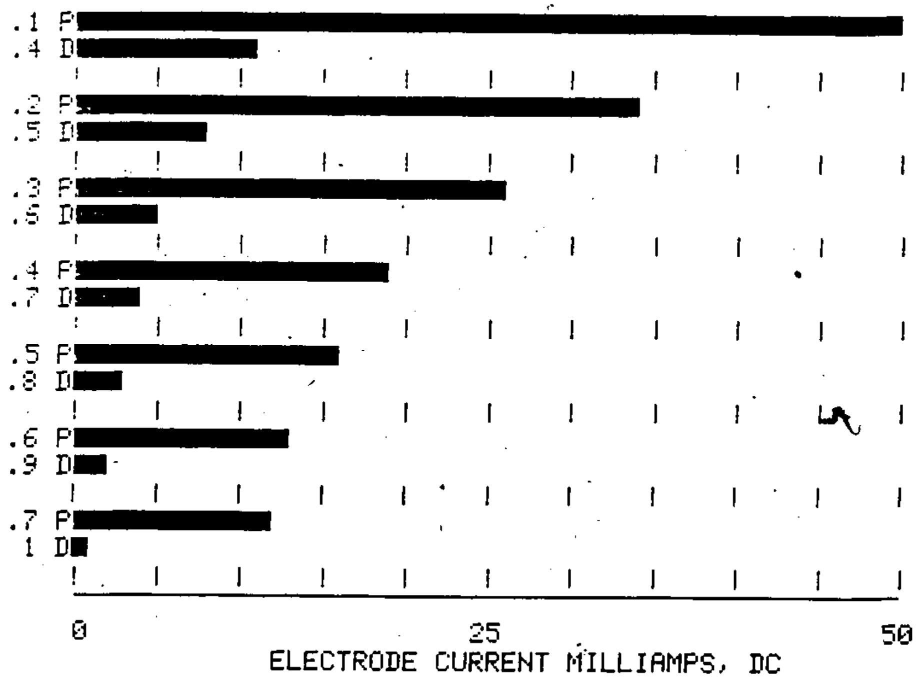

FIGURE. 5.13 C

THROUGHPUT FOR PROXIMAL (P) AND DISTAL (D) INPUTS
CONSTANT BETWEEN RANK SPACING
DENSITY= 6 - SPACING= .3
INPUT-OUTPUT DISTANCE AS SHOWN AT LEFT

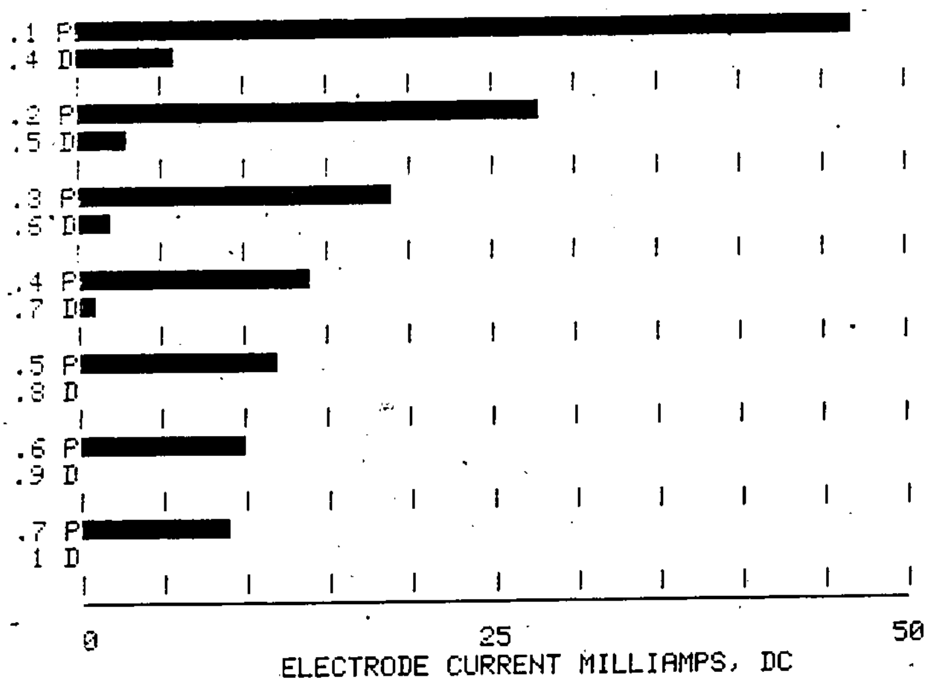

FIGURE. 5.13 D

THROUGHPUT FOR PROXIMAL (P) AND DISTAL (D) INPUTS
CONSTANT BETWEEN RANK SPACING
DENSITY= 10 - SPACING= .3
INPUT-OUTPUT DISTANCE AS SHOWN AT LEFT

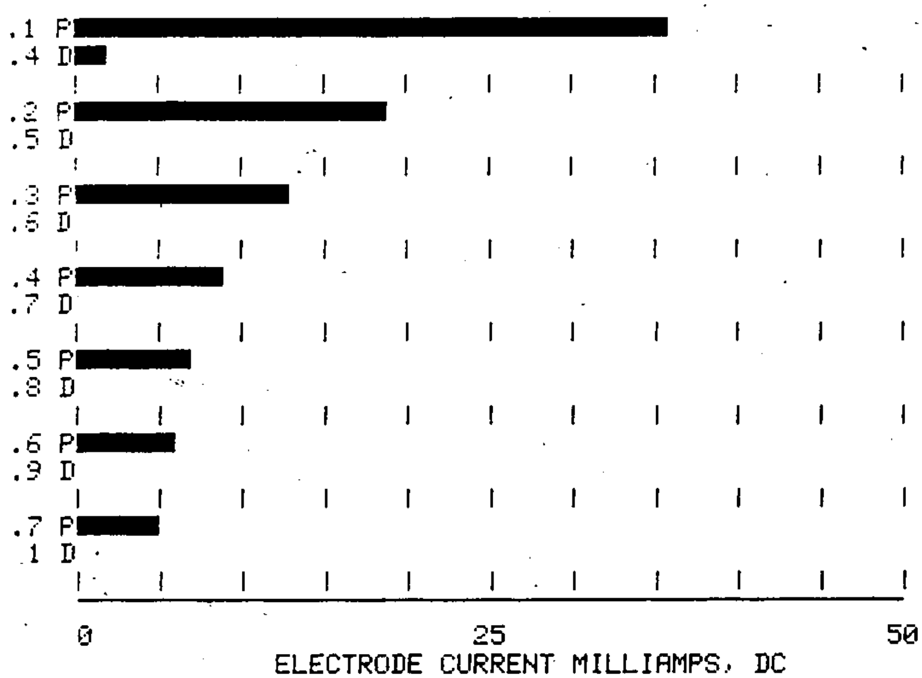

READY.

FIGURE. 5.14

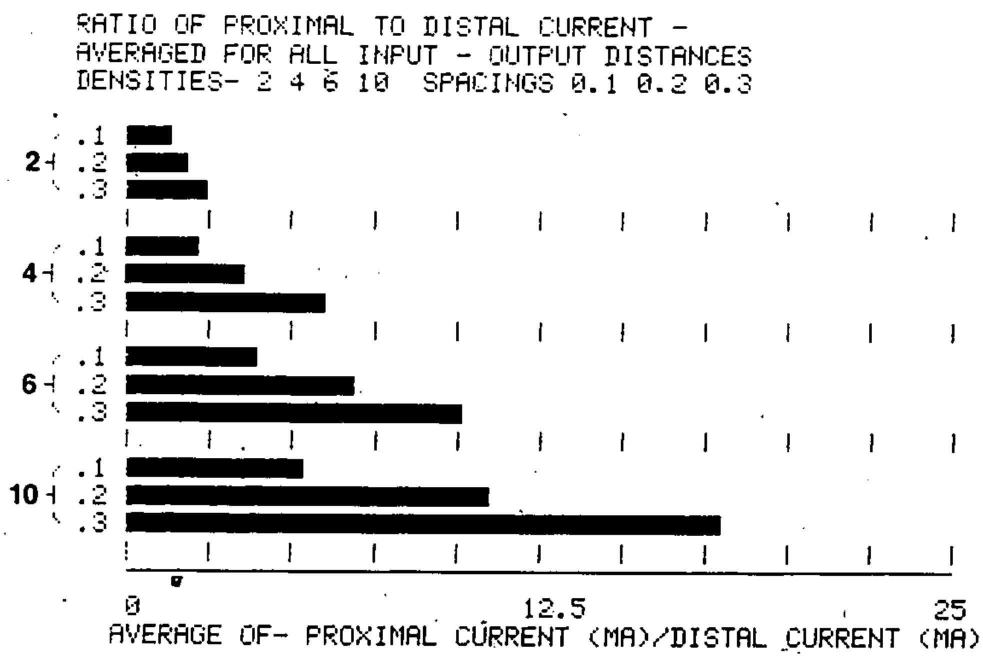
RATIO OF PROXIMAL TO DISTAL CURRENT -
AVERAGED FOR ALL INPUT - OUTPUT DISTANCES
DENSITIES- 2 4 6 10 SPACINGS 0.1 0.2 0.3
2
4
6
10
.1
.2
.3
0
12.5
25
AVERAGE OF- PROXIMAL CURRENT (MA)/DISTAL CURRENT (MA)

FIGURE. 5.15 A

THROUGHPUT FOR PROXIMAL (P) AND DISTAL (D) INPUTS
RANK 1 CONSTANT - RANK 2 VARIABLE
DENSITY= 2
INPUT-OUTPUT DISTANCE AS SHOWN AT LEFT

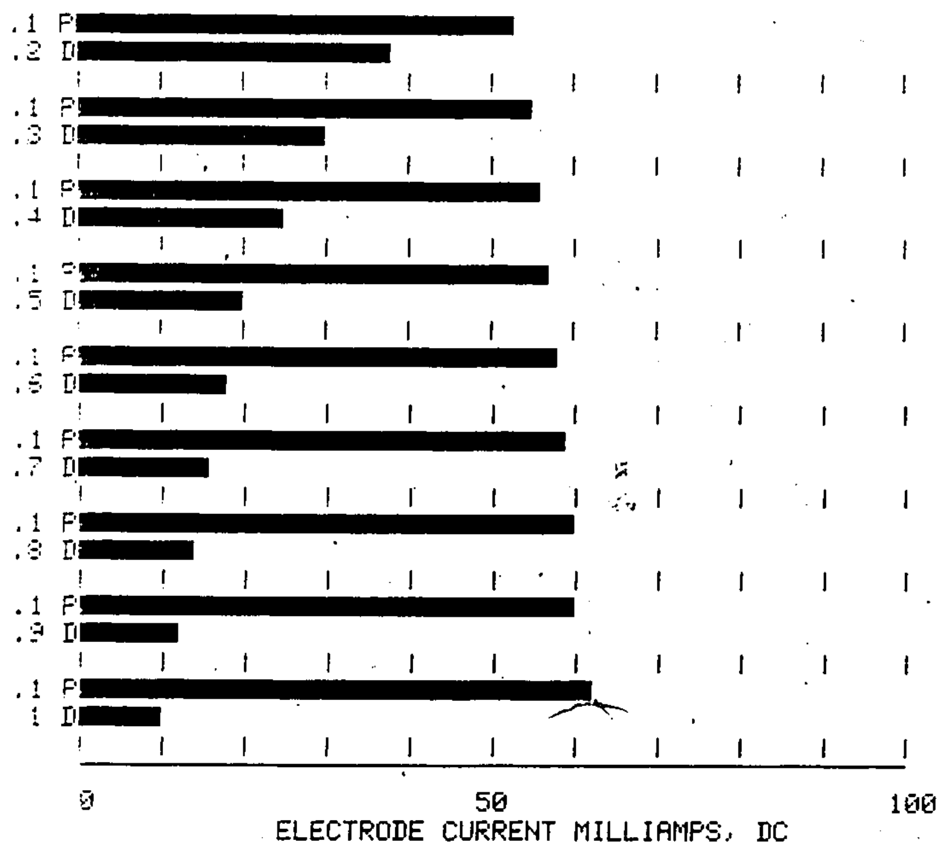

FIGURE. 5.15 B

THROUGHPUT FOR PROXIMAL (P) AND DISTAL (D) INPUTS
RANK 1 CONSTANT - RANK 2 VARIABLE
DENSITY= 4
INPUT-OUTPUT DISTANCE AS SHOWN AT LEFT

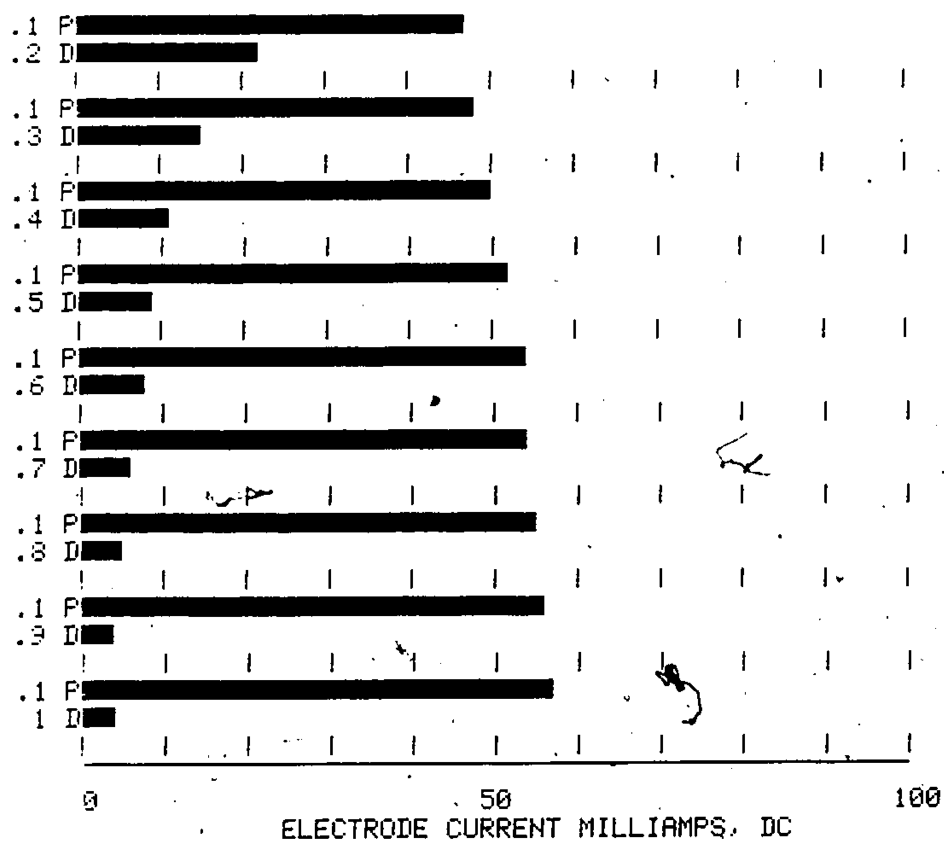

FIGURE. 5.15 C

THROUGHPUT FOR PROXIMAL (P) AND DISTAL (D) INPUTS
RANK 1 CONSTANT - RANK 2 VARIABLE
DENSITY= 6
INPUT-OUTPUT DISTANCE AS SHOWN AT LEFT

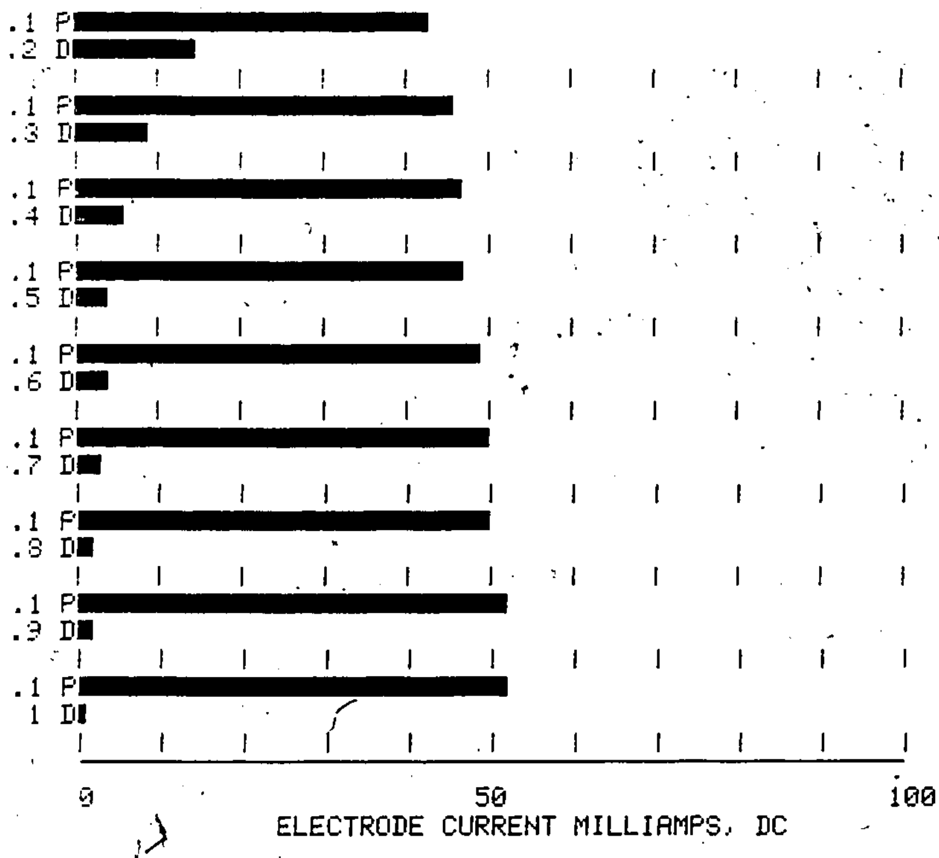

FIGURE. 5.15 D

THROUGHPUT FOR PROXIMAL (P) AND DISTAL (D) INPUTS
RANK 1 CONSTANT - RANK 2 VARIABLE
DENSITY= 10
INPUT-OUTPUT DISTANCE AS SHOWN AT LEFT.

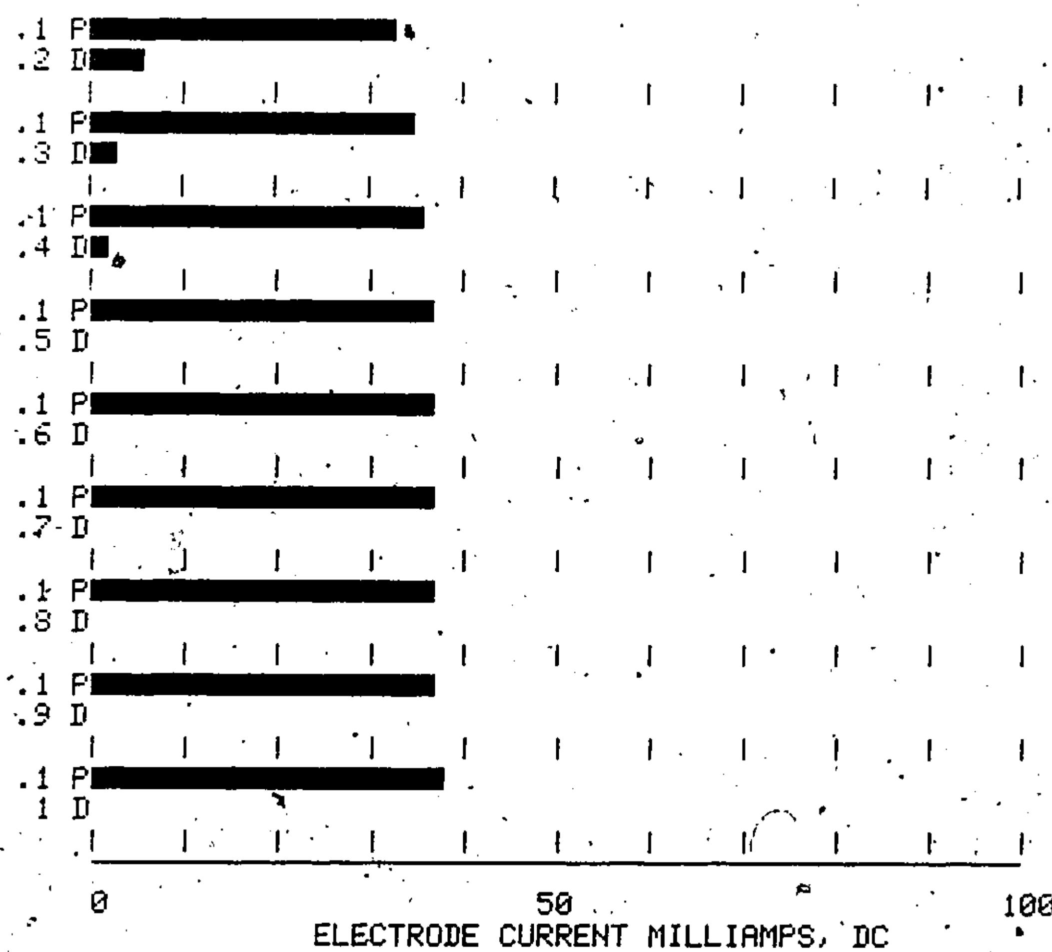

distance of one unit when the proximal rank is positioned at Ø.1 through Ø.9 units from the discharge boundary (Fig. 5.16, A, B, C, and D). Under these conditions, the distal rank shows little change in Q, while the proximal rank varies widely.

5.2.3.4 The Rank Spacing Rule

All of these analyses show that, in general terms, the ratios of individual rank 1 to rank 2 input Q's are direct functions of rank spacing and input density and an inverse function of output distance.

5.2.4 TWO RANK UNEQUAL DENSITY EXPERIMENTS

5.2.4.1 Purpose

These experiments are designed to quantify the effect of increasing inequality of density between two dissimilar ranks of inputs on their relative Q values.

5.2.4.2 Description

As before, two ranks of inputs were introduced along lines parallel to the discharge boundary of the unit square analogue medium. The input density of one rank was fixed at one. The second was given densities of Ø, 1, 2, 4, 6, and 1Ø inputs, spaced according to the formulas in Table 5.1. The rank positions were fixed at Ø.333 and Ø.666 units from the discharge boundary.

FIGURE. 5.16.A

THROUGHPUT FOR PROXIMAL (P) AND DISTAL (D) INPUTS
RANK 1 VARIABLE - RANK 2 CONSTANT
DENSITY= 2
INPUT-OUTPUT DISTANCE AS SHOWN AT LEFT

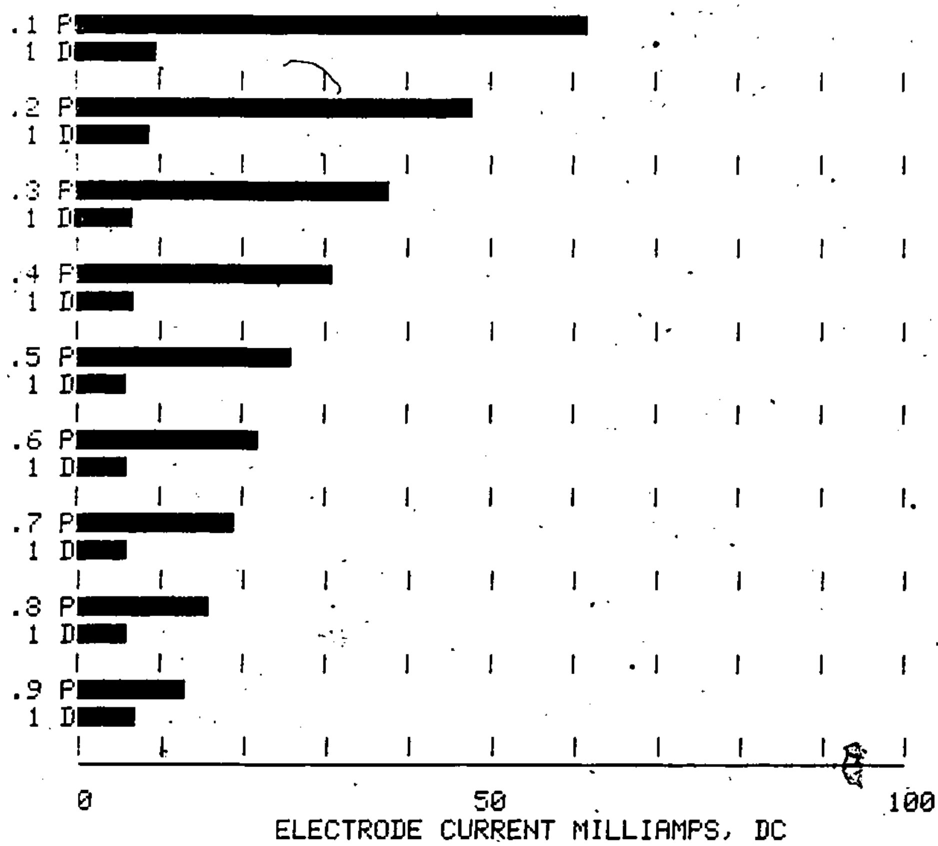

FIGURE. 5.16 B

THROUGHPUT FOR PROXIMAL (P) AND DISTAL (D) INPUTS
RANK 1 VARIABLE - RANK 2 CONSTANT
DENSITY= 4
INPUT-OUTPUT DISTANCE AS SHOWN AT LEFT

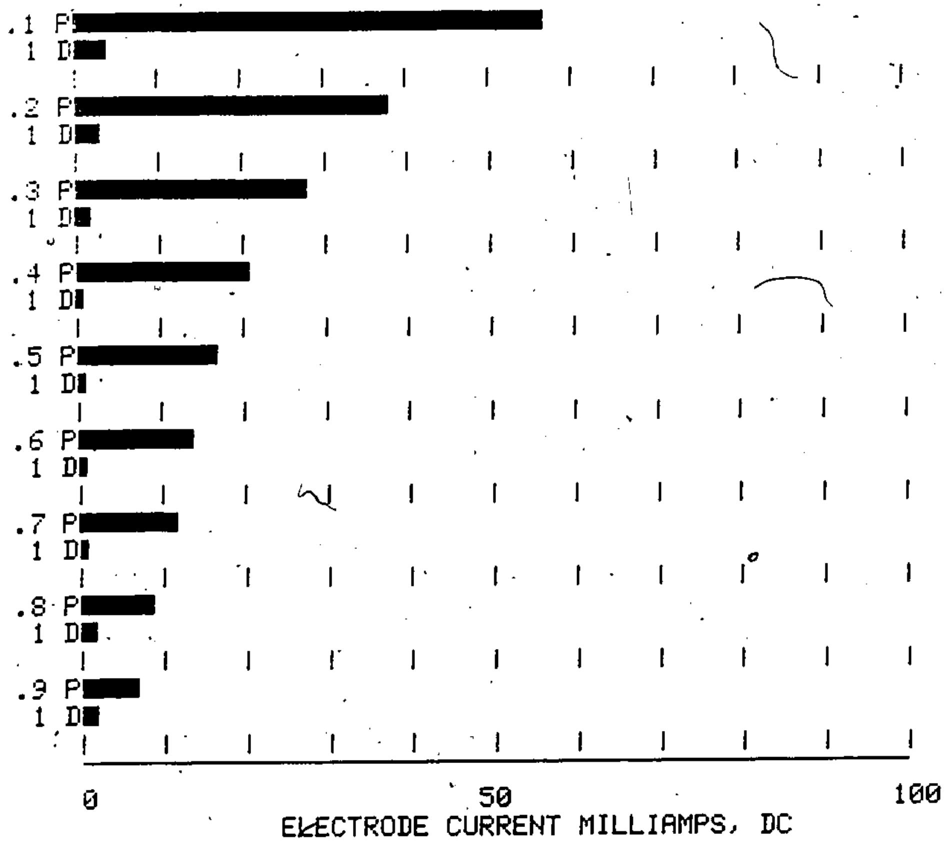

FIGURE. 5.16 C

THROUGHPUT FOR PROXIMAL (P) AND DISTAL (D) INPUTS
RANK 1 VARIABLE - RANK 2 CONSTANT
DENSITY= 6
INPUT-OUTPUT DISTANCE AS SHOWN AT LEFT

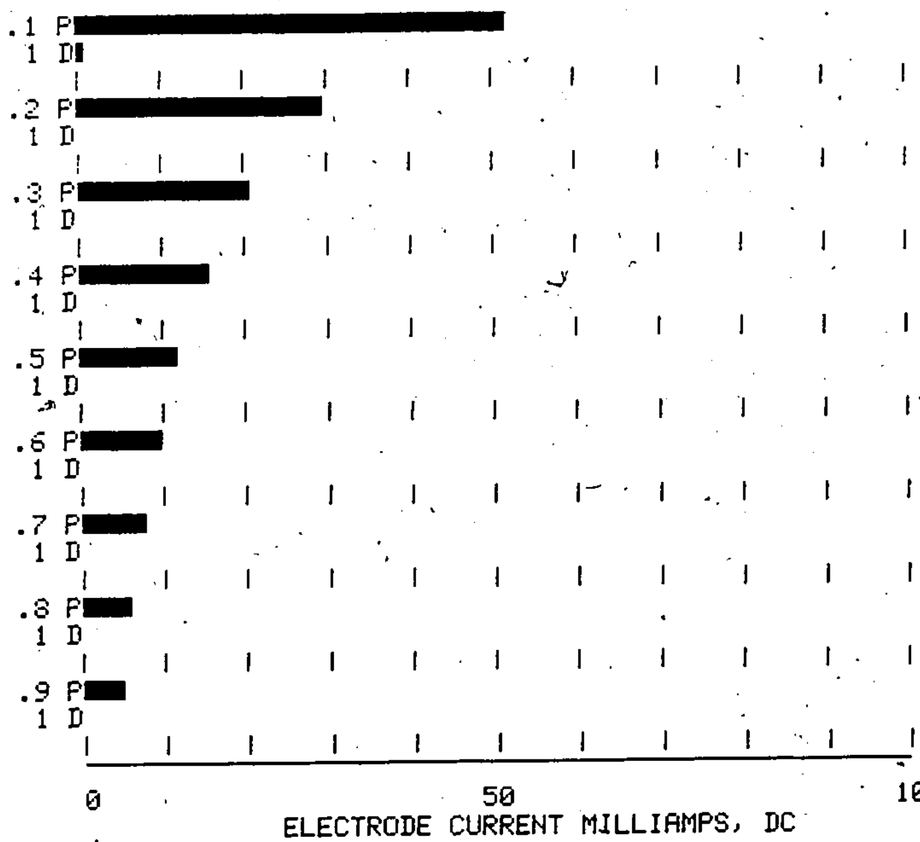

FIGURE. 5.16 D

THROUGHPUT FOR PROXIMAL (P) AND DISTAL (D) INPUTS
RANK 1 VARIABLE - RANK 2 CONSTANT
DENSITY= 10
INPUT-OUTPUT DISTANCE AS SHOWN AT LEFT.

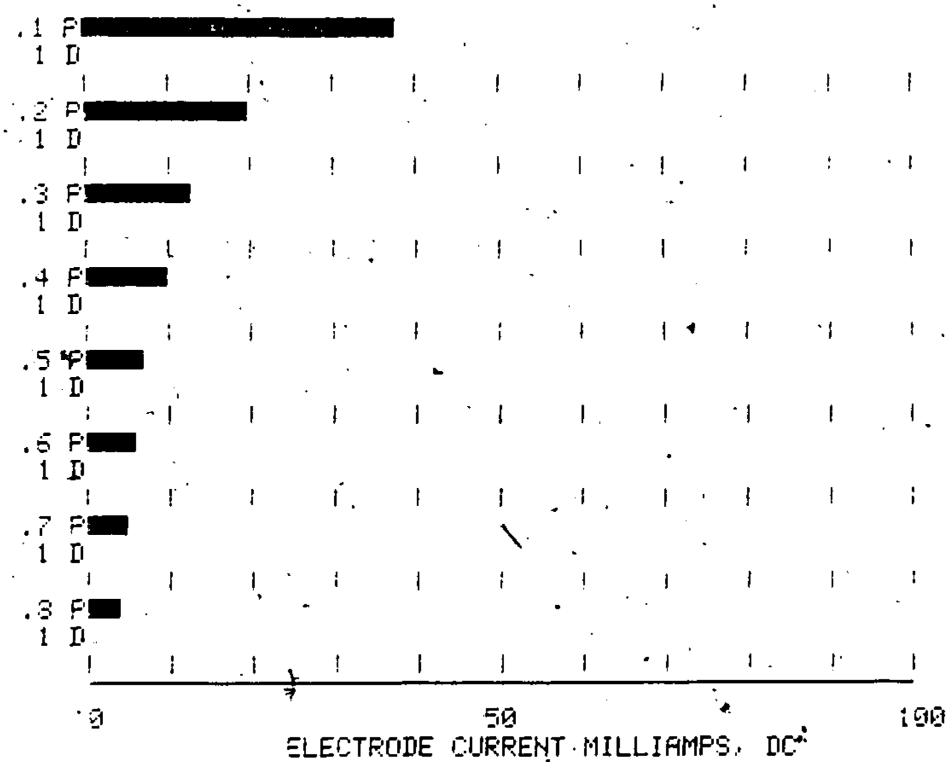

Experiments were conducted with the single input in both the proximal and distal positions. Because the spacing between the electrode of the single input rank and the electrodes in the adjoining rank is non-uniform at densities above two, the electrodes in the multiple input rank will have slightly different Q values. For this reason, average Q values appear in the Table 5.6 and are used in constructing Figures 5.17 and 5.18.

5.2.4.3 Results

The distal rank, whether single or multiple, shows nearly identical individual Q values for a given density of the multiple rank (Fig. 5.17). The distal rank showed a very strong density effect. Q values for both single and multiple distal input ranks were depressed by more than 80% as density increased from 1 to 10. Proximal ranks showed a great disparity between multiple and single rank Q values. The single input proximal rank shows a 26% depression at maximum density, while a multiple input rank shows a depression of 71% over this density range.

Total Q values change little with density when the distal rank is multiple, in comparison to those with the multiple rank in the proximal position (Fig. 5.18). The latter show a 76% increase in total throughput with an increase from density 1 to density 10.

Table 5.6

TWO RANK UNEQUAL DENSITY EXPERIMENTS - INPUT Q (mA)

<table>
<tr><th>POSITION</th><th colspan="10">INPUT NUMBER</th></tr>
<tr><th></th><th>1</th><th>2</th><th>3</th><th>4</th><th>5</th><th>6</th><th>7</th><th>8</th><th>9</th><th>10</th></tr>
<tr><td>Density=10/1</td><td colspan="10"></td></tr>
<tr><td>Distal</td><td colspan="10" align="center">2</td></tr>
<tr><td>Proximal</td><td>10</td><td>10</td><td>10</td><td>10</td><td>10</td><td>10</td><td>10</td><td>10</td><td>10</td><td>10</td></tr>
<tr><td>Distal</td><td>4</td><td>4</td><td>4</td><td>3</td><td>3</td><td>3</td><td>3</td><td>4</td><td>4</td><td>4</td></tr>
<tr><td>Proximal</td><td colspan="10" align="center">26</td></tr>
<tr><td>Density=6/1</td><td colspan="10"></td></tr>
<tr><td>Distal</td><td colspan="6" align="center">6</td><td colspan="4"></td></tr>
<tr><td>Proximal</td><td>16</td><td>16</td><td>16</td><td>16</td><td>16</td><td>16</td><td colspan="4"></td></tr>
<tr><td>Distal</td><td>7</td><td>7</td><td>6</td><td>6</td><td>7</td><td>7</td><td colspan="4"></td></tr>
<tr><td>Proximal</td><td colspan="6" align="center">28</td><td colspan="4"></td></tr>
<tr><td>Density=4/1</td><td colspan="10"></td></tr>
<tr><td>Distal</td><td colspan="4" align="center">9</td><td colspan="6"></td></tr>
<tr><td>Proximal</td><td>21</td><td>21</td><td>21</td><td>21</td><td colspan="6"></td></tr>
<tr><td>Distal</td><td>10</td><td>9</td><td>9</td><td>10</td><td colspan="6"></td></tr>
<tr><td>Proximal</td><td colspan="4" align="center">29</td><td colspan="6"></td></tr>
<tr><td>Density=2/1</td><td colspan="10"></td></tr>
<tr><td>Distal</td><td colspan="2" align="center">17</td><td colspan="8"></td></tr>
<tr><td>Proximal</td><td>30</td><td>30</td><td colspan="8"></td></tr>
<tr><td>Distal</td><td>17</td><td>17</td><td colspan="8"></td></tr>
<tr><td>Proximal</td><td colspan="2" align="center">32</td><td colspan="8"></td></tr>
<tr><td>Density=1/1</td><td colspan="10"></td></tr>
<tr><td>Distal</td><td>23</td><td colspan="9"></td></tr>
<tr><td>Proximal</td><td>35</td><td colspan="9"></td></tr>
</table>

Figure 5.17
Comparison of individual input Q for proximal and distal arrays where the two arrays have differing densities.

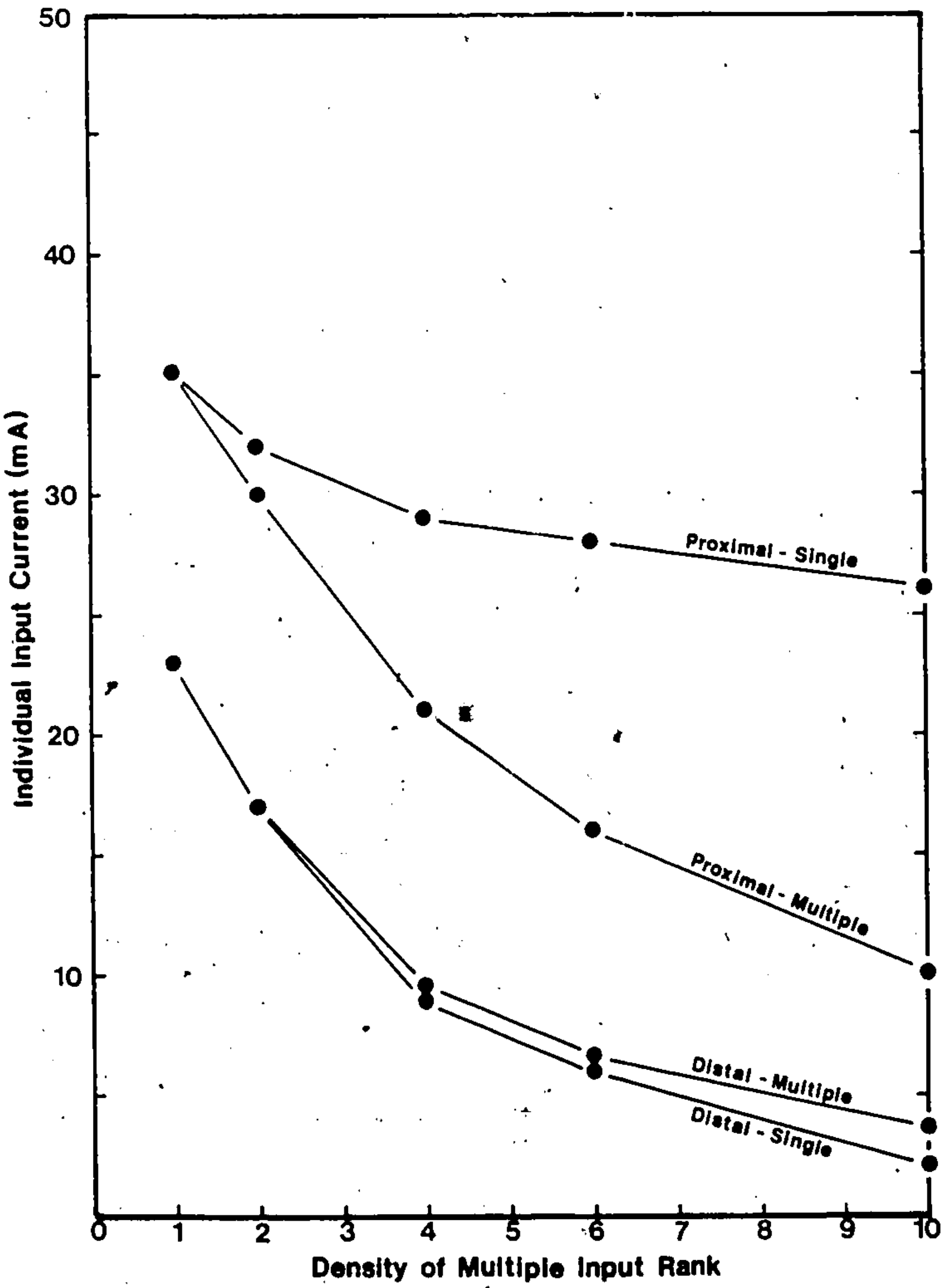
50
40
30
20
10
Individual Input Current (mA)
0 1 2 3 4 5 6 7 8 9 10
Density of Multiple Input Rank
Proximal - Single
Proximal - Multiple
Distal - Multiple
Distal - Single

Figure 5.18
Comparison of total rank input Q for proximal and distal arrays where the two arrays have differing densities.

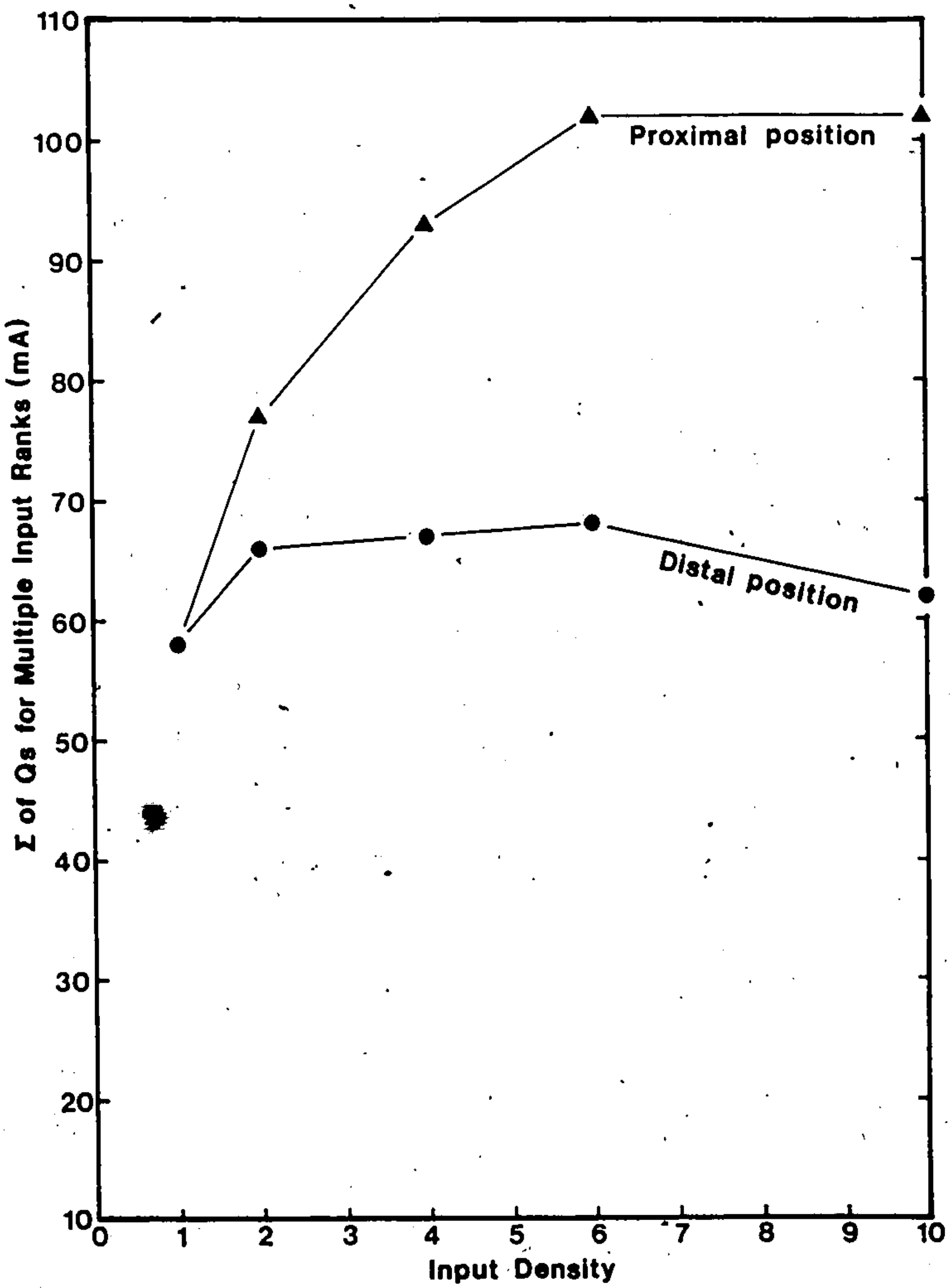
110
100
90
80
70
60
50
40
30
20
10
Σ of Qs for Multiple Input Ranks (mA)
Proximal position
Distal position
0
1
2
3
4
5
6
7
8
9
10
Input Density

5.2.4.4 The Unequal Density Rule

Whether single or multiple, distal input ranks are characterized by small Q values and greatest sensitivity to density. Proximal input ranks have higher Q values with great sensitivity to density when the rank has multiple inputs, and minimal sensitivity to density when the rank is single.

5.3 POINT RESURGENCE

ELECTRIC ANALOGUE EXPERIMENTS

These experiments evaluate initial conditions of flow through inputs to a rectangular bedding plane segment, discharging to a single point. Several input patterns, densities, and spacings were evaluated in terms of flow rate (Q) at the inputs, given a constant head. In analogue terms, input electrode current flow (I) was measured at a constant potential (e).

5.3.1 ASYMMETRICAL MULTIPLE INPUT EXPERIMENTS

5.3.1.1 Purpose

These experiments determine the variation in throughput (Q) for individual inputs as a function of input density and the spacing between a rank of inputs and the single output point. They apply specifically to two dimensional flow fields of square geometry.

5.3.1.2 Description

A linear array of 3, 5, and 10 inputs was established parallel to one of the unit square parting boundaries (Fig. 5.19). The point resurgence was located 0.2 units from that boundary and at a distance from an adjacent boundary equal to 1/2 of the spacing between the inputs. Input spacing followed the rule for earlier experiments (Table 5.1). The distance between the input rank and the output was varied between 0.2 and 0.8 units, measured normal to the input rank axis. Input potentials were held at 20 volts to achieve better resolution for inputs of low Q. Individual currents were measured for each input and corrected for the internal resistance of the measuring instrument.

5.3.1.3 Expected Results

The input output distance for any linear input array discharging to a point cannot be the same for more than two inputs. With the geometry of these experiments, every input has a unique distance from the ouput. Because throughput is inversely related to this quantity, all inputs should differ in this respect. Number 1 inputs (Fig. 5.19) have the shortest mean flow paths and should have the largest Q. Higher numbered inputs should have progressively lower throughput. As the ratio of the orthogonal input output distance to the input array axis length increases, the

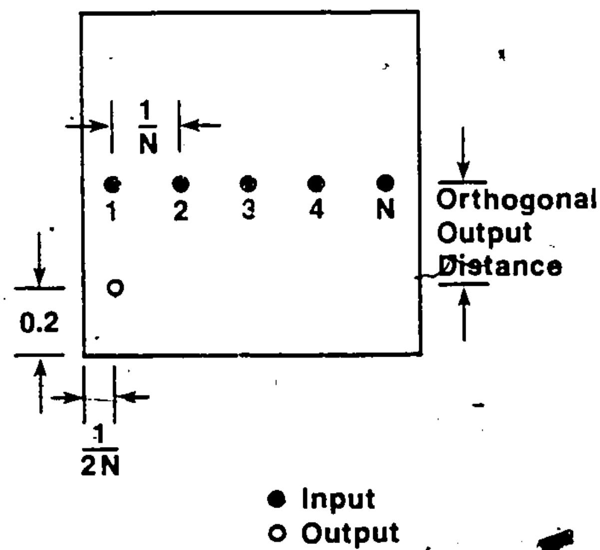

Figure 5.19
Input-output configuration for asymmetrical, multiple input, electric analogue experiments.

length of the mean flow paths for the several inputs becomes more similar. Therefore, their individual Q values should become more similar. Conversely, when the ratio is small, the individual Q values should become more disparate.

As input density increases, we expect that total throughput will increase, but individual input Q values will decrease, based upon the values already obtained in the density experiments. As density increases the mean flow path for distal inputs increases. Thus, it follows that density should also affect the inequality of individual input Q values.

5.3.1.4 Measured Results

The data derived from these experiments are presented in Table 5.7 and Figures 5.20, 5.21, 5.22, and 5.23. The five electrode experiments are typical; they show Q to be strongly influenced by input position (Fig. 5.20). Proximal inputs are characterized by high Q values, with decreasing values for more distal inputs. Figure 5.20 also shows Q values to be a strong inverse function of orthogonal output distance for the proximal electrode (1) and a weak direct function of that distance for the most distal electrode (5).

The data further show that the individual Q values are an inverse function of input density. Figure 5.21 is a plot of Q vs. input positions for input densities of 10, 5,

Table 5.7

ASYMMETRICAL MULTIPLE INPUT EXPERIMENTS - INPUT Q (mA)

Distance	INPUT NUMBER									
	1	2	3	4	5	6	7	8	9	10
Density=10										
4	9	8	7	6	5	4	3	2	2	2
2	19	14	10	7	4	3	2	1	<1	<1
Density=5										
1	50	23	11	6	4					
2	31	20	12	7	5					
3	23	17	12	8	6					
4	18	15	11	8	7					
5	15	13	11	8	7					
6	13	12	10	8	8					
7	12	11	10	8	8					
8	11	10	9	8	7					
Density=3										
4	26	19	14							
2	38	22	13							

Figure 5.2Ø

Comparison of individual input Q for inputs 1 - 5 for orthogonal input-output distances of Ø.1 - Ø.8 units.

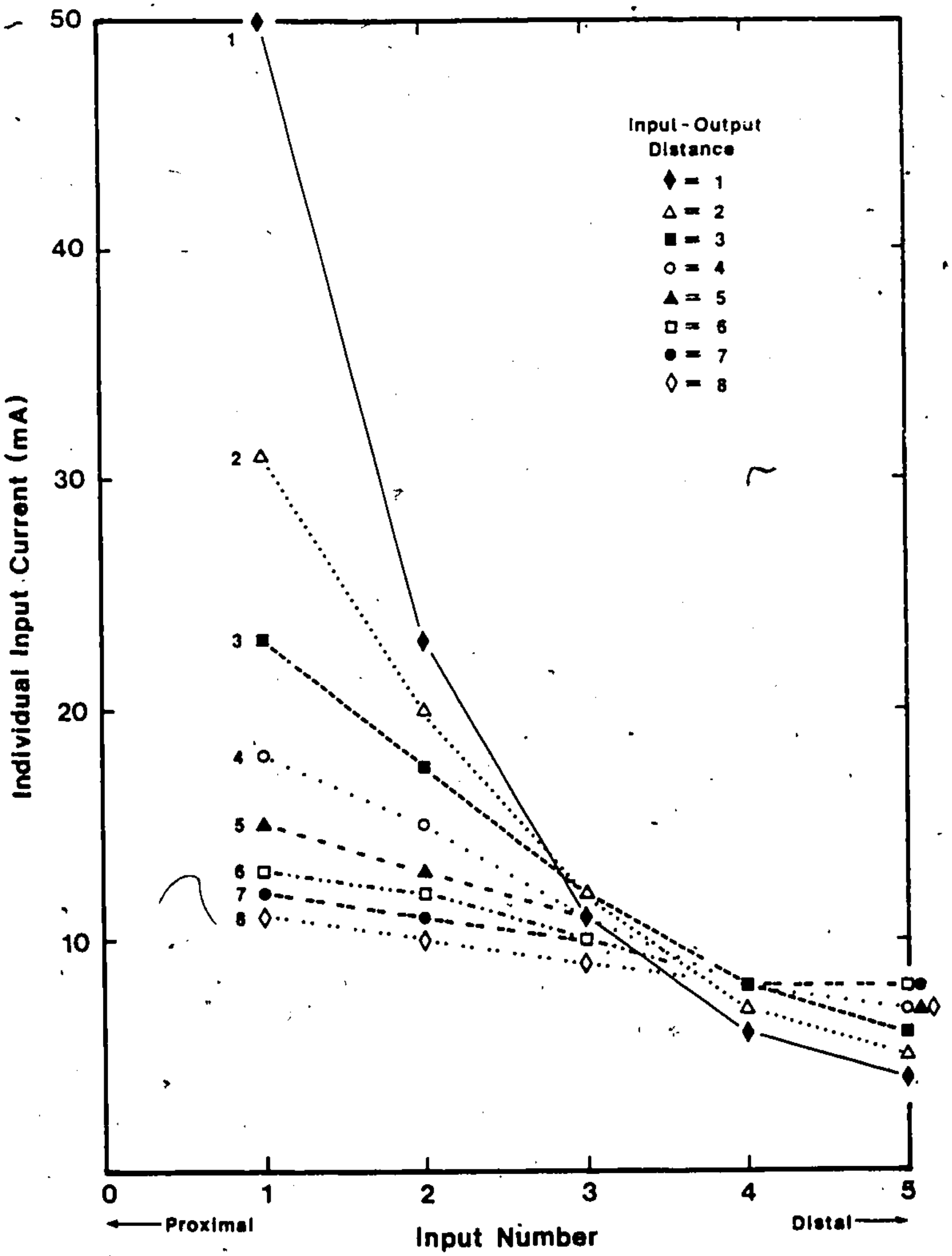
Input - Output
Distance
♦ = 1
△ = 2
■ = 3
○ = 4
▲ = 5
□ = 6
● = 7
◊ = 8
Individual Input Current (mA)
50
40
30
20
10
0
1
2
3
4
5
6
7
8
Proximal
Input Number
Distal

Figure 5.21

Comparison of individual input Q for each input in arrays of densities 3, 5, and 1Ø. Orthogonal input output distance is Ø.4 units.

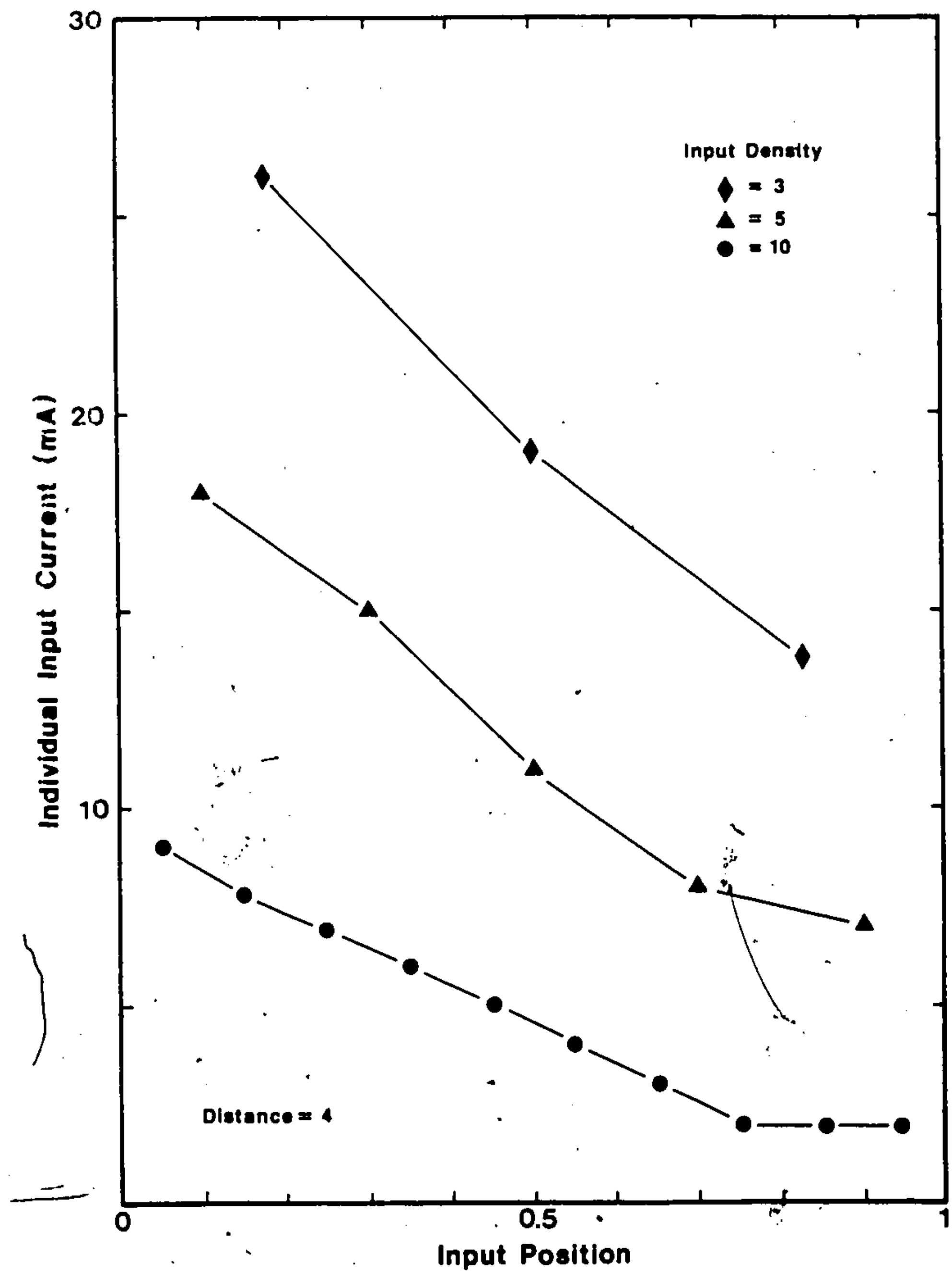
Input Density
= 3
= 5
= 10
Distance = 4
Individual Input Current (mA)
Input Position
30
20
10
0
0.5
1

Figure 5.22

Comparison of individual input Q, as percent of the proximal input, for each input in arrays of densities 3, 5, and 10. Orthogonal input-output distance is 0.4 units.

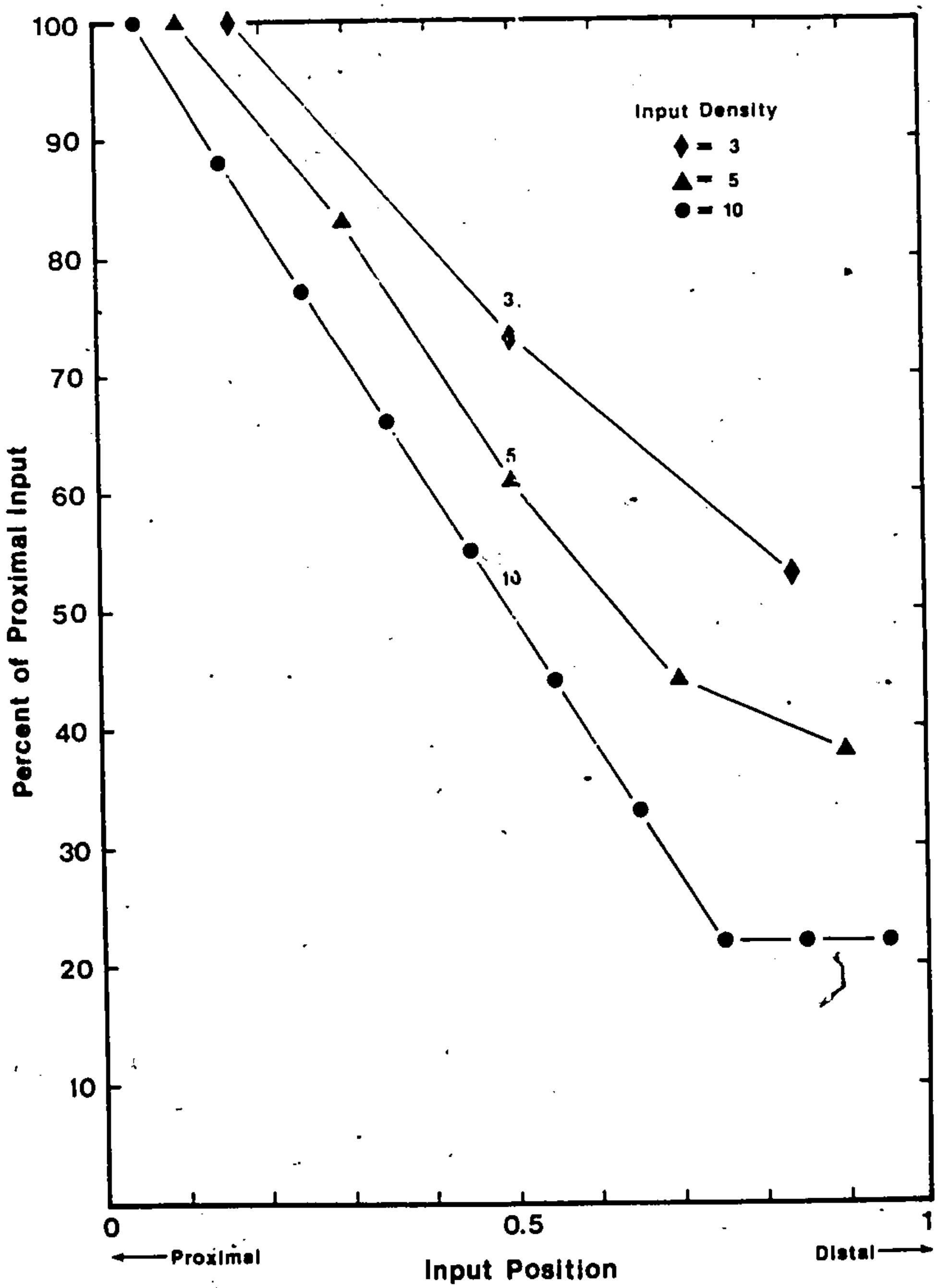

Percent of Proximal Input
100
90
80
70
60
50
40
30
20
10
Input Density
= 3
= 5
= 10
3.
5
10
0
0.5
1
Proximal
Input Position
Distal

Figure 5.23.

Ratio of proximal input Q to distal input Q as a function of orthogonal input-output distance. Error bars denote the value of $\pm$ one digit in the least significant position for the digital current meter.

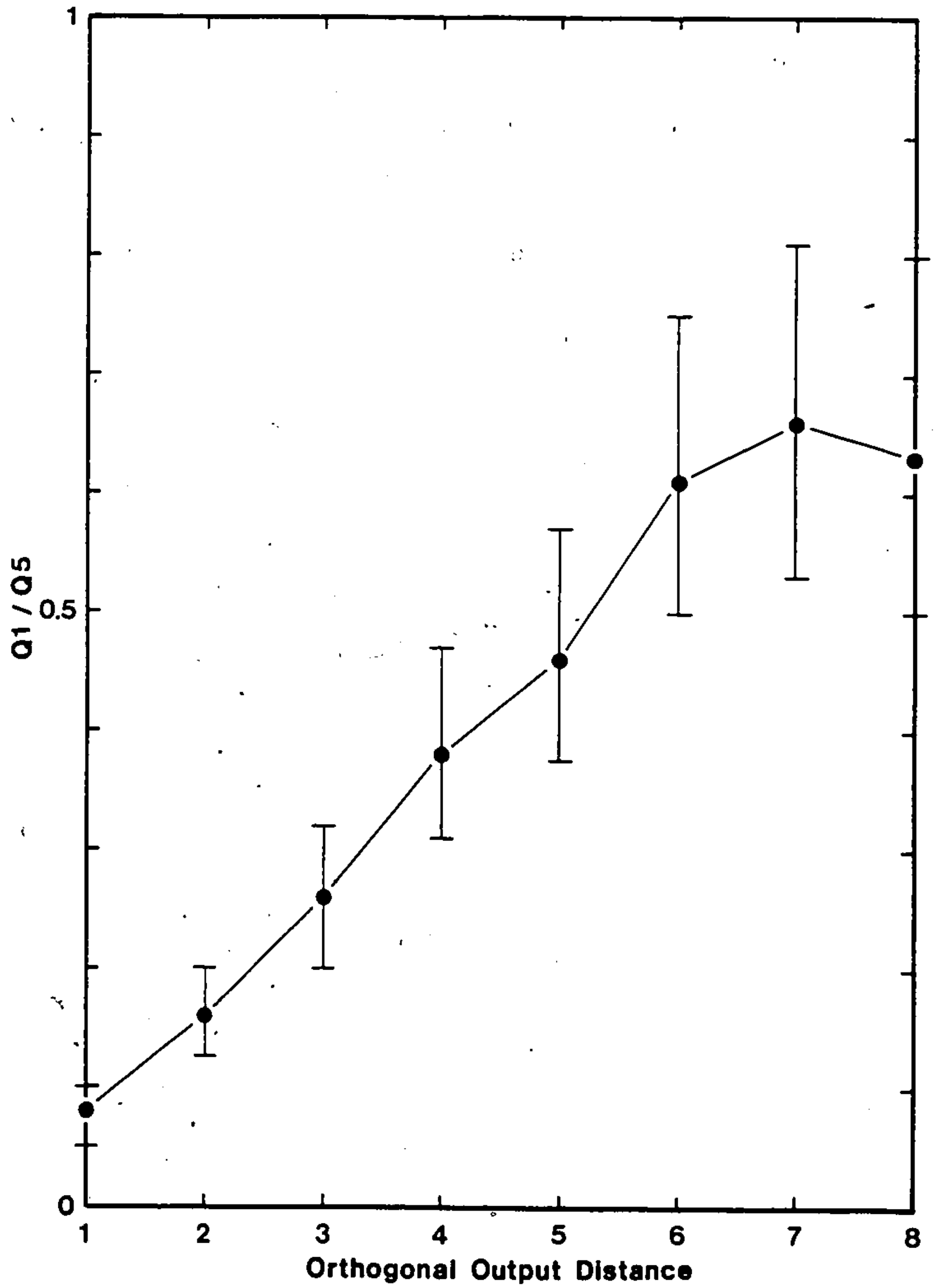
1
0.5
0
Q1 / Q5
1
2
3
4
5
6
7
8
Orthogonal Output Distance

and 3 at a common orthogonal distance of Ø.4 units. The plot indicates Q differences of as much as a factor of 7 for similar positions at different densities. By plotting the individual input Q values as a percent of the proximal value, the effect of density on the disparity of Q values within each experiment can be eliminated, and the proximal-distal disparity compared. Figure 5.22 is such a plot and demonstrates the increase of this inequality with increasing input density. By plotting the ratio of the distal to proximal Q values as a function of orthogonal distance for a single density, the disparity of individual Q values can be assessed (Fig. 5.23). These data confirm the expectation that disparity of these values is an inverse function of the ratio between orthogonal distance and the array axis length. This is to say that, for a given input spread, individual Q values become more similar as their distance from the output point increases.

5.3.1.5 The Asymmetrical Point Resurgence Rules

In hydrologic terms, these experiments indicate that the throughput at a ground water input to a planar parting is maximum for a proximal input and inversely proportional to its orthogonal distace and the input density of the array of which it is a part. Throughput is minimum for a distal input, directly proportional to its orthogonal distance and inversely proportional to input density. Disparity of Q values between proximal and distal inputs is an inverse function of the orthogonal distance/array axis length ratio.

5.3.2 SYMMETRICAL MULTIPLE INPUT EXPERIMENTS

5.3.2.1 Purpose

These experiments deal with collinear, multiple input arrays discharging to a point (Fig. 5.24). They determine the variation in throughput (Q) as a function of input density and position.

5.3.2.2 Description

Successively, 1, 2, 4, 6, and 8 input electrodes were introduced along the central axis of the unit square, electric analogue medium. The sink electrode was fixed at Ø.2 units from the boundary on the same axis. Electrode spacings are given in Table 5.8. It should be noted that the first electrode was fixed at Ø.4 units. All input electrodes were held at a potential of 2Ø volts relative to the sink electrode. Individual currents were measured to the nearest 1 mA and corrected for the internal resistance of the measuring instrument.

5.3.2.3 Expected Results

Like the previous experiments, these consist of linear arrays discharging to a point. Therefore, all inputs

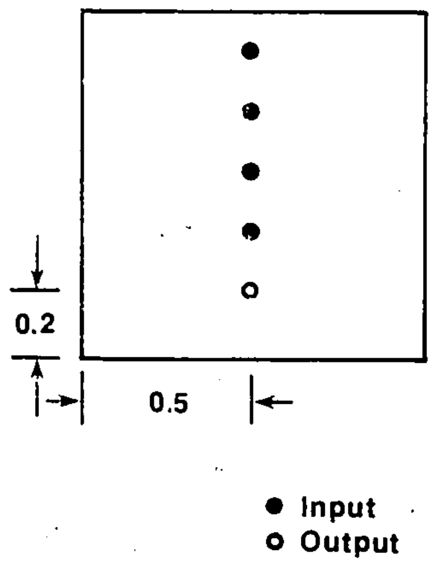

Figure 5.24
Input-output configuration for symmetrical, multiple input, electric analogue experiments.

Table 5.8

SYMMETRICAL POINT RESURGENCE EXPERIMENTS
INPUT POSITIONS

Density	INPUT POSITION (UNITS)							
	1	2	3	4	5	6	7	8
1	Ø.4							
2	Ø.4	Ø.8						
4	Ø.4	Ø.57	Ø.74	Ø.91				
6	Ø.4	Ø.51	Ø.62	Ø.73	Ø.84	Ø.94		
8	Ø.4	Ø.48	Ø.56	Ø.64	Ø.72	Ø.8Ø	Ø.88	Ø.96

have unique mean flow path lengths. Because throughput is inversely related to these distances, the proximal inputs should possess the highest throughput, with decreasing flow for inputs at greater distances. Because the space within the flow medium is divided among all the inputs, we expect decreasing throughput for all inputs as density increases. The sum of all Q values should increase as density increases, but because each additional input extends the line of inputs further from the output, this effect should be less pronounced than in the linear resurgence cases.

5.3.2.4 Measured Results

Figure 5.25 and Table 5.9 shows the recorded data to be consistent with the expectations. The inputs exhibit a systematic lowering of Q with distance from the discharge point. The data also show a lowering of individual Q values with increasing input density. Figure 5.26 shows the throughput at input 1, the stationary input, exhibits a change in Q by a factor of 2.26 with a density increase of 1 to 8. The sum of Q values over all inputs shows a slight increase with increasing density, as expected.

Total Q data from single rank linear resurgence experiments, asymmetrical point resurgence experiments, and symmetrical point resurgence experiments are plotted in Figure 5.27. To standardize the comparisons, these data are taken from experiments where the orthogonal input-output

Figure 5.25
Comparison of individual input Q for each input in symmetrical arrays with densities of 1, 2, 4, 6, and 8.

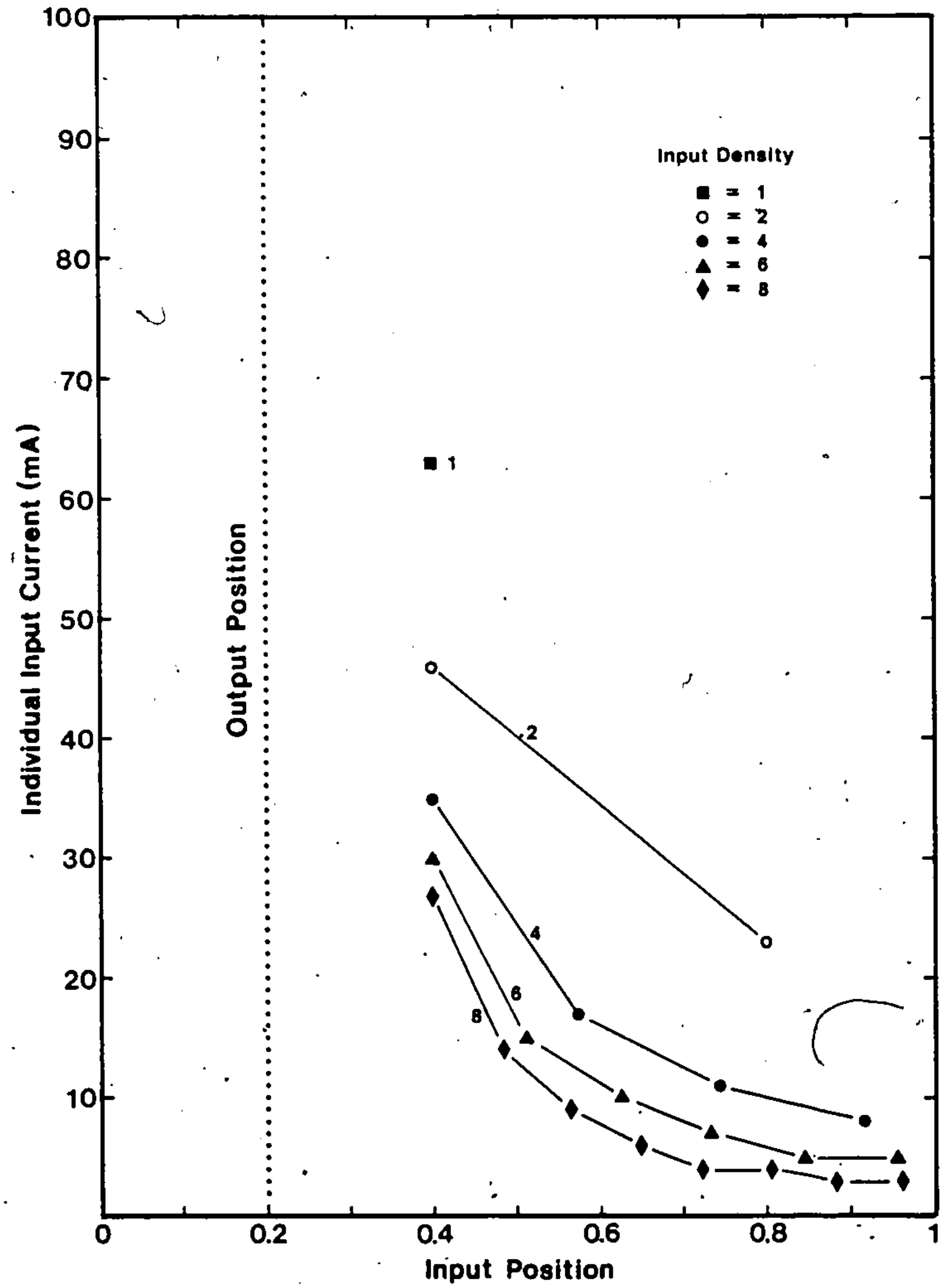
Individual Input Current (mA)
Input Position
Output Position
Input Density
■ = 1
○ = 2
● = 4
▲ = 6
♦ = 8
100
90
80
70
60
50
40
30
20
10
0
0.2
0.4
0.6
0.8
1

Table 5.9

SYMMETRICAL POINT RESURGENCE EXPERIMENTS - INPUT Q (mA)

Density	INPUT NUMBER							
	1	2	3	4	5	6	7	8
1	63							
2	46	23						
4	35	17	11	8				
6	30	15	10	7	5	5		
8	27	14	9	6	4	4	3	3

FIGURE. 5.26

SUM OF Q VALUES FOR EACH INPUT DENSITY
INPUT DENSITIES AS SHOWN AT LEFT
SYMMETRICAL POINT RESURGENCE EXPERIMENTS

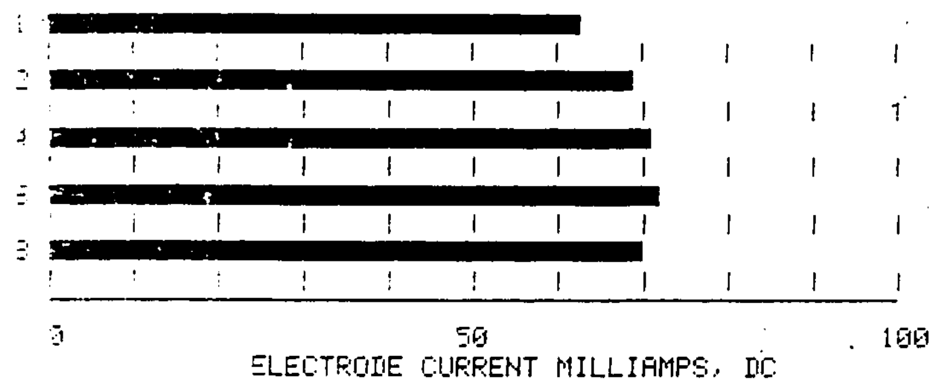

Figure 5.27
Total Q data for single rank linear resurgence, asymmetrical point resurgence, and symmetrical point resurgence experiments.

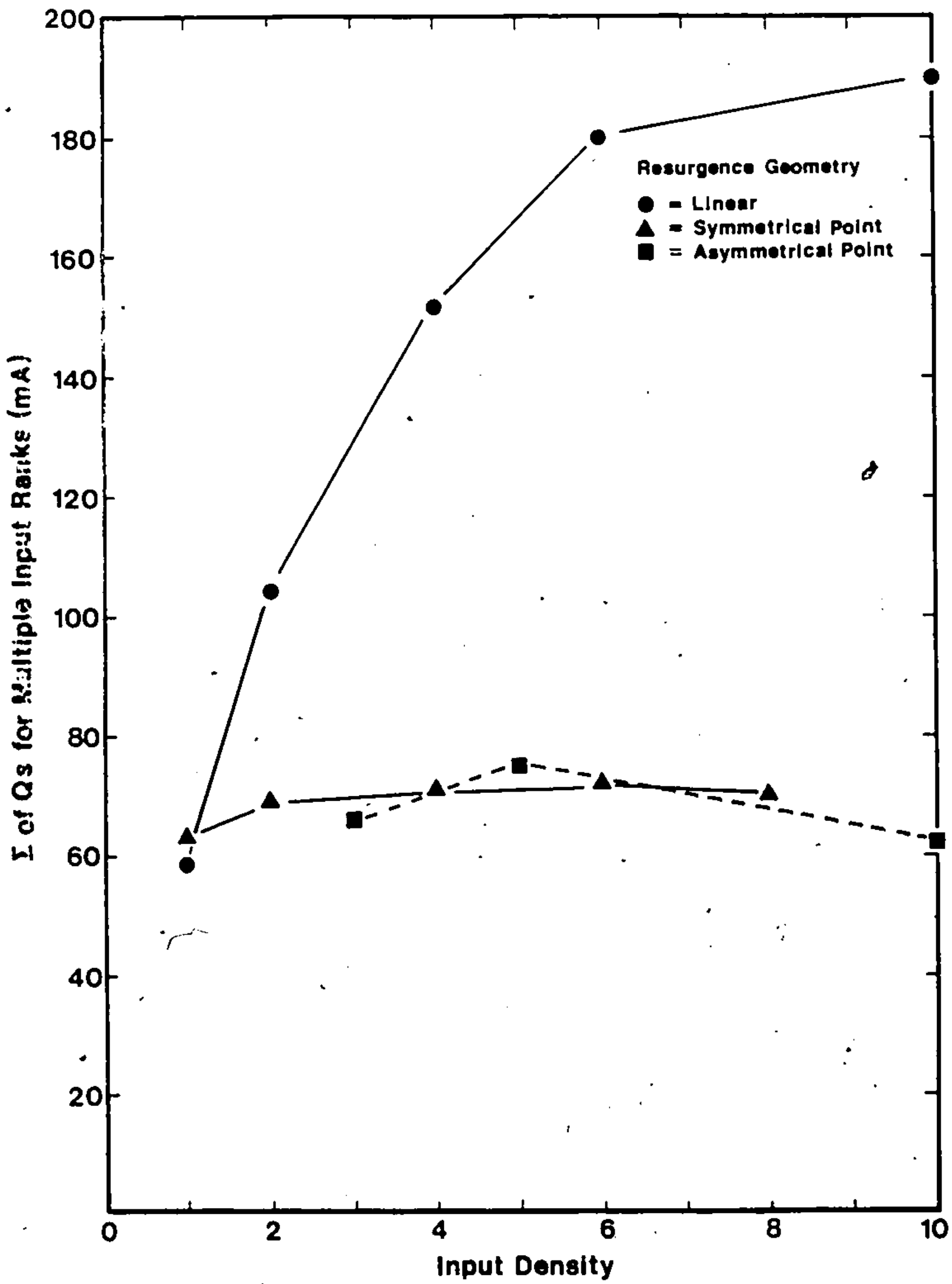

200
180
160
140
120
100
80
60
40
20
0
2
4
6
8
10
Input Density
Σ of Qs for Multiple Input Ranks (mA)
Resurgence Geometry
● = Linear
▲ = Symmetrical Point
■ = Asymmetrical Point

distance is equal to Ø.2 units or, in the case of the symmetrical input experiment, the distance from the proximal input to the output is Ø.2 units.

This comparison reveals that total Q is greatly enhanced by incresing density in the case of linear resurgence experiments. In point resurgence experiments, the gain is very small. This disparity is principally due to the geometry of the input-output systems. In the linear output case, the mean flow path for each input is identical. In the point resurgence cases, the additional inputs have dimishing effectiveness in augmenting the flow because of their increasinly long mean flow paths.

5.3.2.5 Symmetrical Point Resurgence Rules

In hydrologic terms, the symmetrical point resurgence experiments indicate that the throughput at a ground water input to a planar parting is inversely porportional to the output distance and inversely proportional to input density. These rules are a restatement of the distance and density rules formulated for the linear output geometry.

5.4 COMBINED FLOW RULE

The potential for limestone removal along a parting is related directly to the Q per unit area. This quantity is directly proportional to input density, but significantly greater in the presence of linear resurgences.

CHAPTER 6

FLOW ENVELOPE EXPERIMENTS

6.1 INTRODUCTION

These experiments delineate the flow domains associated with the individual inputs of the electric analogue experiments just described. They show clearly the location of the principal flow vector, which coincides well with the early course of the principal tube in a developing network. These experiments also assist in outlining the pattern of network growth for arrays of inputs which are too complex to be easily handled in solution experiments.

The boundaries in these experiments are in every way equivalent to those already described for the electric analogues in Chapter 5. The similitude arguments relating these experiments to natural geologic situations are given in Chapter 3.4. Like the electric analogues, these experiments deal primarily with flow conditions in a state prior to the evolution of significant solution voids in the carbonate rocks.

At several points in the course of this research, the filtration model was used to visualize a flow envelope of special relevance to another experiment. These uses are not reported in this chapter, but are inserted at the point of use. What is reported here are the flow envelope experiments which are of more general use in the remainder of the text.

6.2 THE ORIENTATION EXPERIMENTS

6.2.1 FLOW ENVELOPES, A FUNCTION OF PRESSURE FIELDS

In a series of important papers, Ford (1965, 1968, 1971, 1977) developed the concepts of "dip tubes" and "anastomotic bands" as end members in a series of solution forms found associated with bedding planes. Dip tubes were defined as simple, often solitary, solution forms developed in closely spaced parallel arrays oriented within a few degrees of the dip in steeply inclined carbonate rocks. Anastomotic bands, on the other hand, were described as anastomosing networks of tubes, sometimes in widely spaced subparallel arrays, which are endemic to near horizontally bedded carbonates. It was implicit in Ford's arguments that gravitational differences in these two structural settings, affecting the flow of groundwater entrained in the bedding planes, accounted for these differences.

That these differences of bedding plane forms are correlated with the two different geologic situations is not questioned here. Ford's observations are supported by the this author's own field experience. What is in question is the reason for this dichotomy. Waterman (1975) made an exhaustive search for pattern differences in laboratory solution experiments with a wide range of dip angles and found none.

Darcy (1856) demonstrated that water flows through porous media in response to hydraulic gradient. The standard apparatus used to demonstrate the Darcy relationship is constructed in a manner which permits the flow within the porous medium to be directed at any angle with respect to the gravitational gradient (Fig. 6.1). It can thus be shown that the orientation of the medium has no effect on the velocity of through-flowing fluids. Todd (1960 p. xxx) states:

> "A common misinterpretation of Darcy's Law involves the statement that flow takes place from high to low pressure. For horizontal flow this is true...but for inclined flow, water may actually flow in the direction of increasing pressure."

Figure 6.1 is a case in point.

It can likewise be shown that the form of the flow envelope in a planar conductive medium is also unaffected by its orientation relative to the gravitational gradient.

6.2.2 PURPOSE AND DESCRIPTION OF THE EXPERIMENTS

The purpose of this experiment series is to test the hypothesis that the flow envelope associated with an input point to a planar conductive medium is unaffected by the orientation of the medium. The unit square flow envelope apparatus was provided with a single input point at its

Figure 6.1
Apparatus used for demonstration of the Darcy relationship; after Todd (1959).

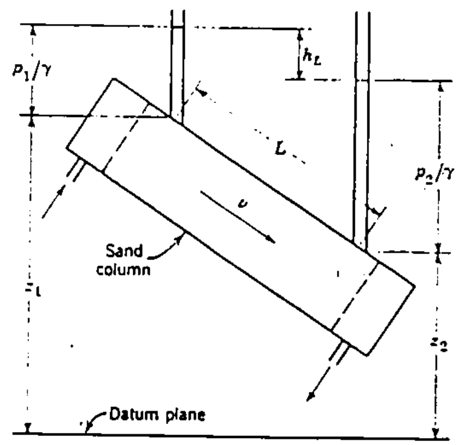

Figure 6.1
Apparatus used for demonstration of the Darcy relationship; after Todd (1959).

center and a linear discharge boundary along one side (Fig. 6.2). A head of 10 cm relative to the output was impressed at the input. The coloured water was permitted to flow until the dye envelope reached a point of tangency with the discharge boundary. This procedure was repeated twice in each of four orientations: horizontal, vertical with upward directed flow, vertical with horizontally directed flow, and vertical with downward directed flow (Fig. 6.2 A-D).

6.2.3 RESULTS

If the orientation of the medium does not affect the flow envelope, the dye patterns in each case should be indistinguishable. Figure 6.2 shows that this is the case. Therefore, the cause of the pattern differences observed by Ford in the two structural settings must lie elsewhere. The explanation may be found in inherent differences in the input-output geometry of the two structural settings. This concept will be explored at length in Chapter 10. It should be noted before leaving this subject, however, that the experiments just described are conducted in a saturated flow environment. Unsaturated flow would evidence a strong gravity orientation. In this instance, the terms saturated and unsaturated are used in the physical rather than the chemical sense, describing the degree to which the pore space is occupied by water. Figure 6.3 depicts an experiment combining saturated and unsaturated flow regions

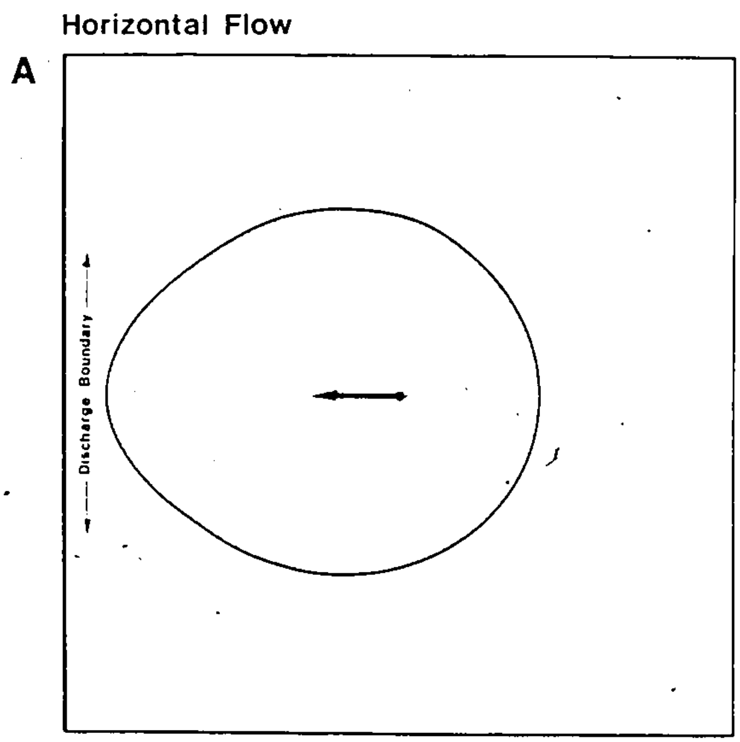

Figure 6.2 A, B, C, D
Flow envelopes for a single point input with four orientations of the principal flow vector.

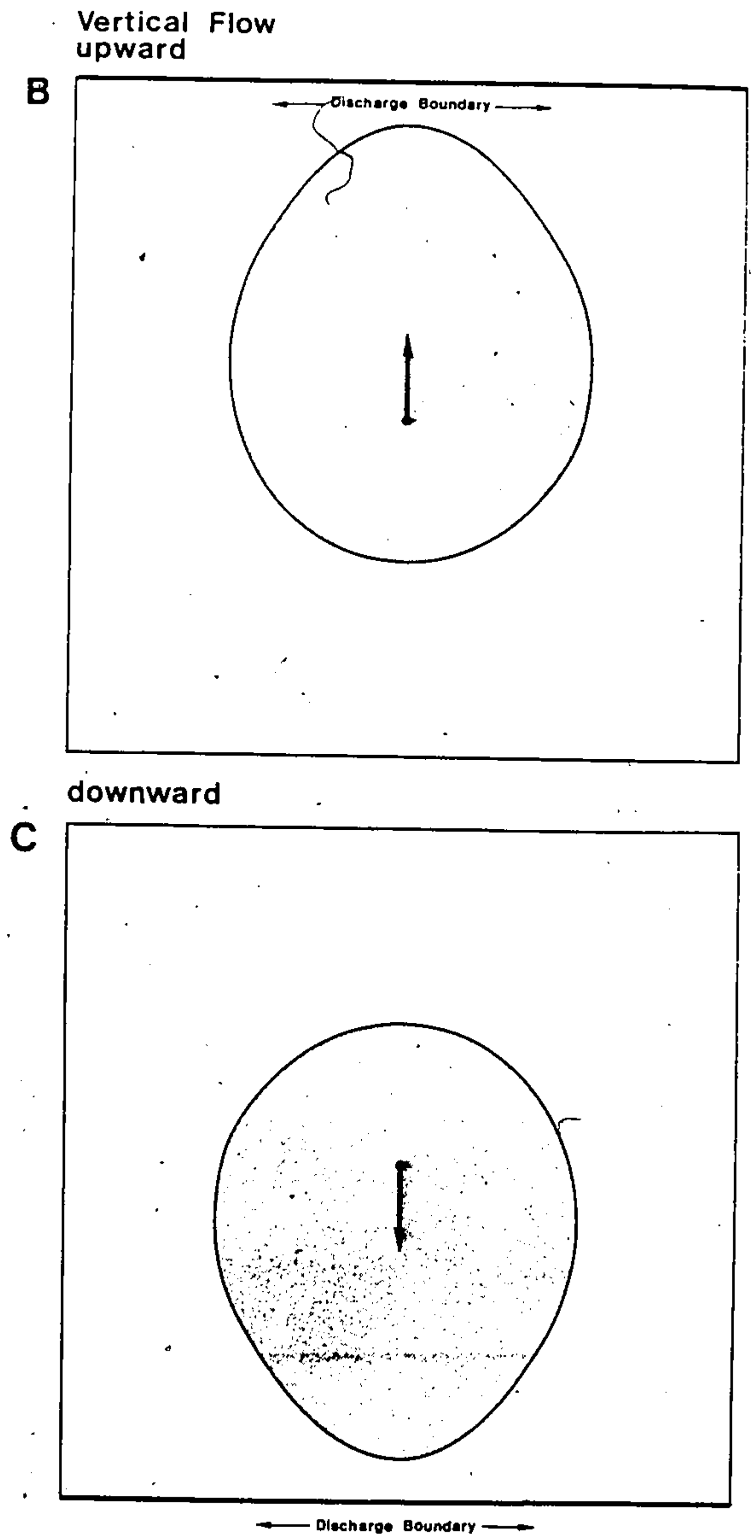
Vertical Flow
upward
B
Discharge Boundary
downward
C
Discharge Boundary

Vertical Flow
lateral

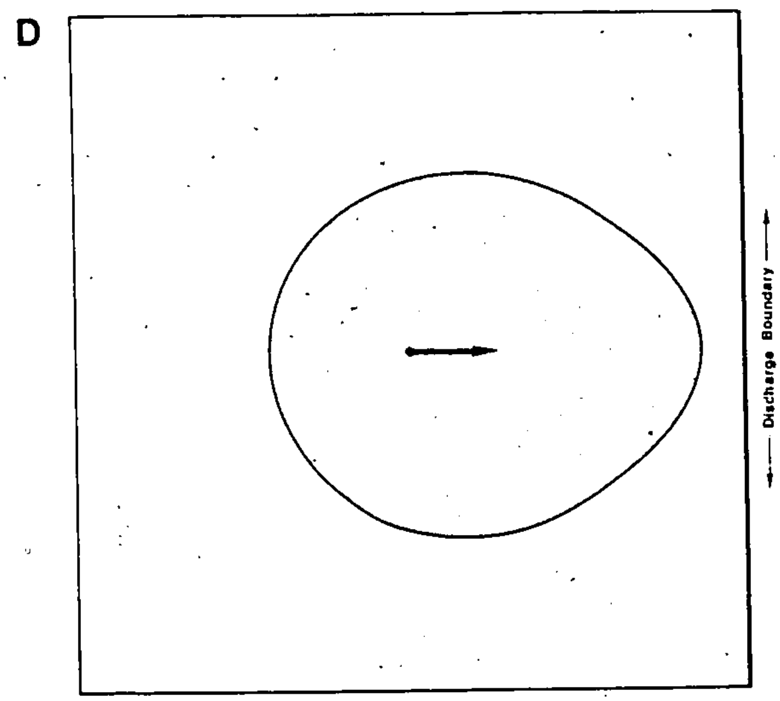

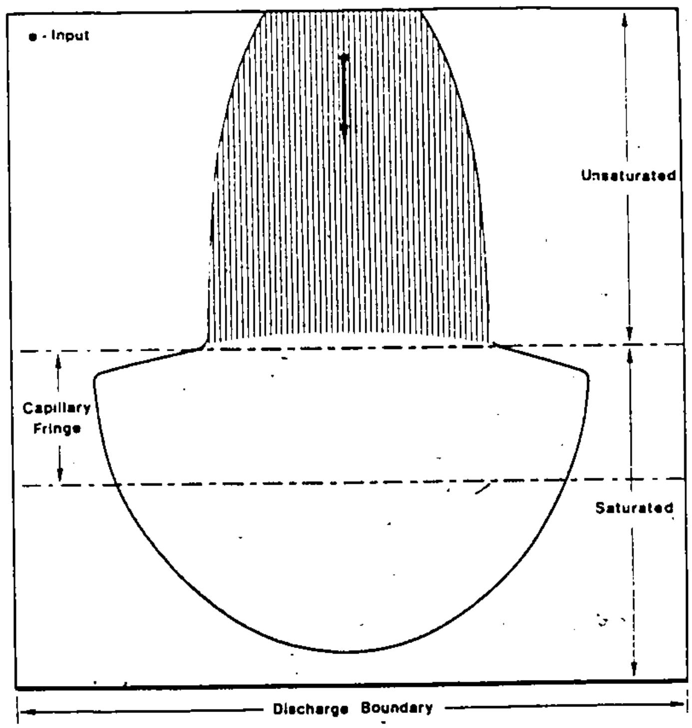

Figure 6.3
Flow envelope for a partly saturated medium with vertical, downward flow.

and demonstrates this control.

6.3 LINEAR RESURGENCE MULTIPLE INPUT EXPERIMENTS

6.3.1 Purpose

These experiments disclose the initial flow boundaries between inputs to a rectangular bedding plane segment discharging to a linear boundary of uniform potential. They also determine the variation in flow envelope geometry for individual inputs as a function of input density and spatial arrangement.

6.3.2 Description

Successively 1, 2, and 4 inputs were established along a line parallel to the discharge boundary of the unit square filtration model. The line was positioned Ø.33 units from the discharge boundary, with individual inputs spaced as shown in Figures 6.4 a and b. Subsequently, a second rank of inputs was established Ø.66 units from the discharge boundary having a density of 4 (Fig. 6.4 c) All inputs were provided with equal head. Experiments were terminated when the discharge boundary appeared to be entirely taken up by the dye tracers.

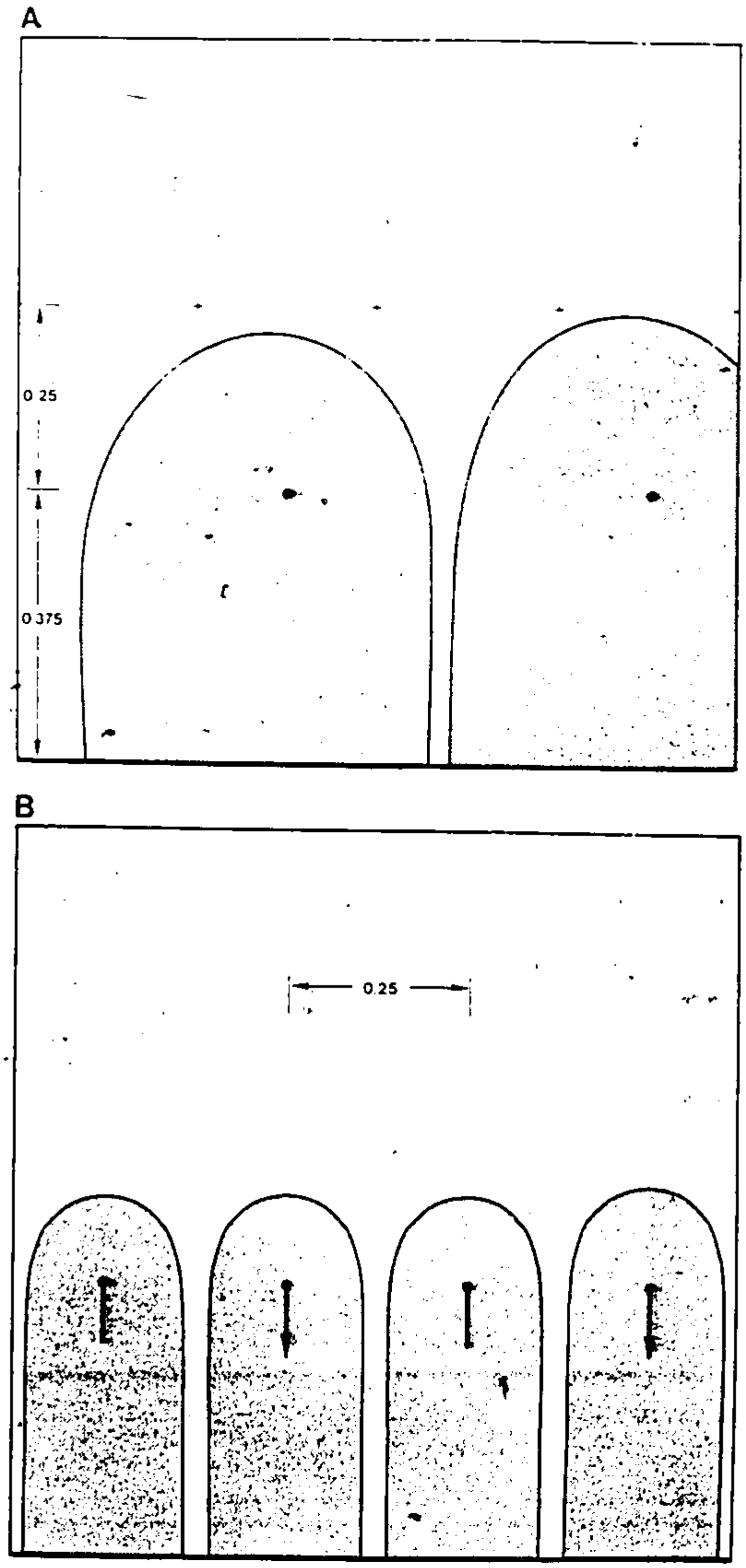
A
0.25
0.375
B
0.25

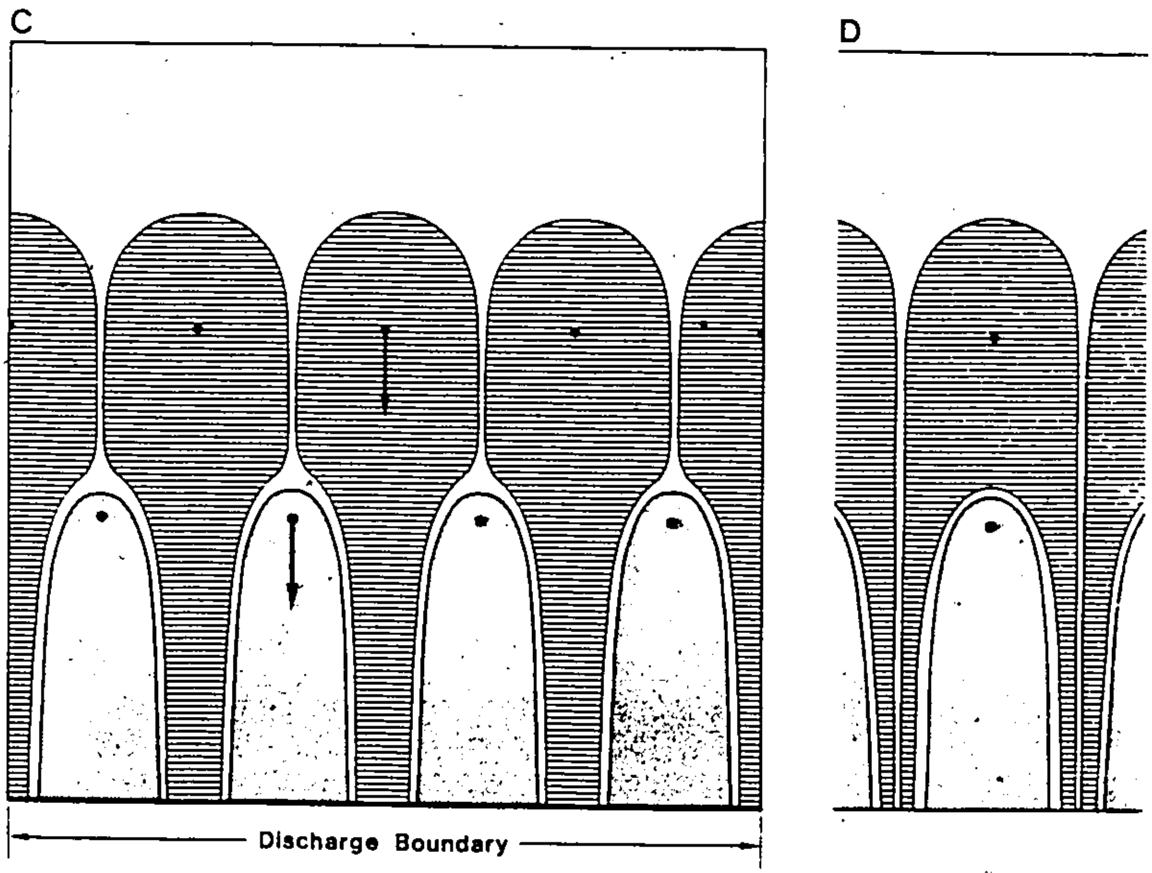

Figure 6.4 A, B, C, D
Flow envelopes for multiple input arrays receiving identical head with a linear discharge boundary.

6.3.3 Observed Results

The results of these experiments are depicted in Figure 6.4. The single input flow envelope occupied the entire discharge boundary, but the envelopes of the two and four input configurations divided this boundary into equal segments.

When the second rank of inputs was added, the space occupied at the discharge boundary by the flow envelopes from the two ranks were unequal (Fig. 6.4 c). The narrower envelopes of the second rank inputs reflect the proportionally lower throughputs for analogous ranks in the electric analogue experiments.

With the second rank inputs configured as shown in Figure 6.4 c, the mean flow vectors are straight and parallel for all of the inputs. By altering the head values, these vectors change. Figure 6.5 shows the effect of increasing or decreasing the head of one of the Rank 1 inputs; an increase produced a divergence of adjacent vectors; a decrease, a convergence. By shifting the second rank one half space along its axis, a bifurcated flow envelope was produced with curved mean flow vectors (Fig. 6.4 d). In this case, the flow envelope of each rank two input appeared at two separate regions of the discharge boundary.

In terms of karst hydrology, these experiments confirm that the flow from individual inputs to a common

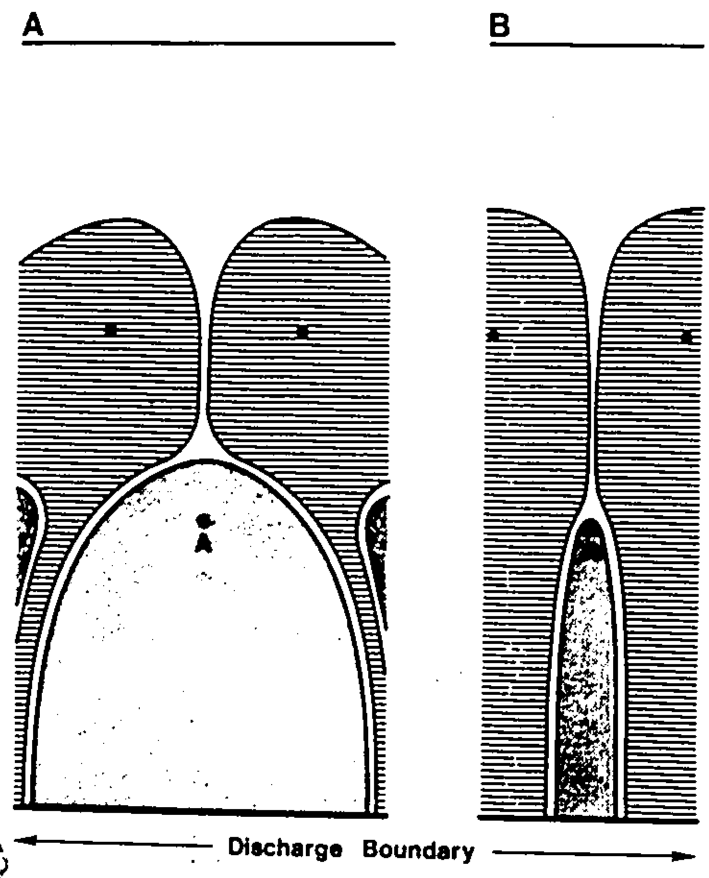

Figure 6.5
Flow envelopes for a two rank multiple input array with one input of variable head. A = Increase B = Decrease Array geometry is equivalent to Figure 6.4.

planar parting remain distinct except for hydrodynamic dispersion and diffusion, and by delineating the mean flow vectors, they show the probable growth vectors of tube networks which propagate from these inputs. The significance of these demonstrations will be discussed further in Chapters 7, 8, and 10.

6.4 POINT RESURGENCE MULTIPLE INPUT EXPERIMENTS

Purpose

These experiments disclose, for a variety of spatial arrangements, the initial flow boundaries between inputs to a rectangular bedding plane segment discharging to a point.

6.4.1 SYMMETRICAL INPUT EXPERIMENTS

6.4.1.1 Description

Four inputs and a single discharge point were established along the central axis of the unit square filtration model. Equal spacing was used between all of the points. Figure 6.6 shows their relationship to the rectangular model boundaries. All inputs were provided with equal head. Experiments were terminated when dye from the majority of the inputs had reached the output point.

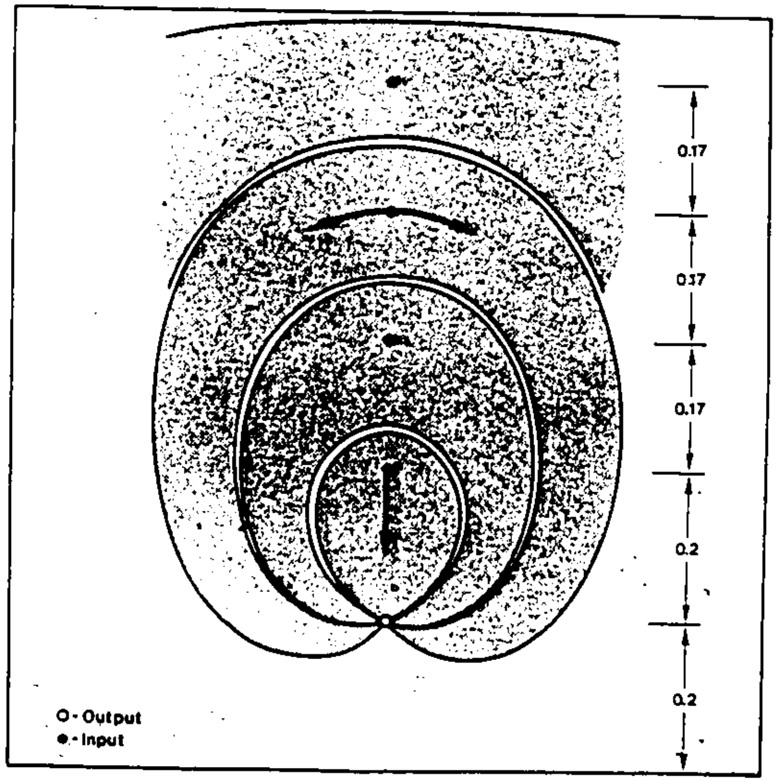

Figure 6.6
Flow envelopes for a symmetrical, multiple input, point discharge array.

6.4.1.2 Observed Results

Figure 6.6 shows the result of this experiment. Input 1, the proximal input, exhibited a flow envelope of lenticular proportions with its principal axis coincident with the input-output axis. The remaining inputs displayed bifurcated flow envelopes surrounding the more proximal inputs. The mean flow vectors diverged from the input-output axis at nearly right angles and connected to the output along lengthy, gently curving paths.

The distribution of the envelopes in the vicinity of the discharge point reflected the relative throughputs of the inputs in a way similar to the linear resurgence experiments. Specifically, the angular distance covered by the flow envelope was approximately proportional to the values determined by the corresponding electric analogues (Chapter 5.3.2.4).

6.4.2 ASYMMETRICAL INPUT ARRAY EXPERIMENTS

6.4.2.1 Description

In the initial experiment, a linear array of four inputs was established parallel to one of the boundaries of the filtration model apparatus. The single point resurgence was located on a line parallel with an adjacent boundary and intersecting the input nearest that boundary. Figure 6.7 shows the relationship of the points to the rectangular boundaries. As before, all inputs were provided with

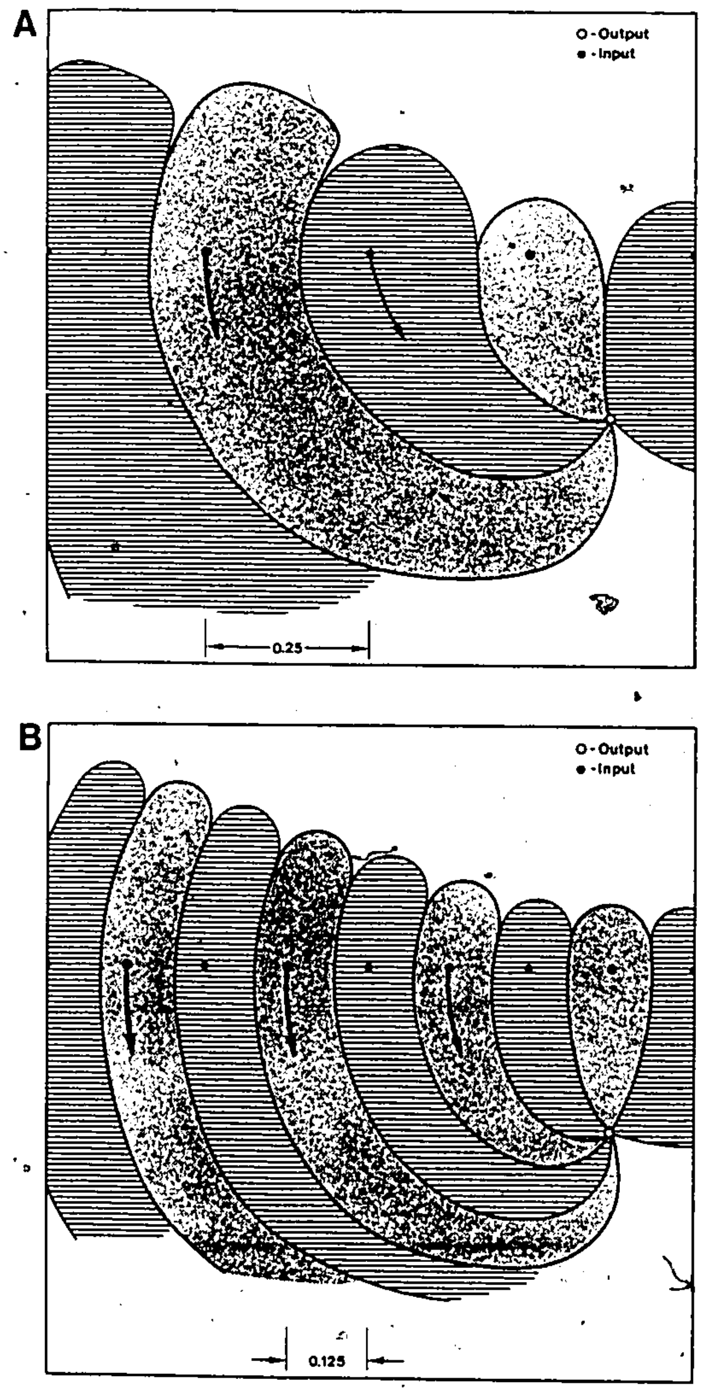
A
O - Output
● - Input
0.25
B
O - Output
● - Input
0.125

identical head, and experiments were terminated when the dye from the majority of the inputs had reached the output point.

6.4.2.2 Observed Results

Figure 6.7A depicts the results of this experiment. Except for minor asymmetry about the input-output axis, the flow envelope of the proximal input was similar to the corresponding element of the preceding experiment. The envelopes associated with the remaining inputs had the form of sweeping single crescents, their radius of curvature increasing with increasing distance from the resurgence.

When input density is increased or the input-output distance increased, the flow envelopes and mean flow vectors become more "J" shaped, with the sections nearest the inputs more nearly straight and parallel (Fig. 6.7B). This demonstrates that the parallelism of these regions is related to the extent to which circulation extends perpendicular to the input array axis.

As before, the distribution of the envelopes in the vicinity of the discharge point reflected the relative throughputs of the inputs in a way similar to the linear resurgence experiments. The angular distance covered by the flow envelope was proportional to the values determined by the corresponding electric analogues, Chapter 5.3.1.4.

The significance of the point resurgence flow envelope demonstrations will be discussed further in Chapters 7, 8, and 1Ø.

CHAPTER 7

SOLUTION EXPERIMENTS

7.1 INTRODUCTION

The solution experiments in laboratory models undertaken as part of this research extend the information on initial flow rates given by the electric analogues and provide a detailed picture of tube network development processes. The input and output configurations of specific experiments relate directly to the geological and geomorphic problems specified in Chapter 1. As before, in the case of the electric analogues, the boundaries in these experiments are analogous to real flow boundaries, including truncations of the bedding plane and interfaces with other flow systems of similar order and scale.

7.1.1 SIMILITUDE

The fundamental similitude arguments relating these experiments to their prototypes are presented in Chapter 3. The specific experiments were designed to achieve geometrical equivalency with natural groundwater systems of the two general types addressed by the electric analogue experiments. They consist of those in nearly horizontally bedded carbonates and those in steeply dipping soluble rocks. Accordingly, the experiments are divided into two general types which differ in their output geometry, linear resurgence, and point resurgence types.

The linear resurgence experiments reflect a situation in which a uniformly conductive bedding plane is truncated in a roughly linear fashion, as by a stream of high Horton order. Such a stream provides a stable regional hydraulic sink and one of comparatively uniform piezometric potential. This type of geometry is most frequently associated with regions of near horizontal strata.

Point resurgence experiments reflect those situations where a relatively horizontally eroding stream intersects a hydraulicly conductive bedding plane at a point, providing a highly localized discharge. This geometry is most frequently associated with regions of steeply dipping strata.

7.2 LINEAR RESURGENCE MULTIPLE INPUT EXPERIMENTS

After determining the nature of the competition between principal and secondary tubes of isolated networks in the 1970-72 work, experiments were undertaken to determine if groups of inputs to a single bedding plane would compete in a similar way.

7.2.1 DESCRIPTION

Five linear resurgence multiple input experiments were performed in a salt medium. These were briefly reported in Ewers, 1972. Similar experiments in a plaster medium, reported below, show results which are qualitatively similar.

Sets of two or four inputs were established on a line parallel with the discharge boundary. All inputs in these experiments were provided with identical fluid potential. The dimensions of these experiments are given in Figure 7.1.

7.2.2 OBSERVED RESULTS

Each of the inputs gave rise to separate distributary networks which initially grew along parallel paths toward the discharge boundary. In plan form, the networks were similar to the results of the single input experiments, possessing clearly defined primary and secondary elements (Fig. 4.2). The major difference was that the networks of the multiple input experiments were narrower and less complexly branched than the single input type. After average network growth had progressed to about 20% of the distance to the output, it was clear that all were not proceeding with equal vigor. The growth rate of the shorter networks declined rapidly while growth rates in the longer increased. The typical two and four input experiments, illustrated in Figure 7.1, show that in each case one network achieved dominance and greatly increased its width and branching tendency as it neared the output boundary.

Figure 7.1
Linear resurgence, multiple input solution experiments; after Ewers (1972).

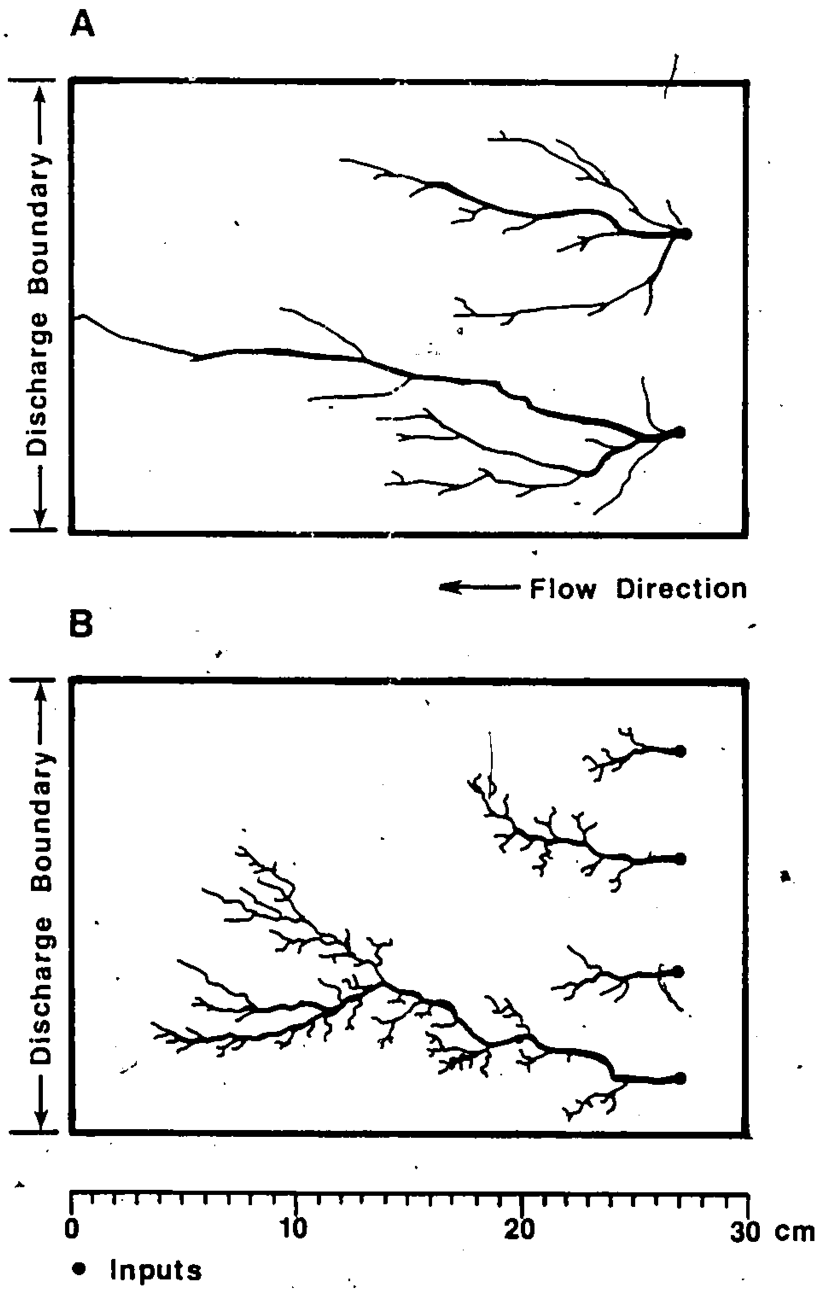
A
Discharge Boundary
Flow Direction
B
Discharge Boundary
0
10
20
30 cm
Inputs

The illustrated experiments were terminated just prior to the establishment of a link between the dominant network and the output. At this time growth of the other networks had decreased to an imperceptible rate.

7.2.3 ANALYSIS OF THE EXPERIMENTS

The experimental results are in agreement with theoretical considerations in terms of network independence, network competition, and the geometry of the individual networks.

7.2.3.1 Network Independence

Each input should give rise to a distributary network of tubes by the processes outlined in Chapter 4. Their growth should be sub-parallel, each network retaining its integrity so long as none has established a low resistance connection with the output. This contention follows directly from consideration of the pressure distribution in the parting. Figure 7.2 is an electric analogue pressure field map for such a configuration before solution modification. It shows that a line can be defined occupying those points which derive their pressure equally from two adjacent inputs. This line of zero pressure differential defines the boundary between the flow domains of the two inputs and is identical with the domain boundary of the flow envelope experiment (Fig. 6.4B). Although this boundary

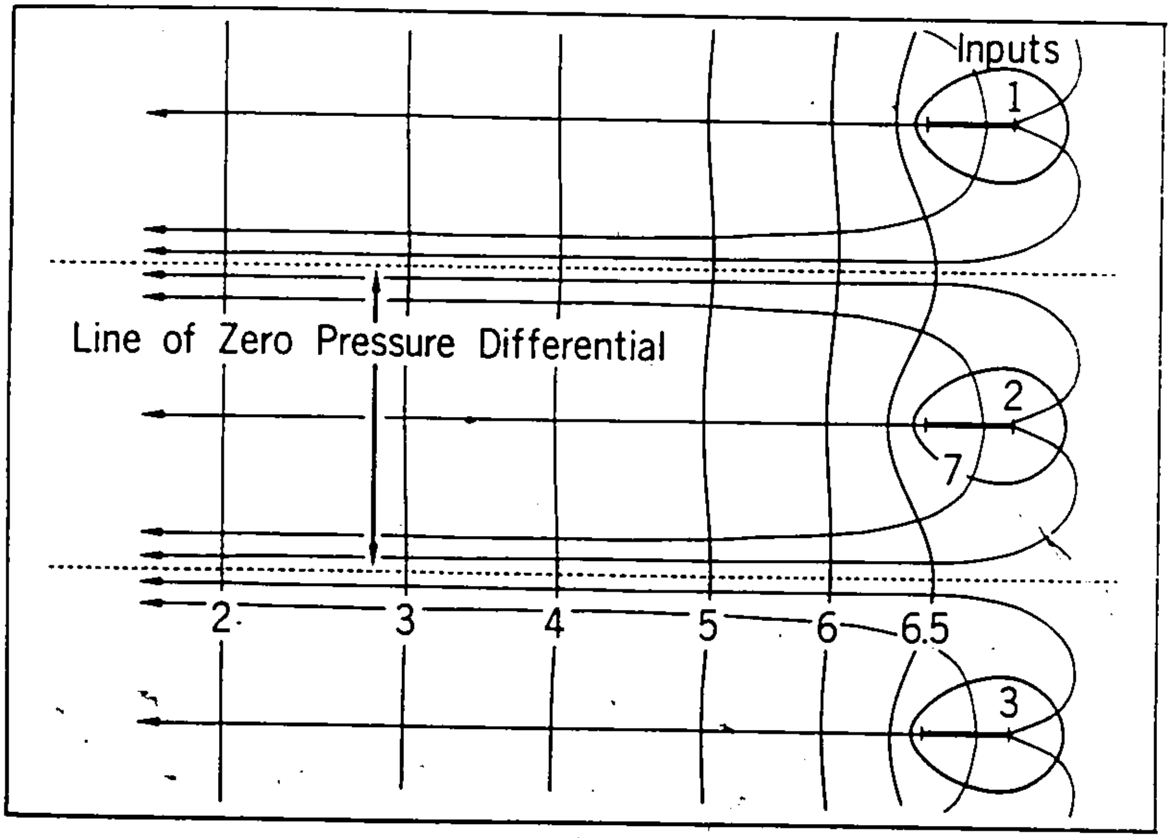

Figure 7.2
Flow field for three co-planar inputs discharging to a linear output boundary; after Ewers (1972). The line of zero pressure differential passes through points which derive their pressure equally from the two adjacent inputs.

will likely not remain fixed as the networks grow and will occupy other positions in the event that the individual input potentials are not equal, it can always be defined so long as there is a net discharge from each tube network into the surrounding parting. A condition of zero discharge occurs for a particular input in the presence of others when the potential at that input is equivalent to the value indicated by a piezometer inserted at the same position.

The movement of the flow domain boundary in response to pressure differences was demonstrated in the flow envelope apparatus. Figure 7.3A shows input B in a piezometer configuration. Figure 7.3B, C and D show increasing head applied at B with corresponding shift of boundaries and the mean flow vectors. The zero pressure differential line is normal to the equipotential lines, and therefore, flow is parallel to it. For this reason, the integrity of the networks is preserved.

7.2.3.2 Network Competition

The relationship between individual networks in close proximity to one another are not significantly different hydraulically from the relationship between the primary and secondary distributary branches in the initial bedding plane solution experiments described in Chapter 4. Therefore, dominant and recessive networks would be expected

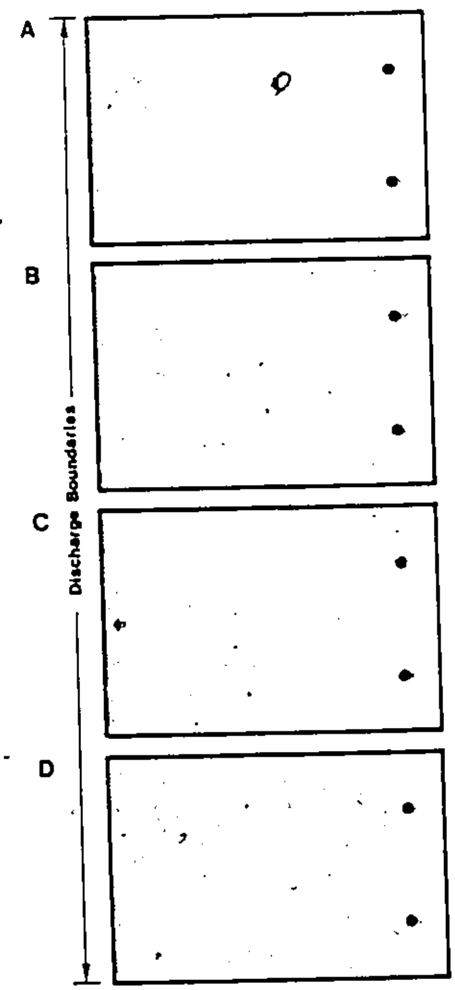

Figure 7.3
Flow envelopes for two inputs with differing heads.

to form in response to small differences in growth potential. A network with a slight initial growth advantage, a dominant input, should increase its discharge space within the bedding plane at the expense of the adjacent networks, augmenting its growth potential. Growth advantages would be related to conditions such as locally higher bedding plane transmissivity or the presence of a minor joint with an orientation parallel to the piezometric slope near the input point. Conversely, an input with reduced growth potential, a recessive input, would confer a competitive advantage upon contiguous networks by providing them with increased discharge space, thus, further reducing its own growth potential. Reduced growth potential could be attributed initially to reduced bedding plane transmissivity in the region of the input or to a delay in establishing the point as an active groundwater input. Thus, we expect a synergistic, positive feedback situation favoring the dominant network.

Pressure field maps, electric analogues, and flow envelope experiments support this analysis. The pressure field maps (Fig. 7.4 A,B,C) show a sharp reduction in gradient for an input with a growth disadvantage in the presence of adjacent advantaged inputs. These pressure fields further show that the magnitude of this disparity of gradient is related, in a direct sense, to the magnitude of the growth advantage. With electric analogue discharge

Figure 7.4 A, B, C

Pressure field maps and principal flow vector gradients for networks of differing length and equal head.

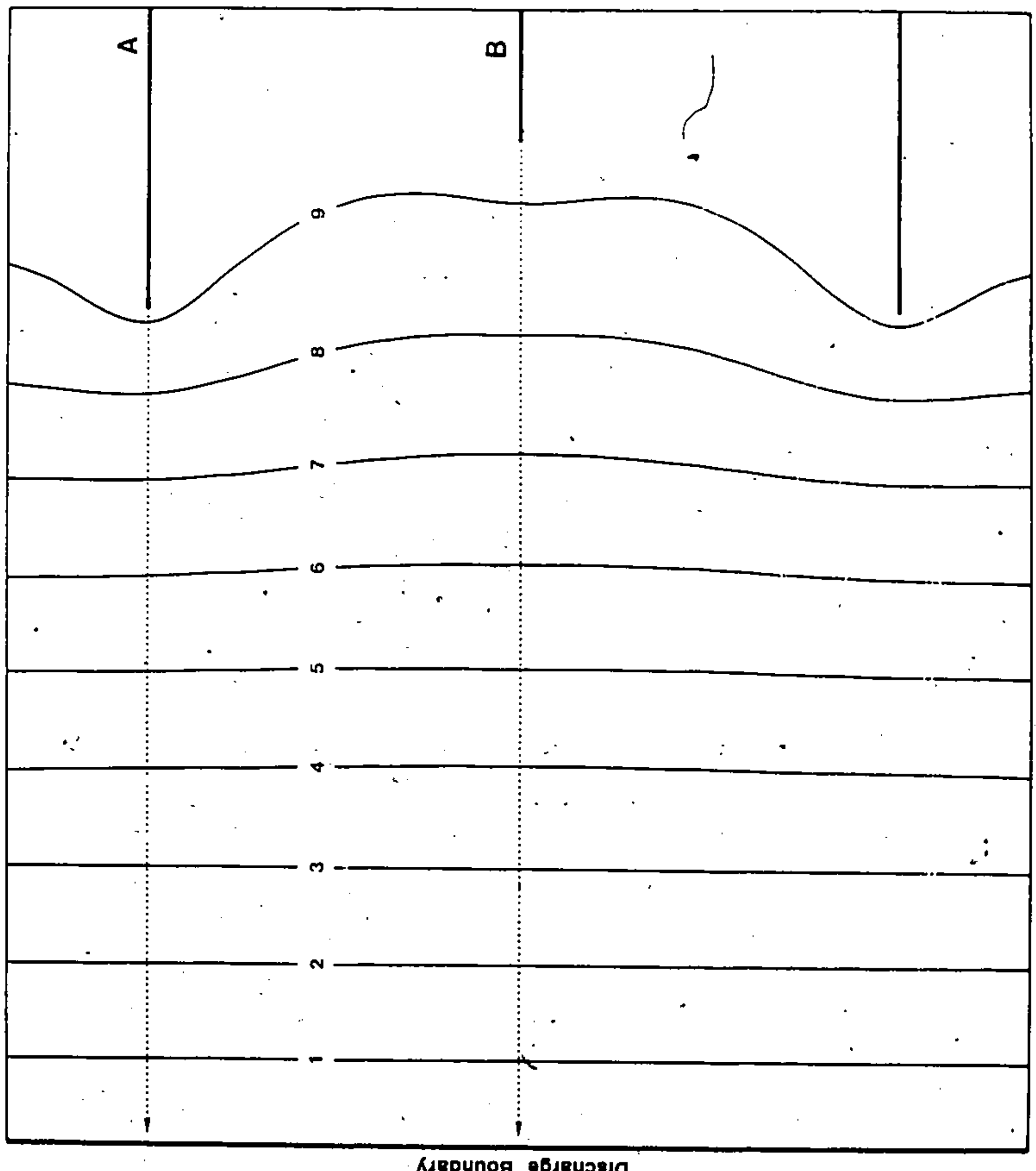

A

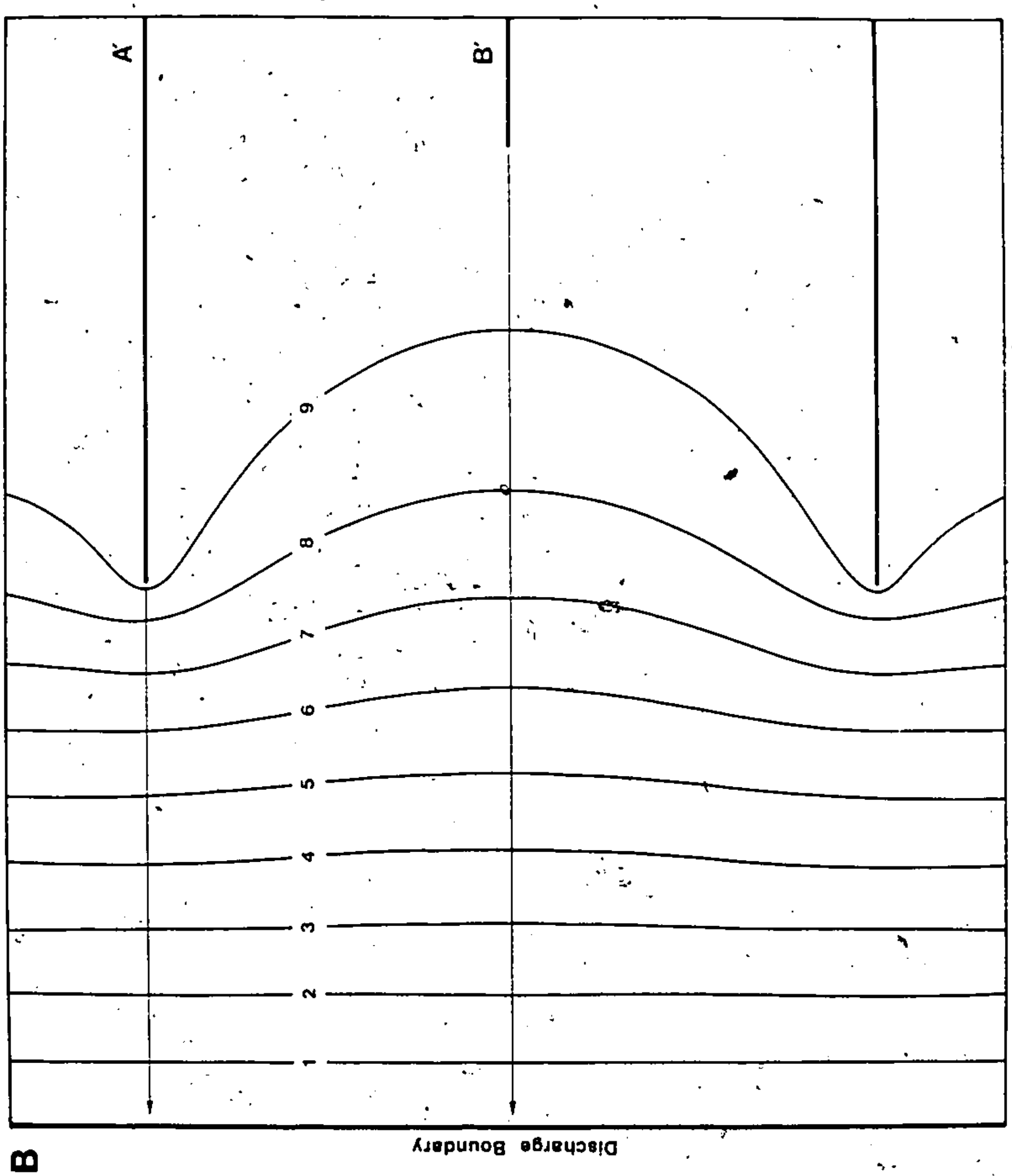
A'
B'
9
8
7
6
5
4
3
2
1
B
Discharge Boundary

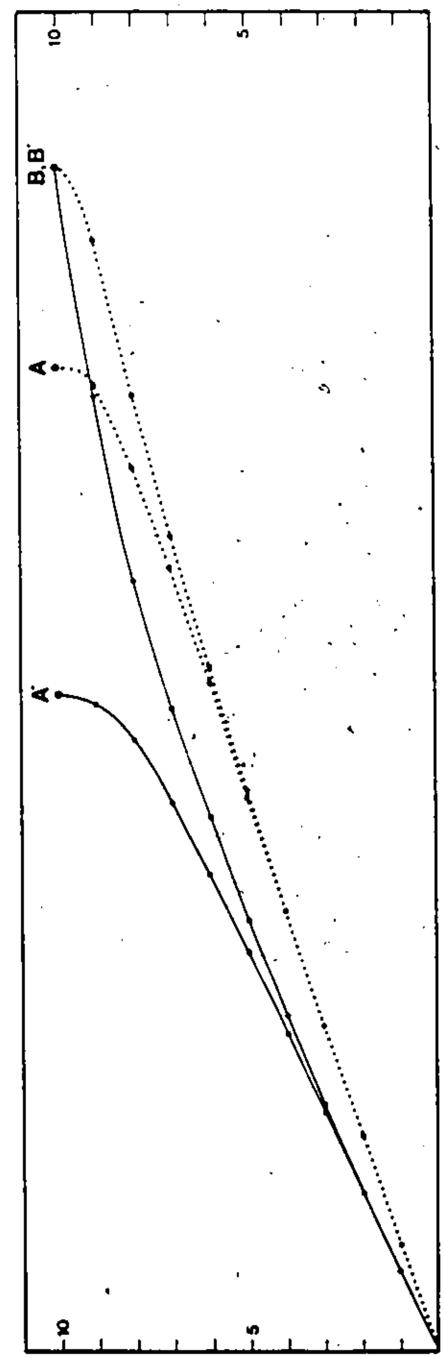

C

experiments, the effect of the gradient change on hydraulic throughput can be qu antified. Two additional types of electric analogue experiments were undertaken to achieve this quantification.

In the first type, the discharge of a recessive input, a point input, was compared with a group of surrounding networks of varying length and input density (Fig. 7.5). These experiments show that a length advantage of 26% of the total input-output distance was necessary to reduce the throughput of the disadvantaged input by 50%, relative to the values for the other inputs, when the input spacing was 100% of the input-output distance (Table 7.1). When input spacing was reduced to 20% of that figure, a length advantage of 10% was sufficient to produce a 50% reduction in throughput.

The second experiments compare the individual throughputs of multiple input systems in the presence of a single dominant network (Fig. 7.6). Figures 7.7A 7.7B and 7.7C show these throughputs expressed in milliamps of electric current as a function of the input position. The data are given separately for varying lengths of the dominant network. These experiments show that throughput is inversely related to both the proximity of the dominant network and its length.

These density and proximity effects can be seen in the solution experiments by comparing the length of the

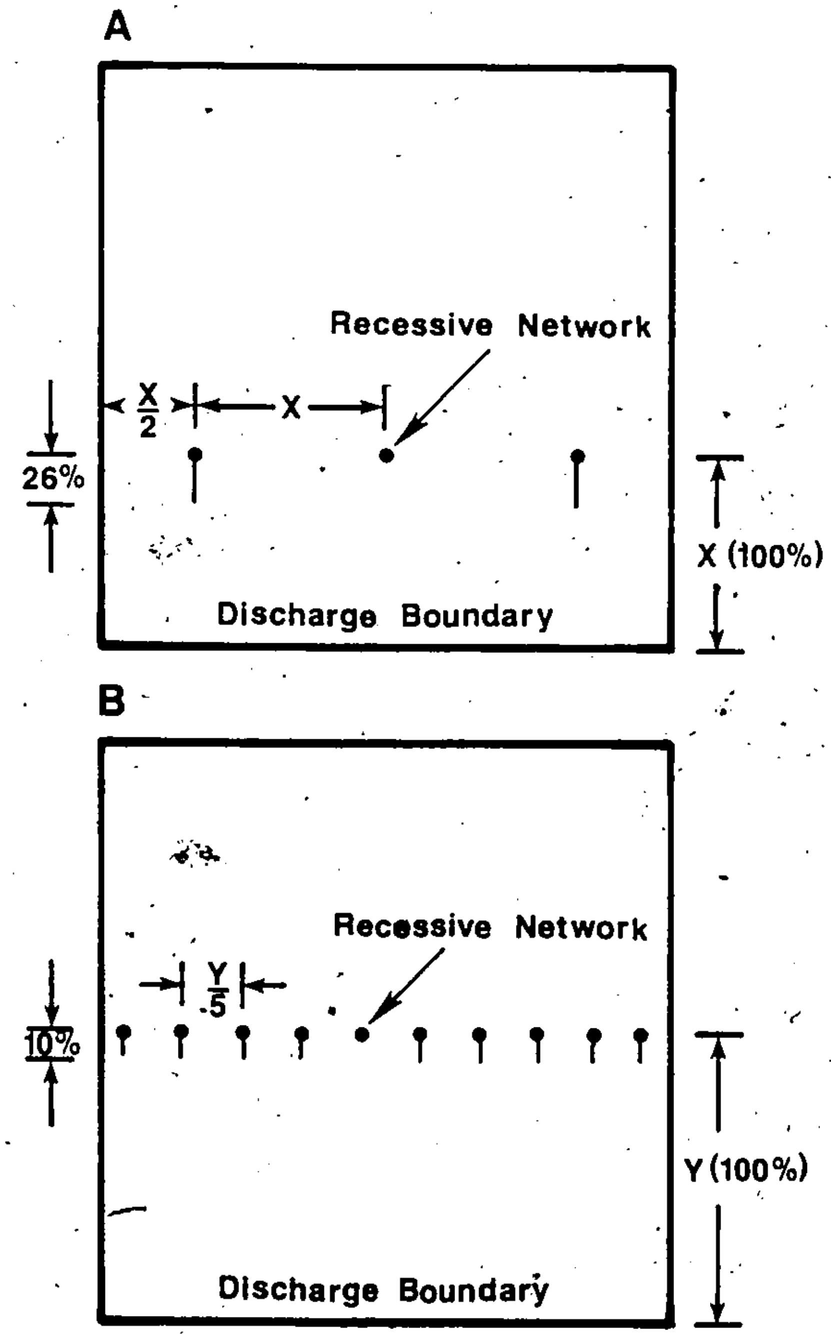

Figure 7.5
Input-output configuration for electric analogue experiments with extended electrodes.

Table 7.1

Input Density	Electrode Current ma. Point	Extended	Electrode length Cm.	% of total path
2	24	50	4.7	26.1
5	10	19	3.0	16.6
10	4	8	1.8	10.0

Electrode length required to produce a 50% change in throughput (Q) for a recessive input (point input) in the presence of equal extended inputs. Data are given for three input densities.

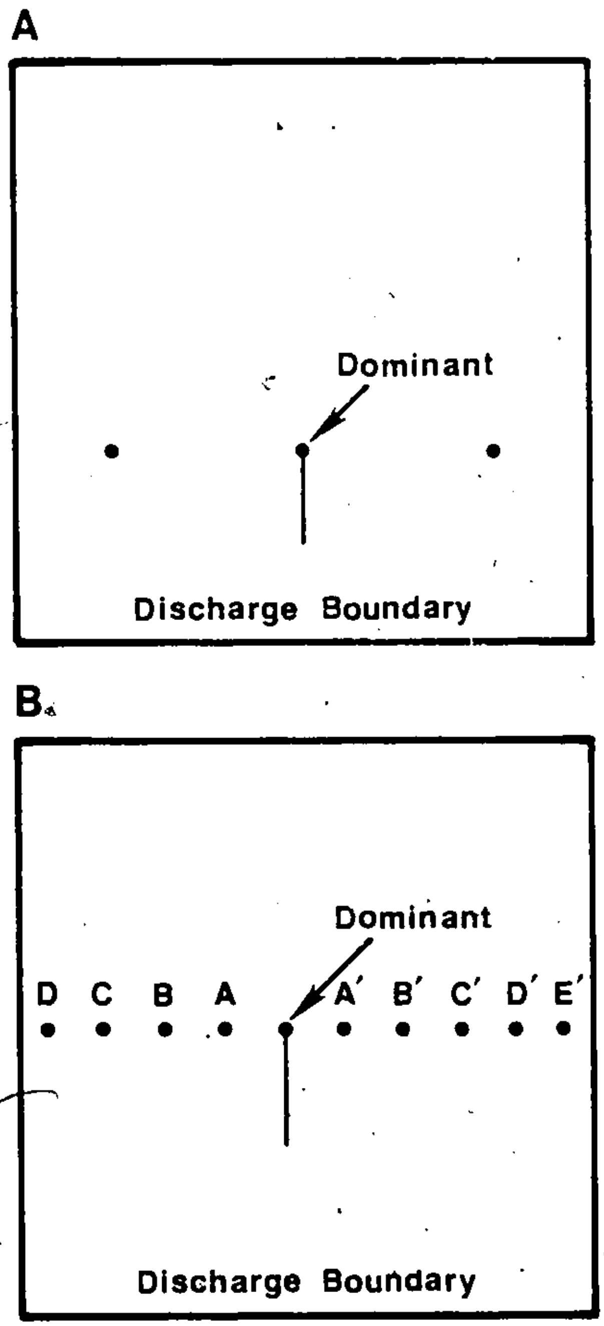

Figure 7.6
Input-output configuration for electric analogue experiments with extended electrodes.

FIGURE. 7.7 A 1

DENSITY 10 - LENGTH OF INPUT 6 = 0.4 UNITS

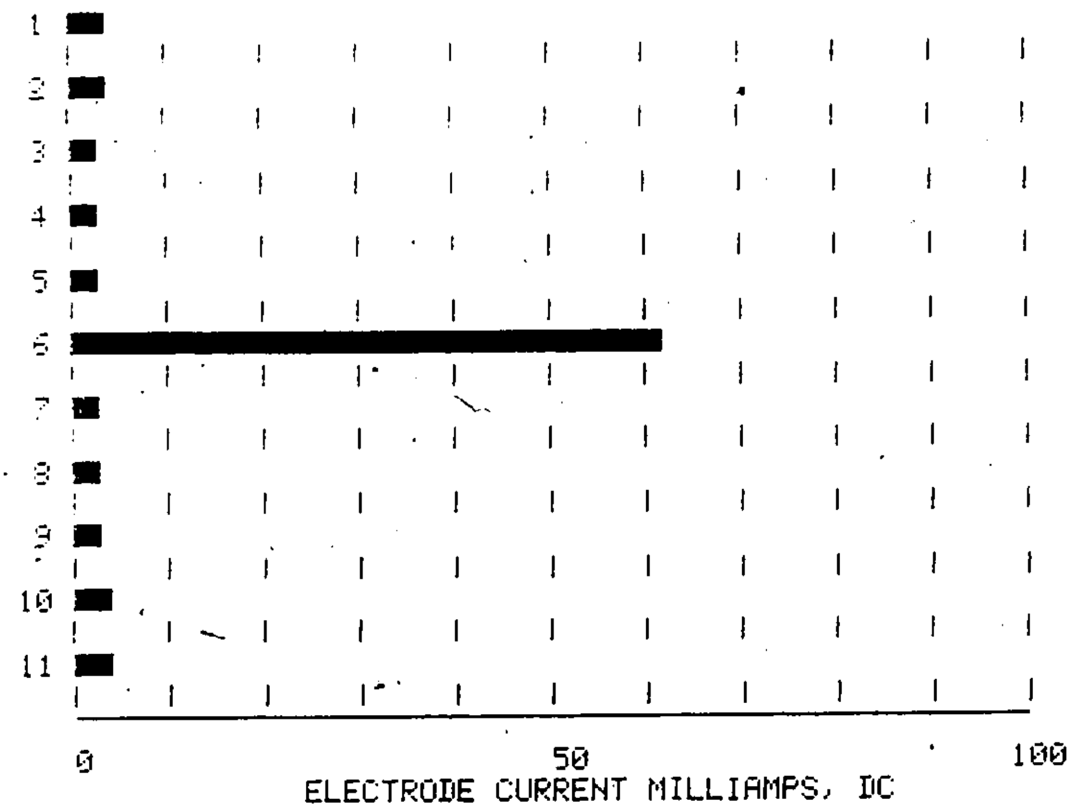

FIGURE. 7.7 A 2

DENSITY 10 - LENGTH OF INPUT 6 =0.2 UNITS

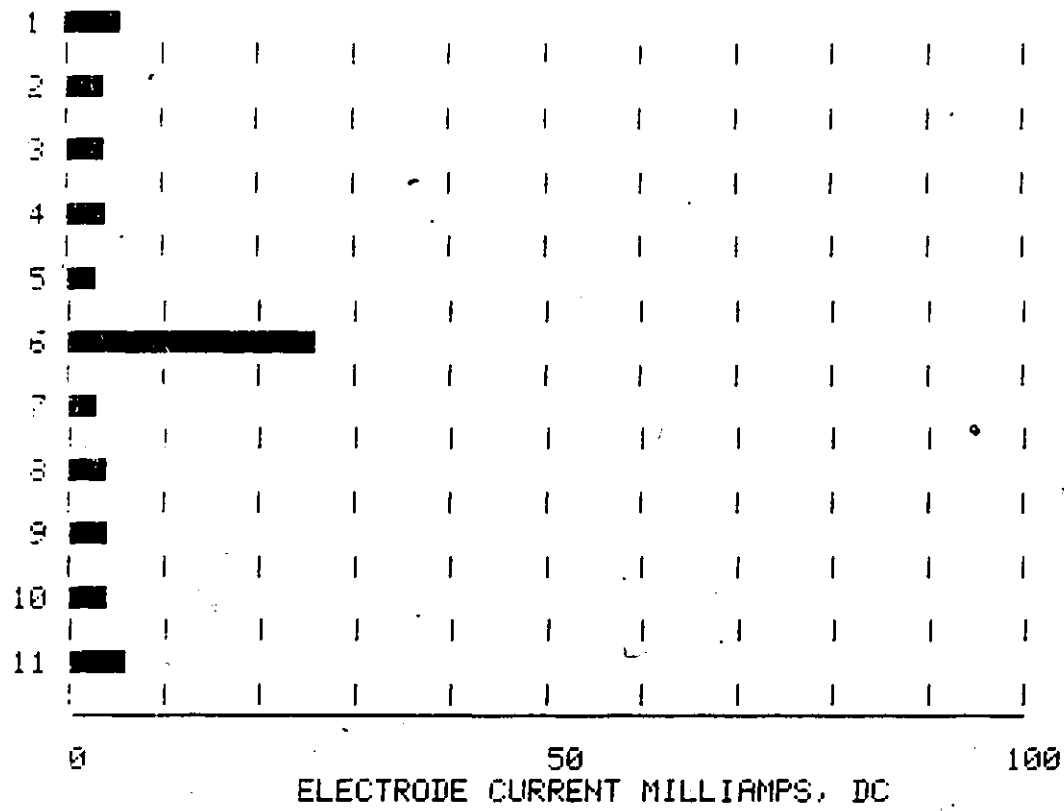

FIGURE 7.7 A 3

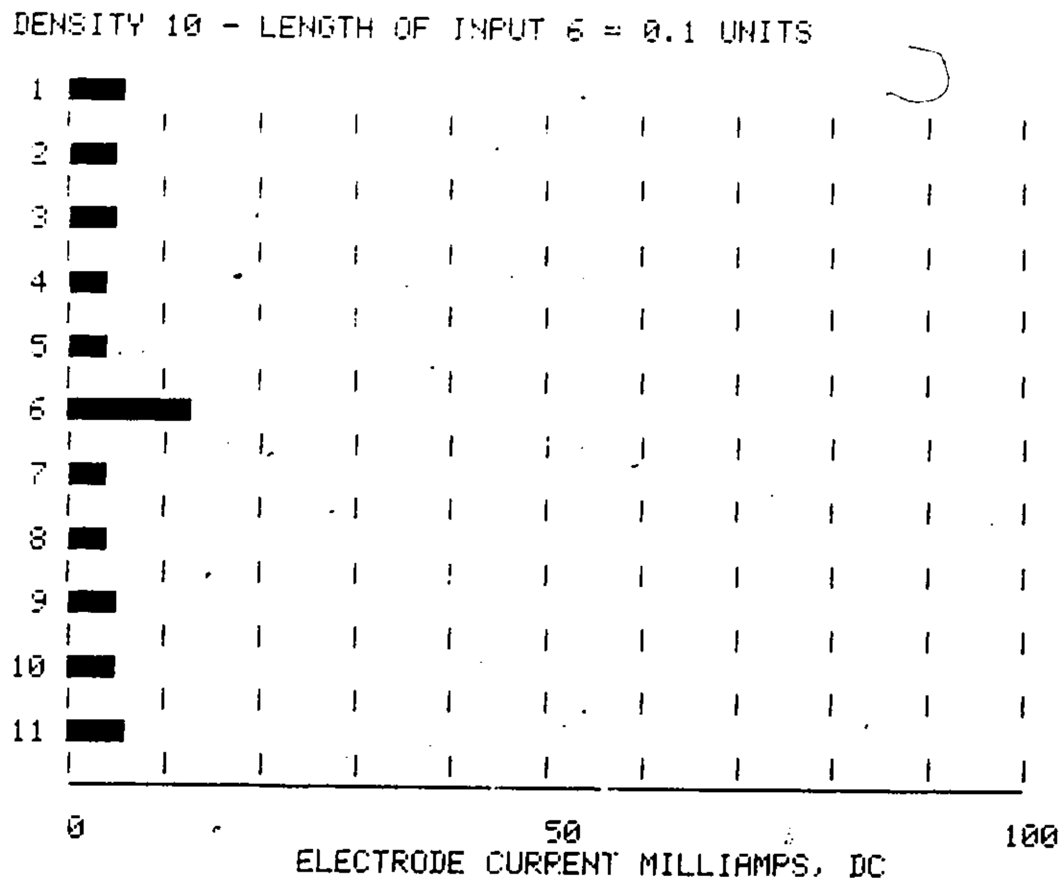
DENSITY 10 - LENGTH OF INPUT 6 = 0.1 UNITS
1
2
3
4
5
6
7
8
9
10
11
0
50
100
ELECTRODE CURRENT MILLIAMPS, DC

FIGURE. 7.7 A 4

DENSITY 10 - LENGTH OF INPUT 6 = 0 UNITS

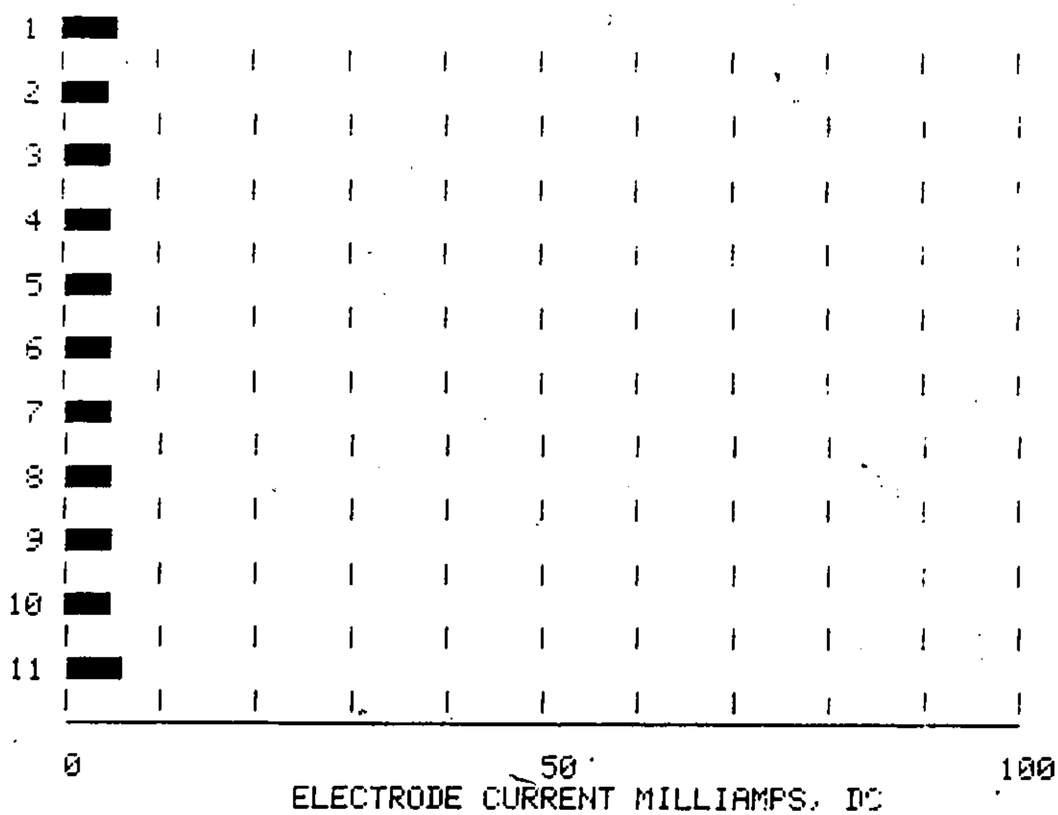

FIGURE. 7.7 B 1

DENSITY 5 - LENGTH OF INPUT 3 = 0.4 UNITS

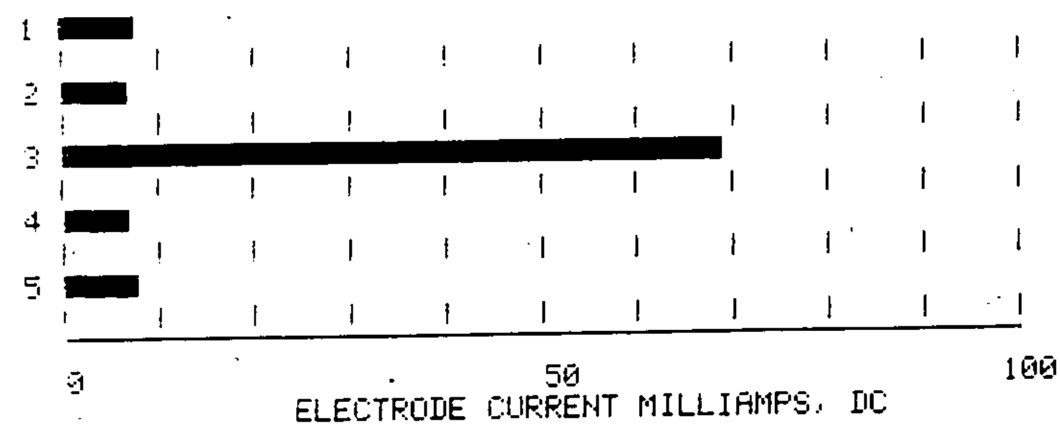

FIGURE. 7.7 B 2

DENSITY 5 - LENGTH OF INPUT 3 = 0.2 UNITS

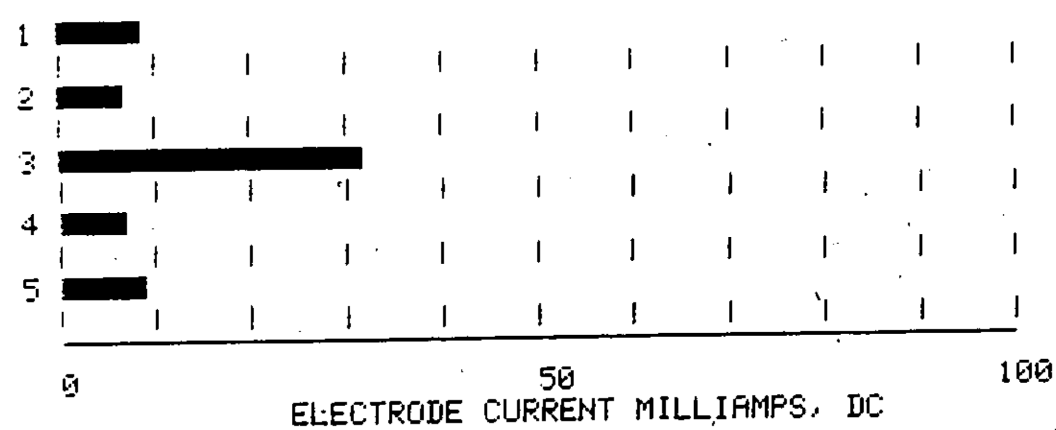

FIGURE. 7.7 B 3

DENSITY 5 - LENGTH OF INPUT 3 = 0.1 UNITS

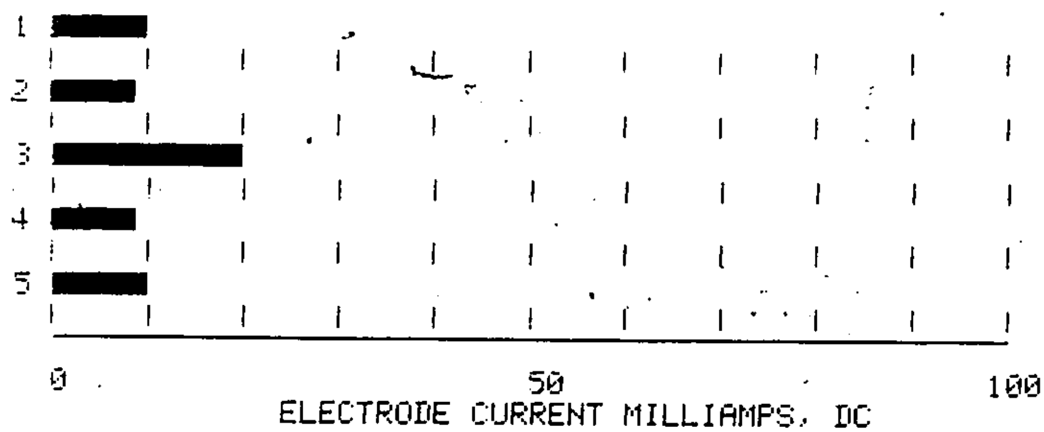

FIGURE. 7.7 B 4

DENSITY 5 - LENGTH OF INPUT 3 = 0 UNITS

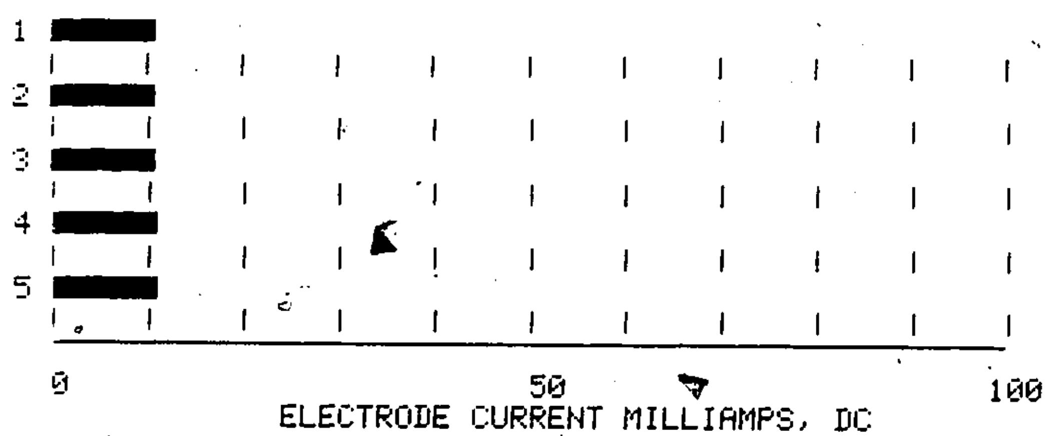

FIGURE. 7.7 C 1

DENSITY 3 - LENGTH OF INPUT 2 = 0.4 UNITS

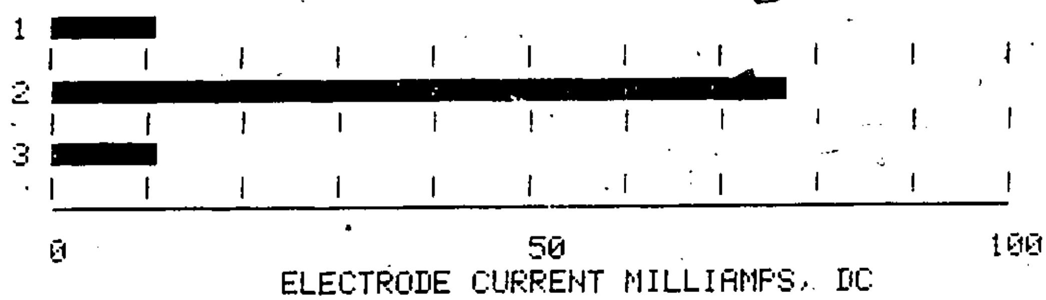

FIGURE. 7.7 C 2

DENSITY 3 - LENGTH OF INPUT 2 = 0.2 UNITS

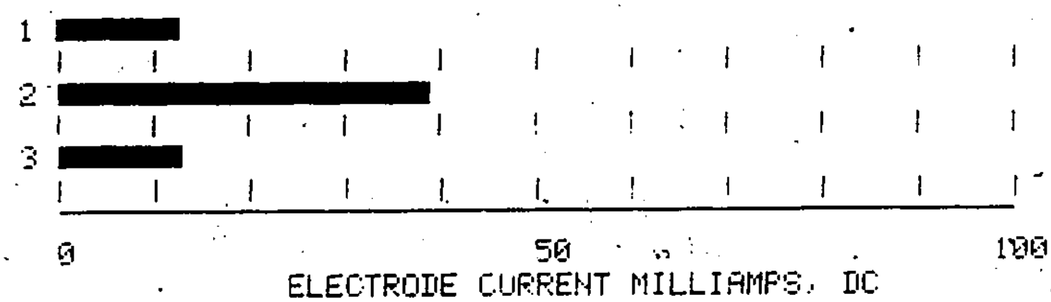

FIGURE. 7.7 C 3

DENSITY 3 - LENGTH OF INPUT 2 = 0.1 UNITS

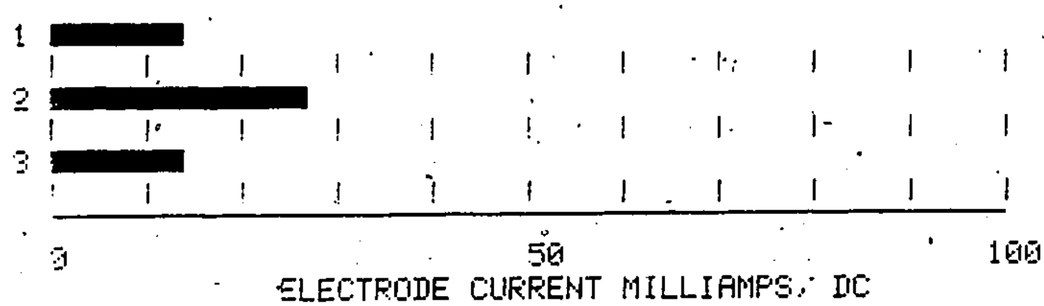

FIGURE. 7.7 C 4

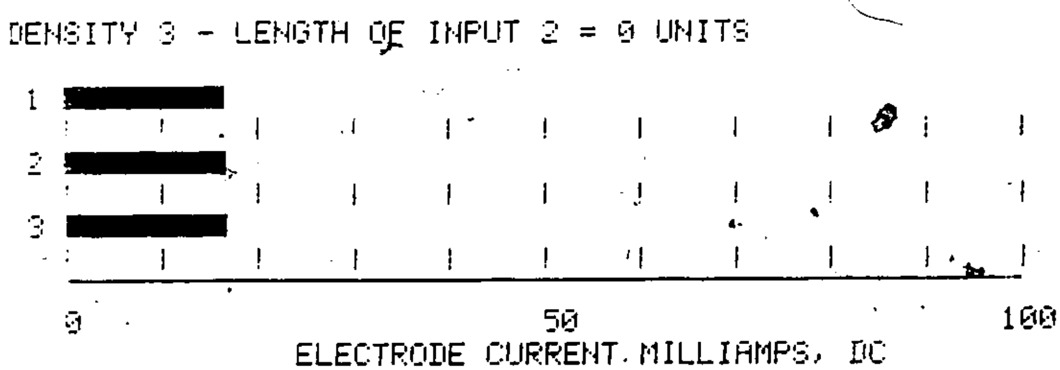
DENSITY 3 - LENGTH OF INPUT 2 = 0 UNITS
1
2
3
0
50
100
ELECTRODE CURRENT MILLIAMPS, DC

recessive networks in Figures 7.1A and 7.1B. Those in the four input experiment s are shorter in comparison to the two input experiments by a factor of two. Figure 7.1B also shows that the network in closest proximity to the dominant network is among the shortest.

On the basis of these experiments we may, therefore, expect that small variations in the parting transmissivity or small temporal variations in the activation of inputs will be effective in causing a condition of divergent competition when network density is high. We may further expect that competition will be intensified when networks are in close proximity to a dominant network.

7.2.3.3 Network Form

A special flow envelope experiment was undertaken to investigate the effect of length differences in multiple input systems. In this experiment, the effective length of an input in a multiple input system was increased by connecting several closely spaced inputs in parallel. The inputs were situated along the mean flow vector from the initial input. These experiments showed that the discharge space for each input in a multiple input system is directly related to the relative network length (Fig. 7.8). This explains the invariably divergent tendency of the dominant network shown in Figure 7.1, as well as the variations in Q noted in Section 7.2.3.2 above.

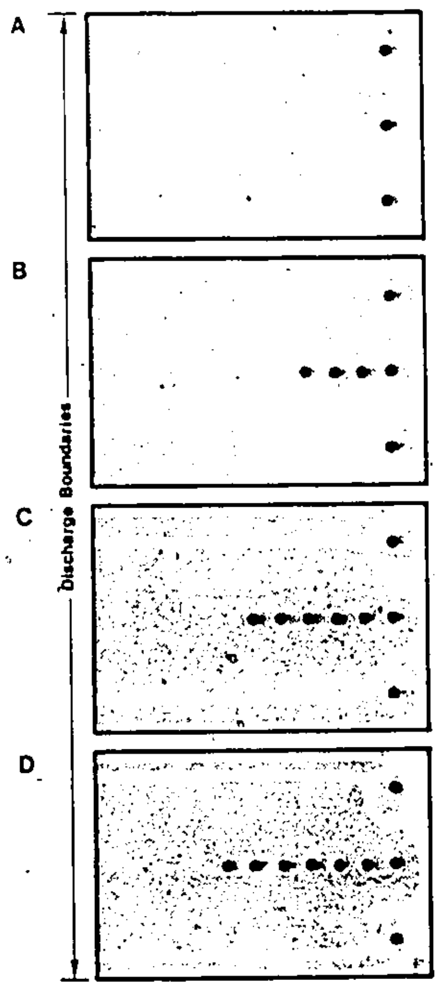

Figure 7.8
Flow envelope change with increasing length of dominant network.

The narrowness of the networks in the multiple input experiments is appa rently due to the narrower flow envelopes and the less divergent flow patterns, indicated by the equipotential lines being nearly parallel to the discharge boundary (Fig. 7.4).

7.2.4 THE MULTIPLE INPUT COMPETITION RULES
(THE LINEAR OUTPUT BOUNDARY CASE)

The results of these early experiments can be summarized in the following rule: where several inputs to a single bedding plane are in close proximity, they will evolve a small number of dominant distributary tube networks of maximum length and a larger number of shorter recessive networks. This divergent competition is intensified with increasing input density and by proximity of the recessive input to the dominant.

7.3 POINT RESURGENCE MULTIPLE INPUT EXPERIMENTS

In contrast to the early solution experiments with resurgences which were coincident with one of the four boundaries of the medium, the experiments in plaster were carried out primarily with point resurgences. These latter may be divided into asymmetrical configurations, where the inputs are colinear and the resurgence is placed to one side, and a symmetrical configuration, where inputs and resurgences are all located on the same axis.

7.3.1 ASYMMETRICAL MULTIPLE INPUT EXPERIMENTS

7.3.1.1 Purpose

The purpose of these experiments was to determine the relative rates and patterns of growth for tube networks, as a function of different densities under boundary conditions typical of steeply inclined strata. They relate specifically to the boundary conditions of the asymmetrical multiple input electric analogue experiments and the complementary flow envelope experiments. In this regard, they provide a test of the speleogenetic implication of those experiments. They also furnish insights into the competition between networks discharging to point resurgences.

7.3.1.2 Description

These experiments were conducted in a plaster medium, with a parting surface of type 100-B of the standard dimensions. A linear array of inputs was established near and parallel to one of the parting boundaries. The single point resurgence was located on a line parallel to an adjacent boundary and intersecting the input nearest that boundary. Three experiment types, employing three input densities and two different scales, were conducted. The scale changes were employed to increase the resolution of the experiments, and to reduce the number of inputs, thereby decreasing the failure rate of the experiments. Because of the scale differences, the input densities are most conveniently expressed in terms of the ratio between the input spacing and the orthogonal distance between the line of inputs and the output. These ratios are 1:4, 1:2, and 1:1 for Types One, Two, and Three respectively. Figure 7.9 shows the relationship of the inputs to the rectangular boundaries. These spacings reflect the rules in Table 5.1. An hydraulic gradient of 1:10 was used in all of the experiments. All inputs for a given experiment were provided with the same absolute head.

7.3.1.3 Expected Results

On the basis of the previous solution experiments with multiple inputs, we expect each input to develop a separate distributary tube network along the parting. The principal direction of that growth should follow the mean flow vector. Initially, the vectors will be those given by the flow envelope experiment depicted in Figure 6.13. Subsequently, the mean flow vectors will be modified by any differential growth of the several networks.

On the basis of the electric analogue experiments (Fig. 5.23), we would expect individual network growth rates in the Type One experiments in this series to be most similar.

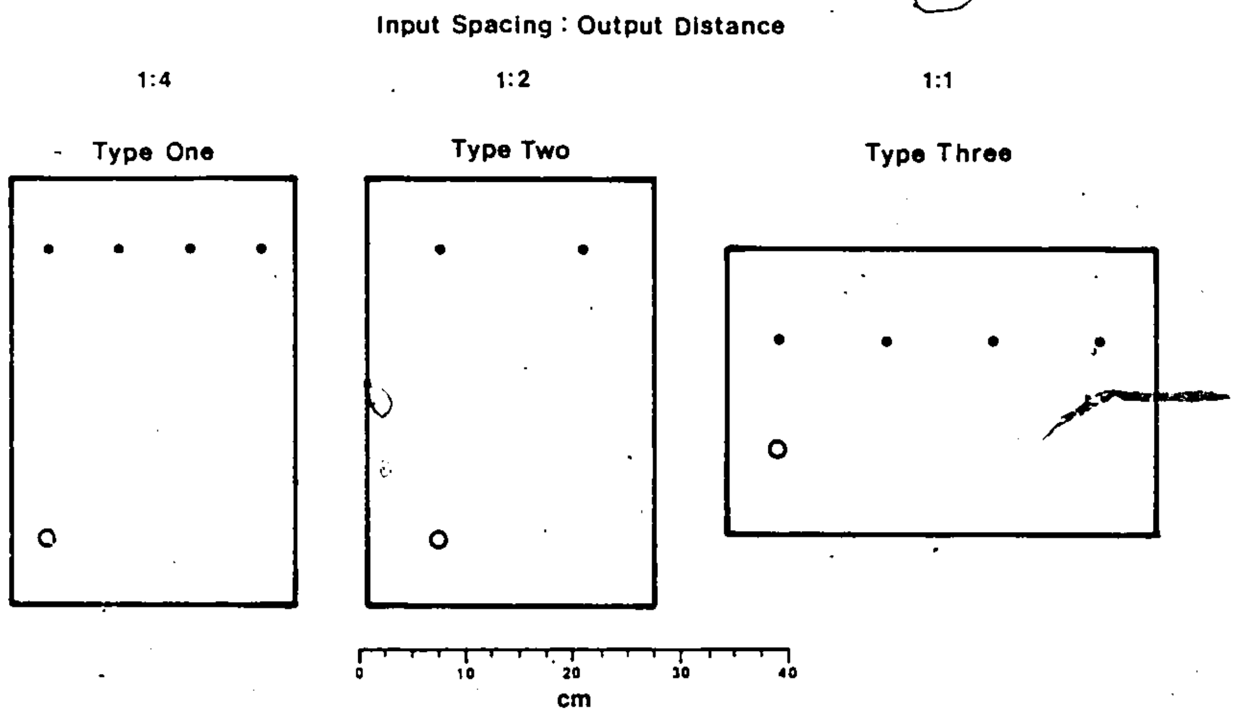

Figure 7.9
Input-output configurations for three types of asymmetrical, point discharge solution experiments.

These have input spacings which are a small fraction of the minimum input-output distance and do not extend laterally by more than that amount. Therefore, their mean flow paths are relatively similar in length. Type Three experiments should show the greatest diversity of growth rate. Their inputs are separated by an amount equal to the minimum input-output distance and extend laterally by three times that amount. Thus, their mean flow paths are relatively dissimilar.

We would anticipate that the high density of inputs in the Type One experiments would lead to slow growth relative to Type Three experiments. This expectation follows from the electric analogue data showing that total input Q is a direct function of density, while individual Q is an inverse density function.

The divergent competition due to length advantage in the linear - resurgence experiments was readily observed. Each input in these arrays had an equal initial Q. In the point resurgence experiments this competition effect should be partly masked by the diverse initial Q's conferred by their position.

7.3.1.4 Experiment Narrative and Results

7.3.1.4.1 Type One Experiments

Figures 7.1ØA-L depict stages in the progress of a typical four input Type One experiment. It also shows the scale and identity of its featues. Input number 1 had a

Figure 7.1Ø
Stages in the progress of a typical type one, asymmetrical, multiple input, point discharge, solution experiment.

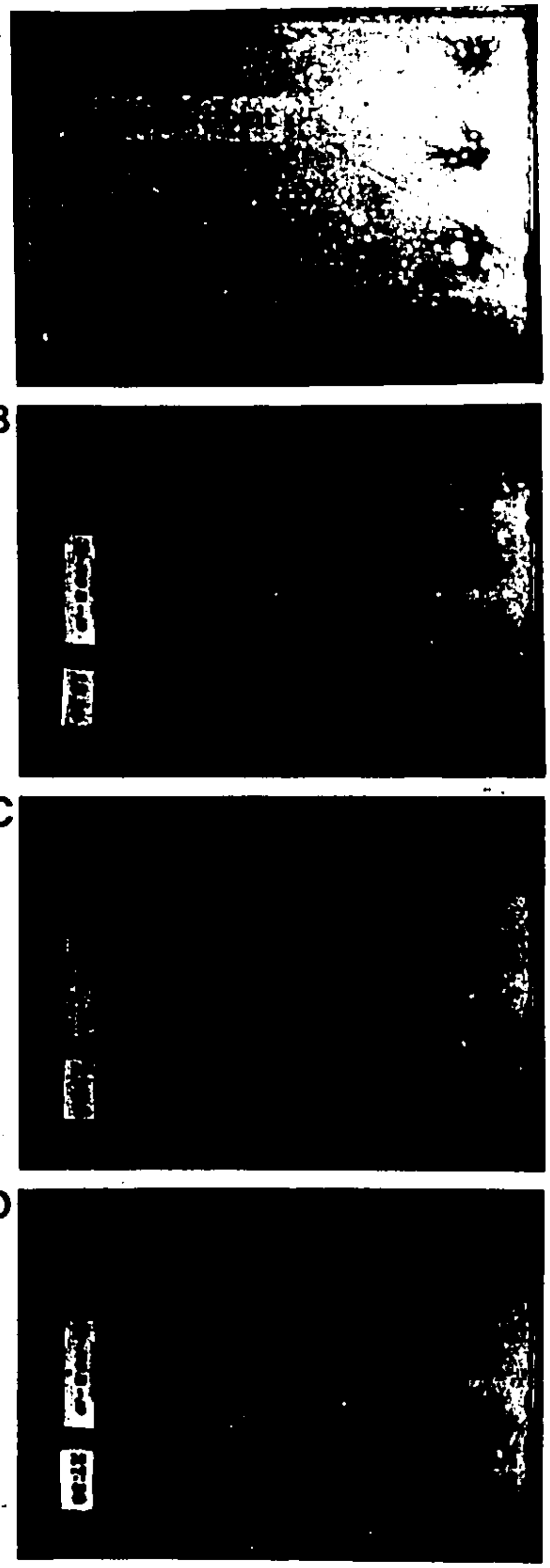

A

Time:12:00 hrs.

Experiment # 3-100-B-10

Flow Left

B

Time:15:30 hrs.

C

Time:21:00 hrs.

D

Time:27:30 hrs.

Time:39:ØØ hrs.

Experiment # 3-1ØØ-B-1Ø

Flow Left

E

Time:45:ØØ hrs.

F

Time:51:ØØ hrs.

G

Time:63:ØØ hrs.

H

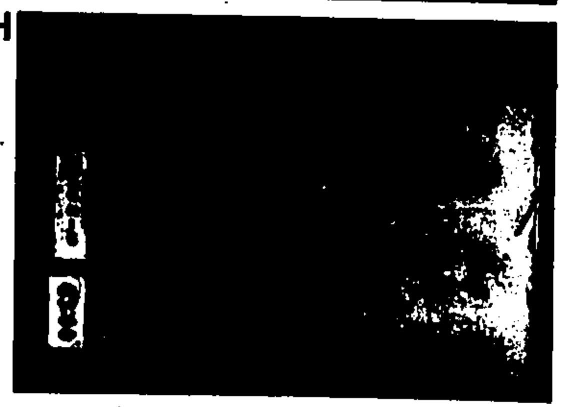

I

Time:72:00 hrs.

Experiment # 3-100-B-10

Flow Left

J

Time:75:00 hrs.

K

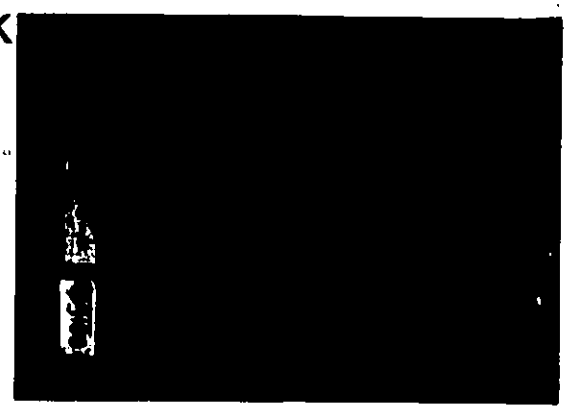

Time:84:00 hrs.

very slight theoretical growth advantage. In terms of straight line distance to the output, there was a difference of 1.1 cm or 4% between inputs 1 and 2. By the same reckoning the distances of inputs 3 and 4 were 12% and 27% longer, respectively, compared to input number 1. These slight geometrical advantages were overcome by hydraulic characteristics of the parting, and by 27 hours into the experiment, 32% of the total experiment time, inputs 2 and 4 had a clear actual growth advantage in terms of tube network length (Figure 7.10D). Growth rates for inputs 1 and 3 had slackened by 45 hours, 53% of the total experiment time, and after 51 hours (60%) no further change could be observed (Figures 7.10G-K). At 63 hours (75%), the growth of network 4 had slowed, and after 72 hours (85%) no further change could be observed (Figures 7.10I-K). Network 2 continued its growth and established a low resistance connection with the output. Figure 7.11 shows the total solvent discharge from the experiment as a function of time. The very steep rise in this value near 84 hours was taken as evidence of a low resistance connection. Table 7.2A shows the length of each network at 84 hours, expressed as a percent of the length of network 2.

7.3.1.4.2 Type Two Experiments

Figure 7.12 A-H depict the progress of a typical two input Type Two experiment. It also shows the scale and

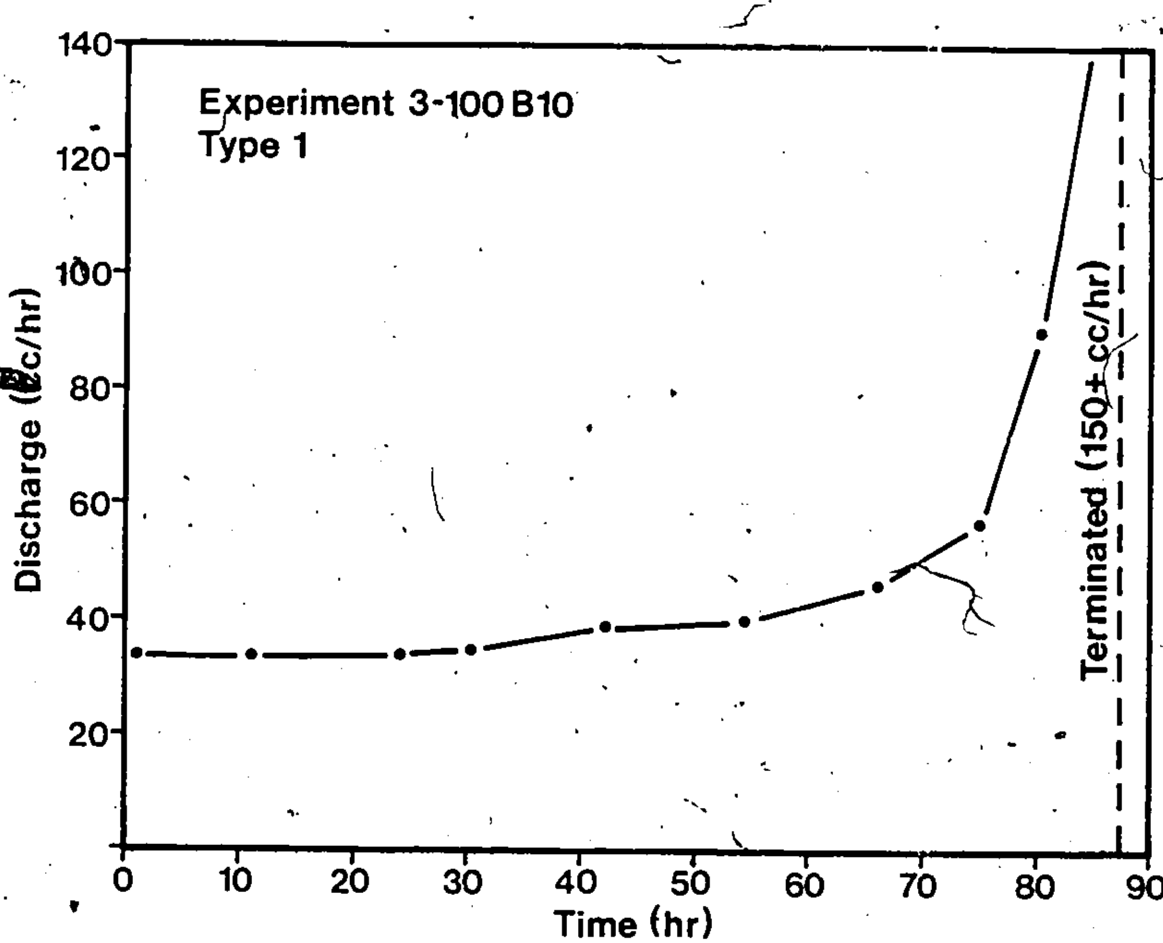

Figure 7.11
Discharge record for a typical type one, asymmetrical, multiple input, point discharge, solution experiment.

Table 7.2A

Network	Length cm.	Percent of Dominant Network length
1	14.5	52
2	28.0	100
3	15.0	53
4	23.5	84

Length of each network in a typical Type One asymmetrical multiple input experiment, expressed in centimeters and percent of the dominant network length.

Table 7.2B

Network	Length cm.	Percent of Dominant Network length
1	28	100
2	14	50

Length of each network in a typical Type Two asymmetrical multiple input experiment, expressed in centimeters and percent of the dominant network length.

Table 7.2C

Network	Length cm.	Percent of Dominant Network length
1	9.0	100
2	3.75	41
3	2.0	22
4	2.0	22

Length of each network in a typical Type Three asymmetrical multiple input experiment, expressed in centimeters and percent of the dominant network length.

identity of its features. Input 1 had a theoretical growth advantage of 3.5 cm or 12% over input 2 in terms of straight line difference to the output. Input 1 achieved a clear actual growth advantage at 18 hours, 23% of the total experiment time (Figure 7.12E). From this point until the conclusion of the experiment, input 2 showed a declining growth rate. Figure 7.13 shows the discharge record of the experiment. The steep rise in this value at 77 hours confirmed the visual observation of a low resistance connection with the output. The lengths of each network at 77 hours are given in Table 7.2B.

7.3.1.4.3 Type Three Experiments

Figure 7.14A-D depicts a typical four input experiment of this type. Input 1 has a clear theoretical advantage in straight line distance to the output. Inputs 2, 3, and 4 were longer by 6.2, 14.6, and 23.5cm (84%, 200%, and 328%) respectively. At 3 hours, 10% of the total experiment time, input 1 had developed an actual growth advantage (Figure 7.14B) but the decline in growth of network 2, 3, and 4 was less dramatic (Figure 7.14C). The steep rise in the discharge rate at about 29 hours confirmed the establishment of a low resistance connection with the output (Fig. 7.15). The lengths of each network at 29 hours are given in Table 7.2C.

Figure 7.12

Stages in the progress of a typical type two, asymmetrical, multiple input, point discharge, solution experiment.

Time:5:00 hrs.

Experiment # 3-100-B-24

Flow Left

A

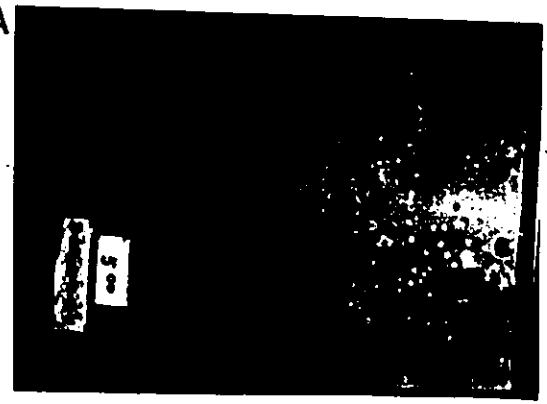

Time:11:00 hrs.

B

Time:18:00 hrs.

C

Time:30:00 hrs.

D

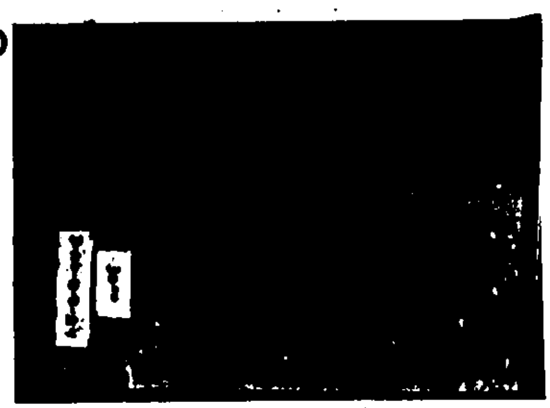

Time:39:ØØ hrs.

Experiment # 3-1ØØ-B-24

Flow Left

E

Time:52:ØØ hrs.

F

Time:77:ØØ hrs.

G

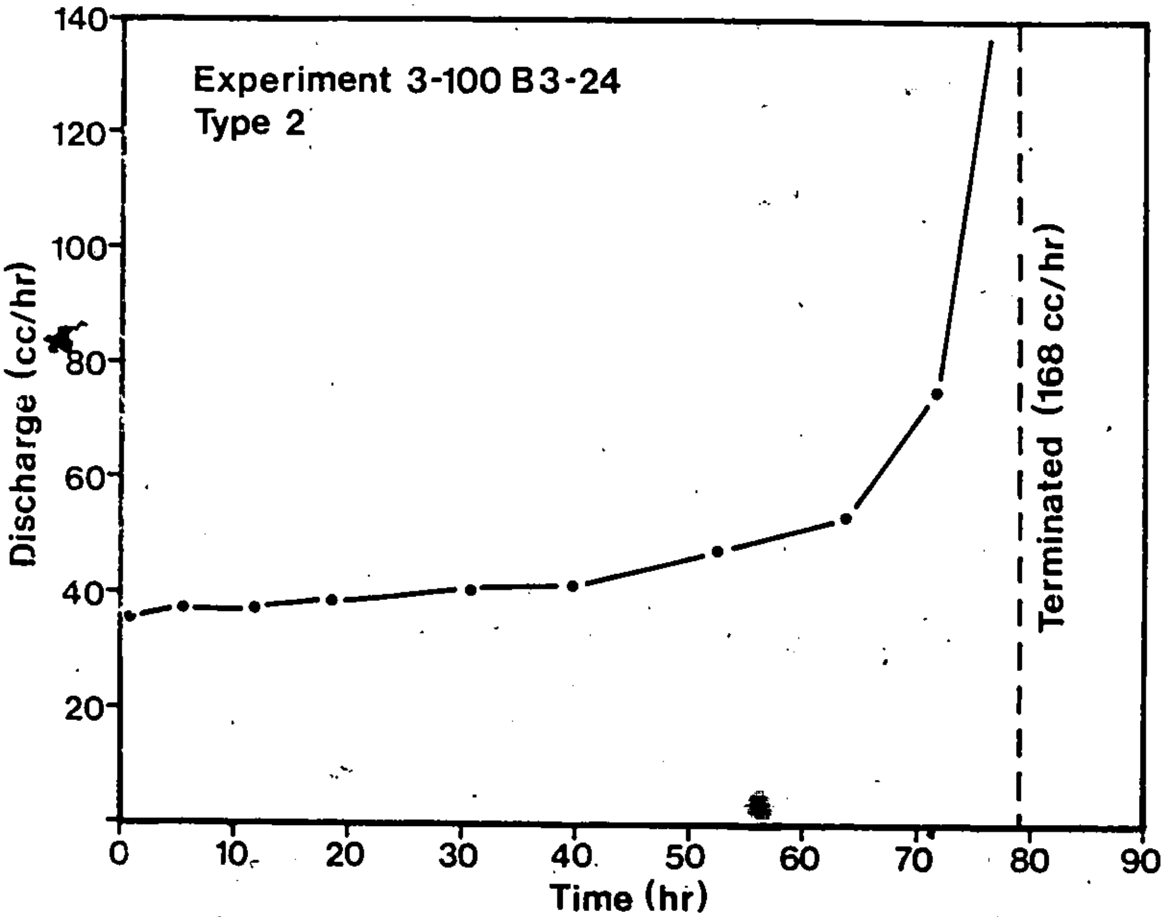

Figure 7.13
Discharge record for a typical type two, asymmetrical, multiple input, point discharge, solution experiment.

Figure 7.14
Stages in the progress of a typical type three, asymmetrical, multiple input, solution experiment.

Time:11:45 hrs.

Experiment # 3-100-B-1-15

Flow Left

A

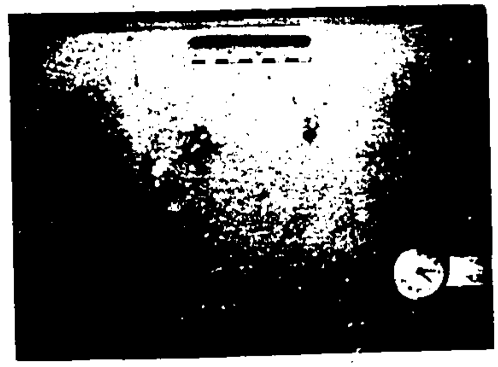

Time:26:00 hrs.

B

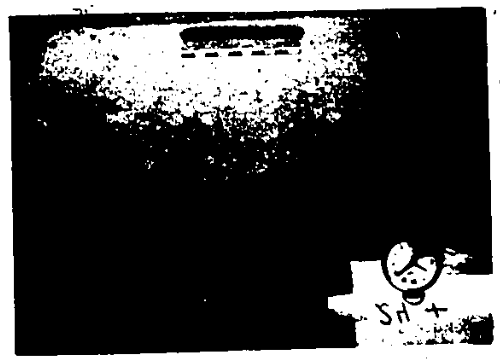

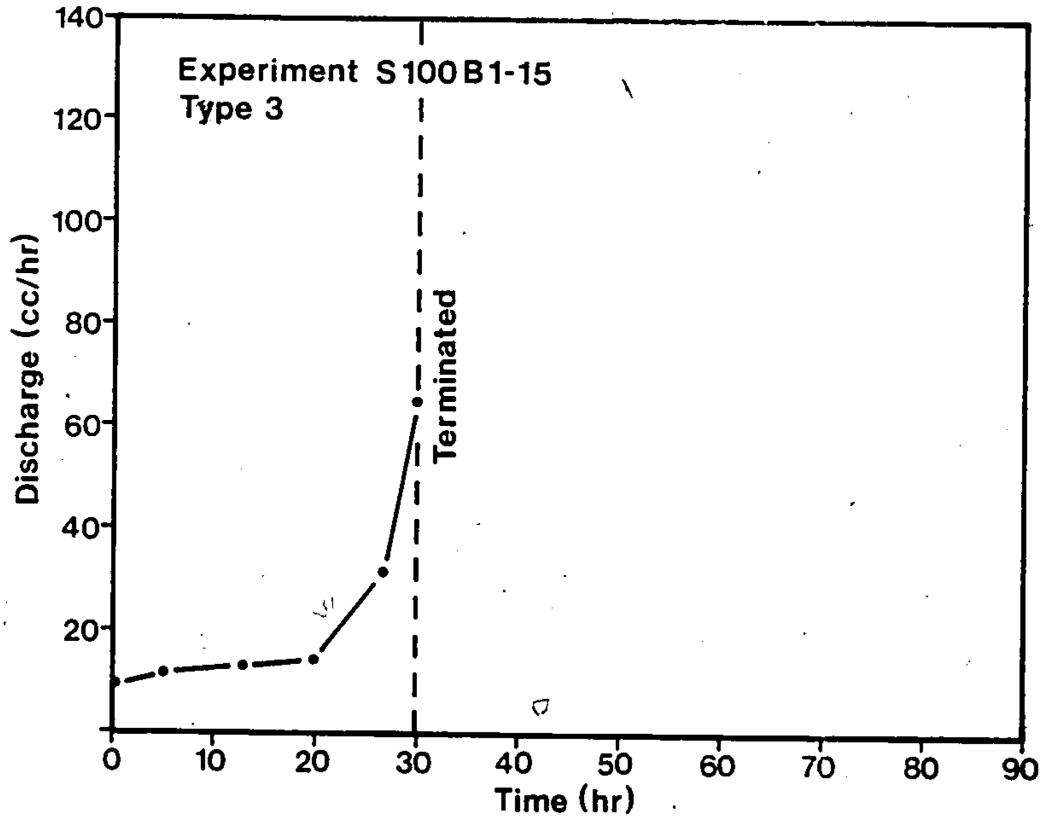

Figure 7.15
Discharge record for a typical type two, asymmetrical, multiple input, point discharge, solution experiment.

7.3.1.5 Summary

In all cases, the several inputs gave rise to separate tube networks as expected. Their growth directions were those predicted by the flow envelope models, with the exception of inputs 3 and 4 of the Type Three experiments. These appear to have been guided by the irregularities of the parting surface.

Individual network growth rates were most similar in the Type One experiments and most diverse in Type Three. Type Two experiments were intermediate in this regard. This is evidenced in two ways. First, the clear differentiation of the dominant network occurred most quickly in Type Three and least quickly in Type One as expected (Table 7.3). Second, the length of all the networks at the time of breakthrough were most similar in Type One. In Type Three, they were most dissimilar. Table 7.2 A, B, C presents these lengths as a percent of the dominant network length.

The high density experiment, Type One, showed the slowest growth as expected; Type Three the most rapid. This is evidenced by the time elapsed for breakthrough of the dominant network (Table 7.4).

7.3.1.6 Multiple Input Competition Rules

(The Asymmetrical Point Resurgence Case)

The results of these experiments can be summarized

Table 7.3

Experiment Type	Elapsed Time	
	Hours	Percent
Type One	27	32
Type Two	18	23
Type Three	3	10

Elapsed time to clear definition of the dominant network for three types of asymmetrical multiple input experiments. Data expressed in hours and percent of total experiment time.

Table 7.4

Experiment Type	Elapsed Time (Hours)
Type One	84
Type Two	77
Type Three	29

Elapsed time to breakthrough of the dominant network for three types of asymmetrical multiple input experiments. Data expressed in hours.

in the following rules. Where the ratio of input spacing to minimum input-output distance is large, the growth competition will be principally controlled by the input geometry. The proximal input will normally develop most rapidly, except in cases where the parting transmissivity or the activation time is well outside the values for the other inputs. Where the ratio of the input spacing to the minimum input-output distance is small, the growth competition between any two adjacent inputs will be principally under control of factors other than the input position. In both cases, however, proximal inputs overall have a higher probabillity of becoming dominant. Unlike the linear output case, point resurgence systems should develop a single dominant network.

7.3.2 SYMMETRICAL MULTIPLE INPUT SOLUTION EXPERIMENTS

7.3.2.1 Purpose

The purpose of these experiments was to determine the relative rates and patterns of growth for tube networks in co-linear multiple input arrays. They relate specifically to the boundary conditions of the symmetrical multiple input electrical analogue experiments and the complementary flow envelope experiments. In this regard, they provide a test of the speleogenetic implications of those experiments. They also furnish insights into the competition between networks discharging to point resurgences.

7.3.2.2 Description

These experiments were conducted in a plaster medium with a parting surface of type 1ØØ-B of the standard dimensions. A linear array of three inputs was established along the central axis of the medium, colinear with the single resurgence point. Equal spacing was used between all of these points. Figure 7.16 shows the relationship of the points to the rectangular boundaries. A hydraulic gradient of 1:1Ø relative to the proximal input was used in all of these experiments. The remaining inputs were provided with the same head.

7.3.2.3 Expected Results

On the basis of the preceding solution experiments involving multiple inputs, each input is expected to develop separate distributary tube networks along the parting. The principal direction of that growth should be directed along the mean flow vectors from each input. Initially, the vectors will be those given by the flow envelope experiment. Subsequently, the mean flow vectors will be modified by any differential growth of the several networks.

On the basis of the symmetrical point resurgence rules derived from the electric analogues, the individual growth rates of the networks would be expected to decrease with increasing distance from the output point.

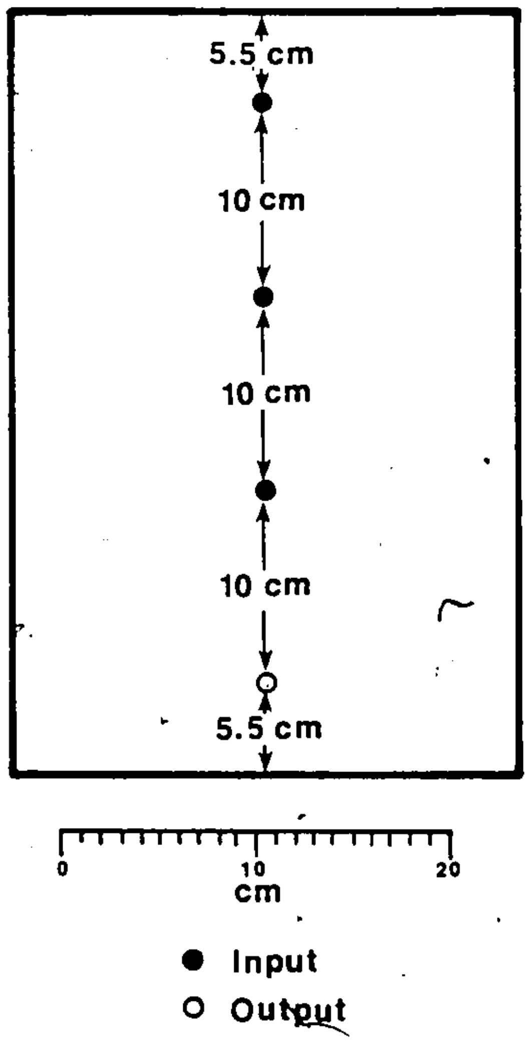

Figure 7.16
Input-output configuration for symmetrical, multiple input, point resurgence solution experiments.

On the basis of the corresponding flow envelope experiments, the flow from all inputs should be symmetrical about the input-output axis. In the case of input 1 (proximal), the highest flow rate, which determines the location of the principal tube, should be coincident with the input-output axis. On a similar basis, inputs 2 and 3, would be expected to divide their flow around the more proximally located inputs. These inputs should, therefore, give rise to a pair of principal tubes extending at right angles and in opposite directions from the input-output axis.

The early competition experiments suggest that the initial slow growth of the networks propagating from inputs 2 and 3 will be further reduced by the growth of the network extending from input 1. This is likewise consistent with the findings of divergent length competition in the asymmetrical point resurgence solution experiments.

7.3.2.4 Experiment Narritive And Results

Figures 7.17A,B depict the progress of a typical symmetrical point resurgence experiment. It also shows the scale and identity of its features.

Careful examination of the experiment surface immediately following the start of solvent flow revealed the presence of a dye front consisting of coloured water from each input which corresponded to the shape of the flow

Figure 7.17
Stages in the progress of a typical symmetrical, multiple input, point resurgence solution experiment.

Time:12:00 hrs.

Experiment # 7-010-B-3-26

Flow Left

A

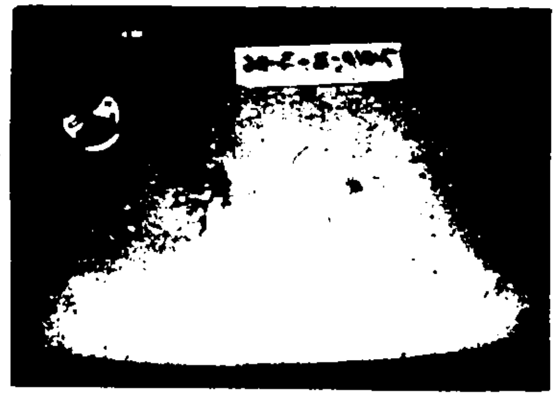

Time:25:00 hrs.

B

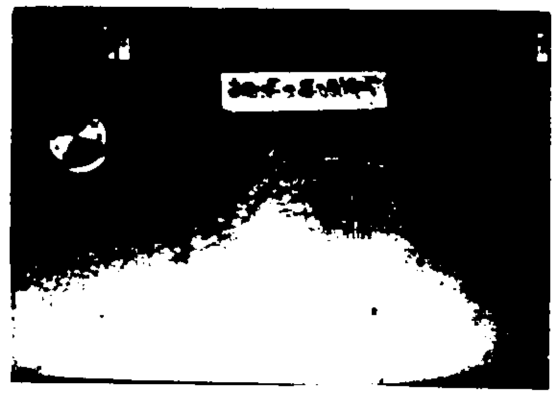

envelopes deduced by experiment in Chapter 6.4.1 (Fig. 7.17A). By four hours, 11 percent of the total experiment time, input 1 had established its growth pattern and was clearly the dominant network. At 18 hours, 50 percent of the total experiment time, small tube networks had extended approximately 5mm from input 2, but no perceptible change had occurred at input 3. At 36 hours, the termination of this phase of the experiment, input 1 had made a low resistance connection with the output. The connection was confirmed by a large increase in throughput (Fig. 7.18) and visually. Still, no perceptible change had occurred at input 3.

This solution experiment and the others of the series confirm the inferences made from the electric analogues and the flow envelope models which have already been stated. They also suggest that the addition of inputs in a system of this geometry has a minimum effect on the total amount of carbonate removed over the time span considered here. It is clear that the quantity of solute removed by solvents entering the experimental reaction surface at inputs 2 and 3 was very small in comparison to that removed by solvent entering by way of input 1.

7.3.2.5 Multiple Input Competition Rules
(The Symmetrical Case)

The results of these experiments can be summarized

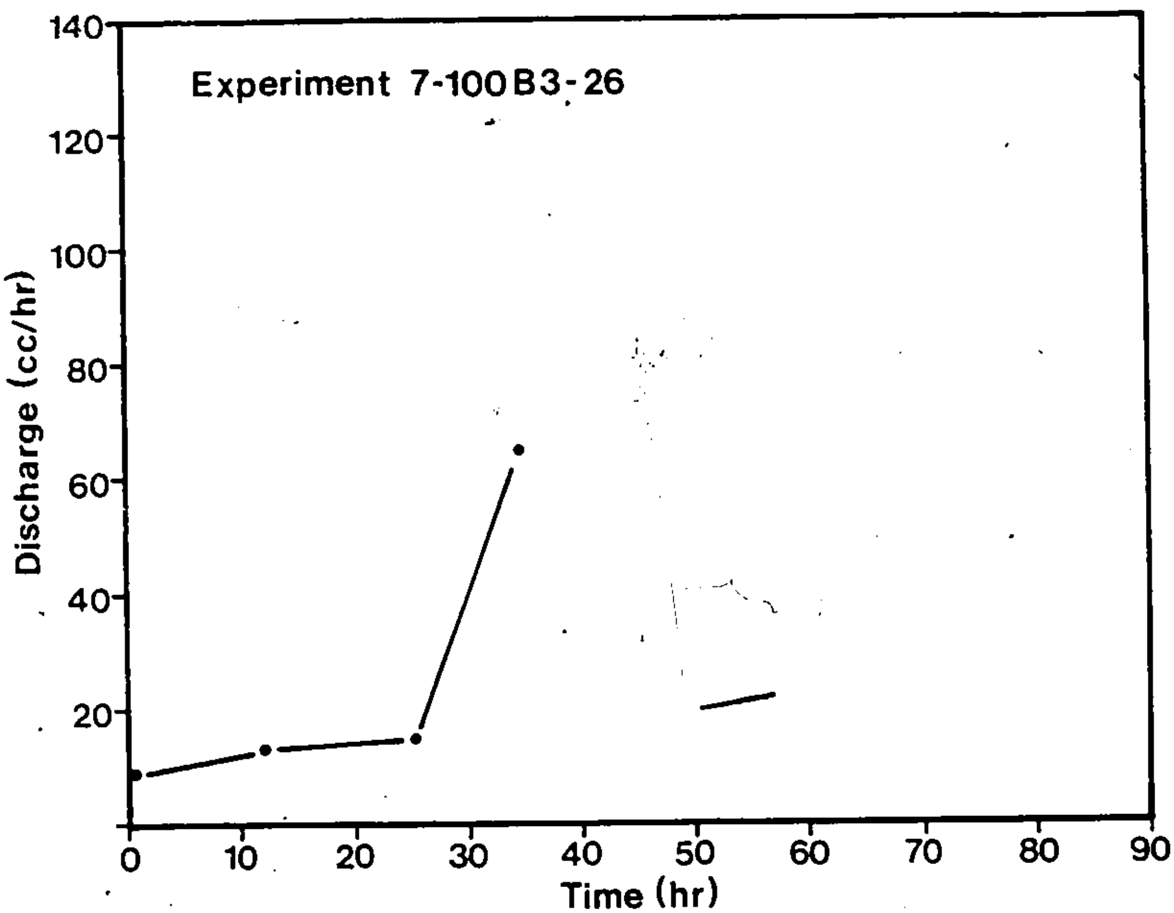

Figure 7.18
Discharge record for a typical symmetrical, multiple input, point resurgence solution experiment.

in the following rules. The competitive advantage of the proximal input in most cases is overwhelming, although it is lessened by increased input density. Of the three configurations considered in this study the inputs of the symmetrical case exhibit the greatest range of growth rates.

CHAPTER 8

THE NETWORK LINKING MODELS

8.1 INTRODUCTION

It has been demonstrated thus far that, to the extent that bedding plane partings in carbonate rocks function as continuous thin tabular resistance elements, the following statements can be made:

1. Each input should give rise to a separate network of distributary tubes.
2. The solution kinetics determine that the network propagate from the input to the resurgence.
3. The rate and direction of that propagation is related to the pressure field within the bedding plane. This is, in turn, related to the geometry of the inputs and resurgences and their relative fluid potentials.
4. As the networks grow, the pressure field must change and networks possessing high growth rate will retard the growth of those with slower growth rates.
5. The hydraulic capacity of a tube network changes abruptly when it achieves a low resistance link with the resurgence.

Prior to the establishment of a low resistance link with the output, the meteoric water catchment for an input is likely to be small because the network's discharge capacity is small. The discharge capacity is determined by the transmissivity of the remaining unaltered bedding plane parting through which the network must discharge, not the network itself. When a network breaches the bedding plane, its principal tube may then be capable of conducting all of the water available to it. In such a case, the head throughout the network will approach the level of the resurgence. This will produce a depression in the hydraulic potential field in the region of the network. Surrounding networks will respond to this pressure field change with an increase in their growth rates and a redirection of their growth toward the low resistance tube. The first of these to link with the initial low resistance tube will become the discharge target for some of the remaining networks. The details of such a linking system depend upon boundary conditions imposed by topography and geologic structure. Three linking models will be investigated: high dip, low dip, and restricted input models. These models encompass the range of common structural and topographic settings in karst regions.

8.2 The High Dip Model

8.2.1 GEOLOGIC AND HYDROLOGIC SETTING

8.2.1.1 Input Geometry

In steeply dipping carbonate sequences, meteoric waters may have direct access to bedding planes. This occurs along the strike, where these partings are truncated by surface erosion. Specific input sites may have greater efficiency if they are localized at points where small allogenic surface streams or minor topographic depressions provide a more continuous water supply (Fig. 8.1).

8.2.1.2 Resurgence Geometry

Resurgences may occur at any point of truncation of the bedding plane lower than the input points, or by way of faults or joints which communicate waters from the bedding plane to a point on the surface at a lower elevation than the inputs. Truncations which commonly provide for drainage of steeply dipping karst rocks are produced by surface erosion parallel to the dip (Fig. 8.1). Such erosion provides drainage for subsurface waters along the strike. Ford (1971) recognized that strike drainage is a common and important characteristic of steeply dipping karst aquifers. Examples of this hydrogeological setting abound: the Crowsnest Pass karst, British Columbia, exhibits drainage to the strike both north and south to a central east-west trending glacial valley which forms the pass (Ford et al., 1972); the Holloch, Muotatal, Switzerland, one of the largest mapped subsurface karst systems, drains via the strike to a fluvio-glacial valley (Bogli, 1970); the central Mendip karst in England (Ford, 1968); Ogof Ffynnon Ddu in

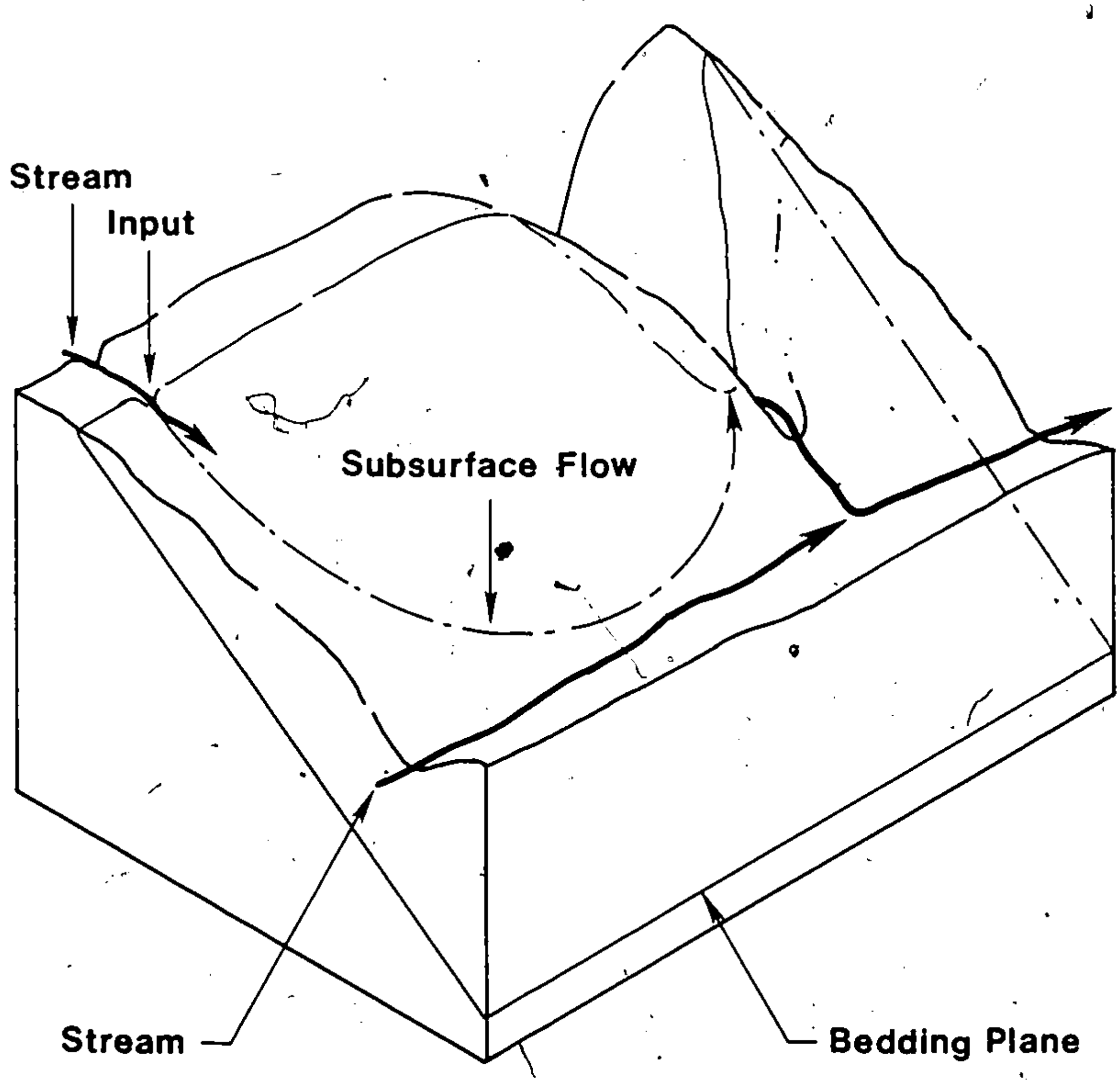

Figure 8.1
Relationships between bedding planes and input-output geometry for steeply dipping beds.

Wales (Charity and Christopher, 1977); the Pine Mountain karst in Kentucky; the Nittany Valley karst in Pennsylvania (Drake and Harmon, 1973); and Postojna Cave, Yugoslavia (Gams, 1965).

8.2.2 EVOLUTION OF THE LINKING PATTERN

Figure 8.2A-E illustrates the development of the high dip linking pattern. In this simplified case (Fig. 8.2A), three inputs are localized along the outcrop of a penetrable bedding plane. A vertical joint is assumed to communicate to the surface from Point P, providing a single resurgence for the discharge of waters entrained in the bedding plane. A driving potential (h) is assumed for all three inputs.

The asymmetrical point resurgence rules (Chapter 5.3) indicate that input 1 will have the highest throughput, with successively smaller Q values for inputs 2 and 3. The asymmetrical point resurgence solution experiments (Chapter 7.3) predict that the growth rates of the tube networks arising from the three inputs will be in proportion to their throughputs. The correspsonding flow envelope experiments (Chapter 6.4.2) indicate that the initial mean flow vectors will be as indicated in Figure 8.2A.

As tube network development proceeds (Fig. 8.2B), the mean flow vectors will be forced to deeper levels by the rapid growth of the network developing from input 1. The

Figure 8.2 A, B, C, D, E
Stages in the evolution of the high dip linking pattern.

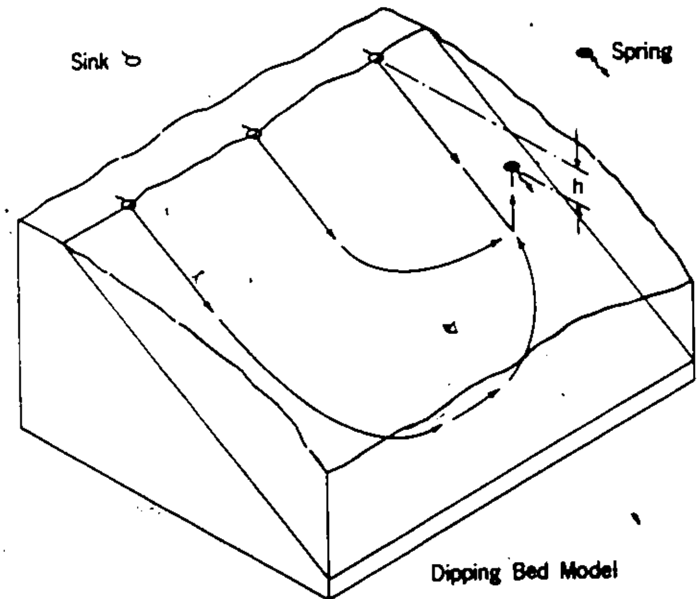

Dipping Bed Model

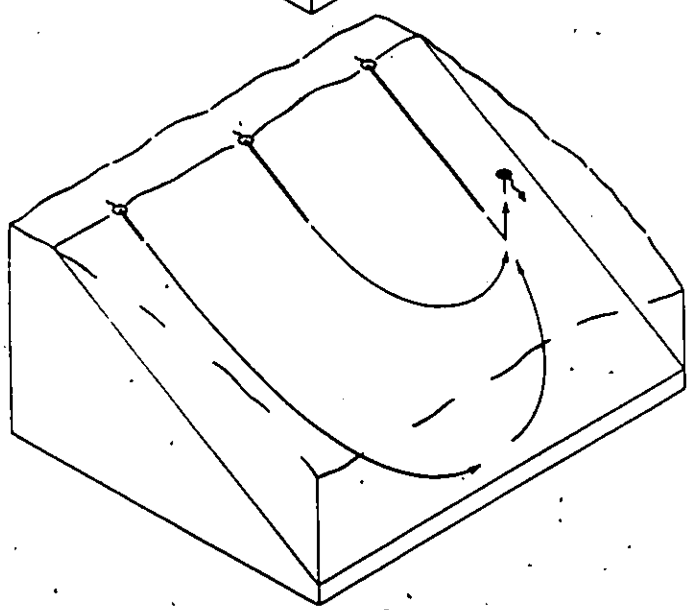

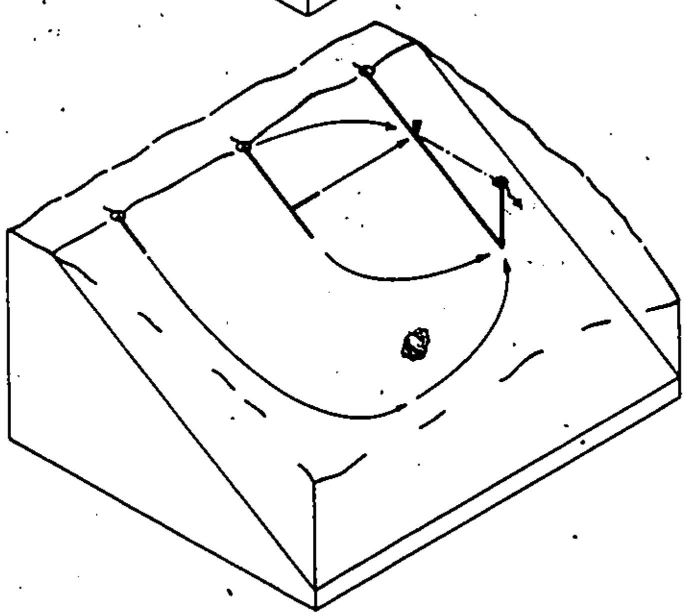

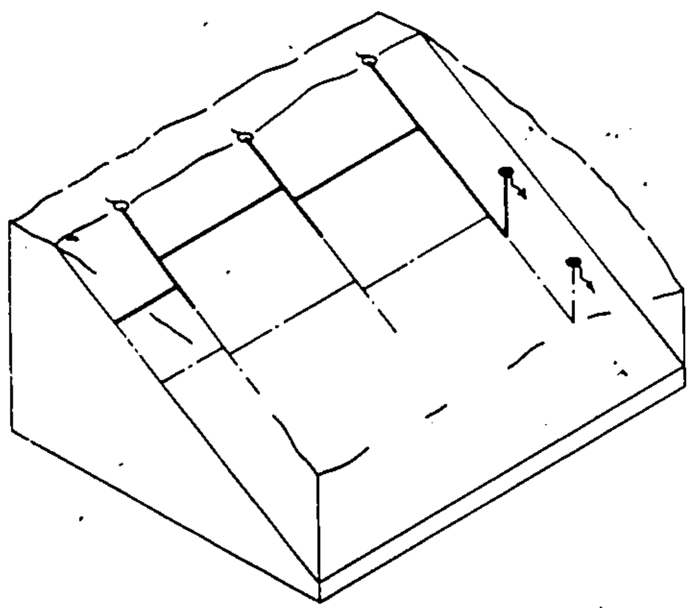

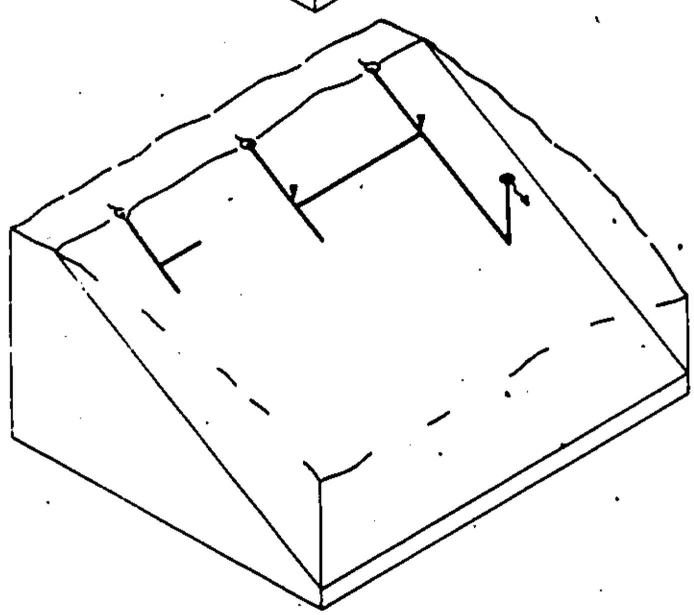

rates of propagation of the networks developing from inputs 2 and 3 will decrease in the manner shown by the network competition experiments (Chapter 7.2). Note that the developing networks are simplified to the extent that principal tubes alone are shown.

In Figure 8.2C, network 1 has completed a low resistance connection to the output, and it is assumed to have enlarged to a degree sufficient to conduct all the water available to input 1 under average circumstances. Because point A is at the same elevation as the resurgence, network 1 will be permanently phreatic below this point and usually vadose above it, given a minimal head to overcome friction. Throughout the permanently phreatic portion, the pressure will be reduced by (h) relative to the condition before establishment of the resurgence connection.

Input 2 (Fig. 8.2C) is developing in response to a head difference or hydraulic potential of (h). Before the breaching of network 1, that head difference was available only at point p via a long discharge path through portions of the bedding plane unmodified by solution. After the breaching of network 1, that head difference became available at all points along network 1 between point A and the resurgence, along flow paths which are significantly shorter. Above point A, progressively smaller head losses are available to network 2. Under these altered conditions, network 2 will discharge in increased amounts to all points along network A. At some site of favorable circumstance, a strike line connection will develop (Fig. 8.2D) which will lower the pressure of network 2 by (h) at all points below B.

Network 2 now possesses the hydraulic characteristics to which network 3 was discharging, and a second strike line connection will evolve. Other inputs existing along the same outcrop line would link to the resurgence by way of intervening networks in a similar way.

8.2.3 REPETITION OF THE LINKING PATTERN

Should the surface erosion processes which established the initial resurgence expose a second lower resurgence, an extension of the existing dip tubes and additional strike connections could evolve. The lower reaches of networks 2 and 3 (Points C and D, Fig. 8.2D) remain in a phreatic condition, even at times when the strike connections may be dry. There would be a reactivation of dip tube propagation from these points, as well as from point P toward the new resurgence. New lower level strike connections would develop in response to low resistance connections to this resurgence in the manner already described (Fig.8.2E). With appropriate hydrogeologic circumstances, this linking scheme could be repeated many times.

8.2.4 FACTORS CONTROLLING STRIKE CONNECTIONS

The location of a strike connection is controlled by two factors: head differences between dip tubes and the distribution of abnormal transmissivity zones between the tube networks. The pressure distribution between a dip tube network, which has evolved a low resistance connection to the resurgence, and adjacent networks, which are not so connected, can be analysed with the help of Figure 8.3A. The three dimensional relationships of the tubes in this figure can be seen in Figure 8.3B.

Input 1 is connected to the resurgence at point G. This connection and the position of the resurgence relative to the dip of the bedding plane controls the water level in network 1 to its midpoint, point D. Inputs 2 and 3 maintain a pressure of one unit above points A' and A" respectively. The pressure in equivalent units for the lettered points along all three networks with respect to atmospheric pressure are listed on Figure 8.3A. Similarily, the pressure differences between adjacent points in the three networks are listed in Table 8-1. It should be noted, that pressure comparisons are the equivalent of head loss comparisons only when the two points lie at equal elevations. Because the flow in this case is principally horizontal, we may assess tube growth rates between these points on the basis of the pressure comparisons. The head

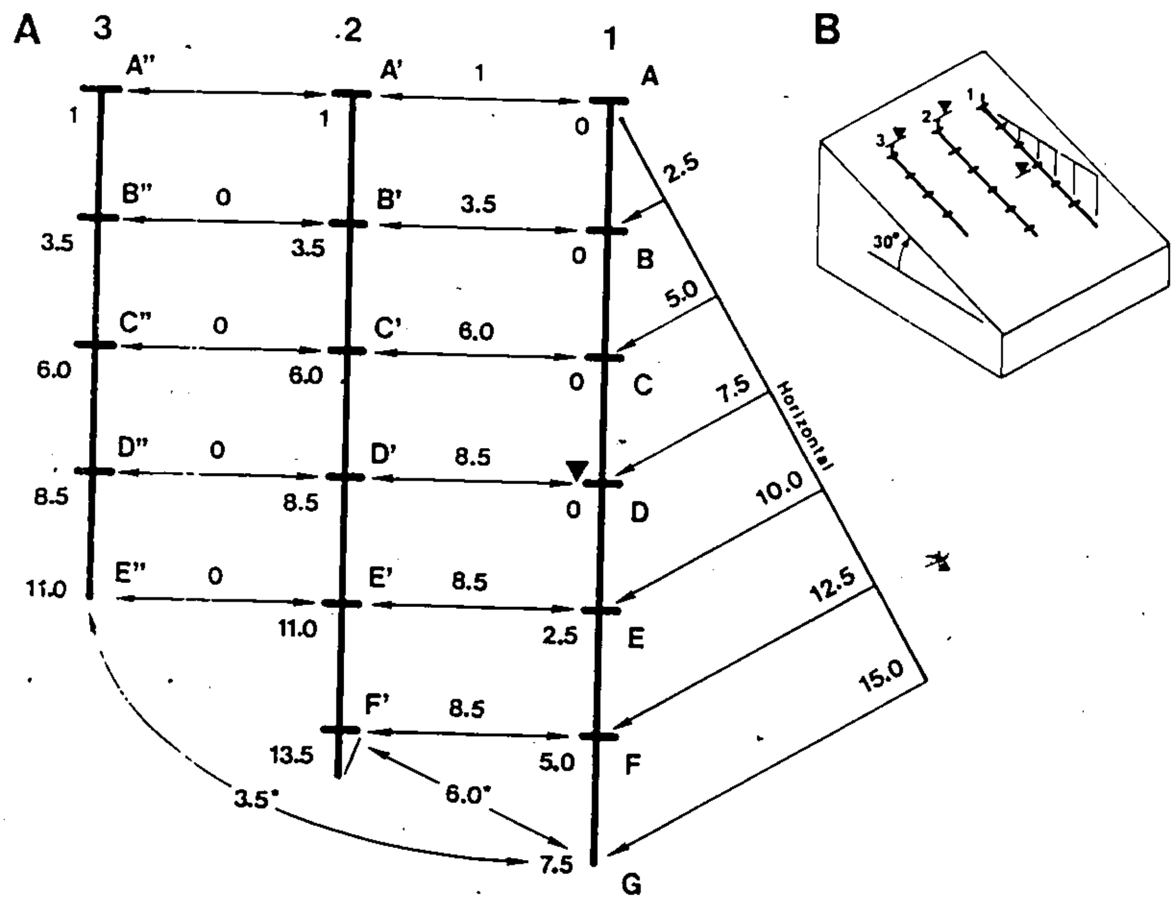

Figure 8,3
Pressure relationships controlling the development of strike oriented conduits between dip tubes.

Table 8-1

Point	Network 1 Head	Head Diff	Network 2 Head	Head Diff.	Network 3 Head
A	Ø	1	1	Ø	1
B	Ø	3.5	3.5	Ø	3.5
C	Ø	6.Ø	6.Ø	Ø	6.Ø
D	Ø	8.5	8.5	Ø	8.5
E	2.5	8.5	11.Ø	Ø	11.Ø
F	5.Ø	8.5	13.5	-	-
G	7.5	-	-	-	-

Head difference values for Figure 8.3.

loss between adjacent points in networks 1 and 2 increases to the level of points D and D'. Below that level, the head difference remains constant. Other factors being equal, initial strike line connection growth should proceed most favorably in the region between the fluid level in the mature dip tube (D) and the terminus of the adjacent dip tube. Connections beyond the terminus are subject to the same fluid potential found at higher potential connecting sites, but the distance along the flow lines is greater and, therefore, the fluid resistance is increased. The tube growth should, thus, be slower, and the likelihood of a connection proportionally less.

In his study of the central Mendip karst, Ford (1968) recognized "true strike subsequent" and "irregular strike subsequent" elements connecting dip oriented tubes. He attributed these pattern differences to the hydraulic characteristics of the bedding plane between the dip tubes. In analyzing this situation, it must be borne in mind that where the bedding plane porosity is ideally uniform, isotropic, and of capillary size, flow will move normal to the flow boundaries in nearly straight and horizontal paths between the sub-parallel dip tubes. This will be true even in the case where one dip tube is partly air filled, as will be shown below. If the actual elements forming the porosity are of uniform hydraulic characteristics, and uniformly and closely spaced, then it will be possible for the flow to select a path and subsequently develop a tube along the ideal, "true strike", path. Per contra, if these elements are of variable hydraulic characteristics, and randomly and widely spaced, then "irregular strike connections" departing significantly from the horizontal are more likely, as Ford suggests.

8.2.5 EXPERIMENTAL VERIFICATION

A special solution experiment was performed to test the foregoing theoretical analysis (Fig. 8.4). Three simplified distributary networks, with branches corresponding to the lettered points of Figure 8.3A, were routed into a plaster block. Inputs and a resurgence were provided at the scale of 1 cm = 1 unit. Solvent flow was initiated with the experimental surface oriented at 30 degrees to the horizontal. Strike line connections began to develop between the corresponding points A through F of networks 1 and 2 as well as from F' to G. The experiment was terminated at 25 hours, prior to the establishment of a complete strike connection. Connections A through D showed increasing length, while D through F were comparable. The F' to G connection had a very slow growth rate. The lengths of the connections are compared in Table 8-2, corroborating the theoretical growth rate analysis.

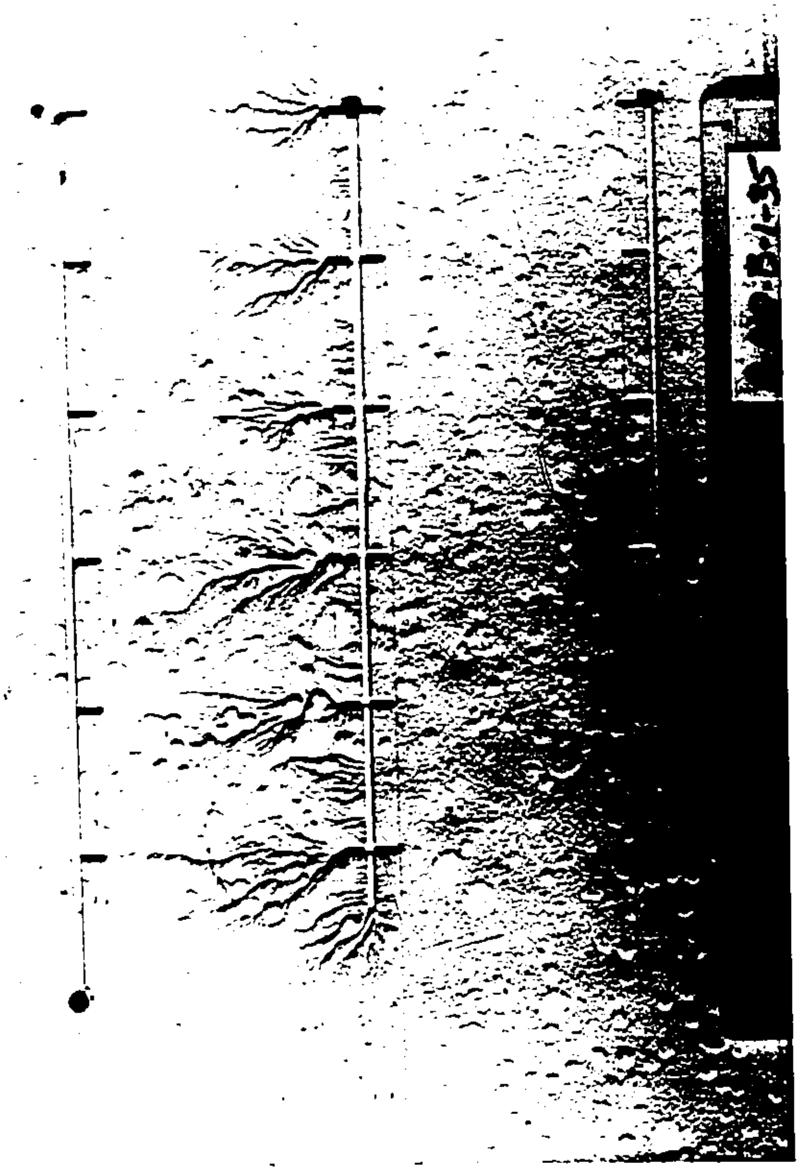

Figure 8.4
Solution experiment showing the development of strike oriented conduits between dip tubes.

Table 8-2

Distributary	Length(mm)	Rank
A-A'	48	6
B-B'	56	5
C-C'	57	4
D-D'	75	3
E-E'	76	2
F-F'	84	1
F'-G	33	7

8.2.6 SUMMARY

The high dip linking scheme can be characterized in the following ways:

1. Subsurface drainage basins should be established by a stepwise integration of small distributary sub-units into a tributary system.

2. The integration of the system should proceed from the resurgence in a headward direction, the opposite of the direction of the network propogation.

3. The plan form of the conduit pattern should develop in what approximates a rectilinear pattern. The elements of that pattern which are oriented parallel to the dip predate the elements which connect them along the strike.

8.3 The Low Dip Model

8.3.1 GEOLOGIC AND HYDROLOGIC SETTING

8.3.1.1 Input Geometry

In near horizontal carbonate sequences, meteoric waters usually have access to bedding planes by way of joints and faults. Cvijic (1893), Chabot (1927), Kunsky (1958), Lavalle (1967), and Williams (1969) among many others, have described the importance of joints and faults in the formation of dolines and the conduction of meteoric water into existing subsurface drainage networks. They should be no less important in the initiation of those networks.

The horizontal aspect of the limestone is likely to produce a situation in which inputs may occur at many points over a large area of the rock unit. It is probable, however, that not all inputs are active from the beginning. Surface erosion processes normally work to a more or less graded profile, which would tend to activate inputs in a systematic sequential manner from regions occupied by higher order streams toward areas of streams of lower order. Where the limestones are capped by impermeable units, stream valleys may be the sites where surface waters may first enter the soluble carbonates. In any case, inputs along stream valleys are likely to be most efficient in developing initial voids in the subsurface in that they may provide a more continuous solvent source.

8.3.1.2 Resurgence Geometry

Resurgences are likely to occur along major stream valleys which truncate the bedding plane at positions lower than the input. These may provide continuous linear exposure over great distances. Depending upon the gradient of the stream and minor structural factors, the resurgence may be initiated in a spotty or even a systematically expanding manner. For the sake of simplicity, the model will be constructed assuming that all inputs and the total length of the resurgence become available simultaneously. Staging of the input and resurgence activation will be dealt with later.

8.3.2 EVOLUTION OF THE LINKING PATTERN

Figure 8.5A-E illustrates the development of the low dip linking pattern. In order to further simplify the analysis, the following non-essential assumptions are made: 1. two ranks of equally spaced inputs are available in positions parallel to the discharge boundary; 2. rank density is twice the rank spacing; 3. vertical joints communicate between the surface and the horizontal bedding plane; 4. an equal head (h) is present at all inputs (Fig. 8.5A).

The rank spacing rules (Chapter 5.2.3) indicate that under the specified conditions, rank 1 inputs will have initial Q values more than ten times those of rank 2. The complementary solution experiment (Chapter 7.3.2) suggests that their growth rates will be in proportion to these Q values. Furthermore, the electric analogue competition experiments (Chapter 7.2.3.2) have shown that, as the rank 1 networks lengthen, the discharge, and therefore, the growth rate of rank 2 networks will decrease (Fig. 8.5B).

Within rank 1, a growth competition should occur of the type seen in the solution experiments in Chapter 7.2. A

Figure 8.5 A, B, C, D, E
Stages in the development of the low dip linking pattern.

A

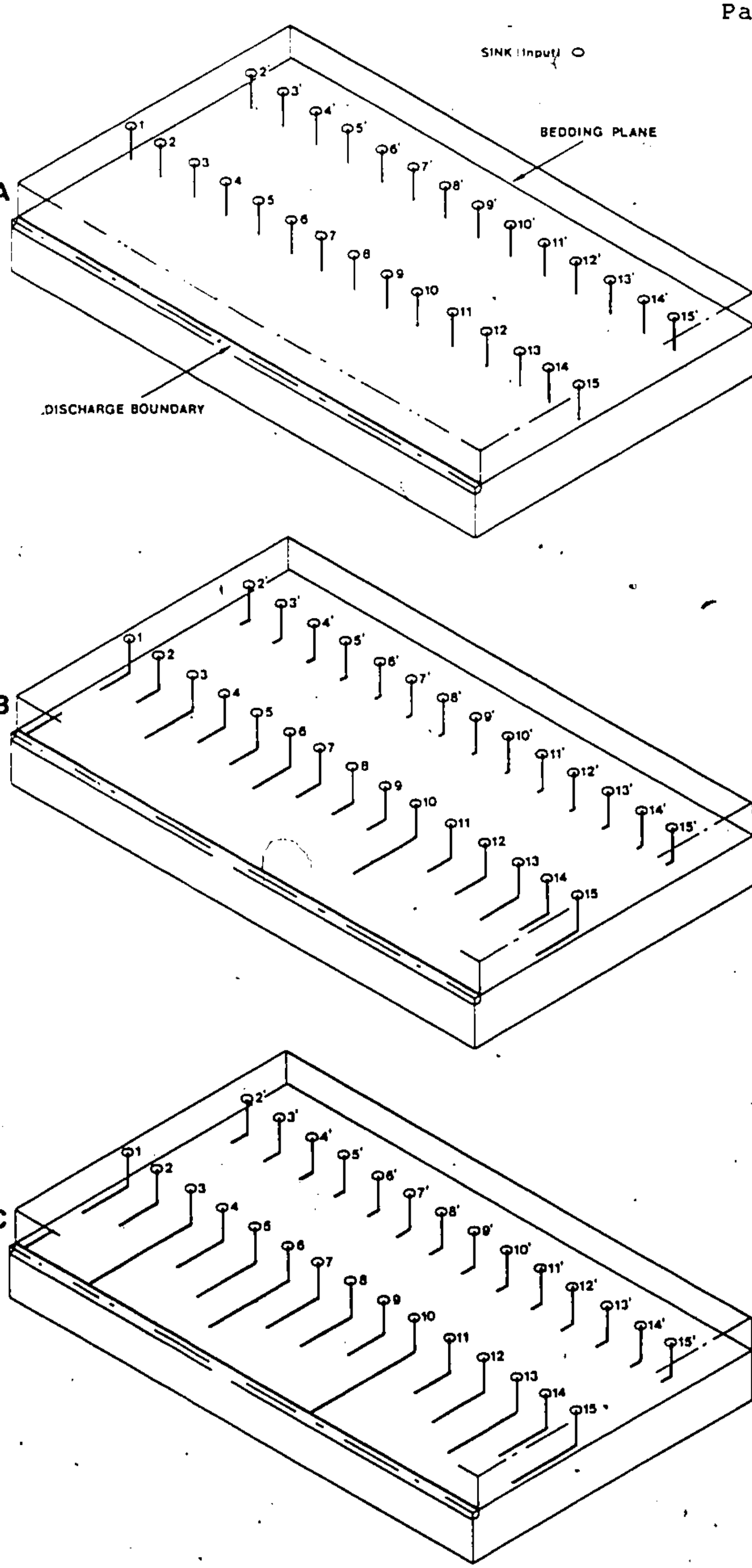
SINK (Input)
BEDDING PLANE
DISCHARGE BOUNDARY
1
2
3
4
5
6
7
8
9
10
11
12
13
14
15
2'
3'
4'
5'
6'
7'
8'
9'
10'
11'
12'
13'
14'
15'

B

C

D

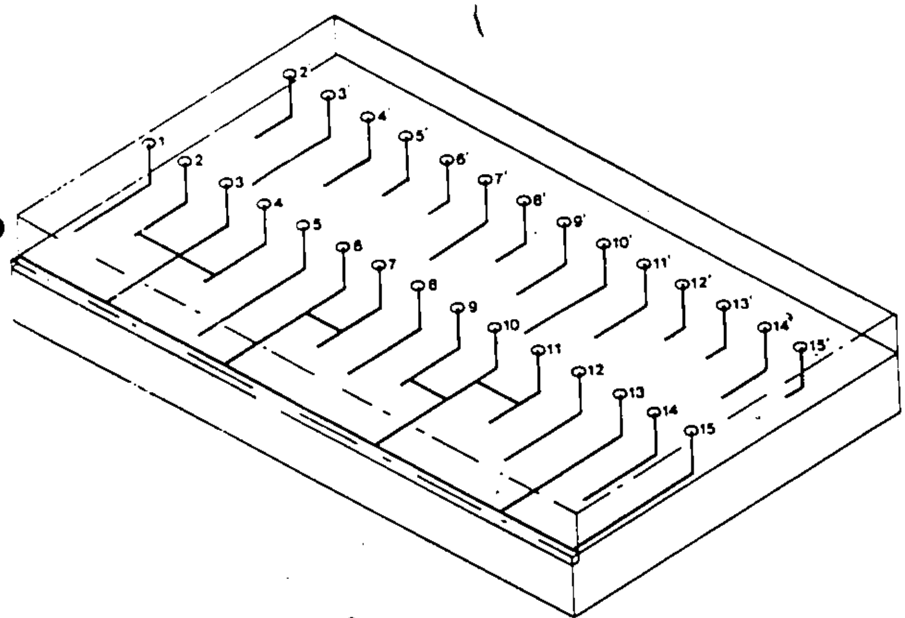
1
2
3
4
5
6
7
8
9
10
11
12
13
14
15
2'
3'
4'
5'
6'
7'
8'
9'
10'
11'
12'
13'
14'
15'

E

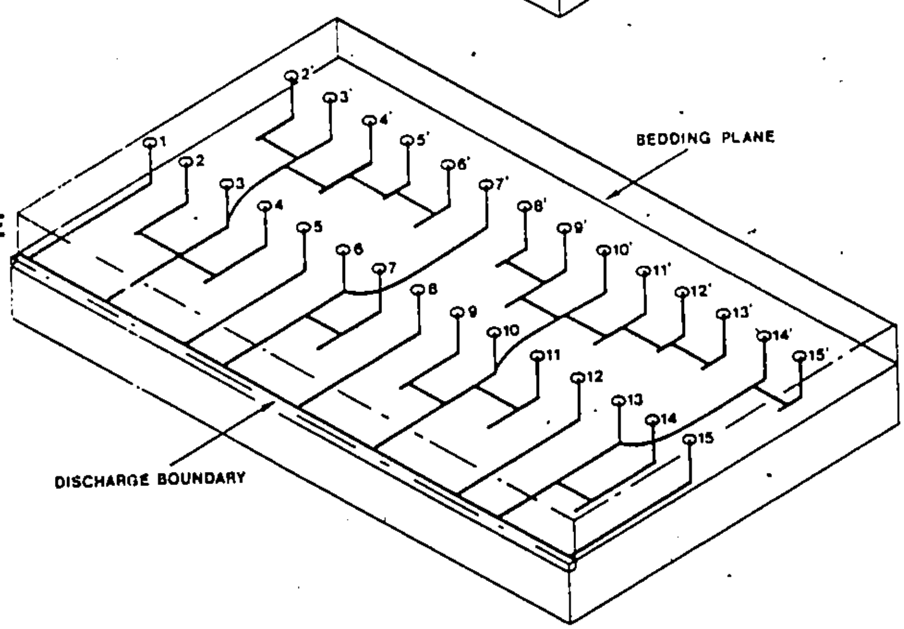
BEDDING PLANE
DISCHARGE BOUNDARY
1
2
3
4
5
6
7
8
9
10
11
12
13
14
15
2'
3'
4'
5'
6'
7'
8'
9'
10'
11'
12'
13'
14'
15'

few rank 1 networks, because of favorable circumstances, will grow rapidly at the expense of neighboring networks. Favorable circumstances would include locally higher bedding plane transmissivity, or the presence of a minor joint near the input, with an orientation parallel to the piezometric slope. These favored networks will establish the initial low resistance connections with the discharge boundary (Fig. 8.5C).

If we assume that the low resistance links can quickly come into equilibrium with the solvent supply, the head at the input of these systems will drop to a value close to that of the discharge boundary. The growth of the two adjacent networks will then be attracted toward them (Fig. 8.5D). In the multiple input linear discharge solution experiments, the networks adjacent to the rapid growth networks were invariably the shortest. This insures that the lateral connection, path A (Fig. 8.5D), has a high probability of being more efficient than continued growth toward the discharge boundary along path B.

With the establishment of the first low resistance link between rank 1 and the discharge boundary, the growth of networks in rank 2 will be stimulated. Their pattern of growth should be similar to the point resurgence model already described, and they should respond with growth rates and directions predicted by the point resurgence electric analogues (Chapter 5.3) and the asymmetrical point resurgence solution experiments (Chapter 7.3). The reason for this type of response is that inputs 3 and 1Ø (Fig. 8.5D) provide the principal discharge for rank 2. Their character is that of point discharges at positions 3 and 1Ø, and only minor flow can take place between the unlinked inputs of rank 1. A potential field map for this configuration is shown in Figure 8.6 and indicates high flow between networks 2 and 3, and 4 and 3, with moderate flow between input 3 and inputs 2', 3', 4', and 5'. The result should be that inputs 3' and 1Ø' will grow rapidly with progressively slower growth for rank 2 inputs of increasing distance from these inputs (Fig. 8.5D). The connection of inputs 9 and 11 to input 1Ø, and 2 and 4 to input 3, should further stimulate the growth of rank 2 inputs. When input 3' and 1Ø' establish low resistance links with their corresponding rank 1 networks, adjacent rank 2 inputs should one by one link to it (Fig. 8.5E).

8.3.3 SUMMARY

The low dip linking scheme can be characterized in the following ways:

1. The number of springs of a given size should be inversely proportional to their drainage area. This is to say a small number of large springs and a large number of small springs should drain the area.

Figure 8.6

Potential fields governing the development of conduits parallel to the discharge boundary in the low dip linking model.

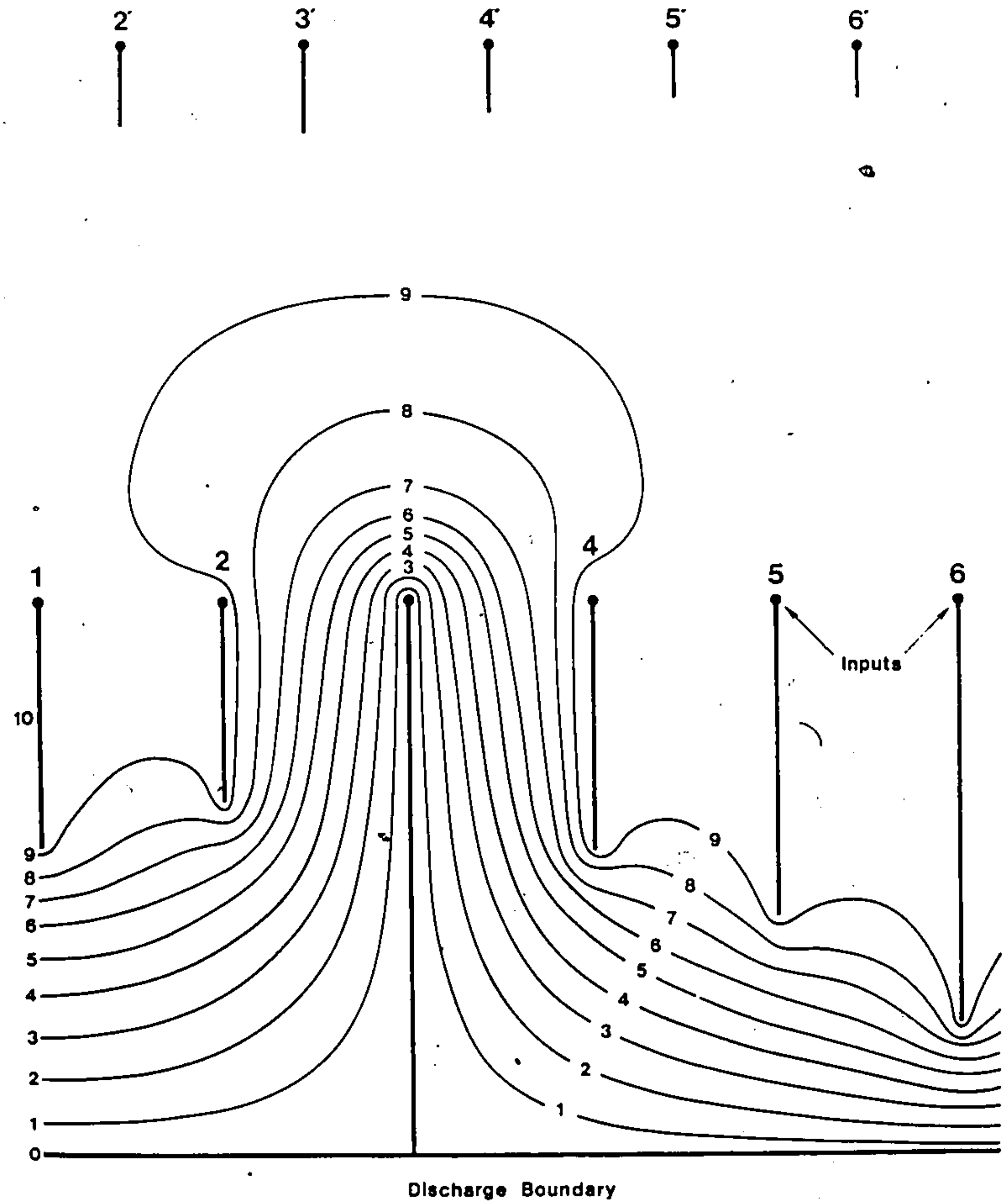
2'
3'
4'
5'
6'
1
2
4
5
6
Inputs
9
8
7
6
5
4
3
2
1
0
10
Discharge Boundary

2. Subsurface drainage basins should be established by the stepwise integration of small distributary sub-units into a tributary system.

3. The integration of the system should proceed from the resurgence in a headward direction, the opposite of the direction of the network propagation.

4. The restriction of the scheme to two ranks is quite arbitrary. Additional ranks could be added, but the tendency for the networks which establish initial connections with the output boundary to broaden their influence with increasing distance into the aquifer seems inescapable.

5. The plan form of the conduit pattern should develop in what approximates a rectilinear trellised pattern. The elements of that pattern, oriented at right angles to the discharge boundary, predate the elements which are parallel to that boundary.

8.4 The Restricted Input Model

8.4.1 GEOLOGIC AND HYDROLOGIC SETTING

Situations frequently arise where geologic structure, lithology, and the character of the surface erosion create conditions for activation of a small number of bedding plane inputs with a compact linear distribution. A peculiar linking pattern occurs in these instances, which is sufficiently distinct to warrant special consideration. The geologic setting involves near horizontal strata with an impermeable lithologic unit overlying the carbonate rocks. Both linear and point resurgences can be envisaged.

8.4.1.1 Input Geometry

Inputs are arranged in linear sets normal to a linear discharge boundary or colinear with a discharge point. In both cases, the spacing between the input arrays is assumed to be large compared to their length. Inputs would occur where fluvial erosion breaches the impermeable stratum. The point of initial breaching and the subsequent activation of additional inputs is related to at least three factors: the stream profile, formation thickness, and minor geological structure. The stream profile determines the point of deepest penetration of the rock mass and, therefore, the point of first outcrop of a covered soluble rock unit (Point A, Fig. 8.7). Thinning of the capping units and thickening of the carbonates can predispose a point to early access by meteoric waters (Point B, Fig. 8.7) as can anticlinal structures (Point C, Fig. 8.7). In all cases joints may play an important role in admitting the meteoric waters to the subsurface.

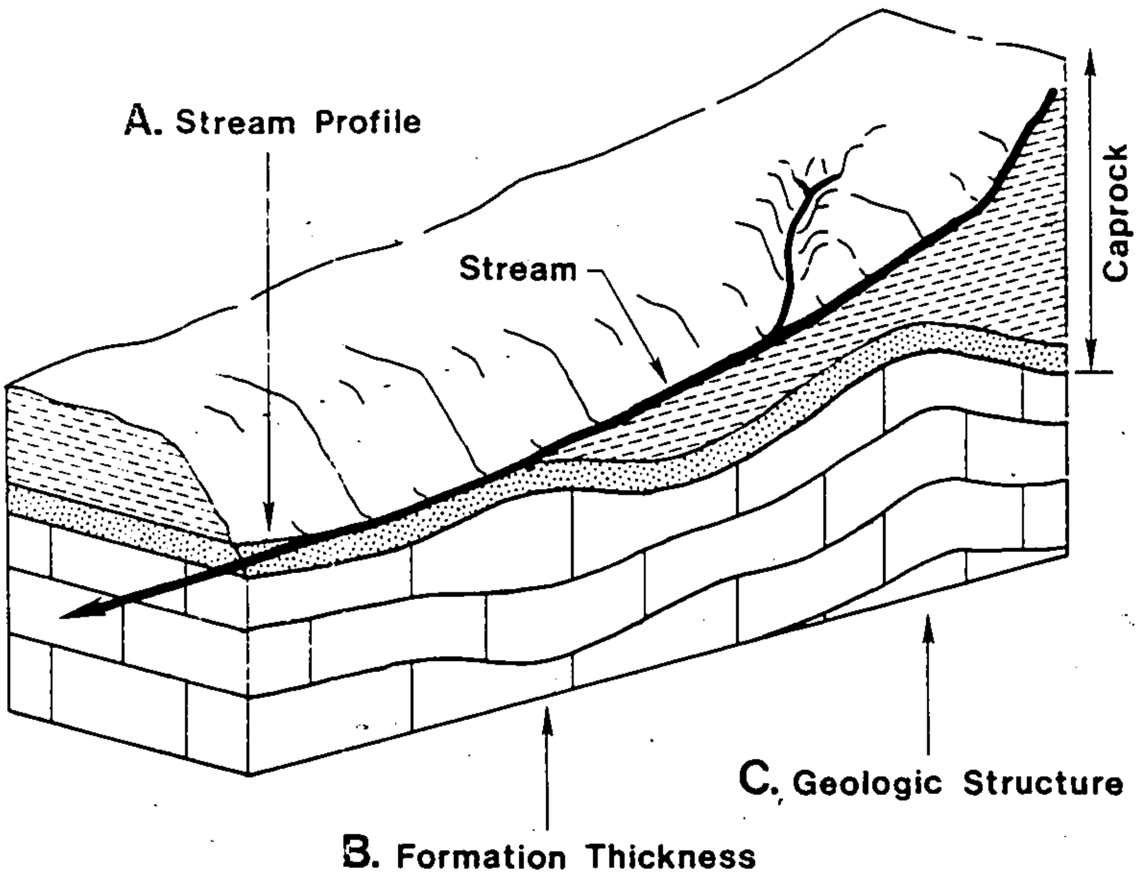

Figure 8.7
Factors governing the location of surface water inputs in the restricted input model.

8.4.1.2 Resurgence Geometry

Linear resurgences could occur in situations similar to those outlined in Chapter 5.1.2. Point resurgences may be localized along the same stream course or an adjacent one by the same factors which operate relative to the inputs. In both the linear and point resurgence cases, vertical joints may be important in transmitting the groundwaters from the bedding planes to the surface.

8.4.2 EVOLUTION OF THE LINKING PATTERN

Figures 8.8A-E illustrate the development of the restricted input linking pattern. In this idealized case, three inputs and a single point resurgence occur along a stream course where an impermeable cap rock has been breached. Groundwater is assumed to be conducted to and from the bedding plane by way of joints. Equal driving potentials h1, h2, and h3 are assumed for the inputs. The symmetrical multiple input rule (Chapter 5.3.2) indicates that input 1 will have the highest throughput with successively smaller Q values for Inputs 2 and 3. The symmetrical point resurgence solution experiments (Chapter 7.3.2) predict that the growth rates of the tube networks arising from the three inputs will be in proportion to their throughputs. These experiments and the corresponding flow envelope experiments (Chapter 6.4.1) indicate that the

Figure 8.8 A, B, C, D, E

Stages in the development of the restricted input linking pattern.

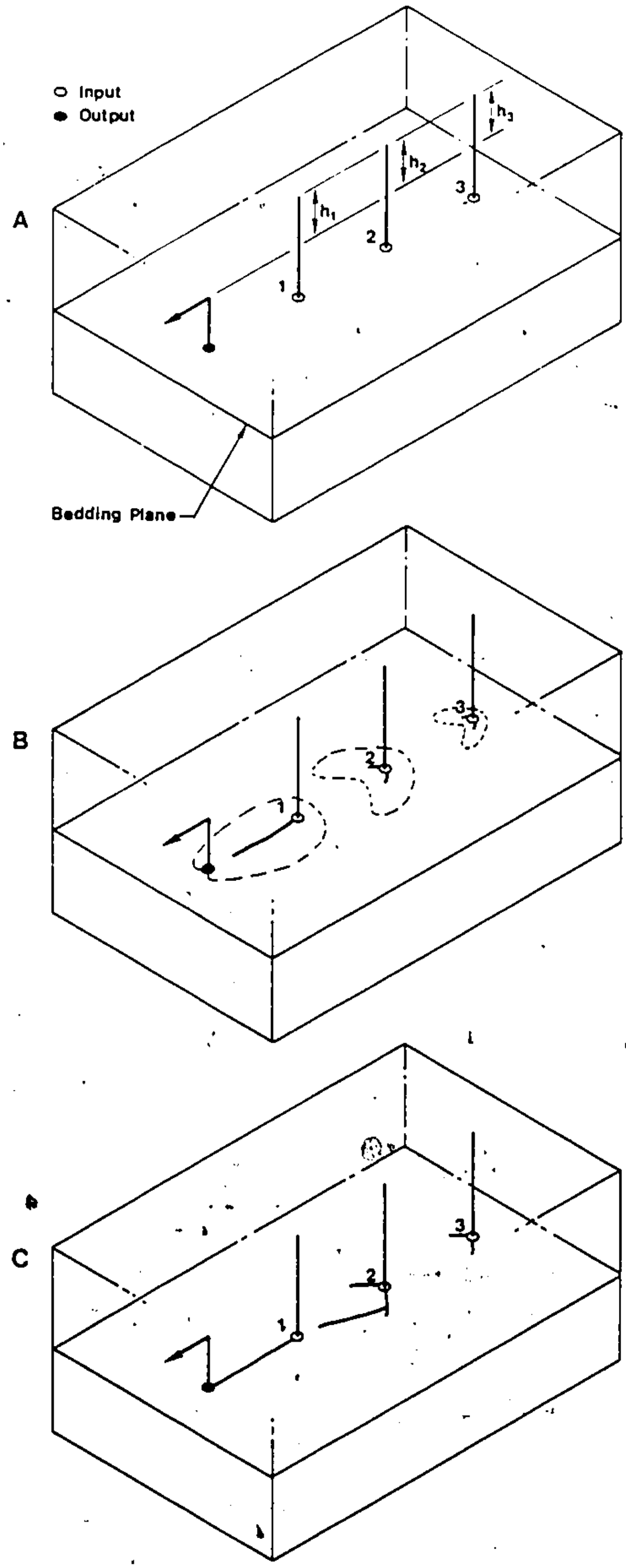
Input
Output
A
h1
h2
h3
1
2
3
Bedding Plane
B
1
2
3
C
1
2
3

D

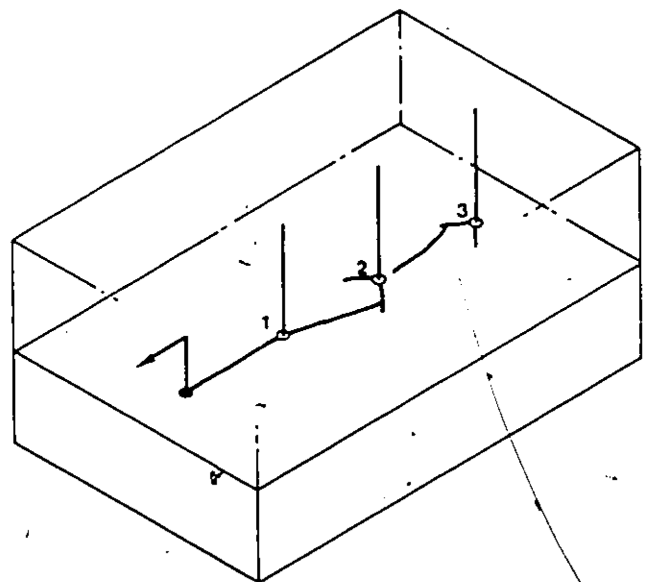

E

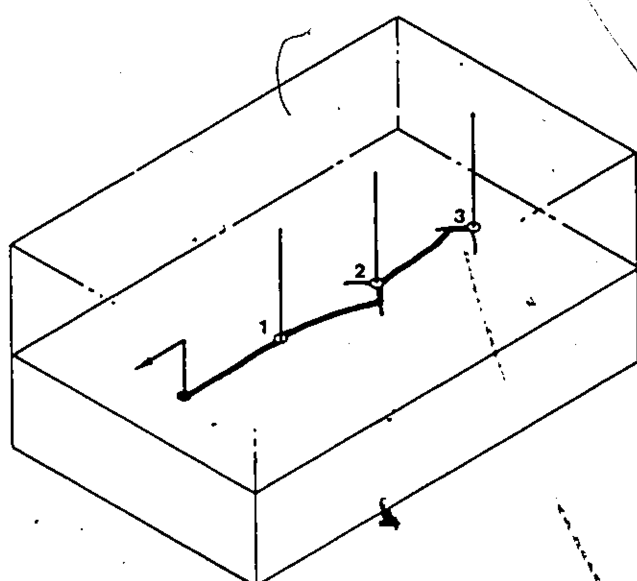

flow from Input 1, the proximal input, is symmetrical about the input-output axis and the flow envelope will possess an ovoid shape. A single principal tube should develop along the piezometric slope, bifurcating the flow envelope. Inputs 2 and 3, however, exhibit a two lobed flow envelope and generate a pair of principal tubes which form relatively independently (Fig. 8.8B).

In Figure 8.8C the network forming from input 1 has completed a low resistance connection to the output, and it is assumed to have enlarged to a diameter sufficient to conduct all of the water available at input 1 under average conditions. Therefore, the head at input 1 will drop to the level of the resurgence, and the network function at all points will change from source to sink for groundwaters entrained in the bedding plane. The discharge boundary is, thereby, altered from a point with limited capacity to one of linear dimension equal to the perimeter of network 1 with greatly increased capacity. In response to this increase and its newly established proximity to an output boundary, network 2 should commence rapid growth. The extension of this network will take place along a route which combines already existing tubes with the shortest available path to form a link with network 1. This reasoning follows directly from the point and linear distance rules developed in Chapter 5.

Network 3 should show increased growth following the conversion of network 1 to phase II. This increased activity is also due to the increased discharge capacity of the bedding plane and the decreased length of its principal flow vectors (Fig. 8.8C). Subsequent to the linking of networks 1 and 2, network 3 should commence growth to complete a low resistance link with network 2, in the manner already described for that input (Fig. 8.8D and E).

8.4.3 EXPERIMENTAL VERIFICATION

Because of the simplicity of this input-output configuration, the linking scheme is easily verified in solution experiments. By extending the symmetrical point resurgence experiments beyond the state of those reported in Chapter 7.3.2, low resistance links were established between the number one input and the resurgence. By setting the solvent supply rate to the inputs at appropriate values, or by simply eliminating the solvent supply to inputs after they had linked to the resurgence or adjacent networks, the linking pattern could be experimentally observed. Figure 8.9A through 8.9D depicts such an experiment. The pattern is that predicted by the model.

Simple logic suggests and the solution experiments verify that there is good reason for such a linking system to be operable in nature: it is simply more efficient. Where the possibility exists to drive a groundwater conduit over a given distance from a single input or from several

Figure 8.9
Stages in the development of the restricted input linking pattern shown by a solution experiment.

Time:48:ØØ hrs.

Experiment # 7-Ø1Ø-B-3-26

Flow Left

A

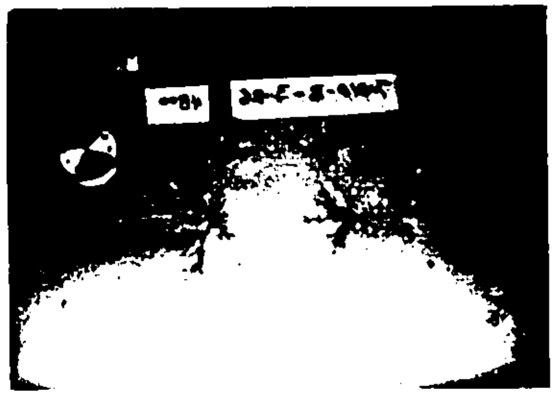

Time:6Ø:ØØ hrs.

B

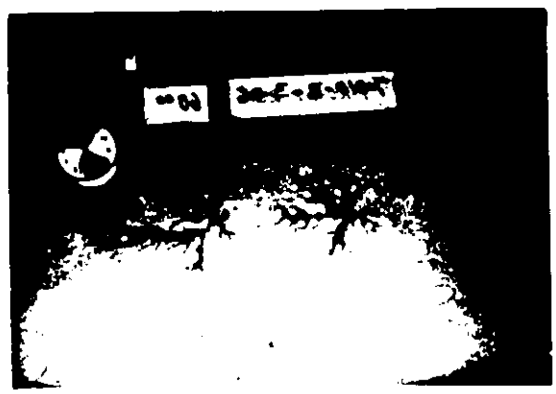

Time:72:ØØ hrs.

C

Time:96:ØØ hrs.

D

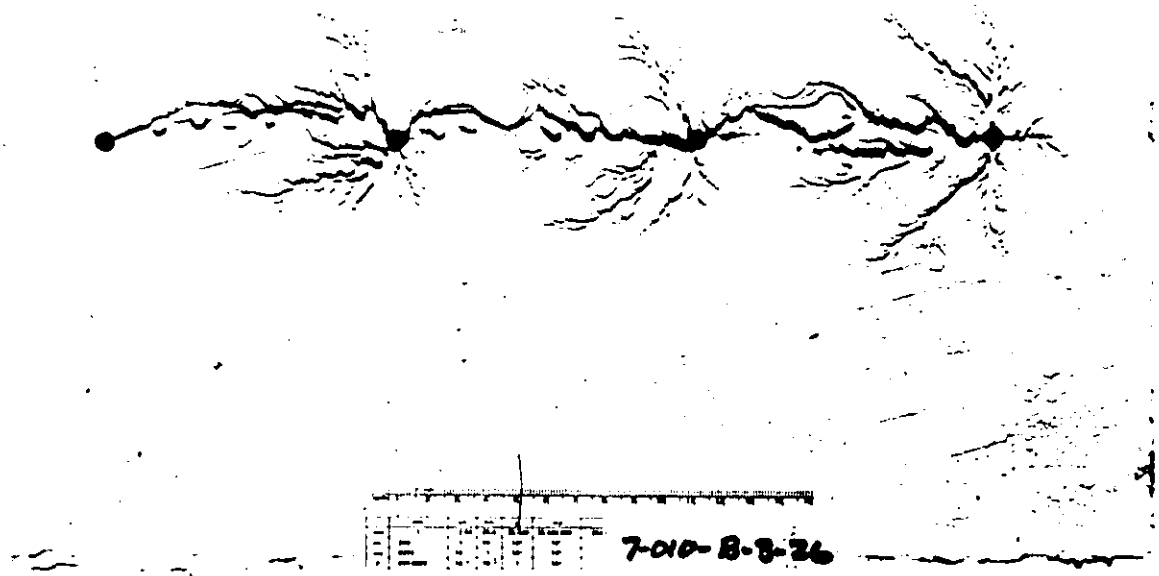

E. The completed experiment.

intermediately spaced inputs in a linking scheme, the multiple input system will prove more efficient in terms of time. This assumes that equal driving potential exists at each input. Figure 8.10 illustrates this principle. It can be seen that the gradient or piezometric potential curve in the multiple input system is greater in the active portion of the bedding plane. Solution experiments show that for a three input system the average rate of propagation of the principal tube in experiments 15 and 16 was 3.1 mm/h over a distance of 300 mm. Single input experiments 21 and 27, utilizing similar driving potentials and parting characteristics, had average propagation rates one-third less over a distance one-third shorter (Table 8C).

8.4.4 SUMMARY

The restricted input linking scheme can be characterized in the following ways:

1. As in the other linking schemes, subsurface drainage basins should be established by the stepwise integration of small distributary sub-units into a tributary system.

2. Similarly, the integration of the system should proceed from the resurgence in a headward direction, the opposite of the direction of the network propagation.

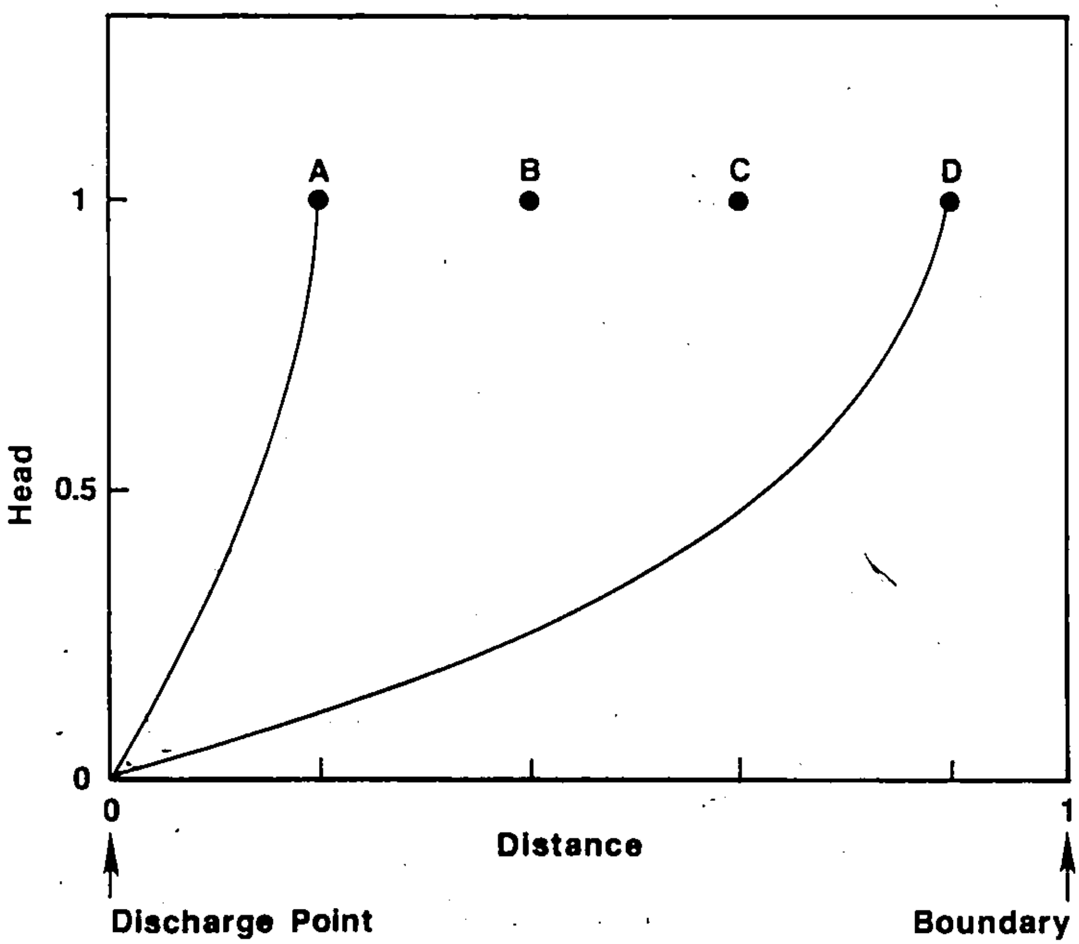

Figure 8.10
Gradients associated with the proximal and distal inputs in a symmetrical point resurgence array. The gradients are shown projected orthogonally onto a vertical plane passing through the input and discharge points.

3. The plan form of the conduit pattern should be simple, linear, and unbranched and may parallel the stream course from which it originated.

CHAPTER 9

FIELD EVIDENCE

9.1 A LOW DIP MODEL EXAMPLE - THE MAMMOTH CAVE REGION

This area comprises one of the worlds largest and most extensively studied low dip karsts. Mammoth Cave, known to European descendants since ca. 1790, is the world's largest known system of solution conduits, comprising more than 360 km (Cave Research Foundation, 1981, personal communication). In excess of 550 km of passages have been mapped within the region (Quinlan & Ewers 1981). The most complete recent reviews of the hydrology and geomorphology are by White et al. (1970), Quinlan (1970), and Quinlan and Ewers (1981-a). This abundance of information, together with a regional dip of one degree or less, make it an ideal place to test the low dip model.

9.1.1 THE GEOGRAPHICAL SETTING

The Mammoth Cave Region, also known as the Central Kentucky Karst, is located in the Mississippian Plateaus of west-central Kentucky. The boundaries of the region are arbitrarily drawn at major allogenic surface streams (Fig. 9.1); on the south and southwest by Barren River, on the south by Beaver Creek, on the east by Little Barren River

Figure 9.1
The Mammoth Cave Region, Kentucky.

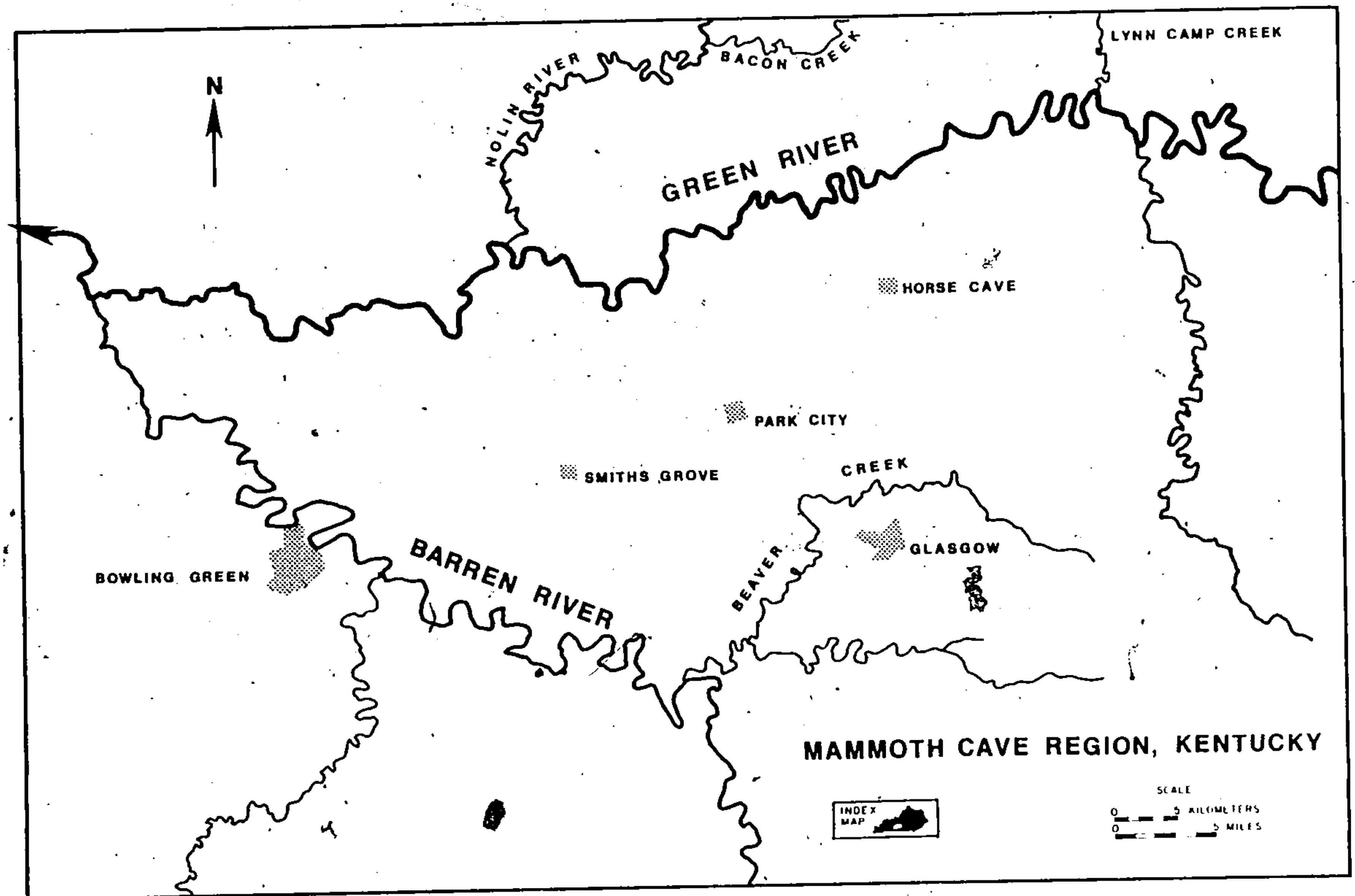
MAMMOTH CAVE REGION, KENTUCKY
N
LYNN CAMP CREEK
NOLIN RIVER
BACON CREEK
GREEN RIVER
HORSE CAVE
PARK CITY
SMITHS GROVE
CREEK
BEAVER
GLASGOW
BOWLING GREEN
BARREN RIVER
INDEX MAP
SCALE
0
5 KILOMETERS
0
5 MILES

and Lynn Camp Creek, on the north by Bacon Creek, and on the northwest by Nolin River and Green River.

9.1.2 THE GEOLOGIC SETTING

9.1.2.1 Lithology

No modern study of the petrology and sedimentary environments of the formations outcropping in the Mammoth Cave Region has been made. Figure 9.2 (after Pohl, 1970) is the best published summary of the stratigraphy. General reviews of the broader regional stratigraphy have been made by Swan (1963) and by Rice et al. (1979).

9.1.2.2 Structure

The regional structure is shown in Figure 9.3. The area lies west of the Cincinnati Arch in the southeast corner of the Illinois Basin. More specifically, it lies at the eastern end of the Moorman Syncline, a structure that is bounded on the south by the Pennyrile Fault System and on the north and east by the Rough Creek Fault System (Kraus and Treworgy, 1979). The region contains many smaller anticlinal structures which appear to be disharmonic folds near the axis of the region-wide syncline. The east-west trending monocline that is coincident with the Chester Escarpment, west of Park City, and the two en echelon monoclines east of Park City are attributed to faulting in the subsurface (Quinlan and Ewers, 1981-A). The only fault

Figure 9.2
Stratigraphy of the Mammoth Cave Region; from Pohl (1970).

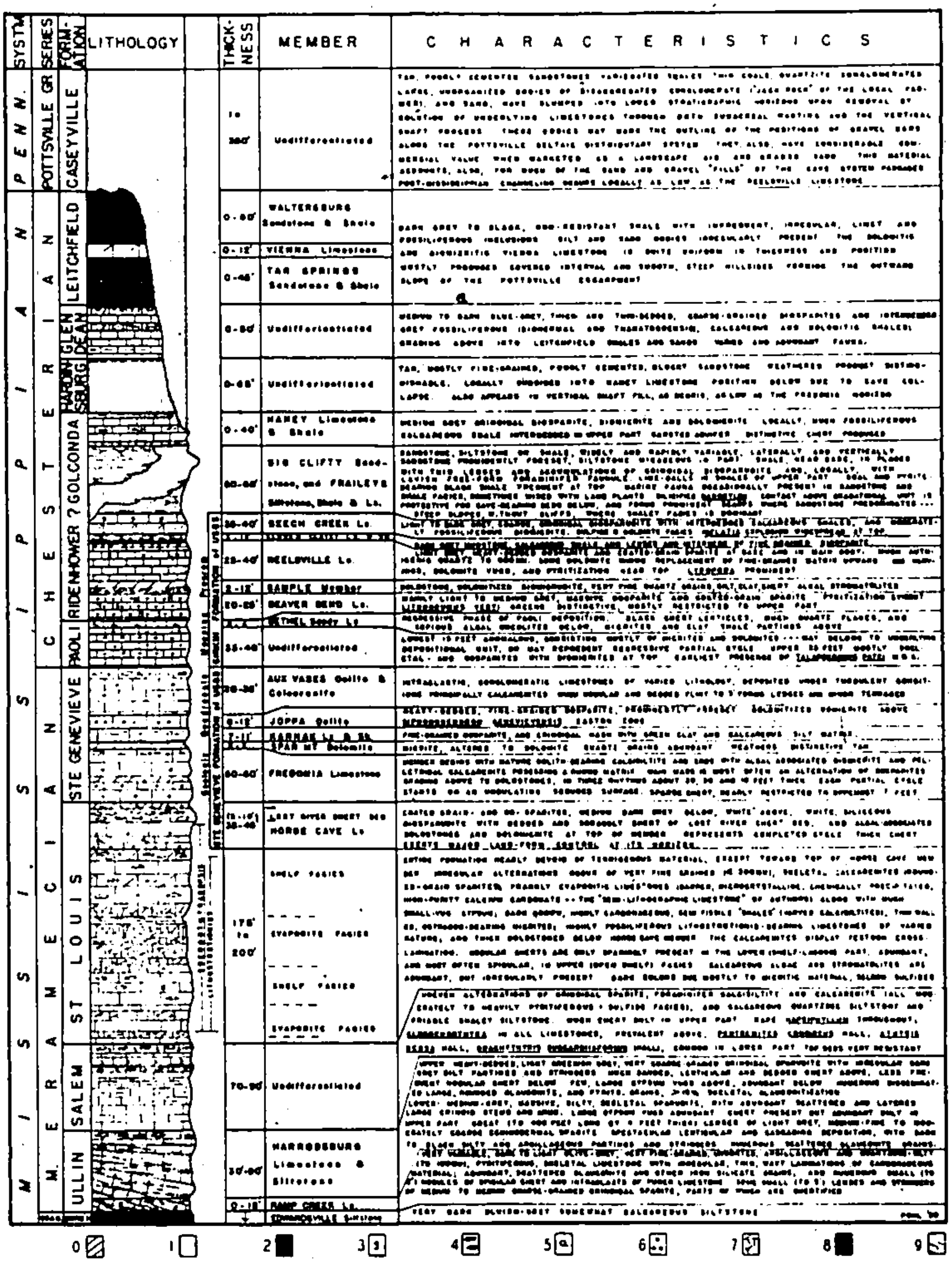
SYSTEM
SERIES
FORMATION
LITHOLOGY
THICKNESS
MEMBER
CHARACTERISTICS
PENN.
MISSISSIPPIAN
POTTSVILLE GR.
CASEYVILLE
CHESTERIAN
LEITCHFIELD
GLEN DEAN
HARDINSBURG
GOLCONDA
RIDENHOWER
PAOLI
MERAMECIAN
STE GENEVIEVE
ST LOUIS
SALEM
ULLIN
WALTERSBURG Sandstone & Shale
VIENNA Limestone
TAR SPRINGS Sandstone & Shale
Undifferentiated
HANEY Limestone & Shale
BIG CLIFTY Sandstone, and FRAILEYS Siltstone, Shale & Ls.
BEECH CREEK Ls.
REELSVILLE Ls.
SAMPLE Member
BEAVER BEND Ls.
BETHEL Sandy Ls
AUX VASES Oolite & Calcarenite
JOPPA Oolite
KARNAK Ls & Sh.
SPAR MT Dolomite
FREDONIA Limestone
LOST RIVER CHERT BED
HORSE CAVE Ls
SHELF FACIES
EVAPORITE FACIES
HARRODSBURG Limestone & Siltstone
RAMP CREEK Ls.
EDWARDSVILLE Siltstone
0
1
2
3
4
5
6
7
8
9

in the Mammoth Cave region is the Cub Run Fault, part of the Rough Creek System. Dips range from less than 0.5 degree to nearly 4 degrees; overall, the dip is 1 degree or less toward the northwest.

9.1.2.3 Geomorphology

The landform map (Fig. 9.4) is also a generalized geologic map. The grey tone on this map indicates the outcrop of the Big Clifty sandstone and younger rocks, chiefly siliclastic. These rocks cap portions of the upland areas in the northern part of the region. A series of dry valleys, formerly extending from the the Sinkhole Plain northward to Green River, cross this area. These, and lesser valleys, now drain internally through karstic depressions.

The streamless region in this figure, the Sinkhole Plain, is the outcrop area of the Girkin and Ste. Genevieve and the upper two-thirds of the St. Louis formations, chiefly limestone. Here karstic depressions with depths in excess of six metres (dolines, sinkholes, and karst windows) number as high as 100 per square kilometer. Where the Lost River chert (upper St. Louis, see Pohl 1970) underlies the plain at shallow depth, the infiltration of soil is prevented and the infiltration of water is reduced, thereby impeding the development of sinks (Woodson 1981).

The unshaded area of the map, drained by surface

Figure 9.3
Structure Map for the Mammoth Cave Region; from Quinlan and Ewers (1981a).

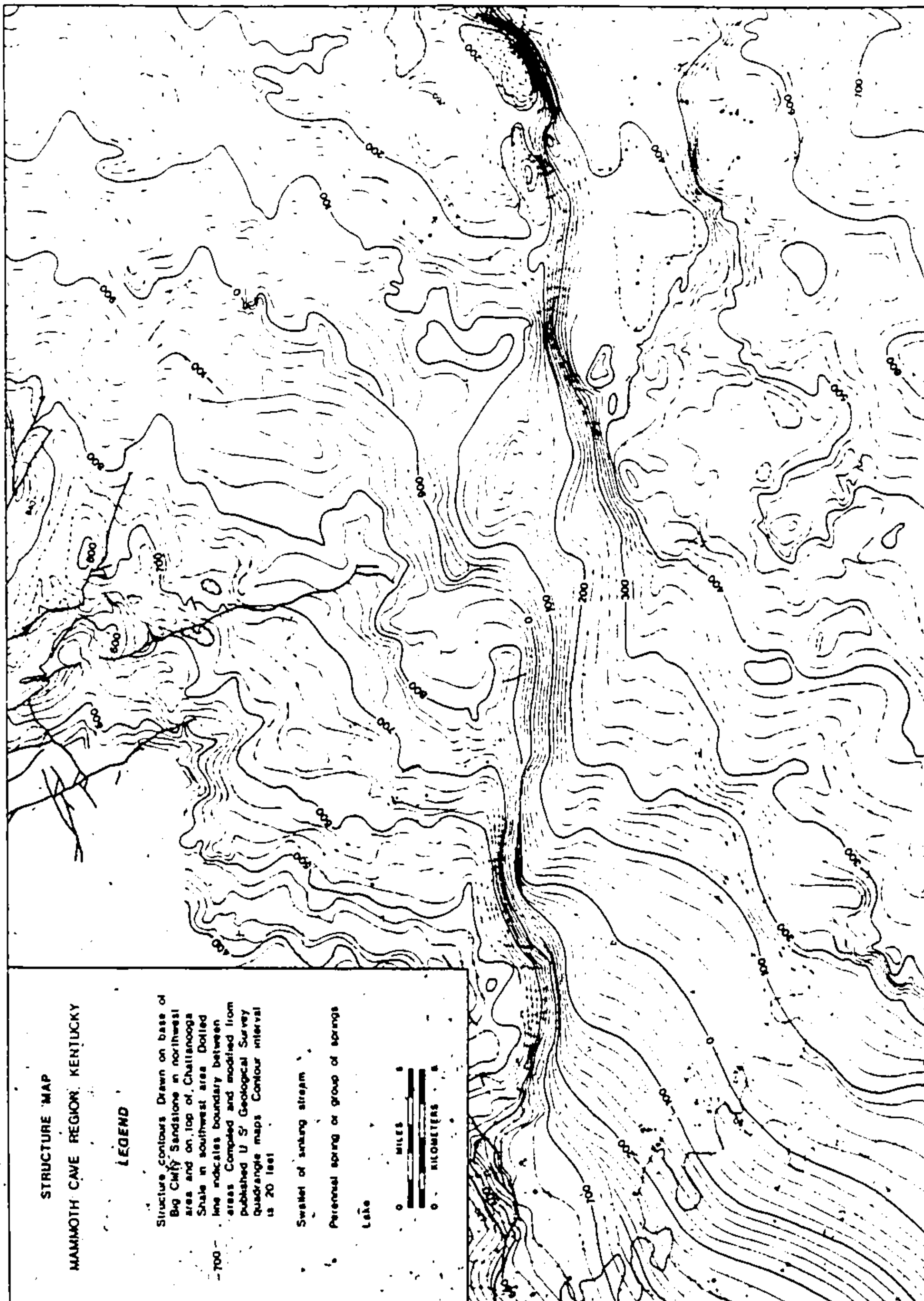
STRUCTURE MAP
MAMMOTH CAVE REGION, KENTUCKY
LEGEND
Structure contours Drawn on base of Big Clifty Sandstone in northwest area and on top of Chattanooga Shale in southwest area Dotted line indicates boundary between areas Compiled and modified from published U S Geological Survey quadrangle maps Contour interval is 20 feet
Swallet of sinking stream
Perennial spring or group of springs
Lake
MILES
KILOMETERS
0
100
200
300
400
500
600
700
800
900

Figure 9.4
Landform map for the Mammoth Cave Region, from Quinlan and Ewers (1981a).

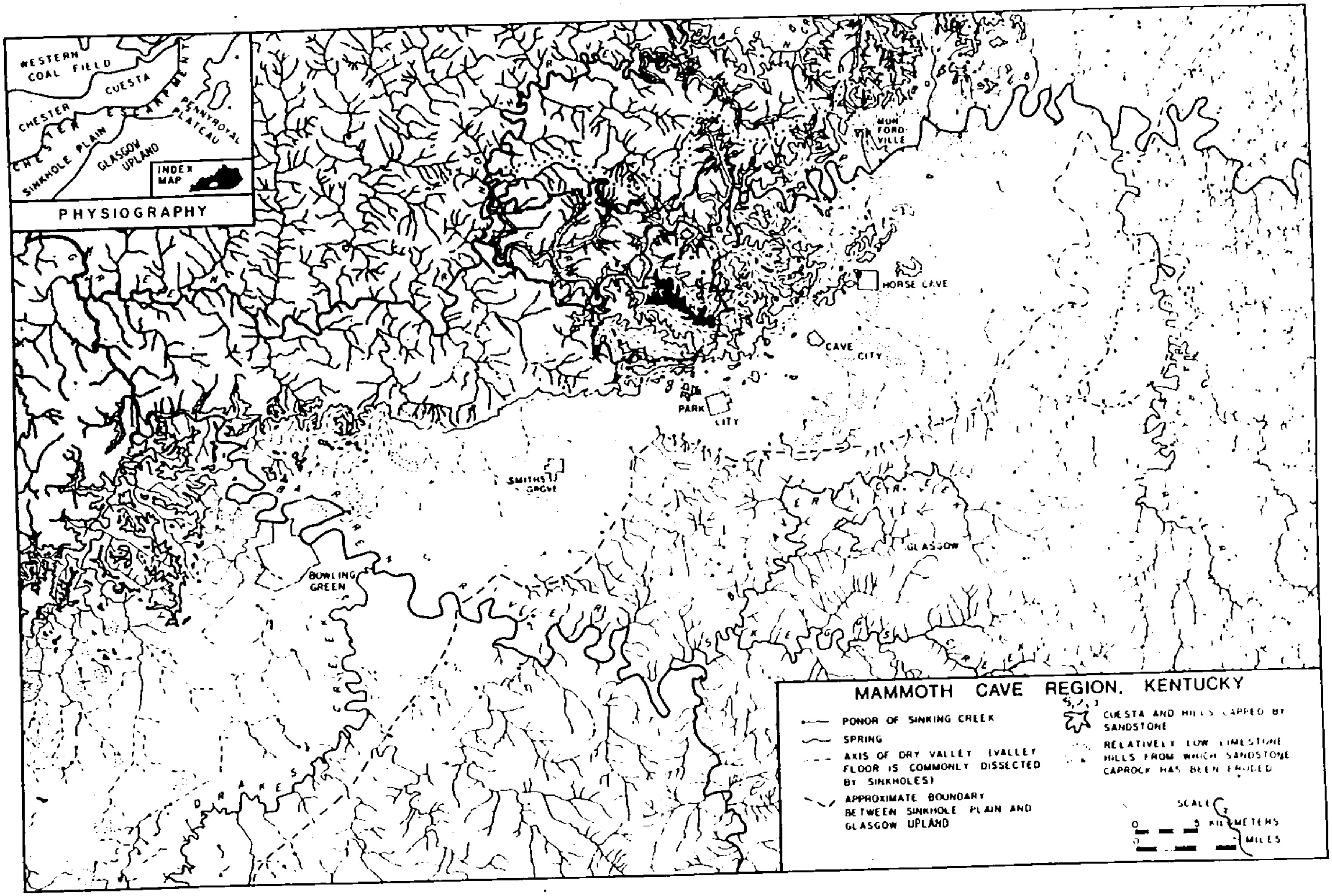
MAMMOTH CAVE REGION, KENTUCKY
PONOR OF SINKING CREEK
SPRING
AXIS OF DRY VALLEY (VALLEY FLOOR IS COMMONLY DISSECTED BY SINKHOLES)
APPROXIMATE BOUNDARY BETWEEN SINKHOLE PLAIN AND GLASGOW UPLAND
CUESTA AND HILLS CAPPED BY SANDSTONE
RELATIVELY LOW LIMESTONE HILLS FROM WHICH SANDSTONE CAPROCK HAS BEEN ERODED
SCALE
0
5
KILOMETERS
MILES
WESTERN COAL FIELD
CUESTA
CHESTER
CHESTER ESCARPMENT
PENNYROYAL PLATEAU
SINKHOLE PLAIN
GLASGOW UPLAND
INDEX MAP
PHYSIOGRAPHY
MUNFORDVILLE
HORSE CAVE
CAVE CITY
PARK CITY
SMITHS GROVE
GLASGOW
BOWLING GREEN

streams, is the outcrop of the lower two-thirds of the St. Louis plus older rocks, chiefly limestones and interbedded silty and clayey limestones. These rocks form the Glasgow Upland. The Bon Ayre Nose, the northwest-plunging anticlinal structure southwest of Park City (Fig. 9.3), brings the lower St. Louis rocks into outcrop further north than elsewhere and narrows the Sinkhole Plain in that region.

9.1.2.4 Hydrology

The principal aquifer is composed chiefly of the St. Louis and Ste. Genevieve limestones but also, in the northwest, the Girkin limestone. Groundwater in this aquifer is perched on shaley and silty units in the lower third of the St. Louis and at the top of the Salem-Warsaw. The total aquifer thickness is approximately 140 m. Water flows from the swamps of the Glasgow Upland by a combination of surface and subsurface routes. These feed small perennial and ephemeral springs that are the source of streams that sink at the southern and eastern margins of the Sinkhole Plain. Water from these swallets flows to cave streams. The low order cave streams join to form intermediate and, finally, high order trunk streams that discharge at major springs along the Barren, Green, and Little Barren Rivers. In addition to these allogenic waters, the cave streams are fed by authigenic runoff into sinkholes and by direct infiltration throughout the Sinkhole Plain. The portions of the cave streams that pass beneath the Chester Cuesta may be fed not only from the Sinkhole Plain but also by runoff from the ridgetops by way of vertical shafts, infiltration from karst valleys, and by spring discharge from a perched aquifer in the Haney limestone. This latter source is perched upon the sandstones and shales of the Big Clifty and Fraileys formations. This drainage also enters the lower aquifer by way of vertical shafts.

The groundwater basins were studied by Miotke and Papenberg (1972), Wells (1973), and Hess (1974), but the pesent knowledge of the groundwater basins and their flow patterns has been gained principally through the work of J. F. Quinlan, reported in Quinlan and Ewers (1981-A & B), Quinlan and Ray (1981), Quinlan and Rowe (1977, 1978), and Quinlan et al.. (1977). Semi-quantitative water tracing techniques employing fluorescein, optical brightners, and existing heavy metals in municipal sewage effluents have been the principal investigative tools. In addition, piezometric surface mapping, cave mapping, and geochemical investigations have been used. These methods are summarized in Quinlan (1981).

In all more than 600 dye traces have been performed. Water from a single sinking stream has been traced as much as 27 km via streams in as many as three different caves, three karst windows. It is rare in karst studies to have so many observation points between the dye input and its ultimate resurgence. This condition greatly enhances the understanding of the aquifer. The observed fact that a large number of inputs flow to a smaller number of resurgence points indicates that the present flow is primarily through a system of tributary conduits. Major elements of this system accessible to direct inspection are commonly as much as 15 m wide and, at many points, accomodate water level rises of as much as 30 m in response to heavy rains. Flow velocities commonly range from 10 to 400 m/hr.

9.1.3 THE MODEL COMPARISON

The model comparison focuses upon the basin shapes and sizes, and the plan form of the conduits, factors which are the verifiable characteristics stated in sections 7.2.2 and 8.3.3.

9.1.3.1 Basin Characteristics

Twenty-two groundwater basins, plus additional sub-basins, are recognized. All discharge to springs on the Green, Barren, and Little Barren Rivers (Fig. 9.5). The size of these basins ranges from less than one square kilometre, with an estimated base flow of 0.003 cubic meters per second, to 740 square kilometres, with an estimated base

Figure 9.5 [SEE REAR POCKET]
Groundwater basins in the Mammoth Cave Region, showing springs, major caves, dye traces, and potentiometric surface; by Quinlan and Ray (1981).

flow of 1 cubic meter per second. Further, these basins exhibit a wide diversity of plan form, especially when considered separately from the areas drained by surface streams. For example, both the Turnhole Spring and the Bear Wallow groundwater basins extend entirely across the sinkhole plain and headward of neighboring basins. In plan form, they posess the shape of a mushroom rooted in Green River. In contrast, the other basins are more narrow and conform better to the pear-shape proportions of a typical surface drainage basin.

The dye traces depicted in Figure 9.5 are shown as curved lines, drawn perpendicular to the equipotential lines of the mapped piezometric surface. They link dye input and recovery points, but do not show the actual position of the subsurface conduits. The convergence of trace lines to a circled point indicate a true convergence at a tracer recovery point. Confluences not so marked are conjectural, based upon piezometric surface data.

Basins 3 & 14 (Fig. 9.5) are of major proportions and conform to the model tributary systems draining through networks 3 and 10 (Fig. 8.5). Like their natural counterparts, these model tributary systems extend laterally in their headwaters and take drainage from upstream of lesser networks 1, 5, 8, 12, and 15. These smaller model units conform to basins 2, 6, 7, 10, 12, and 13 in the prototype. Basin 14C, though partly linked to the main part of basin 14, is similar to networks 6 and 13 in the model.

9.1.3.2 Conduit Pattern Characteristics

Most of the drainage trunks revealed by dye tracing are unexplorable to an extent that would reveal their actual plan form. One of the major exceptions to this statement is the upper reaches of the Turnhole Spring system, comprising Parker Cave (Quinlan and Rowe, 1978). Here 11 km of mapped passage reveals five sub-parallel stream conduits with irregularly offset cross connections. The phreatic portion of these conduits possess an elliptical cross section with the major axis of the ellipse parallel to the bedding. The axes of these tubes are also parallel to the bedding planes. These characteristics are interpreted to mean that initial solution porosity development was directed along these partings. The condits form a trellised pattern (Fig. 9.6) which is not due to the influence of a joint system. Criteria for recognition of joint control include: 1. a visible joint in the rock surface enclosing the passage which is parallel to its long dimension, 2. a lenticular passage cross-section, with the joint coincident with the long dimension of the cross-section, 3. straight reaches of passage an order of magnitude longer than the mean passage width. A careful inspection of the ceiling throughout the cave reveals only occasional solution widened joints and only short sections of passage parallel to one of the joint

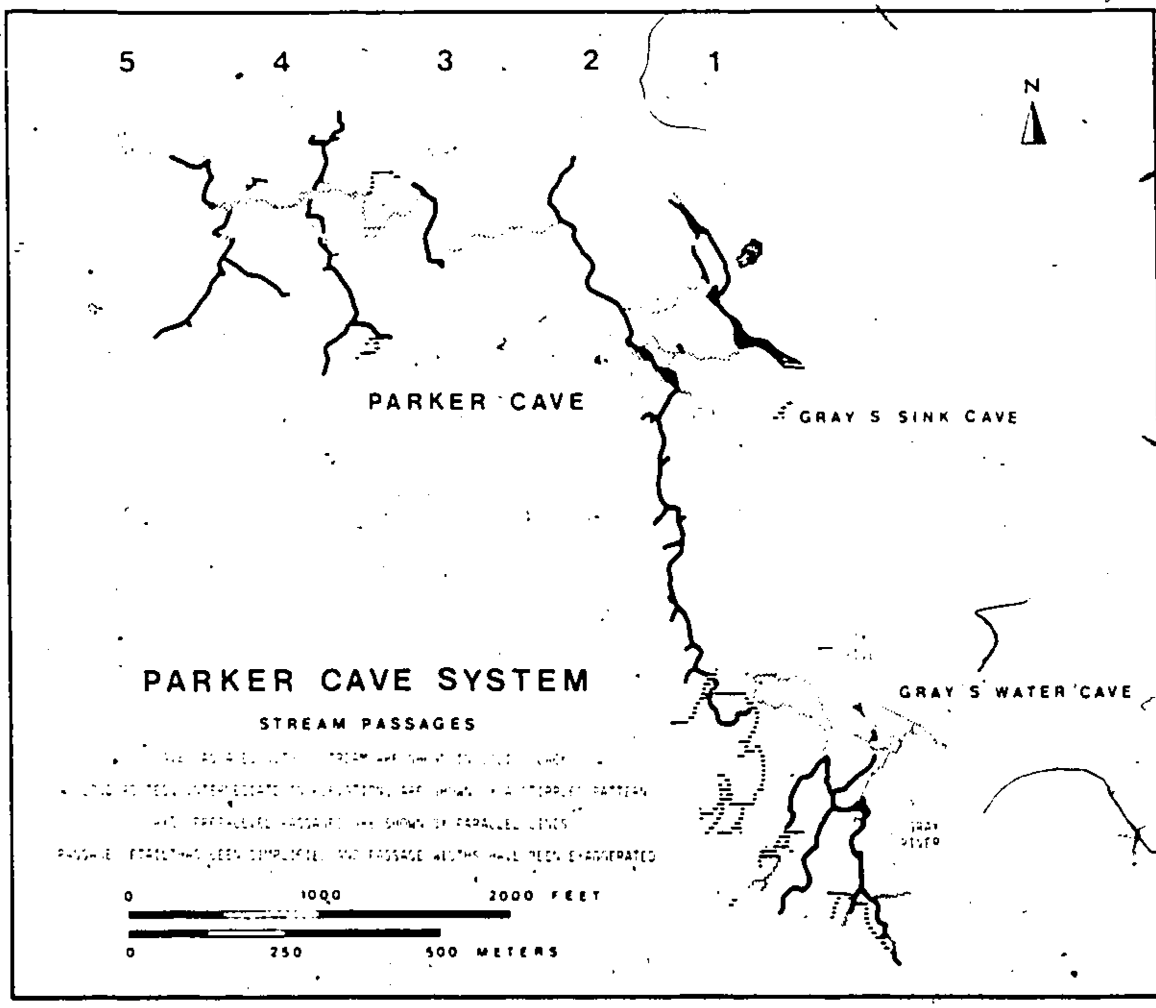

Figure 9.6
The Parker Cave System, From Quinlan and Ewers, (1981a). Stream flow, shown in black, is to the north. Dip is also north.

sets. The passage morphology in these sections as elsewhere is not suggestive of joint control. Quinlan (personal communication) has performed a similar inspection and concurs in these findings. Ford (1968) refers to such a trellised pattern as composed of "dip tubes" and "strike subsequent tubes". He clearly referred to structural dip and strike of the bedding plane in which the tubes form and clearly inferred their sequential development with the adjective subsequent. These concepts may also be applied to the relationship of the tubes to strike and dip of the hydraulic potential surface. In the Mammoth Cave case, however, the structural dip and the dip of the hydraulic potential surface are essentially the same.

This trellised pattern of conduits presently functions in a complex way which is related to their enlargement history (see Quinlan and Rowe, 1978), but two salient points should be emphasized. First, each of the parallel dip oriented streams, with the exception of Brown River, exhibits an abrupt reduction of cross-sectional area downstream from the strike connection. Second, except for the link between Parker and Brown Rivers, the strike connection is of proportions equal to the Parker River cross-section, the largest of the streams except for Brown River. These conditions are consistent with development of a series of small parallel conduits down the piezometric slope, with the subsequent integration of these primitive tubes along routes parallel to the discharge boundary. Later enlargement of this framework has left the tubes downstream from the strike connection in a near-primitive state.

The relationships between inputs east and west of the known Parker Cave system and the hydrology of inputs closer to the discharge boundary argue strongly for the existence of a similar trellised pattern of dip tubes and strike subsequent conduits beneath these adjacent areas. Figure 9.7 shows that dye traces from inputs in the vicinity of Park City, north of Parker Cave, flow northward to Cedar Sink and discharge at Turnhole Spring. Thirteen inputs of allogenic waters adjacent to Parker Cave, together with the five Parker Cave streams, bypass the nearby Park City inputs. These must flow westward and then northward, first to Mill Hole and thence to Turnhole Spring via Cedar Sink. Eleven of these inputs are integrated by strike oriented flow and discharge through Parker Cave via Brown River. During high stage, a portion of the Brown River flow, and most of the Parker River, North Creek, Sulphur River, and Crayfish Canyon discharge are integrated by the strike passage (Cross County Expressway) and flow westward to join the Brown River drainage at an unknown point. At base flow the strike connection ceases to carry water, and all of these dip oriented tubes flow northward to integrate at unknown points.

Figure 9.7
The Turnhole groundwater basin, from the Mammoth Cave Region; from Quinlan and Ewers, (1981a).

Legend-----------

12 - Sinking streams at the Lower St. Louis Contact
13 - Parker Cave
23 - Procter Cave
26 - Park City
T - Turnhole Spring
C - Cedar Sink
M - Mill Hole

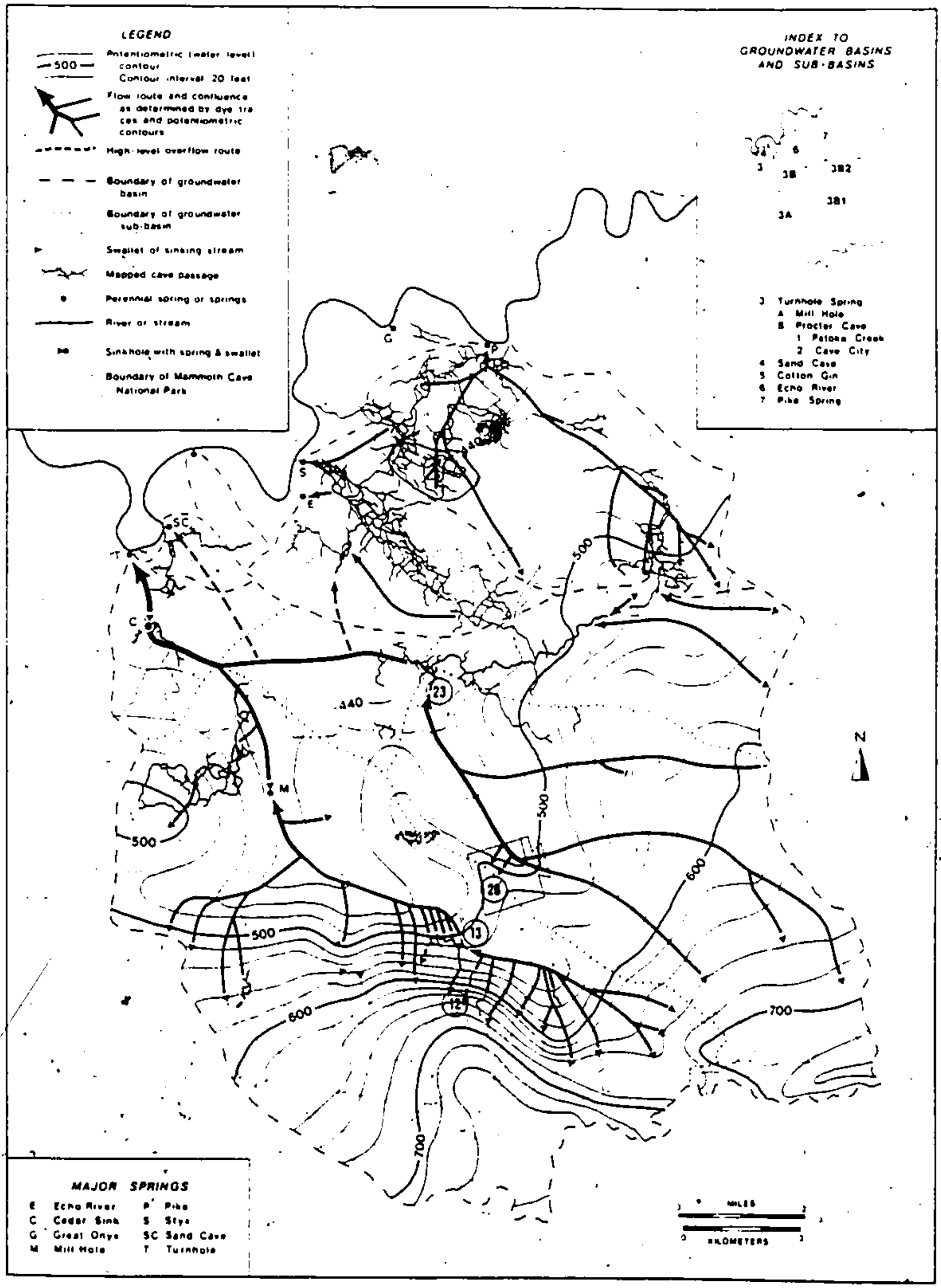
LEGEND
500
Potentiometric (water level) contour
Contour interval 20 feet
Flow route and confluence as determined by dye traces and potentiometric contours
High-level overflow route
Boundary of groundwater basin
Boundary of groundwater sub-basin
Swallet of sinking stream
Mapped cave passage
Perennial spring or springs
River or stream
Sinkhole with spring & swallet
Boundary of Mammoth Cave National Park
INDEX TO GROUNDWATER BASINS AND SUB-BASINS
3 Turnhole Spring
A Mill Hole
B Procter Cave
1 Patoka Creek
2 Cave City
4 Sand Cave
5 Cotton Gin
6 Echo River
7 Pike Spring
G
P
S
E
SC
T
C
M
23
440
500
600
700
28
13
12
N
MAJOR SPRINGS
E Echo River
C Cedar Sink
G Great Onyx
M Mill Hole
P Pike
S Styx
SC Sand Cave
T Turnhole
MILES
KILOMETERS

All of the major groundwater basins are characterized by discharge from springs fed by caves with a distributary pattern of flow. This pattern can be directly observed as in the case of the Hidden River sub-basin (Fig. 9.5) or inferred from chemical characteristics and dye tracing (see Quinlan and Rowe, 1977). In each groundwater basin, the discharge appears at numerous springs, particularly at high stage (Fig. 9.8). These distributaries range in width from 45 m to as much as 10.9 km, and possess as many as 18 discharge points. The situation at the Hidden River complex suggests that the present spring orifices may be part of an older distributary system. A major proportion of the basin discharge rises 17 m at point A (Fig. 9.9) from a lower trunk conduit. Quinlan and Rowe (1977) suggest that this trunk may have discharged to Green River through springs now covered by the 15 m of post-Pleistocene infilling of the river gorge. A high level trunk at B, together with a filled remnant at C, probably associated with a higher stand of Green River, may well have established the basic distributary framework now in use. Palmer (1975) refers to these distributaries as floodwater mazes with genetic connotations. There can be no doubt that, during certain flow conditions, up stream distributary conduits receive flood water from Green River and discharge this flow through their down stream conterparts (Quinlan & Rowe, 1977), and that in so doing, they are enlarged.

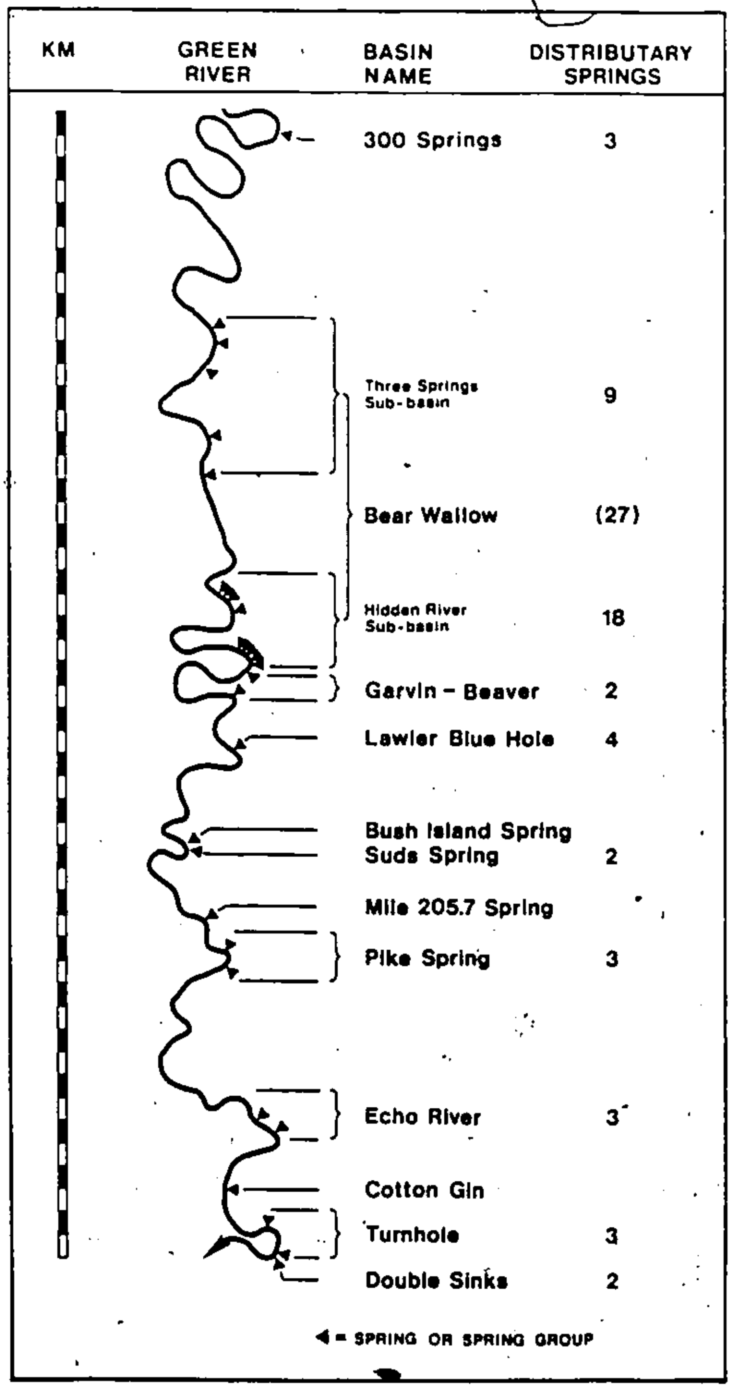

Figure 9.8

Distributary springs associated with the groundwater basins of the Mammoth Cave Region.

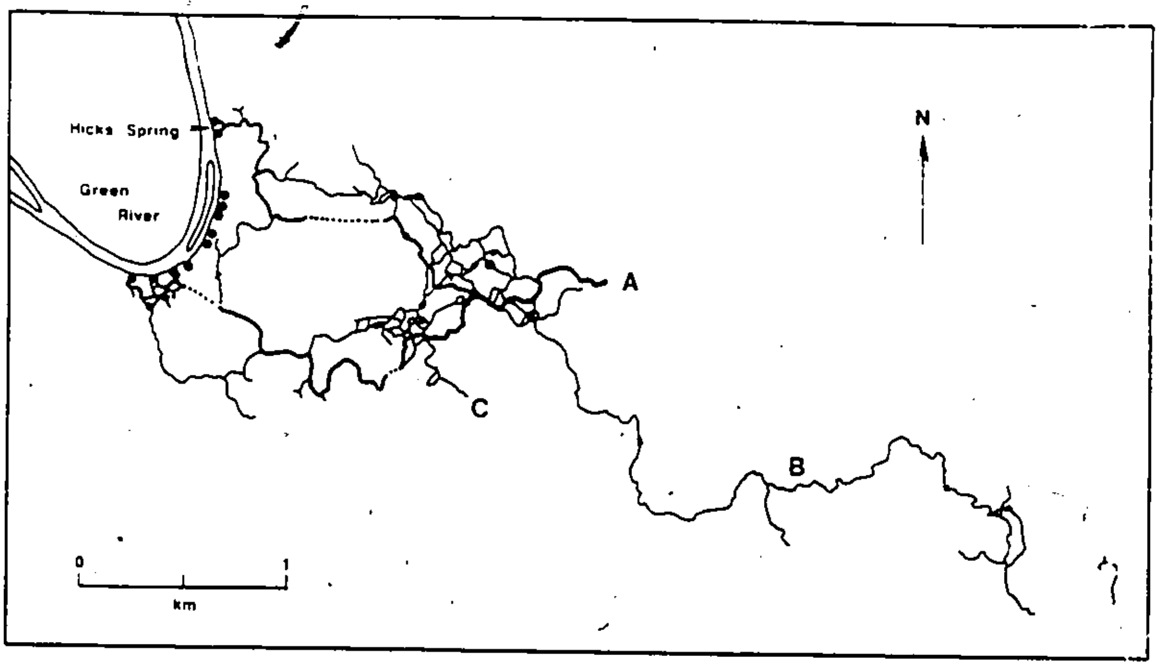

Figure 9.9
Known conduits of the Hicks Spring distributary of the Bear Wallow groundwater basin, Mammoth Cave Region, from Quinlan and Ewers (1981a).

However, their similarity to the distributary branching observed in laboratory networks as they neared the discharge boundary (Chapter 7) and their ubiquitous occurrence suggests that they are a fundamental feature of subsurface solution along bedding planes.

9.1.3.3 The Sequence Of Basin Development.

The low dip model invokes several means by which individual input-output pairs may achieve competitive advantage over neighboring inputs. These include favorable joints, locally higher bedding plane transmissivity, and the time sequence of resurgence activation. The Mammoth Cave Region is sufficiently well understood geologically that some speculations can be offered regarding the operation of these factors there. These have been discussed by Quinlan & Ewers (1981 b). Of special importance to these speculations are the capping sandstones and shales of the Big Clifty and Fraileys Members, and the Lost River Chert bed of the uppermost St. Louis Formation. These can be shown to function as aquicludes or, at some locations, as aquitards. Of equal importance to the speculations is the entrenchment history of the Green River. Subsequent to the establishment of the valleys which cross the Chester Cuesta, a period of entrenchment occurred which, on the basis of paleomagnetic evidence, began at least 900,000 years b.p. (Schmidt, 1981). There is no geomorphic evidence of significant changes in the course of Green River or its two tributaries, the Barren and Little Barren Rivers, since that entrenchment. Finally, a period of valley-infilling has occurred to as much as 20 m at Mammoth Cave.

In order to create a karst aquifer, meteoric water or allogenic surface runoff must have access to the soluble rocks. This must occur in a topographic setting where significant fluid potential can be achieved relative to active discharge points. The conditions of geologic structure, stratigraphy, and the boundary conditions imposed by the Green and Barren Rivers suggest a sequential opening of the limestones to karstification. If we assume that all of the valley bottoms crossing the Chester Cuesta have been at almost the same elevation at any given time during the entrenchment of Green River, Figure 9.10 and subsequent figures would depict the sequence of exposure of the recharge and discharge areas within the region. This assumption is not unreasonable in view of the fact that present streams possess gradients less steep than the dip. In this figure, no attempt has been made to infer the location of former valleys above the Sinkhole Plain. The sandstone-limestone boundaries on these figures separate the area of possible limestone exposure along such valleys from areas completely covered by the Big Clifty for a given stage of valley deepening. The exposure of the limestone is presumed to take place by normal fluvial processes, not

Figure 9.10

Distribution of the caprock in the Mammoth Cave Region at a valley deepening stage of 900 ft. Tributary valleys to the Green River are not shown. From Quinlan and Ewers (1981b).

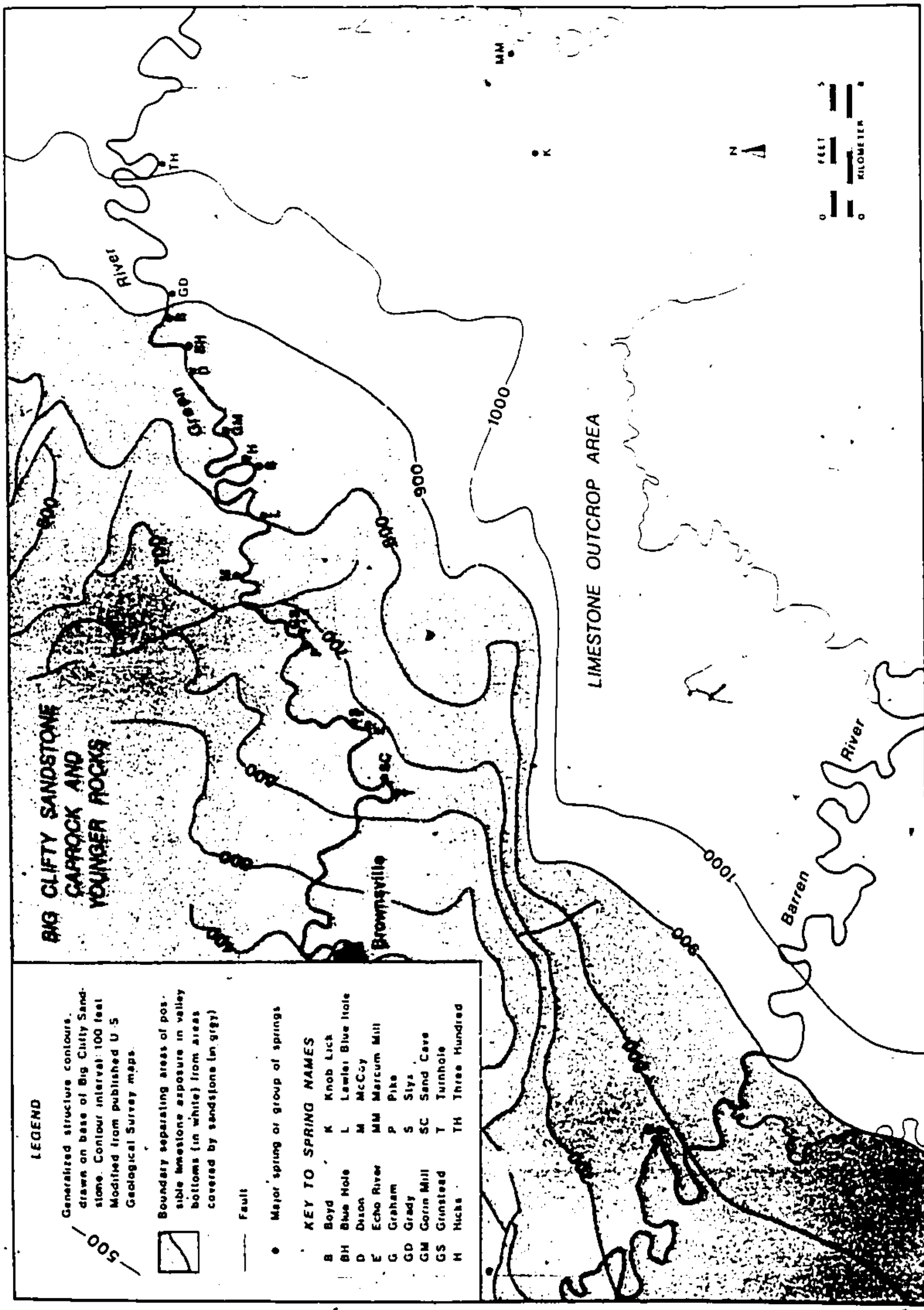
BIG CLIFTY SANDSTONE CAPROCK AND YOUNGER ROCKS
LIMESTONE OUTCROP AREA
Green River
Barren River
Brownsville
FEET
KILOMETER
N
LEGEND
500
Generalized structure contours drawn on base of Big Clifty Sandstone. Contour interval: 100 feet. Modified from published U.S. Geological Survey maps.
Boundary separating areas of possible limestone exposure in valley bottoms (in white) from areas covered by sandstone (in gray)
Fault
Major spring or group of springs
KEY TO SPRING NAMES
B Boyd
BH Blue Hole
D Dixon
E Echo River
G Graham
GD Grady
GM Gorin Mill
GS Grinstead
H Hicks
K Knob Lick
L Lawler Blue Hole
M McCoy
MM Marcum Mill
P Pike
S Styx
SC Sand Cave
T Turnhole
TH Three Hundred

solutional mass wasting. The figures are based upon the United States Geological Survey maps which use the English system. In order to avoid interpolations which could compound any existing error, English units are retained.

At the arbitrarily selected valley deepening stage of 900 feet, a large belt of limestone is exposed, but groundwater discharge from its rocks can take place only at the eastern margin, at Green River, and the western margin, at Barren River. At both discharge areas, the subsurface flow from local inputs should readily generate solution porosity. In the center of this exposed limestone belt, both flow and the development of solution porosity will be comparatively sluggish. As the porosity development at the discharge points begins to drain the margins of the limestone belt, conduit development will become integrated and extend gradually headward as outlined in the model, thus establishing two principal drainage basins (Fig. 9.11). Although the drainage divide has been drawn midway between the discharge points, reflecting the presumed water movement, the solution modification of the limestone in the divide area would most likely have progressed but a short distance into the rock. At this stage, integrated solution voids should develop only near the discharge points.

Discharge points can be established along the north-central margin of the limestone belt at progessivly lower stages of valley deepening. This sequence of

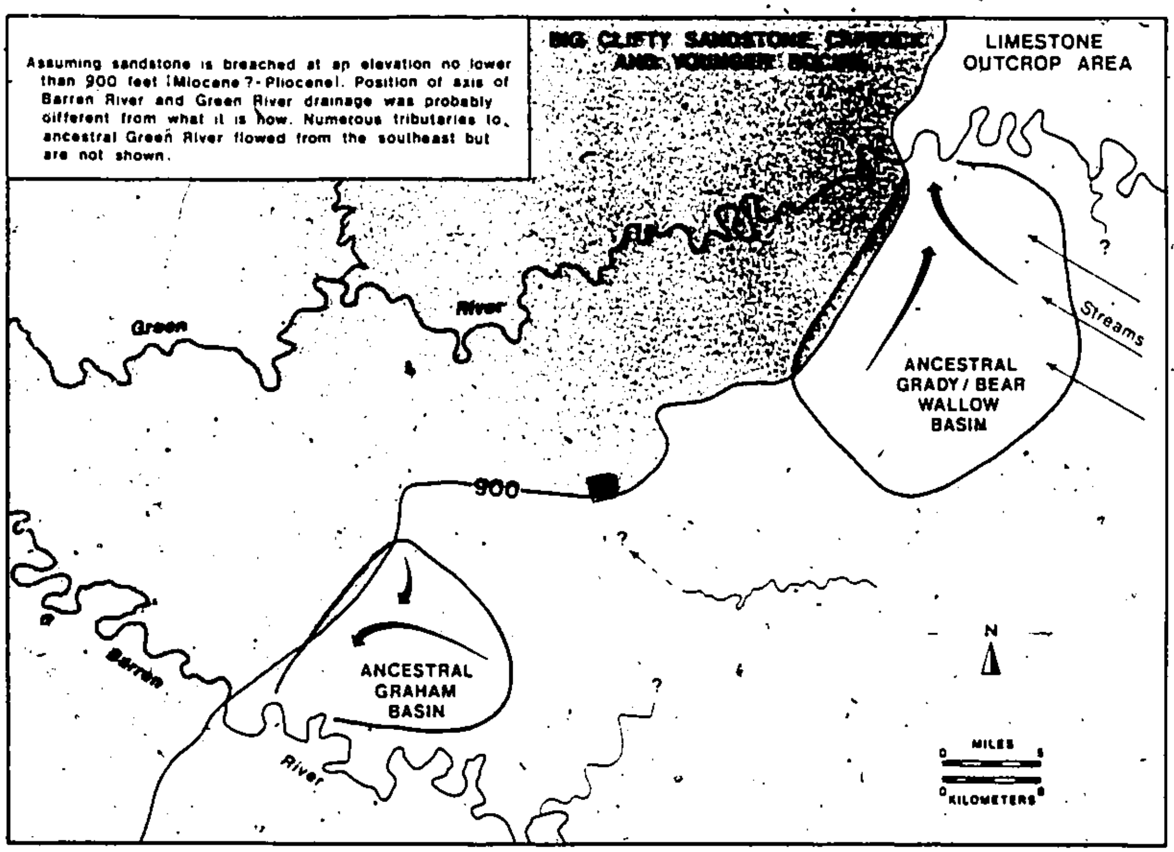

Figure 9.11
Initial groundwater flow in the Mammoth Cave Region at a valley deepening stage of 900 ft., from Quinlan and Ewers, (1981b).

development is depicted in greater detail in Figure 9.12. The ancestral spring sites at present day Pike Spring and Echo River Spring, together with their respective distributaries, Grinstead and Styx Springs, were all exposed at the same elevation, 680 ft., and the same time. During this process of spring initiation the drainage of the central portion of the limestone belt could now begin with the growth of the north-flowing groundwater basins (Fig. 9.13 A).

The published 700 and 680 foot structural contours on the peculiar anticlinal feature at Pike Spring (Haynes, 1964) have been straightened, even though by doing so the conceptually attractive possibility of Pike Spring being the first to form is eliminated. The feature is not present in the subjacent limestones (Arthur N. Palmer, oral communication, 1978).

It is assumed that springs which may have formed in the bottom of the tributary streams at spillover points were unimportant. Such springs are generally fed by shallow circulation, and all of the basins under consideration here are characterized by deeper circulation.

The present day groundwater basins (Fig. 9.5 & 9.13 B), with one exception, the Turnhole Spring Basin, to be discussed later, appear consistent with this interpretation. The Graham Springs and Bear Wallow Basins are the largest; their ancestral spring points were almost certainly the

Figure 9.12

Progressive exposure of limestone along the Green River and its tributary valleys at six stages of valley deepening. Letter key for springs is the same as Figure 9.10. From Quinlan and Ewers (1981b).

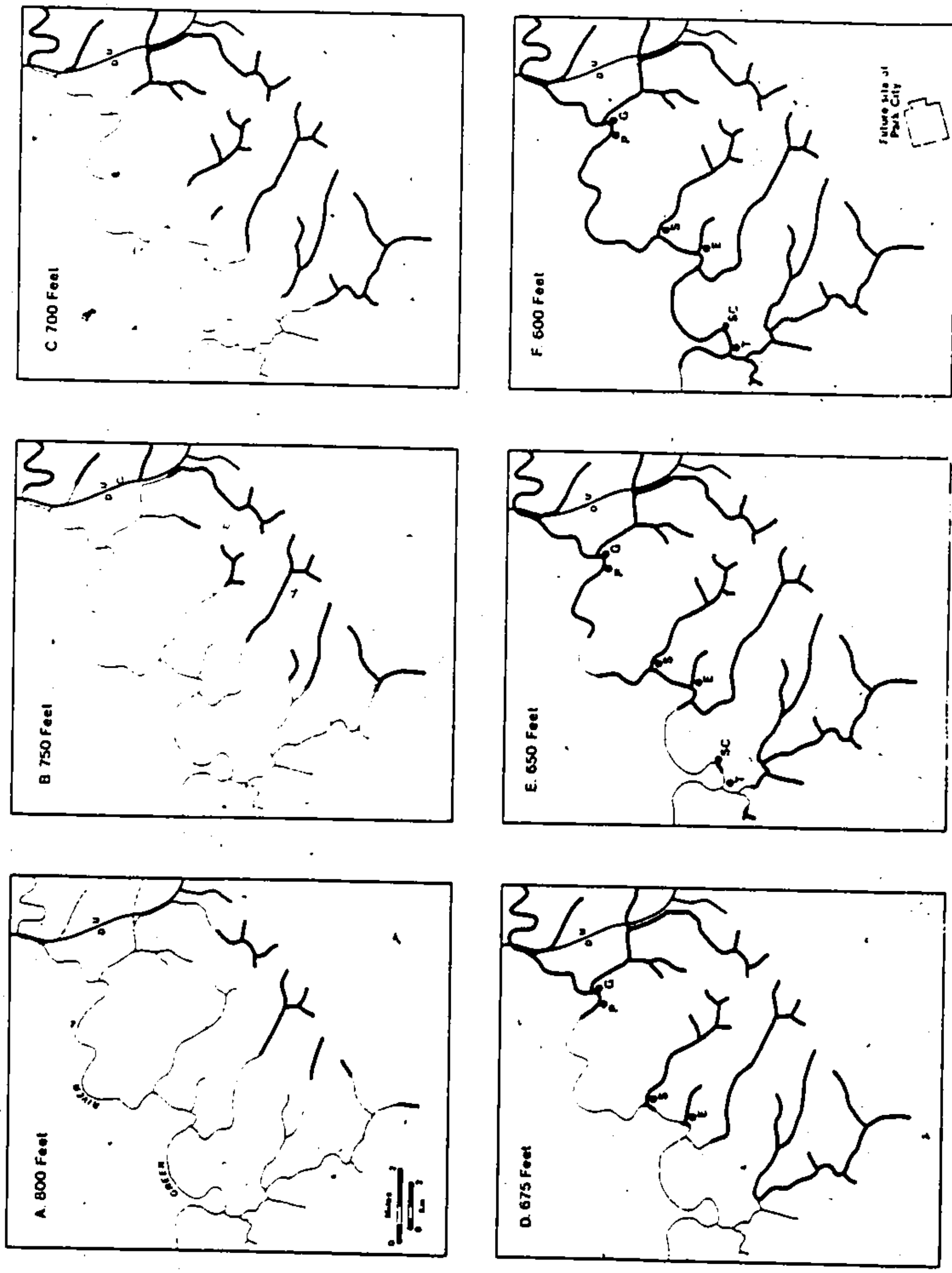
C 700 Feet
F. 600 Feet
Future site of Park City
B 750 Feet
E. 650 Feet
A. 800 Feet
GREEN
RIVER
D. 675 Feet

A

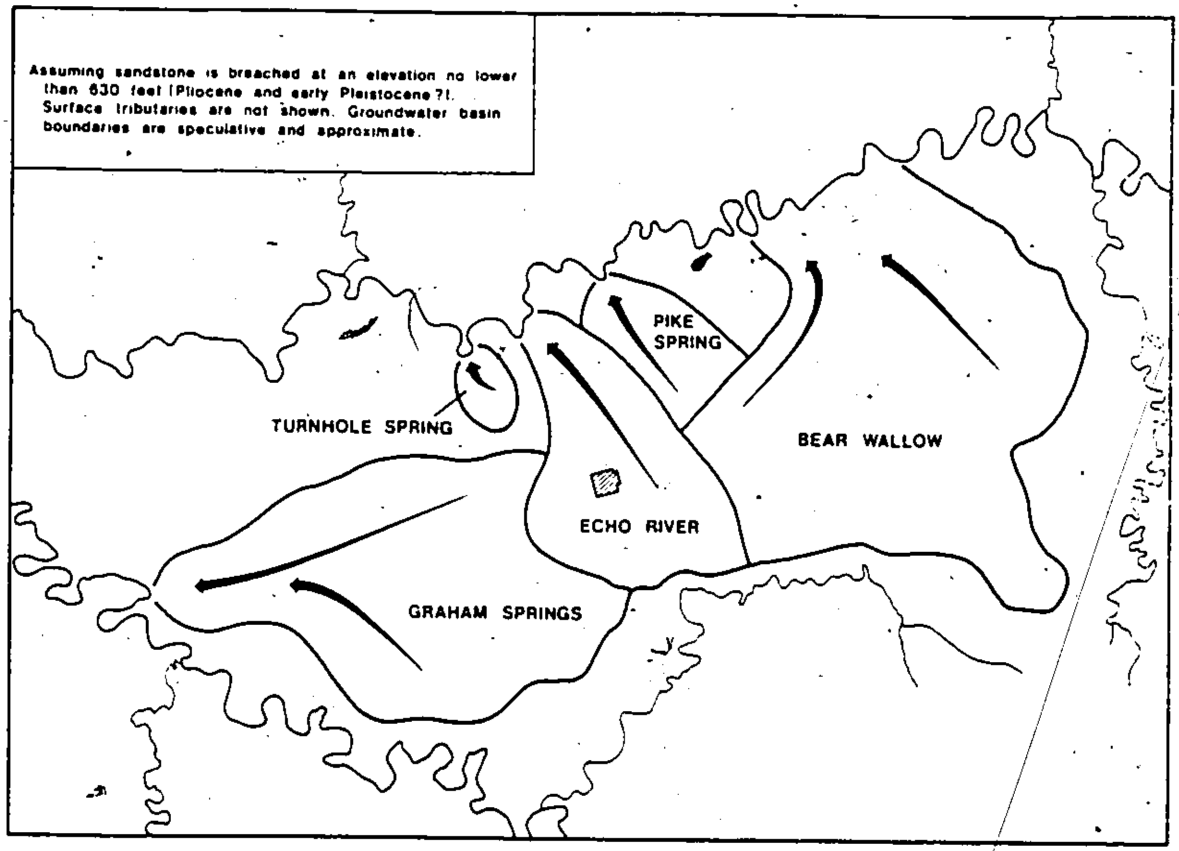

Figure 9.13 A, B

Early and present groundwater basins in the Mammoth Cave Region.

B

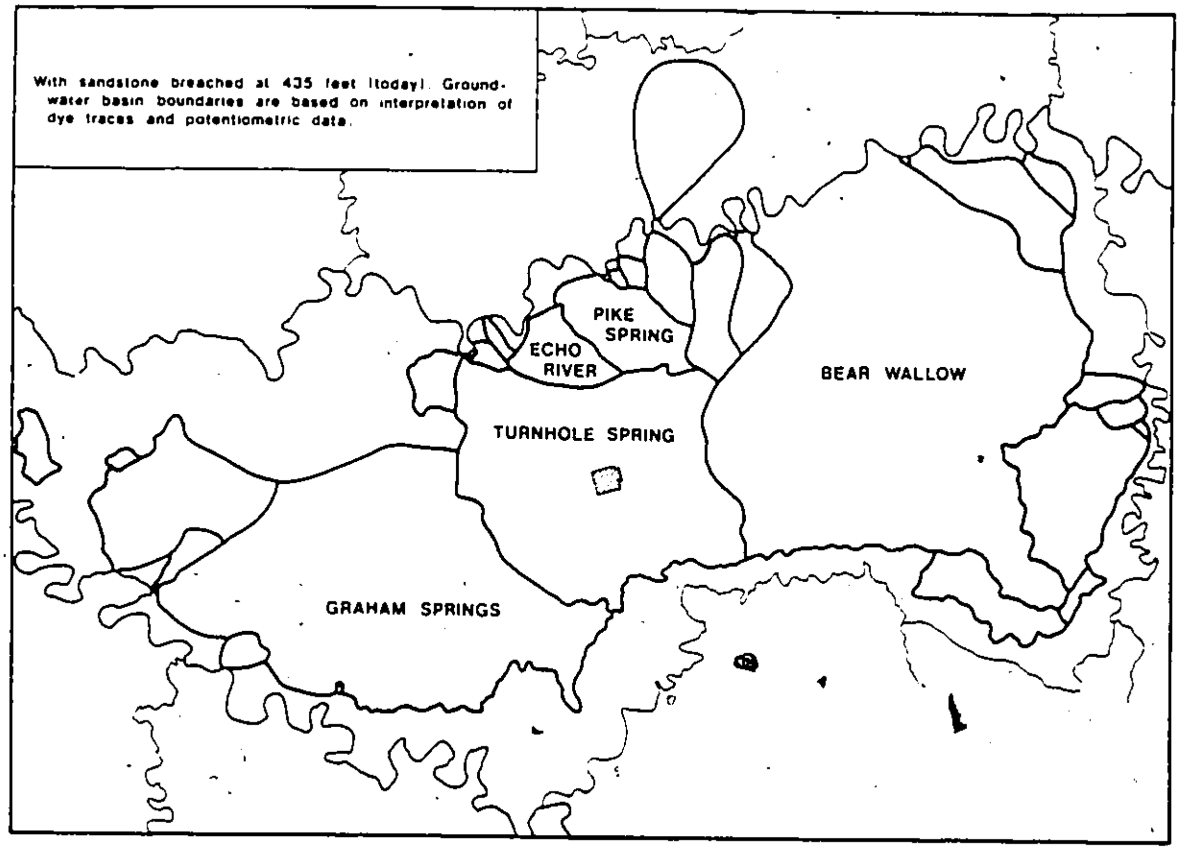
With sandstone breached at 435 feet (today). Ground-water basin boundaries are based on interpretation of dye traces and potentiometric data.
PIKE SPRING
ECHO RIVER
BEAR WALLOW
TURNHOLE SPRING
GRAHAM SPRINGS

first to be initiated. The present principal springs in both basins, however, are lower than the points of earliest possible breaching. Hicks Spring (Fig. 9.10) in the Bear Wallow Basin is the principal spring. It is considerably west of the point of first breaching and lower. Grady Spring is located 13 km upstream (eastward) and higher, much nearer the point of first breaching. It is, by this interpretation the oldest surviving spring in the basin, while Hicks Spring is the youngest. Progressive movement of a basin spring point downstream is not unexpected and has long been recognized. No comparable higher level ancestral spring has yet been identified in the Graham Springs basin.

It is also interesting to note that the Bear Wallow basin extends headward of the Garvin-Beaver and Lawler basins. This is interpreted to be a consequence of its time related competitive advantage in integrating the groundwater flow of this area, conferred by the structure in concert with the erosion processes. If the Garvin-Beaver and Lawler basin ancestral springs had been initiated contemporaneously with the Bear Wallow springs they should have evolved to a greater extent southeastward, and the Bear Wallow basin would be smaller. Although this explanation seems satisfactory, it should be noted that the headward boundary of the Garvin-Beaver and Lawler basins with the Bear Wallow basin is adjacent to the remarkably straight northeast-southwest trending portion of the Chester

Escarpment, which is referred to as the Horse Cave Lineament (Quinlan and Ewers, 1981). The lineament also nearly coincides with a major trough in the potentiometric surface (Fig. 9.5). The cause of the lineament is unknown, but it is possible that it localized the development of solution permeability in the aquifer, a permeability that because of its efficiency, has not yet been pirated by the smaller, younger, higher gradient basins.

The large size of the Turnhole Spring basin is somewhat perplexing. Like the Bear Wallow basin, it extends headward of the adjacent basins but does so in spite of its apparently late initiation. It may be that some structural feature such as a joint or fault compromised the integrity of the caprock or increased the transmissivity of the limestone south of the spring point. Either condition could have given the basin a competitive advantage, but no evidence for such features exists. The proximity of Turnhole Spring to the monocline west of Park City may have provided a shorter, higher gradient path for groundwater flow. Also, the paleo-valley crossing the Turnhole Spring basin, Cedar Spring Valley, is larger than the paleo-valleys associated with the neighboring Pike and Echo Spring basins. The larger and presumably deeper valley would have increased the probability of inputs occurring close to the spring and at an earlier time than in the adjacent valleys. These conditions could have given the basin a competitive advantage.

The position of Turnhole Spring, downstream from the Echo River and Pike Spring basins, may confer a slight head advantage, allowing it to extend headward at a faster rate or pirate the headwater conduits of the adjacent basins. This capture hypothesis is supported by the fact that present day Echo River has captured Styx, and Pike Spring is interpreted to have captured Grinstead (Quinlan and Ewers, 1981 A). In each case, the capturing spring is downstream about one half mile. Also, large paleo-drainage trunks, such as Kentucky Avenue in Mammoth Cave, argue for a larger basin than presently exists upstream from these springs. Explorers have recently discovered a connection in Roppel Cave (Quinlan and Ewers, 1981, Fig. 7) in the Pike Spring basin with a lower river passage dye-traced to Procter Cave and thence to Turnhole Spring (Jim Borden, oral communication, February, 1981). This suggests that piracy of the headwaters of Pike Spring basin by Turnhole drainage may be occurring now. There is also evidence for piracy of the headwaters of Graham Springs by Turnhole drainage. Crump Cave, a dry high level trunk passage, consists of a single conduit 13 m wide and more than 16 m high located near the headwaters of the present Graham Springs basin. Wells (1973) showed that the paleo-flow of this huge passage was toward the present discharge boundary of the basin. The proximity of this major trunk to the boundary of the

Turnhole Spring, one kilometer to the east, suggests that the headwaters of the Graham Springs groundwater basin, the recharge area for the Crump Cave passage when a river flowed through it, have been captured by Turnhole Spring (Quinlan and Ewers 1981, Stop 27). Thus it could be that the Echo River Basin, not Turnhole, was of intermediate size extending to the southern margin of the sinkhole plain as depicted in Figure 9.13, and that this catchment and part of the Graham Springs Basin have subsequently been acquired by Turnhole Spring.

Although the caprock was breached at both Pike Spring and Echo-Styx spring at about the same time (675 ft.), it is tempting to conclude that Pike Spring was the first of those related to Mammoth Cave to commence flow. Collins Avenue, elevation 690 feet, is the highest passage in Crystal Cave, part of the Flint Ridge portion of Mammoth Cave, and trends toward Pike Spring. Gothic Avenue, at the much lower elevation of 600 feet, is the highest passage in Mammoth Cave, and is nearest to Echo-Styx springs. This conclusion, however, would be inappropriate. It is based upon the debatable assumption that the passages had to be graded to the level of Green River. They could well have been 20 or even 60 or more feet below the river when they formed.

As if matters were not already sufficiently complex, there remains the interpretation of the influence of the

Lost River Chert. This unit is frequently associated with the perching of small springs. On the summary diagram (Fig. 9.14), its breaching relative to some present spring points is shown. The Bear Wallow Basin springs emerge from below the chert, yet the basin must have been established above this horizon. Thus, it must be concluded that the influence of an established set of subsurface drainage trunks is so strong that a lithologic discontinuity of this magnitude is not sufficient to cause major disruption of the established system. This conclusion is further supported by the fact that water sinking in the Lawler basin passes through the Lost River Chert before rising at Lawler Bluehole spring.

The interpretation of available evidence suggests that the stripping of the caprock, in conjunction with the structure, has conferred the competitive advantages which are reflected in the size and juxtaposition of the principal groundwater basins in the Mammoth Cave Region. This sequence is summarized in Figure 9.14.

9.1.4 SUMMARY

The correspondence between the theoretical model and the available data from the Mammoth Cave Region is most encouraging. Thus far, the five points listed above which summarize the model are met. Further exploration will undoubtedly reveal additional passages beneath the Sinkhole Plain with which the model may be further tested.

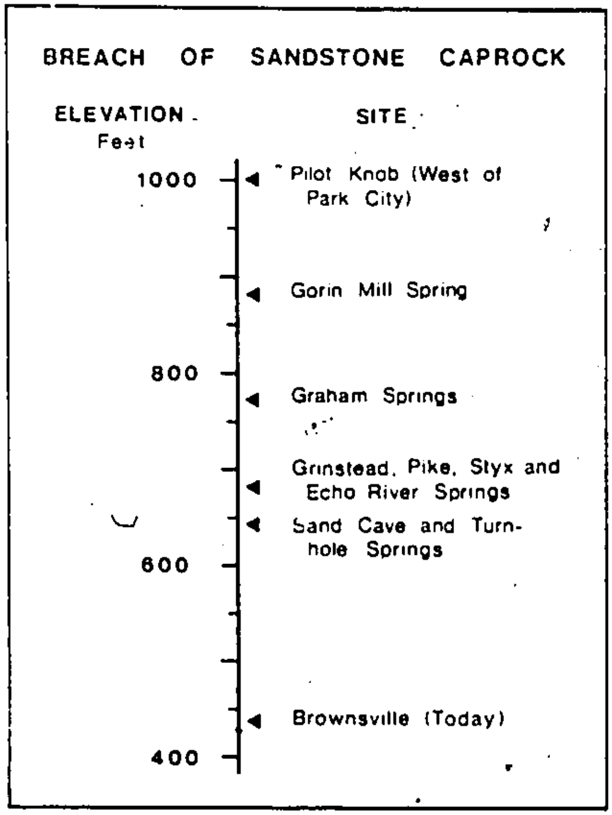

Figure 9.14
Summary of elevations (and therefore relative times) at which the caprock was breached at spring sites along Green River.

9.2 A HIGH DIP MODEL EXAMPLE

- THE HOLLOCH

The Holloch, known to Swiss explorers since 1875, is one of the major caverns of the world. It consists of more than 130 km of surveyed passage, linked with a theodolite survey. The survey and maps were prepared by members of the Arbeitsgemeinschaft Hollochforschung, under the scientific direction of Prof. Dr. Alfred Bogli. At least 50% of the known passages are developed in a single planar parting, having a dip of 12 to 25 degrees. These characteristics make it an ideal place to test the high dip model.

9.2.1 THE GEOGRAPHICAL SETTING

The Holloch is located in north-central Switzerland, 38 kilometres east of Lucerne, in the canton of Schwyz (Fig. 9.15). More specifically, it lies south of the Starzlenbach River, near its confluence with the Muota River. The region is within the northern-most portion of the Alps, a region of limestone mountains referred to as the Glarus Alps.

9.2.2 THE GEOLOGIC SETTING

9.2.2.1 Lithology

The region is underlain by lower Cretaceous, Urgonian rocks. These are principally limestone but include clayey and cherty limestones, glauconitic sandstones, marls,

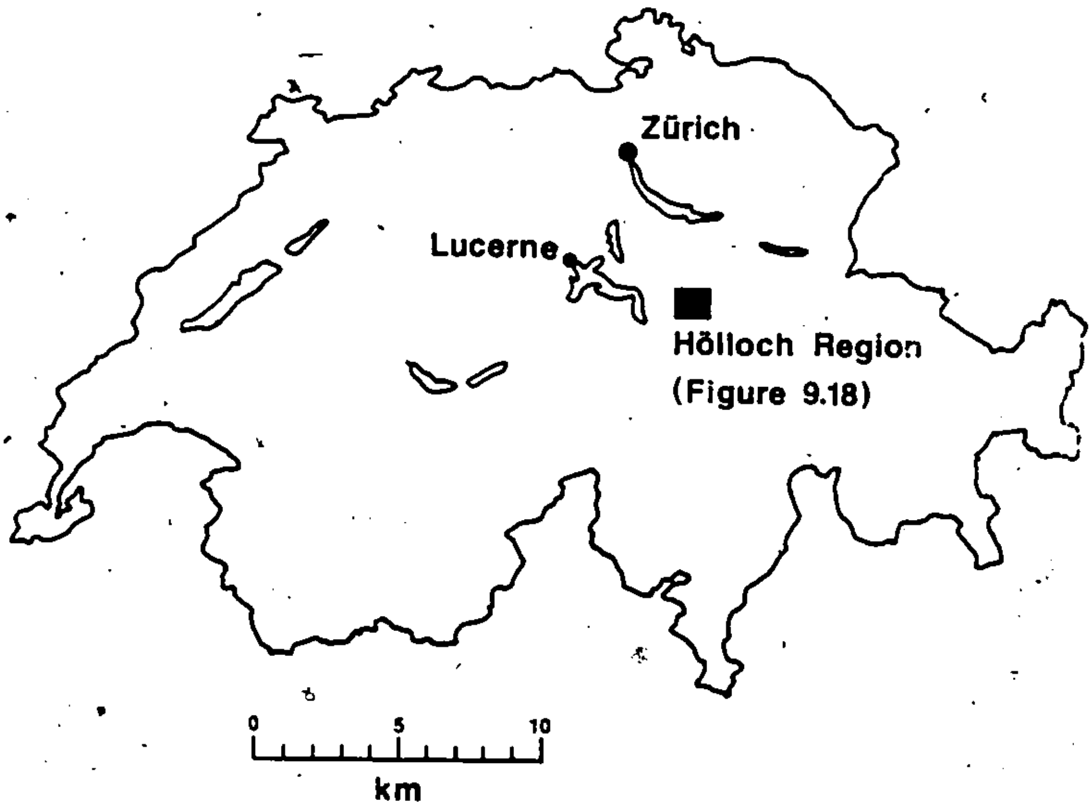

Figure 9.15
Location of the Holloch region in Switzerland.

and shales. Figure 9.16, after Bogli (1970), describes a typical section. The Holloch is developed primarily in the Schrattenkalk, a pure limestone composed of 92 to 98% calcium carbonate.

9.2.2.2 Structure

The regional structure is shown in Figure 9.17. The principal structural feature associated with the Holloch is the Axendecke, comprised of three subsidiary thrust sheets, the Silberndecke, the Bachistockdecke, and the Axendecke (sensu stricto). A varying amount of the upper portion of the lithologic section shown in Figure 9.16, including the Seewerkalk and upper Shrattenkalk, is repeated three times. The lithologically lower Kieselkalk is intercalated complexly with these minor thrust sheets on their up dip side. The principal portion of the Holloch, the Hauptsystem, comprising 86 km, is confined to the Bachistockdecke. The Upper system of conduits, the Hochsystem, comprising 23 km, is formed in the Silberndecke (Bogli, 1970). Many of the bedding planes show features indicating that they were the locus of tectonic slippage. The Osirisgang and Sphinx, in particular, show well developed mylonites along the exposed bedding plane.

9.2.2.3 Geomorphology

This region of Switzerland has been subjected to

Figure 9.16
Stratigraphy in the Holloch region, Switzerland; after Bogli (1970).

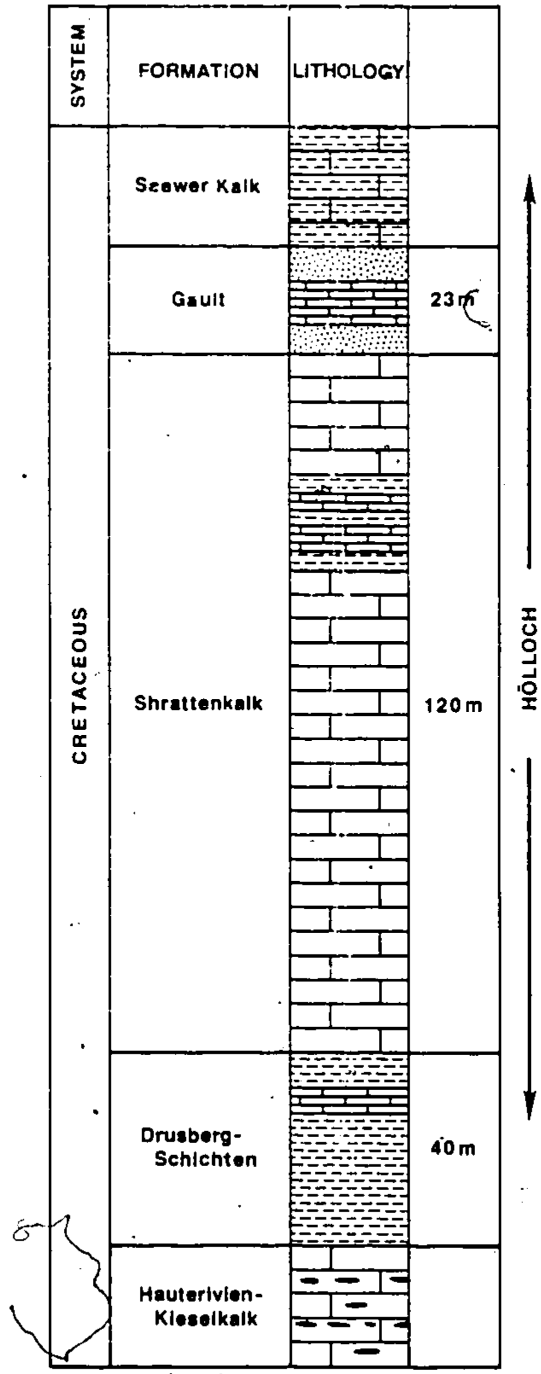

After Bögli,(1970)

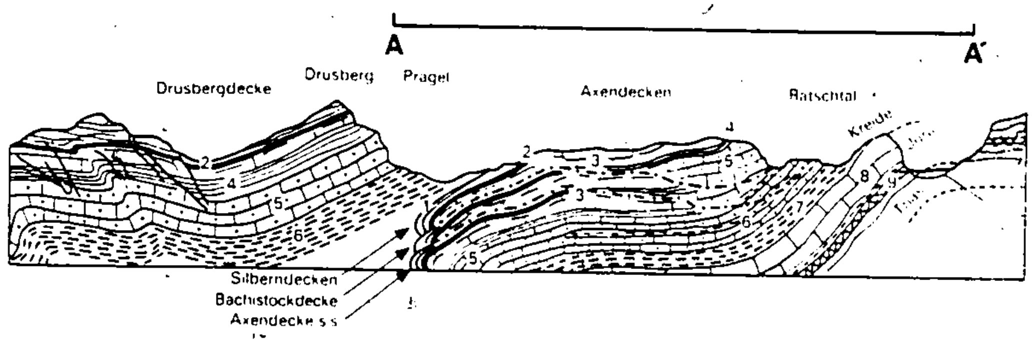

Figure 9.17
Regional structure near the Holloch, Switzerland, from Bogli (1970). Key: 1-Flysch, 2-Seewerkalk, 3-Schrattenkalk, 4-Drusbergerschichten, 5-Kieselkalk, 6-Valanginienmergel, 7-Zementsteinschichten.

intense alpine glacial erosion. It is probable that this erosion has been episodic, given the abundance of evidence for a sucession of glacial advances during the Pleistocene. Several authors have cited gomorphic evidence to support such a scenario in this region. Krieg (1954, 1955) cited levels of subsurface conduits as evidence for a sequential lowering of the valleys. Shauberger (1955) analysed the position of cave entrances in the region and found correlations with several presumed erosion surfaces. Arnsburger (1955) and Trimmel (1955) rejected these analyses and attributed the correlations, in part, to lithologic causes. Bogli (1966, 1968) noted a glacially polished valley bottom at 750 m, which he attributed to the first interglacial period. This physical evidence is less than overwhelming. Until techniques such as isotopic dating of stalactites are employed in working out a firmly based chronology for the cave conduits at the various elevations, the question may not be satisfactorily resolved.

Bogli (1970) estimated that 43% of a 623 square kilometre area draining to the Muota river, which includes the catchment of the Holloch, is karstified. The terrains directly overlying the Holloch exhibit a variety of karren forms, sinks, and swallets. These features form local catchments and hydraulic inputs to the conduit system, 100 to 900 metres below. Except for one vadose shaft, they do not, however, provide access to the cavern due to their filling of debris from the most recent glacial period (P. Berg, Personal communication, July, 1981). Few can be penetrated to a depth of more than 20 metres.

9.2.2.4 Hydrology

The area base level is presently controlled by the Muota River which flows, in part, across the strike and integrates strike-aligned flow of several tributary valleys (Fig. 9.18). Surface streams occupy these valleys where they are alluviated or are underlain by non-karstifiable rocks. The regions of limestone outcrop are drained internally, and their flow resurges at a series of springs along the Muota Valley. Like the surface streams, the subsurface drainage is directed along the strike.

Precipitation in the area is relatively high and altitude dependant. The annual precipitation at an elevation of 610 m in the Muota Valley averages 1990 mm. At 1200 to 2300 m in the region overlying the Holloch, it is approximatly 2400 mm per year (Bogli, 1970).

The Holloch is located beneath 22 square kilometers of karst terrain. The precipitation of this catchment resurges at the Schleichender Brunnen. This spring has an annual discharge in excess of 50 million cubic meters (Bogli, 1970). This discharge easily accounts for a precipitation of 2400 mm over this 22 square kilometre area, assuming zero evapotranspiration. Like the other tributary

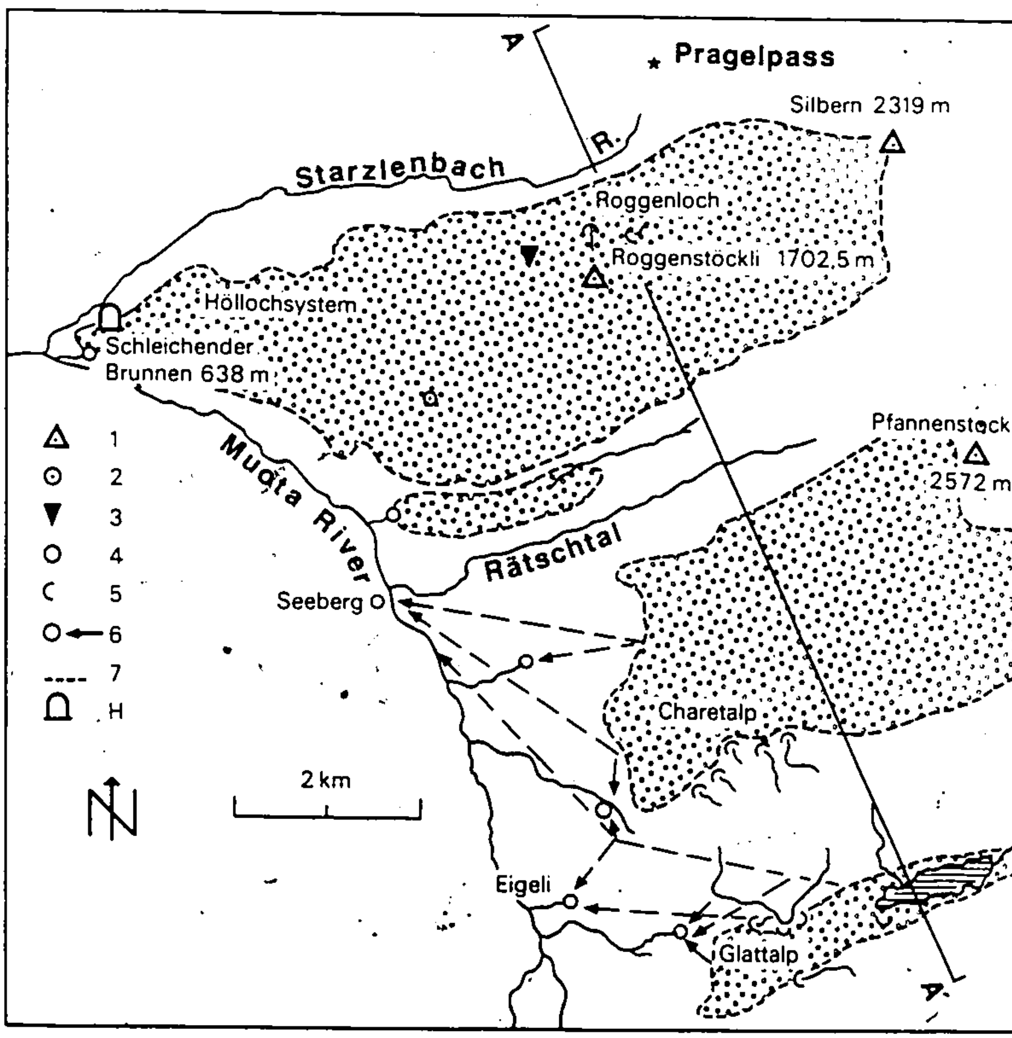

Figure 9.18
Hydrology of the Holloch area; from Bogli (1970). Key: 1-Mountain summit, 2-Sinkhole, 4-Karst springs, 5-Stream sinks, 6-Dye traces, 7-Boundary of karst rocks, 8-Holloch entrance. A-A' shows the location of the section in Figure 9.17.

systems to the Muota in Figure 9.18, this catchment is characterized by westward drainage along the strike.

9.2.3 THE MODEL COMPARISON

In this case, the model comparison focuses principally upon the three dimensional pattern of the conduits and their evolving hydraulic function. This analysis is based upon evaluation of mapped passages in the middle portion of the Holloch (Fig. 9.19). This portion is bounded on the east by a north-south trending fault zone passing through the Sielgang, Sturzgang, and Orgelwand; on the north by the Schlundgang and Rabengang; on the west by the Riesengang; and on the south by the tributary passages of the Domgang and Himmelsgang. The northern boundary is the lowest part of the region normally above the phreatic zone and, as such, represents the present practical limit of direct exploration for speleogenetic analysis. The southern boundary, the highest area under consideration, displays an early phreatic morphology but is partly obscured by more recent sediment infilling and vadose processes, some of which remain active. It was deemed unwise to extend the analysis to higher portions of the cave for these reasons. Representative sections of this region were investigated in detail as part of this research.

Following the analysis by Ford (1965, 1968) of the conduits in Swildon's Hole in the central Mendip Hills,

Figure 9.19

The conduits of the middle portion of the Holloch showing dip and strike oriented elements, after Bogli (1970).

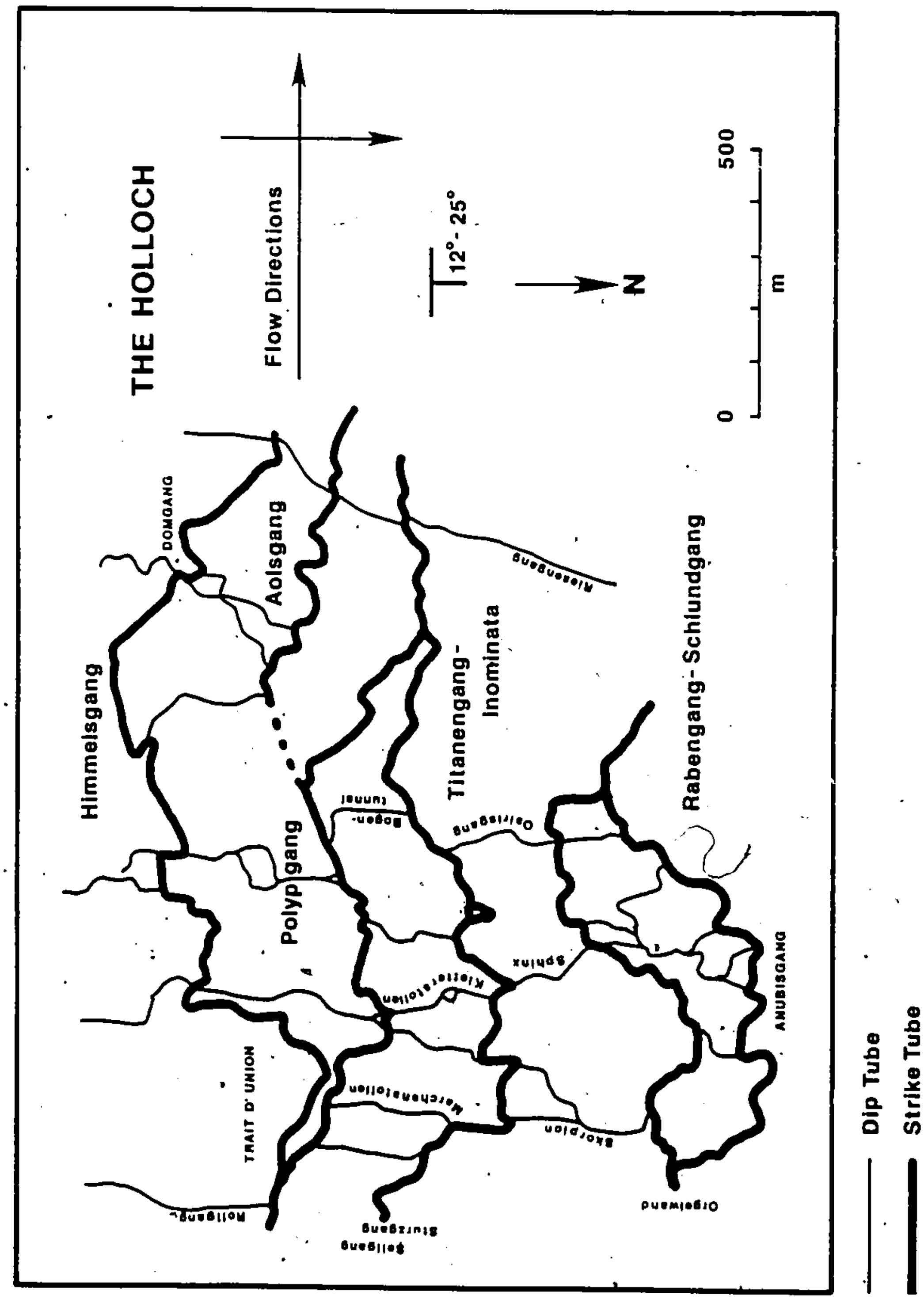
THE HOLLOCH
Flow Directions
12°-25°
N
0
500
m
Himmelsgang
Domgang
Aolsgang
Riesengang
Titanengang-Inominata
Rabengang-Schlundgang
Polypgang
Bogen-tunnel
Osirisgang
Sphinx
Kletterstollen
Anubisgang
Trait d' Union
Marchenstollen
Skorpion
Orgelwand
Rollgang
Sturzgang
Seilgang
Dip Tube
Strike Tube

England, the conduits of the Holloch can be divided into two principal types. The first is oriented approximately parallel to the dip. Examples include Riesengang, Osirisgang, Sphinx, Scorpion, the northern part of Polypgang, Bogentunnel, Kletterstollen, and Marchenstollen. The mean diameter of these conduits is typically two to three meters. The second conduit type is directed approximately parallel to the strike. These form three principal east-west trunks within the larger conduit network. The uppermost trunk extends from 900 m. to 1000 m. and is composed of the Himmelsgang and Trait d' Union conduits. The second trunk composed of Styx, Innominata, and Titanengang lies at an intermediate level, between 725 m and 880 m. The lowest trunk, composed of the lowest part of Osirisgang, Anubisgang, and Schlundgang lies between the permanently phreatic zone at 643 m and about 750 m. These two conduit types are referred to here as dip and strike elements, respectively. Both are elliptical to lenticular in cross section, with a bedding/thrust plane occupying a position in the middle or lower part of the section. The tubes frequently possess anastomotic networks extending laterally, with diminishing size, along the bedding plane. A generalized cross section from the region of Sphinx is depicted in Figure 9.20.

Entrenchment features, indicative of vadose activity, are conspicuous by their absence. Only minor

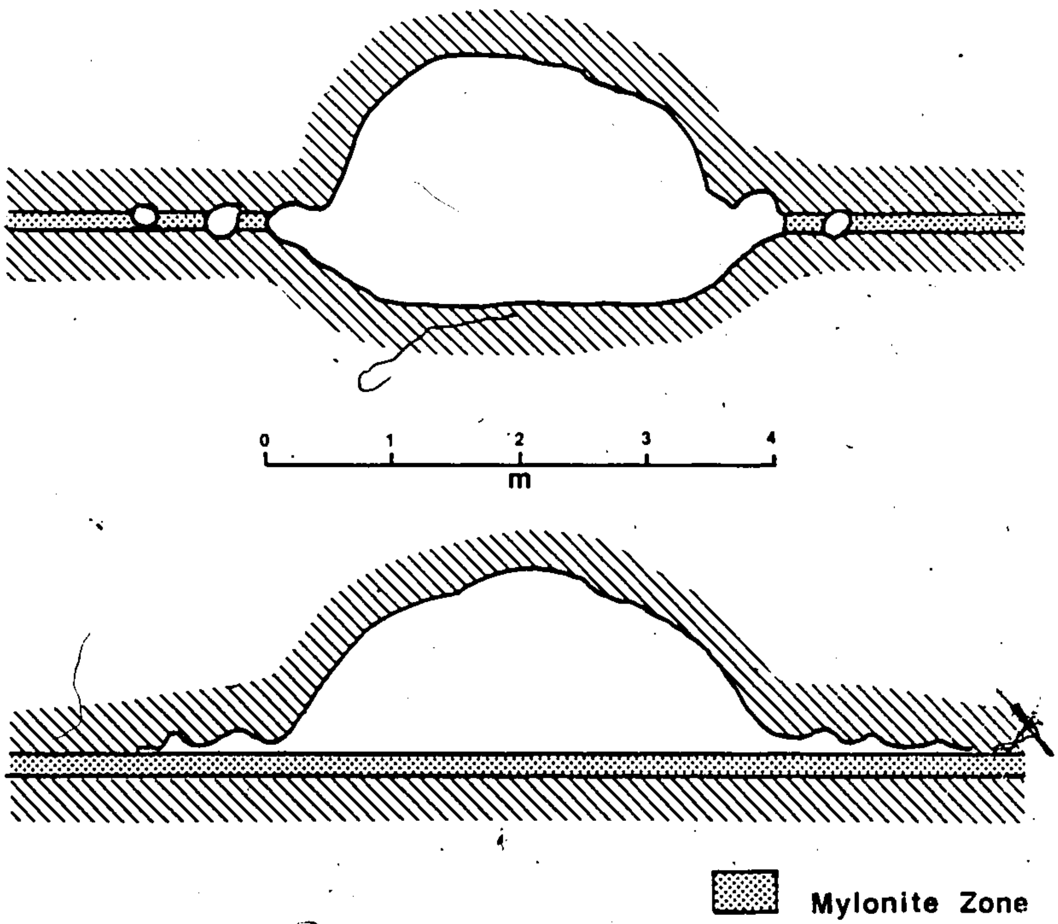

Figure 9.2Ø
Typical dip tube cross-sections from the region of Sphinx, the Holloch.

runnels, a few centimeters in width and depth, indicate any activity of this type. These are found principally in the middle and upper portions of the cave.

Joints normal to the bedding planes are quite common, and their orientation is consistent with the direction of principal stress involved in the movement of the thrust plane (Fig. 9.21). These joints are, however, of minor importance in determining the orientation of the dip and strike directed tubes. This contention is supported by the observation that very few joints along the ceiling showed any enlargement, and the tendency for conduits in the study region to follow such features, whether they are enlarged or not, is very rare.

This combination of morphological characteristics suggests that phreatic flow along bedding planes was responsible for their initial development. The characteristics further suggest that phreatic flow was responsible for the enlargement of the primitive conduits to their present size.

The dip-oriented elements of the cave pattern have apparently formed in a down dip direction. This interpretation is based upon two factors. First, they extend obliquely downward from the surface, where inputs are most likely to occur, following the most reasonable direction for potential loss. Second, scallop flow directions indicate that they have enlarged to their present

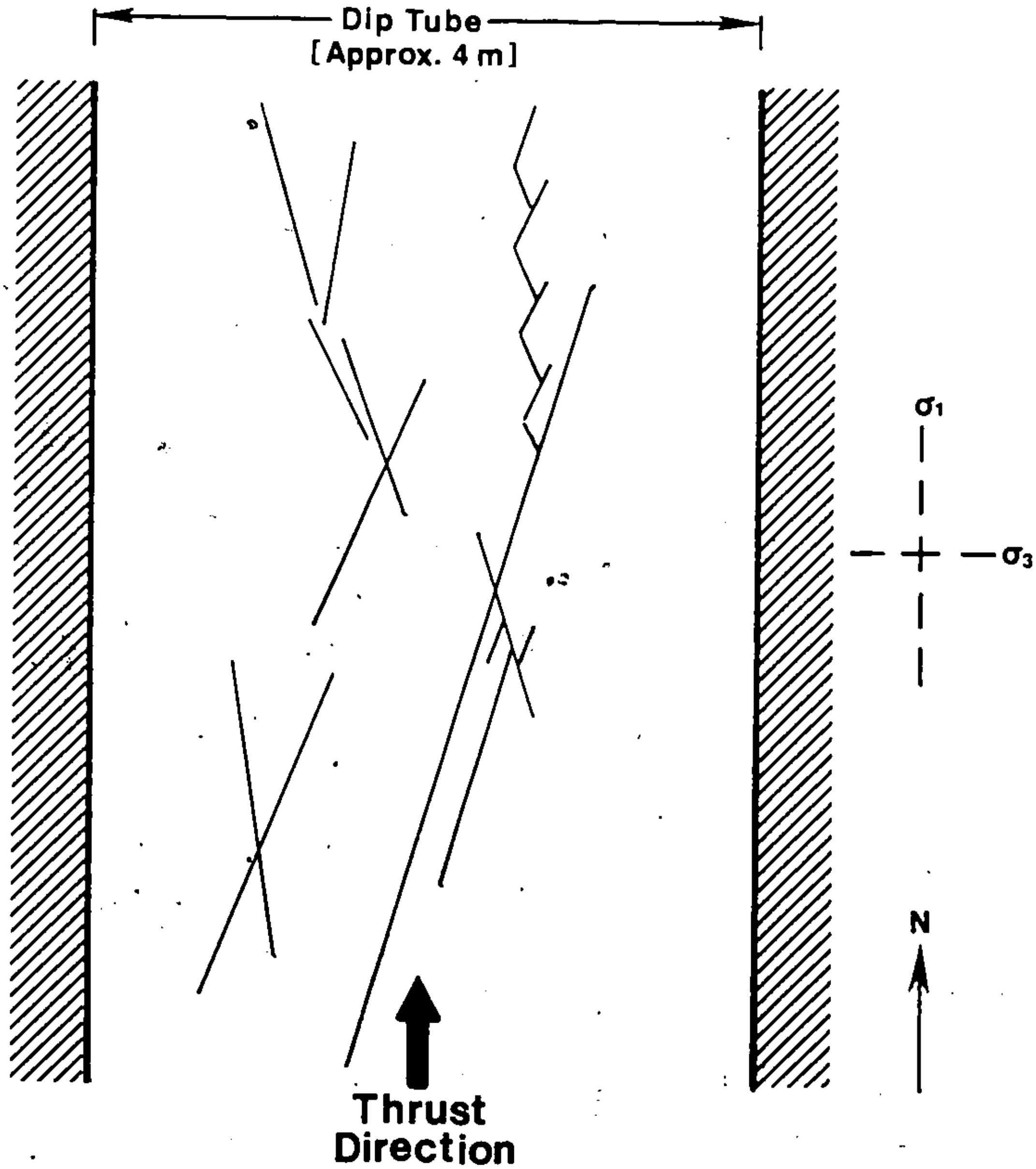

Figure 9.21
Plan view of a dip tube in the region of Osirisgang, showing tectonic fractures.

size by down dip flow. This latter evidence may or may not be indicative of initial flow direction. The strike oriented elements are most likely to have developed and enlarged by flow in a westward direction. Flow to the east, away from the Muota Valley, seems unlikely at any stage of development. Such flow would be counter to the most reasonable and shortest direction for potential loss. Recharge areas rise eastward at present, to elevations of 1700 m above the Muota, at the summit of Silbern (2319 m). In addition, scallops indicate that the most recent flow was principally westward in these tubes at all elevations where they were investigated. The conduit flow directions and phreatic morphology of the strike and dip conduits in the middle section of the Holloch are consistent with the requirements of the high dip model. A more important test of the model, however, is the temporal order of their development. The model requires that the dip elements predate the strike element which connects them. The Titanengang is the largest, simplest, and most intensively studied of the strike systems (Fig. 9.19). This conduit, nearly two kilometers in length, posesses a series of offsets which invariably occur at junctures with dip elements. At each of these points, the strike element is abruptly offset up or down dip to continue its course sub-parallel to the strike at a higher or lower level. The short segment of dip element involved in the offset is, in every case, enlarged to the typical dimensions of the strike conduit. These relationships are most simply explained by the strike elements having formed subsequent to the smaller dip elements. The model also requires that the strike elements linking the dip tubes be established in a sequential manner from the output toward the most distant part of the catchment. There is no way at present to determine if the western portions of the Titanengang predate the eastern elements. However, the irregular offsets and wide vertical range of this continuous, constant diameter passage, formed within what appears to be a single dipping bedding plane, strongly suggests that it was not formed as a single entity.

The function of the passages in their present form is quite clear. The phreatic portion of the system has been confirmed by dye traces to conduct water from beyond the eastern limit of the known cave, along the strike, to the resurgence at Schleichender Brunnen, elevation 638 m (Bögli, 1970). When these phreatic conduits have insufficient capacity, the lowest level of normally dry conduits is flooded, namely Anubisgang - Schlundgang. With increasing runoff, a higher but minor strike trunk, Rabengang, becomes filled. When water levels reach 734 m, these trunks in combination with the Hauptgang, in the extreme western portion of the system, conduct water to the surface via the historic entrance. Because of the irregular elevation of the strike elements, dip tubes are likely to be called into play from time to time during floods, to convey water downward from higher to lower strike levels. Such flow would occur when the water level falls below the highest level of a strike trunk. Thus, the principal enlargement of the strike elements may take place in a phreatic environment at base flow, while enlargement by high flow, in epiphreatic conditions, seems to characterize the dip elements.

This scheme explains why the presently visible inputs in the higher portions of the system are so grossly underfit with respect to the dip conduits and why the two types of conduits are relatively similar in size, in spite of the great disparity in their catchments. These inputs are little more than trickles. Even this flow does not presently traverse the intermediate elevations of the system. For example, nowhere in the Innominata or Titanengang are such flows evident, even during the period of heavy rainfall when this study was conducted. This suggests that they pass along undiscovered routes in parallel but lower bedding planes.

Enlargement of the passages must also have taken place following a somewhat different scheme during periods of glacial advance. At these times, discharge points at the valley bottoms are likely to have been sealed by glacier ice, and abandoned strike trunks, with their related discharge points, would be reactivated and enlarged. Lower strike trunks would carry flow from the most distant inputs fed by downward flow in the distal dip elements, while proximal dip elements would have conducted flow upward (Fig. 9.19). This renewed phreatic flow could erase vadose features in the affected conduits, thus explaining their present rarity. The only direct evidence for glacial flooding, observed during the study, was the total lack of sediment in the Titanengang, while sediments were in generous supply throughout the higher part of the system, in Osirisgang and, to a lesser extent, in the other dip elements below the Titanengang. This passage would seem to have escaped all episodes of slack water sediment deposition since it was last flushed clean by rapid through-flowing waters. This suggests that, following this cleansing, flood crests simply did not reach it, due to a relatively sudden lowering of water levels. The melting of a glacial plug at the elevation of the present resurgence is certainly a rapid and plausible means of accomplishing this lowering. Such evidence is admittedly quite circumstantial, but the striking cleanliness of this passage, even in such prime sediment traps as the loop east of the junction with Osirisgang, is difficult to overemphasize, and demands explanation.

9.2.4 SUMMARY

The morphology of the middle portion of the Holloch is not inconsistent with its evolution in the manner described in the high dip model. This would proceed from inputs arrayed along the strike in a down dip direction with ultimate discharge to the west at an elevation at or above 1000 m. As the proximal inputs link to the discharge point, a series of strike oriented conduits develop, one at a time, linking the dip tubes at elevations near, but below, the 1000 m. discharge point. This would establish the Himmelsgang trunk. With the development of a lower level discharge point at about 900 m, continued development of dip tubes could proceed, and a new series of strike links could develop as before. This would give rise to the Titanengang trunk. The level of 900 m is chosen because the highest point in the Titanengang is at about 885 m, and a phreatic morphology is preserved there. Thus, the spillover point in the system must have been above that point. With the development of a resurgence near the level of the historic entrance, 734 m, a third set of dip tubes could be formed, followed by the evolution of the strike trunks at the elevation of Anubisgang and Rabengang.

It is interesting, and perhaps significant, that the highest levels of the system extend along the strike the shortest distance, while the lowest levels cover the greatest span, extending to the known eastern limits. The model requires that the integration of the dip tubes take place sequentially, beginning in the discharge region. The older higher level trunks should posess a shorter strike line extent than the younger deeper trunks because they were abandoned before integration had proceeded to its present degree." Figures 9.22 A & B show that the highest strike elements at the level of Galerie des 800.m and Galerie du Jura extend no further eastward than Rollgang. Himmelsgang extends an additional 0.5 km. and may include Lehmschollengang for a total of nearly 1 km. The Titanengang extends at least through S.A.C. Gang as far as Bivouac 3 into the region of Versturzgang, a distance of 2 km. beyond Himmelsgang. Bogli (1966) infers that a portion of Hoffnungsgang and Schluchtgang, totalling an additional 1.6 km, may also be related to this strike system. The elevation of this section (Fig. 9.22 B) strongly suggests that this is the case, although the physical connection between the two is somewhat obscure. The lowest accessible level extends through the lower portions of S.A.C. Gang, through Pagodengang to Reinacherstollen, 5.5 km more distant from the present day resurgence than the highest, and presumably oldest, level. Thus, even the overall plan appears to conform to the model requirements.

9.2.5 AN ADDITIONAL EXAMPLE OF THE HIGH DIP MODEL

In contrast to the the Holloch, Ogof Ffynnon Ddu, one of the largest caves in the British Isles, is intimately associated with joints(O'Reilly, 1973). Here 40 km of

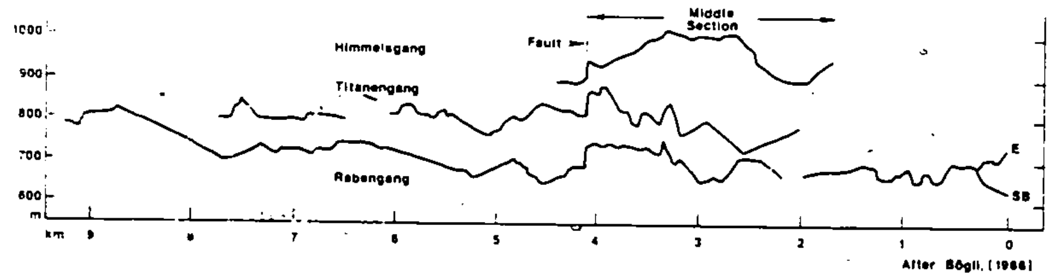

Figure 9.22
Plan view of the Holloch [SEE REAR POCKET] and vertical section parallel to the strike, from Bogli (1970).

conduits are developed in the flank of a complex, asymmetric, anticlinal structure. A sequence of cavernous Carboniferous limestones, dipping southward at an average angle of 15 degrees, is underlain by Devonian Old Red Sandstone. The limestones are overlain by Namurian quartzite conglomerates (Millstone Grit) (Fig. 9.23). These units are faulted in a northeast-southwest direction, parallel to the principal anticline, and in a north-south direction (Weaver, 1971) (Fig. 9.23). This latter fault direction is less persistent and parallels a series of minor anticlines (Charity and Christopher, 1977a, 1977b). Joints are clearly visible in the cave, which are sub-parallel to these faults and minor folds, as well as the regional dip.

The conduits are phreatic bedding plane tubes, which frequently follow the joints. The observed fact that the major axis of the cross section of the phreatic portions of the tubes is horizontal rather than vertical is the rational for this designation. The joints seem to provide only a guiding influence relative to the plan form. Glennie (1948) and O'Reilly (1973), among others, have noted this relationship. Frequently, the phreatic forms are modified by past and present vadose entrenchment.

Figure 9.23 shows that, like the Holloch, the conduits of Ogof Ffynnon Ddu can be divided into two groups: a set of dip tubes and several sets of irregular strike subsequent tubes. Seventeen dip tubes presently carry

Figure 9.23
Structure, conduit pattern, and areal extent of sandstones in the region of Ogof Ffynnon Ddu, Wales; after Charity and Christopher (1977a).

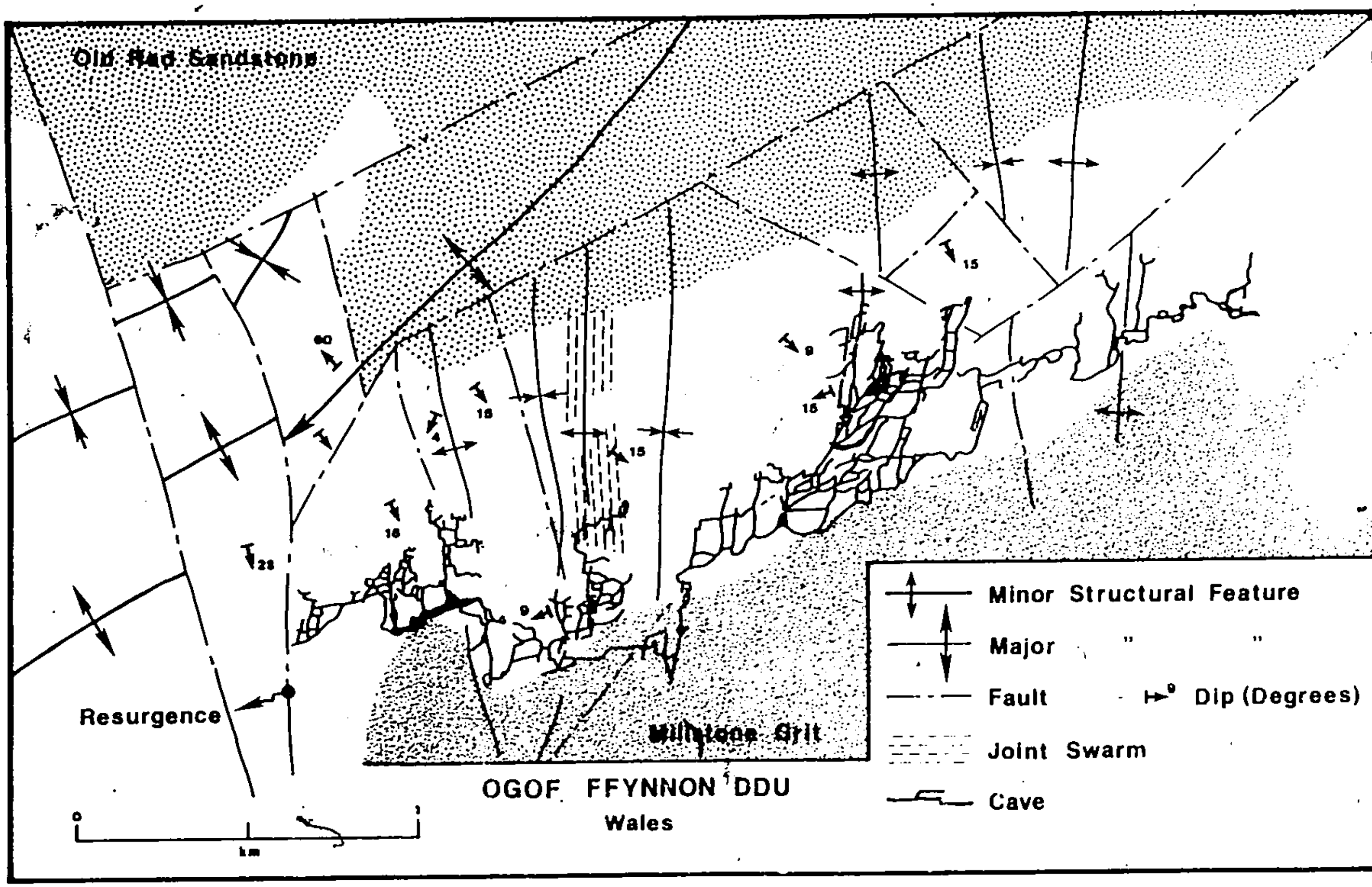
Old Red Sandstone
Millstone Grit
Resurgence
Minor Structural Feature
Major " "
Fault
Dip (Degrees)
Joint Swarm
Cave
0
km
1
OGOF FFYNNON DDU
Wales

vadose streams which are tributary to the principal subsurface stream. This channel is deeply entrenched along the topographically lowest strike conduit.

9.3 A RESTRICTED INPUT MODEL EXAMPLE
- CAVE CREEK

The Cave Creek area contains six known units of subsurface conduits totaling 17 km in length which form part of a once fully integrated system of limestone caves. The inputs to this system are confined to a narrow zone, no more than a few hundred meters across, where stream erosion has breached an impermeable caprock consisting of sandstones and shales. This system of conduits and inputs is relatively isolated from others and provides an almost ideal test of the restricted input model.

9.3.1 THE GEOGRAPHICAL SETTING

Cave Creek, a tributary of the Cumberland River, is located in south-central Kentucky, in Pulaski County. The area is depicted on the Hail quadrangle map of the United States Geological Survey 7.5 minute series and the geologic map of the Hail quadrangle by Smith et al (1973). The area is part of a larger karst region which extends from just south of the Ohio River, southward along the Appalachian Highlands escarpment through Tennessee.

9.3.2 THE GEOLOGICAL SETTING

9.3.2.1 Lithology

The region is underlain by sedimentary rocks, largely limestones, sandstones, and shales of Upper Mississippian and Lower Pennsylvanian age. Figure 9.24 shows a representative stratigraphic section from the area. The nomenclature of these rock units is borrowed, in part, from Tennessee, Illinois, and West Virginia and varies considerably between adjacent geological maps and between workers. This nomenclature is presently under revision by the Kentucky Geological Survey. Because of this confusion, a second nomenclature, frequently used by earlier workers, is also included in Figure 9.24.

9.3.2.2 Structure

The area lies on the eastern flank of the Cincinnati Arch, a broad, low, north-south trending anticlinal feature which can be traced from southern Michigan through Cincinnati to northern Alabama. On a regional basis, the rocks may, therefore, be described as dipping gently toward the east-southeast at 3.5 - 9 meters per kilometer. Locally, however, a considerable amount of subtle structure can be discerned. In the region of specific interest, a small anticlinal feature extends over the point of confluence between the Cumberland River and Cave Creek (Fig. 9.25).

9.3.2.3 Geomorphology

The region lies at the edge of the maturely

Figure 9.24
Stratigraphy in the Cave Creek area, Kentucky, from Ewers (1972).

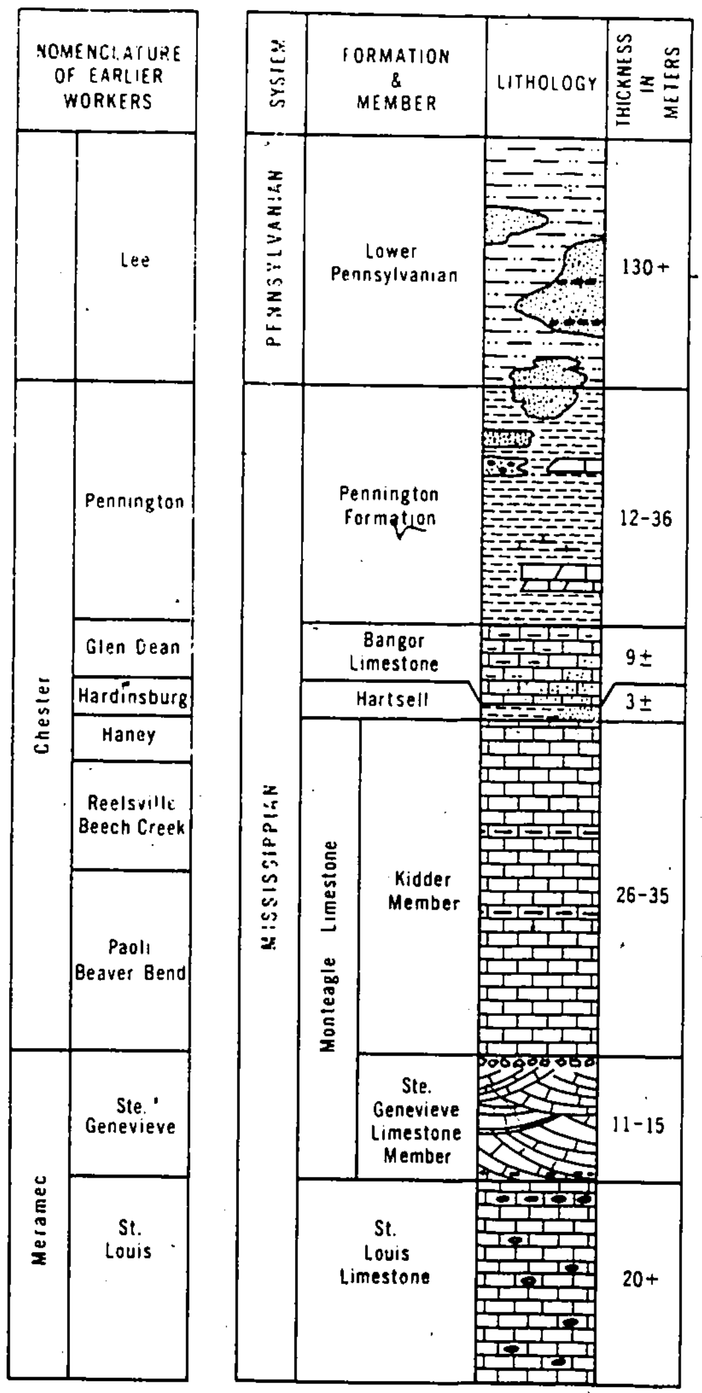

After McFarlan & Walker (1956)

After Lewis, (1972)

Figure 9.25

Structure and caprock distribution in the Cave Creek area, Kentucky; adapted from Smith et al. (1973). Structure contours are drawn on the Hartselle formation in the north and on the Rockcastle member in the south.

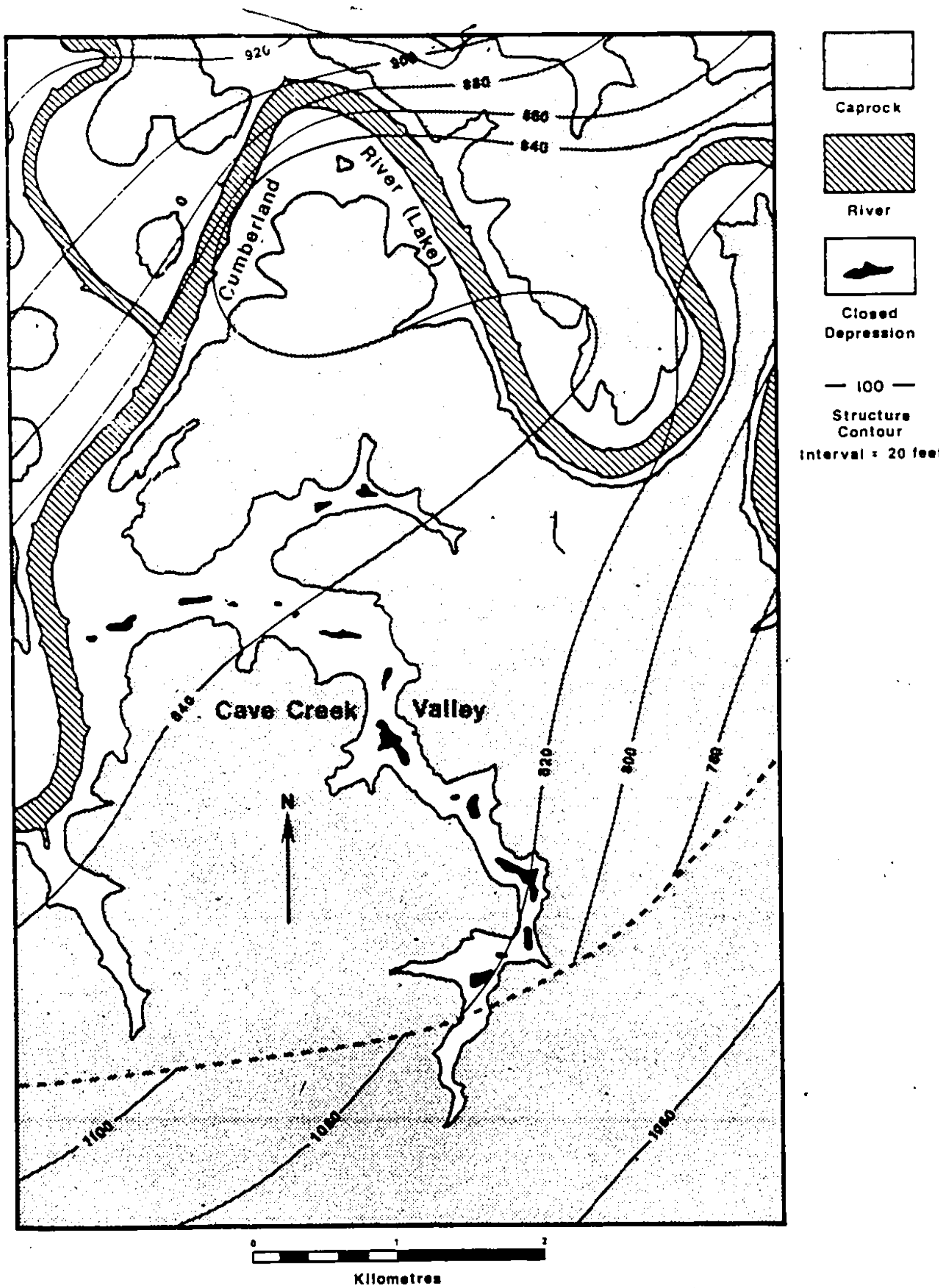

920
900
880
860
840
Cumberland
River (Lake)
Cave Creek
Valley
840
820
800
780
N
1100
1080
1060
0
1
2
Kilometres
Caprock
River
Closed Depression
100
Structure Contour
Interval = 20 feet

dissected western margin of the Cumberland Plateau. The plateau is capped with basal Pennsylvanian clastics of a highly variable nature. They range from cross-bedded conglomerates, locally referred to as the Rockcastle Member by Hatch (1963), to siltstones, shales, and coals. The hilltops in the plateau region have an elevation of 375 m. Maximum relief here is 155 m.

An area of knobs occurs in a narrow strip normally 5 - 6 kilometers wide along the edge of the plateau. These detached plateau remnants have summit heights up to about 365 m and rise about 100 m above the intervening surface. This surface is developed on the Kidder and Ste. Genevieve limestones and is marked by numerous sinks and solution valleys. To the west of the knobs is a gently rolling surface, continuous with that between the knobs, which forms the Highland Rim, a part of the Interior Low Plateau Province (Fenneman, 1938).

The Cumberland River flows in a narrow gorge for 64 km through the dissected portion of the escarpment. Evidence suggests that the gorge here was formed, in part, by the retreat of Cumberland Falls from near Burnside, Kentucky, to its present location upstream from the town. The falls retreats as it undermines the the resistant Rockcastle Conglomerate cap rock, exposing the easily eroded shales, siltstones, and poorly cemented sandstones of the Lee and Pennington formations (McFarlan, 1943). The development of the gorge is closely related to the evolution of the karst in Cave Creek, as will be demonstrated below.

The erosion of Cave Creek Valley has breached the caprock and exposed the Monteagle and Ste. Genevieve limestones along the valley sides and bottom. This exposure extends for 5.75 km east and southward from its confluence with the Cumberland River.

Cave Creek Valley can be characterized as a karst valley, due to its irregular profile and its internal drainage. There are many other valleys of similar character along the escarpment.

9.3.2.4 Hydrology

The drainage in the region is controlled by the Cumberland River and, since 1952, by its artificial pool created by Wolf Creek Dam. The normal pool elevation for Lake Cumberland is 220 m, 5 m above the pre-impoundment level at the mouth of Cave Creek. The areas of discontinuous sandstone and conglomerates act as granular aquifers, perched upon the impermeable shales of the Lower Pennsylvanian and Upper Mississippian. These give rise to numerous diffuse seeps and springs, which are occasionally tapped for domestic water supplies. Where exposed, the limestone units develop subsurface conduit drainage. This secondary solution porosity is not restricted to any particular stratigraphic horizon within the limestone, although there is some tendency for surface streams to be maintained where the upper St. Louis limestones lie directly beneath the surface. This suggests that this unit may be less soluble, or otherwise less conducive to karstification (Romanik,1981; Morris, 1981).

Cave Creek Valley contains several hundred closed depressions and is without continuous surface flow, even under conditions of extreme precipitation. At least thirty well defined wet weather tributaries, carrying allogenic waters from the caprock, extend to the valley bottom, where they sink (Fig. 9.25). The resurgence for these waters is assumed to lie at the Cumberland River beneath its present artificial pool. A large spring, downstream from the valley mouth and on the same side of the river, appears on early topographic maps (Mayfield & Withers, 1929) and is reported by longterm residents of the area. This spring is presumed to be the resurgence.

9.3.3 THE MODEL COMPARISON

The known passages associated with Cave Creek Valley form a three dimensional network which closely follows the valley axis (Fig. 9.26). The network ranges vertically between 207 m and 263 m. The course of the subsurface flow which traversed these conduits, neglecting minor deviations, extends for a distance of 4.8 km. Figure 9.26 depicts this generalized path as line "A-B". There is no reason to

Figure 9.26 A, B

Conduit pattern and generalized subsurface flow route beneath the Cave Creek area. For discussion of paths A-B and A-C see page 35Ø. Cave information was provided courtesy of Mr. Louis Simpson.

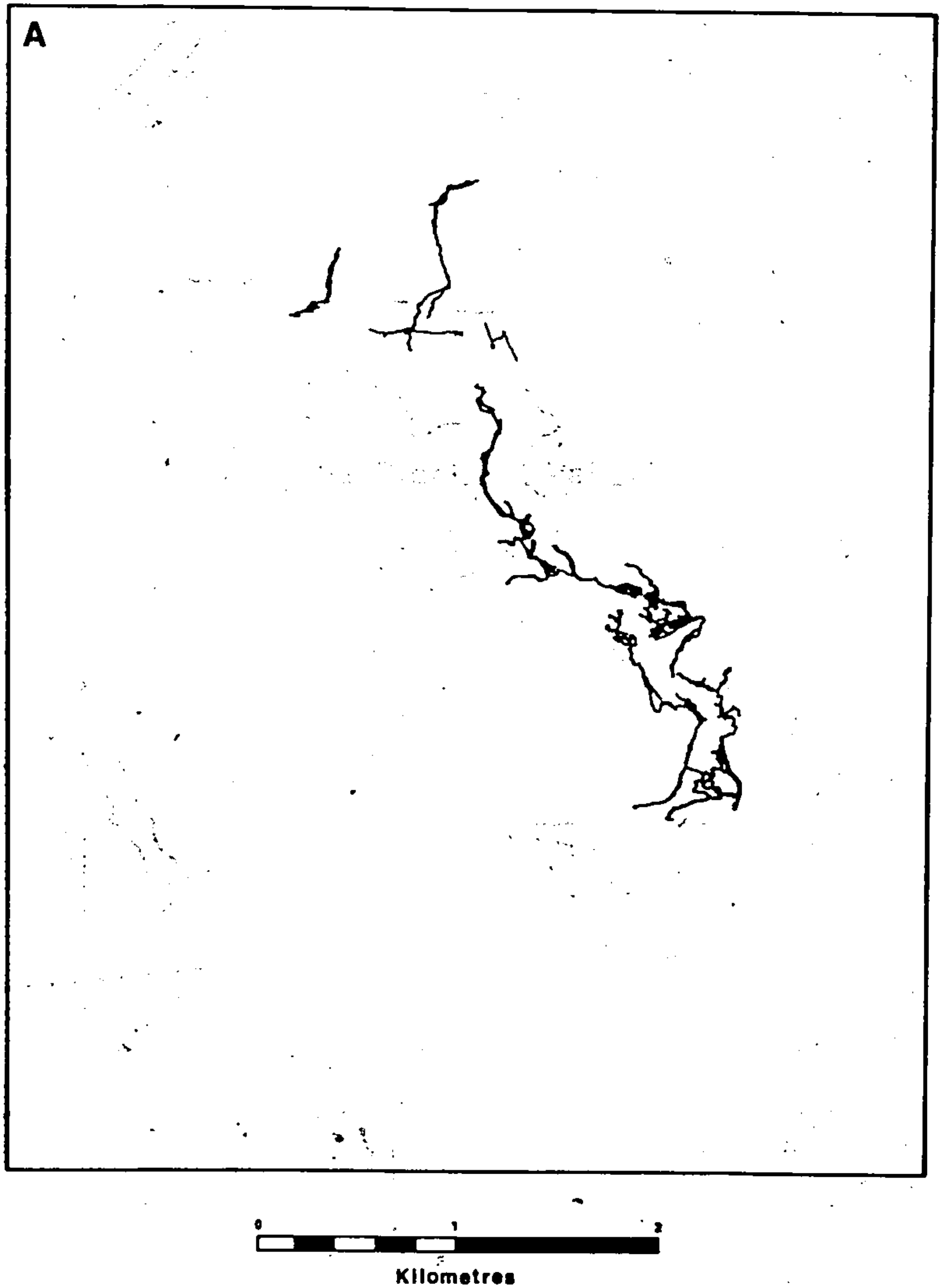
A
0
1
2
Kilometres

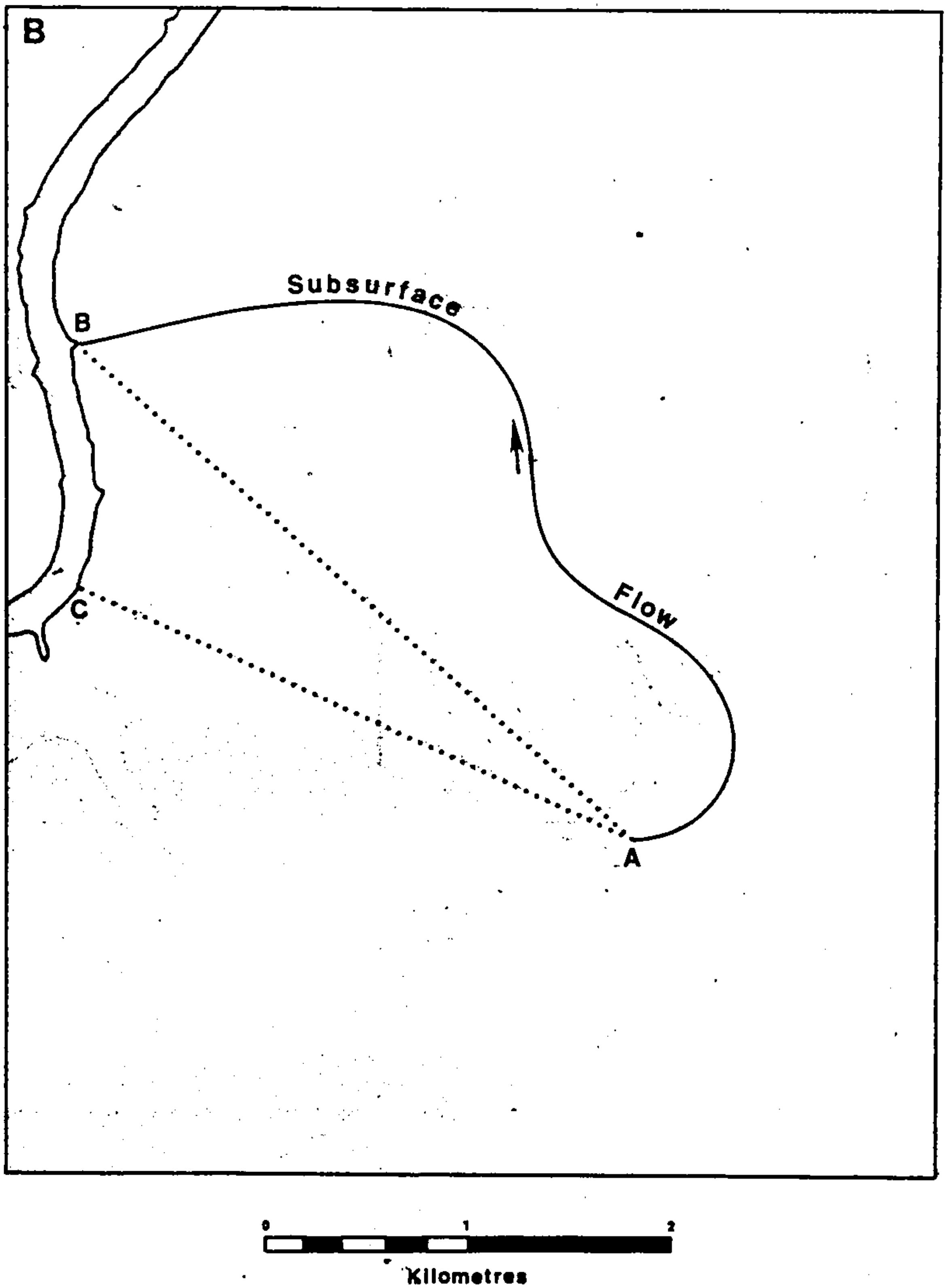
B
B
C
A
Subsurface
Flow
0
1
2
Kilometres

believe that flow from the region of the sink at "A" could not be conducted along path "A-C" or on the direct course to "B". No structural or lithologic barriers to such flow are known or seem likely. In fact, a considerable advantage would seem to exist along these latter courses. Their lengths are 3 km and 3.6 km, compared to 4.8 km. Thus they should have 62.5 and 75 percent, respectively, of the resistance of the longer course. The gradient would be 1:3 and 1:3.6 compared to 1:4.8, a significant increase. Stratigraphically, point "C" is about two meters lower than point "B" and, therefore, if the entrenchment of the Cumberland River proceeded uniformly, point "C" may not have been able to discharge waters from the limestone as early.

In the face of these theoretical advantages, the known conduits follow the longer, lower gradient course. It seems reasonable, given the geomorphic setting, that the following events would have occurred. First, as the falls receded past the mouth of Cave Creek Valley the stream, flowing then upon the caprock sequence, began gradually exposing the limestone along Cave Creek to significant hydraulic pressure gradients. This exposure, by reason of the dip as well as the gradient of the stream, would have proceeded from the valley mouth in an upstream direction. The localization of the first breaching at the creek mouth, rather than at other points along this reach of the river, is assured by the presence of the minor anticline at this point (Fig. 9.25). Second, upon the exposure of a suitable structural discontinuity for admitting water to the limestone bedding planes, the development of one or more subsurface conduits between this input and the Cumberland River would have occurred. Third, as additional inputs evolved, they developed conduits linking to the previously completed conduits.

In support of this scenario are three pieces of evidence. First, only four kilometers of passage, less than 25 percent of the total known, extends beneath the caprock on the valley flanks. This indicates that the targets for conduit development lay along the valley bottom. Second, there are several regions of conduit mazes directly connected with the trunk conduits that presently lie close to the surface and near the valley center. These appear to have functioned as specific sites of input. The most complicated mazes are located in the upper part of the valley, suggesting that those in the lower part, and so formed earlier, may have been partly destroyed. Third, many of the high elevation mazes are in the form of phreatic canyons. The morphology of these conduits suggests that they have enlarged upwards from a horizontal bedding plane network (Fig. 9.27) or from a descending primitive tube network, following a combination of joints and bedding planes. This enlargement normally occurs in a turbulent regime when sediments are carried into the conduit.

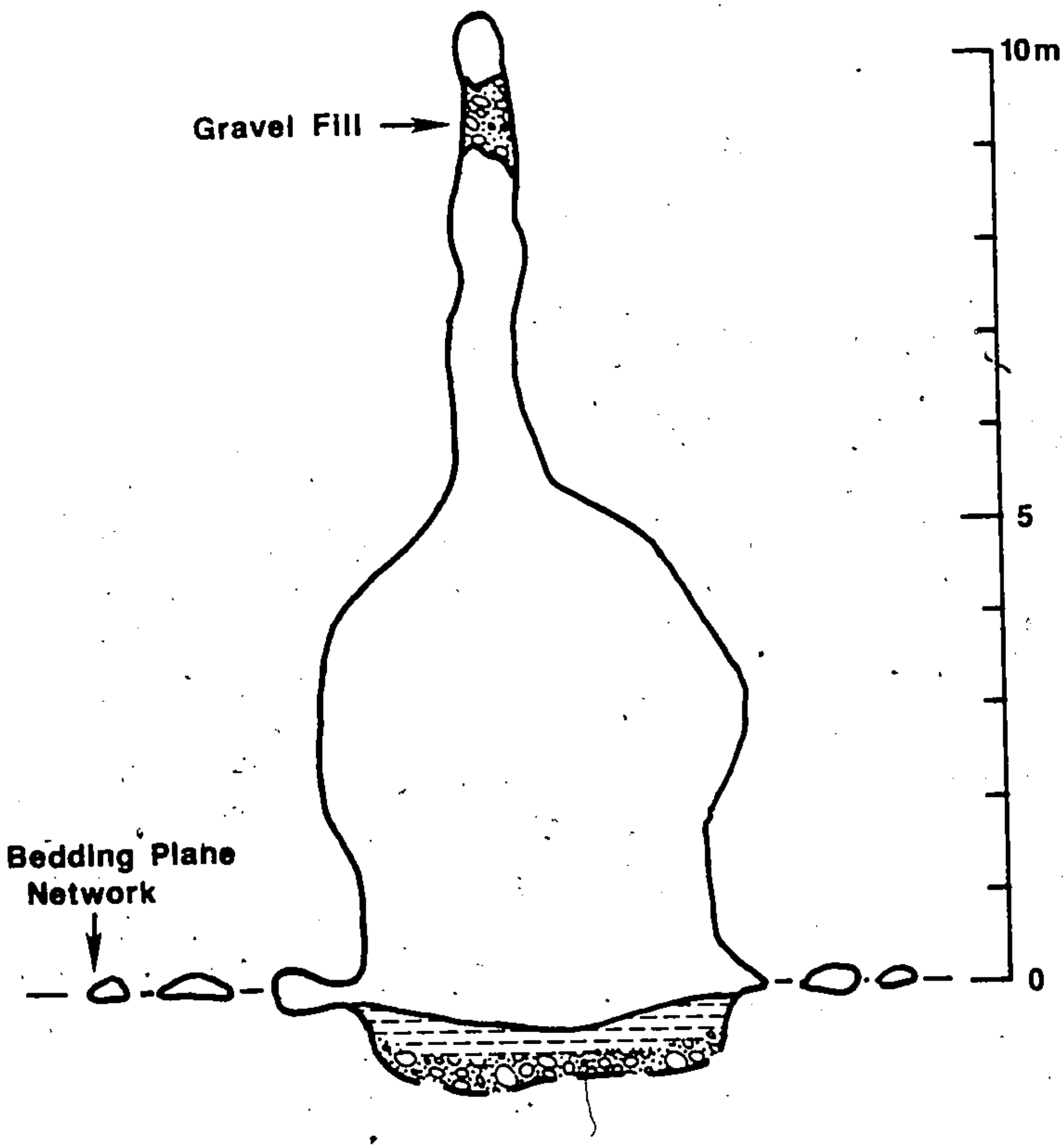

Figure 9.27
Phreatic canyon from Goldson's Cave, Cave Creek Kentucky. This conduit is inferred to have formed upward from the bedding plane network under phreatic conditions. Note the remnant of gravel fill in the top of the canyon.

This would have occurred only after a conduit had established a low resistance link to its discharge target. The sediments armour the lower portion of the conduit and concentrate dissolution at the ceiling. Frequently, the passage shows meander forms which propagate upward and downstream, similar to the presumed growth of eskers in glacial ice (Embleton & King, 1971, pp. 370-382), thus verifying the presence of this mode of enlargement. The downstream direction of flow is deduced from scallops on the walls, the imbrication of gravels where they exist, and from the assumption that flow was from the valley inputs toward the major trunks. All of these methods give a consistent flow direction. This mechanism has been discussed by Ewers (1977), Passini (1973, 1967) who uses the term antigravitational erosion, and Renault (1970) who uses the term paragenesis. This latter evidence strongly suggests that the main conduit development was truly phreatic, not simply epiphreatic. Furthermore, it supports the contention that the mazes were input points.

The passages illustrated in Figure 9.26 represent two fairly distinct levels of conduit development, one between 200 m and 225 m, and another between 225 m and 240 m. Although these ranges overlap, the juxtaposition of passages confirm that they are parts of two distinct trunks. This suggests that development of primitive phreatic tubes may have occurred at several horizons, with the upper level enlarging to trunk proportions first. Later, when the river had entrenched further, the lower level enlarged and became active.

9.3.4 SUMMARY

The morphology of the conduits beneath Cave Creek Valley are consistent with their having evolved in the manner described in the restricted input model. The fact that alternate, but unused, pathways of steeper gradient for discharge of the headwaters of the system exist, argues strongly that the theoretical growth advantages of the multiple input system stated in Chapter 8.4.3 are real.

CHAPTER 10

DISCUSSION AND SYNTHESIS

10.1 THE FUNDAMENTAL ASSUMPTIONS

This research, and the models which are its result, rest upon the assumptions generally considered applicable to flow fields which arise from the application of the Laplace equations. In addition, it rests upon the following three fundamental assumptions peculiar to the subject.

A. It is assumed that a genetic relationship exists between the many conduits in karst aquifers, having the form of elliptical tubes of phreatic character and the bedding planes they follow. This includes the conduits cited in the previous chapter.

In support of this assumption is the widely published data, of many origins, on the low primary permeability of Paleozoic limestones with which this study deals. For example, Choquett and Prey (1970), Davis and DeWiest (1966, p348), and Freeze and Cherry (1979, p29) list limestone permeabilities of less than 0.1 millidarcies when fracture porosity is not considered. It is not unreasonable then to assume that secondary permeability, joints and bedding planes, should provide the capillary spaces through which the bulk of groundwater movement will occur. Early workers such as Martell (1921) and Swinnerton (1932) pointed out the importance of these partings.

Bedding planes have been shown by several authors to be clearly associated with phreatic conduits, and quantitatively more closely associated with these conduits than joints. Ewers (1972), in an analysis of more than 20 km of subsurface conduits in south-central Kentucky showed that 93% of these were apparently related to bedding planes. Deike (1967) found joints of very limited importance in the development of subsurface karst in the Mammoth Cave region, and by implication, that bedding planes are of great importance. Ford (1971) reported that, in his field experience, the ratio of bedding plane to joint passages commonly ranges from 10:1 to 100:1 in those caves where bedding planes are of any importance at all.

The reasons for the overwhelming importance of bedding planes in this regard is not difficult to understand. Bedding planes are frequently more common than major joints and their lateral extent is often much greater, often reaching all boundaries of a limestone mass. Joints which do traverse an entire rock mass can carry groundwaters only along a single horizontal vector, which may not coincide with the regional hydraulic potential field. Bedding planes are capable of conducting flow along any horizontal vector. Even in those cases where complementary joint sets may provide a continuous capilliary opening to the limestone boundary, it is not clear that it will be enlarged. Ford (1971) pointed out that groundwater flowing through a network of joints is required to make many turns at joint intersections. Such a course is one of high resistance and vulnerable to capture by a straighter, more efficient bedding plane with which the joint almost certainly intersects.

Bedding planes, therefore, should frequently be the best candidates for the capillary space through which groundwater initially moves in limestones, and the assumption that the aforementioned conduits are genetically related to them appears justified.

B. It is further assumed that groundwater moving in the primitive capilliary spaces, be they joints or bedding planes, attain the bulk of their solvent load after having moved a matter of meters through the rock. A corollary to this assumption is the concept that these waters must do the bulk of their geomorphic work within a short distance of encountering such capilliary space.

The arguments in Chapter 2 suggest that our knowledge of limestone dissolution kinetics leaves somthing to be desired in terms of detail, but that in a gross way we understand the process. White (1977), in bringing together the work of Berner and Morse (1974), Plummer and Wigley (1976), Curl (1976), and Weyl (1958), showed that this assumption is apparently well founded. In fact, he concludes his remarks on limestone dissolution kinetics with the statement that: "The (kinetics) mechanism...is not in disagreement with the local headloss model of Ewers", the general model under consideration in the present work.

C. It is assumed that a water filled capilliary space exists, along at least some bedding planes, which functions as a very thin, more or less continuous, permeable zone through which pressure from input points may be transmitted. It is in this area of the speleogenesis problem that our lack of knowledge is most profound and least quantitative. The author has observed in Indiana, Ohio, Kentucky, and West Virginia quarries that certain bedding planes tend to seep and that noticeable seepage from these same horizons may be derived from more than one quarry face. This indicates a degree of homogeneity and isotropy in the transmissivity of these horizons. It is also observed that few wells in cavern forming limestones are totally dry, although they may not produce significantly. This too, argues for isotropy in the capilliary spaces. It may, therfore, be concluded, at least tentatively, that this assumption is not implausible.

If these assumptions are accepted, at least five deductions logically follow, which summarize the major concepts of this thesis.

1. Propagation of solution porosity must proceed

from input points toward the resurgence. Acceptance of assumption A, above, allows no other type of geometrical change.

2. The propagation of solution porosity is related to the solvent throughput which is, in turn, related to the geometry of the input, output, and impermeable boundaries. The electric analogues demonstrate that throughput at individual inputs is inversly related to distance and density. The separation of multiple ranks influences the throughput of proximal ranks in a direct way, while affecting distal ranks inversely. These generalizations apply equally to point and linear resurgence geometries, although they differ in detail. These statements follow from the generally accepted rules governing potential fields.

3. The solvent action of the groundwater flow in carbonate aquifers produces changes in its hydraulic characteristics, which are accompanied by continuous adjustment of the hydraulic potential field. This statement follows directly from deduction 1 above. The initial enlargement along individual flow paths only in the vicinity of the input reduces the head loss in this region, thus, concentrating it in the unaltered regions of the capillary space. This concept was developed in sections 3.5.3 and 4.3.1.

4. The adjustments in the potential field, as a result of unequal growth of solution porosity from multiple input points, reduces the discharge through all nearby inputs, thus reducing their growth potential. This statement follows directly from assumption C, that the capillary space along a favorable bedding plane is a continuous permeable zone, as far as the extent of that parting.

5. If hydraulic potential within a dominant network drops when it links with the output boundary, it will attract the discharge and reorient the growth direction of nearby networks. This statement follows directly from C above. The result of this process is a tributary conduit system composed of distributary elements.

In Chapter 8, this basic scheme has been applied to three general types of boundary conditions. In terms of process these models are indistinguishable. The specific geometries of the resulting networks, however, are specific to the boundary conditions, and, in the case of the high dip model, the pattern can be repeated several times. Master drainage trunks in the steep dip model are directed along the strike, while in the low dip case they are oriented normal to a linear discharge boundary. In the Mammoth Cave low dip example (Chapter 9.1), the master drainage is down the dip. The strike and dip orientation and the degree of dip are significant only in that they tend to direct the probabilities toward a point or linear discharge condition. It would have been as valid to call them point resurgence and linear resurgence models.

10.2 THE DETERMINISTIC Vs. THE STOCHASTIC VIEW

Perhaps this work's most significant departure from that of most previous workers is its emphasis on the control of solution conduit propagation and integration by stochastic variables, with the subsequent, continuous modification of their growth rates and directions by these variables. Implicit in the models of most other workers in this area of research is the assumption that a clearly defined path, a physical opening through the rock, exists from the onset of speleogenesis which is simply enlarged, simultaneously at all points along its length, to hydraulically important dimensions. This deterministic view is particularly evident among the water table theorists and those who have focused on the solution kinetics. Members of the first group, which includes Swinnerton (1932), Sweeting (1950), Davies (1960), and Moore (1966), focused upon a specific region proximate and parallel to the water table. They argued, a priori, that it would be the clear winner in any route competition. The second group was more restrictive in their consideration of a preferred route.

White (1969), Wigley (1973), and Curl (1974) considered the enlargement of primitive voids in limestones as simple input-output units, without consideration of the larger potential field of which such elements are a part.

The present research, while recognizing that lithic discontinuities with a wide range of permeabilities exist in karstifiable rocks, acknowledges the stochastic processes governing speleogenesis. It is perfectly clear, for instance, that only a small proportion of bedding planes are conducive to cavern development. At times, these display some feature which may explain their preferential selection. These include shale partings, chert fillings, slickensiding, brecciation (Ford, 1965; Renault, 1967; Waltham, 1971) and differential solubility of the beds (Rauch and White, 1970). To the degree that penetrable partings are rare within the limestone mass, the speleogenetic processes may be said to be deterministic. Similar statements can be made with respect to joints and faults (Ford and Ewers 1978).

If one of these discontinuities should be sufficiently high in permeability, it is probable that it would predetermine the route of solution enlargement to the virtual exclusion of all others in its vicinity. However, in most lengthy caves, single joint or fault determined conduits and single tubes in a penetrable bedding plane are the exception. The conduit patterns are generally complex and irregular, involving many tributary elements. The fact that these elements are tributary to one another suggests that they formed as part of a continuous flow field. It is precisely these conditions which the present model requires. It predicts that competitive forces related to internally or externally derived controls on the pressure distribution within the flow field will influence the final pattern. These controls include:

1. The input and output geometry.
2. The sequence of initiation of the inputs.
3. The pressure at the input points.
4. The transmissivity of the parting and the areal variability of the transmissivity.
5. The geometry of the solution porosity associated with each input during solution modification.

With the exception of number four, all of these controls are time dependant stochastic processes. Therefore, it may be assumed that the pattern evolves with continuous readjustments, of a stochastic character. The stochastic readjustments operate within the deterministic framework of penetrable regions of the rock mass.

It seems reasonable that a continuum should exist between two rare situations. The first is entirely stochastic, in that the rock mass contains a high density of low permeability penetrable fissures. Here, the continuously changing stochastic forces alone select the route of conduit formation. The other situation is entirely deterministic. A single high permeability element alone controls the course of conduit evolution. If experience with other geologic continua are taken as our guide, we may expect that in the great majority of cases the controlling factors will consist of a mix of stochastic and deterministic processes. These arguments bear a strong similarity to the contentions of Ford (Ford and Ewers, 1978) in which penetrable fissure frequency was shown as the controlling factor in the degree to which conduit systems follow a water table course.

The significance of these arguments is two fold. First, they imply severe limitations to the deterministic approach and, second, they imply limits to both our theoretical understanding and the utility of the models. No matter what degree of sophistication our knowledge of the rock characteristics attain, there are chance occurrences, both internally and externally, with respect to the rock mass, that will require probabilistic statements relative to the course of conduit development in carbonates. The carbonate hydrogeologist or geomorphologist is, thus, in a situation analogous to that of the modern physicist with respect to determinism. The determinists argued that to the extent that we know the vector, inertia, and other characteristics of every particle of the universe, intelligence regarding its past and future could be deduced to any degree of sphistication. No less a luminary than

Laplace defined the aim of scientific effort as being "...to approximate without limit to the intelligence we have just imagined" (Eddington, 1934). More recently, the indeterminists have demonstrated, through constructs like the Heisenburg uncertainty principal, that the necessary information may be theoretically unattainable (Eddington, 1934). Similarly, the carbonate specialist faces uncertainties which may be theoretically unattainable. For example, the pattern of conduit development may frequently be determined by which of two similar crystals or, indeed, which of two indistinguishable molecules of carbonate mineral at a flow divergence dissolve first. This situation may be analagous to determining which of two atoms of a single radioactive species will decay first.

In a practical sense, it appears that we must deal with many uncertainties which, while not fundamentally unknowable, may only be treated in a probabilistic manner. These would include such past events as the order of initiation of the inputs and their effective hydraulic potential, and may also include their location. In some cases, in perhaps most cases, the evidence may be erased by the weathering process or too indistinctive to identify. For example, if the models developed in this research are valid, it follows that the pattern of conduits could be laid down by very small quantities of groundwater flow. All that is required for a given input point to be effective is a quantity of flow sufficient to maintain a reasonable hydraulic potential on the virgin bedding plane. It is conceivable that such an input point would not evolve a catchment capable of supplying quantities of water larger than this minimum amount. This input, although possibly of great importance to the pattern plan, may be difficult to identify in the cave, and altogether impossible to recognize at the surface.

In adopting this stochastic viewpoint the present work gains inspiration from and bears certain similarities to the work of Rhoades and Sinacori (1941). Their work contains two salient points. First, they pointed out for the first time that the solvent action of the groundwater moving through a carbonate aquifer produces changes in its hydraulic characteristics, which are accompanied by continuous adjustment of the form of the flow field. Second, they showed that as a consequence of this dynamic flow field concept, subsurface drainage networks should propagate in a headward direction from a spring or discharge point. This second point was based upon the assumption that the concentration of flow in the region surrounding the discharge would engender the most rapid solution. Although Rhoades and Sinacori presented no field evidence in support of these concepts, it is evident to the most casual observer of the morphology of karst regions that the number of sink points is large, the number of large springs is small, and that the conduit systems connecting these two types of features must form tributary networks. These characteristics are precisely those which the Rhoades and Sinacori model predicts.

The kinetics of limestone solution require that the solution openings propagate from the inputs toward the discharge boundary. However, when viewing the karst subsurface at a scale which encompasses many inputs, the individual input-output pairs become links in a tributary system. This system propagates in a headward direction, in a manner which is grossly like that predicted by the Rhoades and Sinacori model. In detail, however, it is considerably different, but characterized by processes which continuously readjust the potential field through stochastic agencies. Thus, Rhoades and Sinacori appear to be right but for the wrong reasons.

1Ø.3 THE DIP TUBE - ANASTOMOTIC BAND PROBLEM

In Chapter 6.2, it was demonstrated that the morphologic differences between bedding plane tubes in steeply dipping rocks and flat-lying rocks described by Ford (1977, 1971, 1968, 1965) are not due to gravitational effects. Ford developed the concepts of "dip tubes" and "anastomotic bands" as end members in a series of these solution forms. Dip tubes were defined as simple, often solitary, solution forms developed in closely spaced parallel arrays, oriented within a few degrees of the dip, in steeply inclined carbonate rocks. Anastomotic bands, on the other hand, were described as anastomosing networks of tubes, sometimes in widely spaced subparallel arrays, which are endemic to near horizontally bedded carbonates.

The experiments in Chapter 6.4.2 and Chapter 7.3 suggest that the dip and the complexity of the tube networks may be related by way of the boundary conditions. In those cases where the input density is very high, flow envelopes are shown to be narrowed. During the course of the present research, several solution experiments were performed with single point inputs and single point outputs (Fig. 10.1). These showed that the tube network was concentrated in the central region of the flow domain. When the flow envelopes are narrowed by increasing density, the complexity of the tube network could be severely restricted. The type 1, 2, and 3 experiments show an increasing complexity of form as the effective density is decreased. When compared to Figure 10.1 a full continuum from anastomotic bands to dip tubes can be seen.

Thus, in the steeply dipping case, where surface waters may be expected to have access to the erosionally truncated bedding plane at many points, a large number of closely spaced parallel conduits should occur. This close spacing should cause them to approach the form of simple tubes. Where the karstifiable rocks are flat-lying, meteoric waters will have less frequent access to the

Figure 1Ø.1
Conduit pattern developed in solution experiment 4-1ØØ-B-2-23 with the "B" surface. Headloss equals 2 cm.

bedding planes. Although the resulting conduits may be parallel, their pattern will be more complex as a result of the decreased density.

An additional control on network complexity in the solution experiments is the size and distribution of high and low permeability areas on the simulated bedding plane. Experiments conducted on the S 100 surface produced extremely complex sets of anastomotic tubes (Fig. 10.2). The S 100 B surface with large areas of low transmissivity produced more dendritic more strongly channelized tubes of larger vertical dimension (Fig. 10.1). The more uniform transmissivity of the S 100 surface apparently retarded the channelization process, while the more variable surface enhanced it. An S 100 C surface containing joints, as well as the features of the S 100 B surface, produced, as expected, a tube pattern of further reduced complexity (Fig. 10.3).

10.4 THE PROBLEM OF MAZE CAVES

In his very interesting paper on the rate of enlargement of parallel conduits in soluble rocks, Curl (1974) demonstrated, on a theoretical basis, that the diameters of these conduits should be convergent. This analysis was based upon mass transfer considerations and the flow characteristics expected in pipes. He draws two conclusions from this analysis. First, the standard

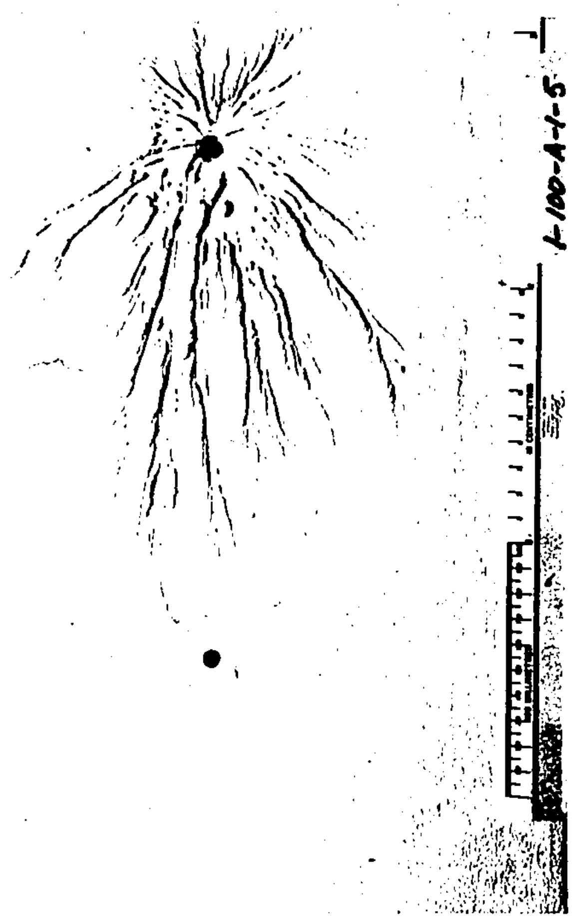

Figure 1Ø.2
Conduit pattern developed in solution experiment 1-1ØØ-A-1-5 with the "A" surface. Headloss is identical to Figure 1Ø.1.

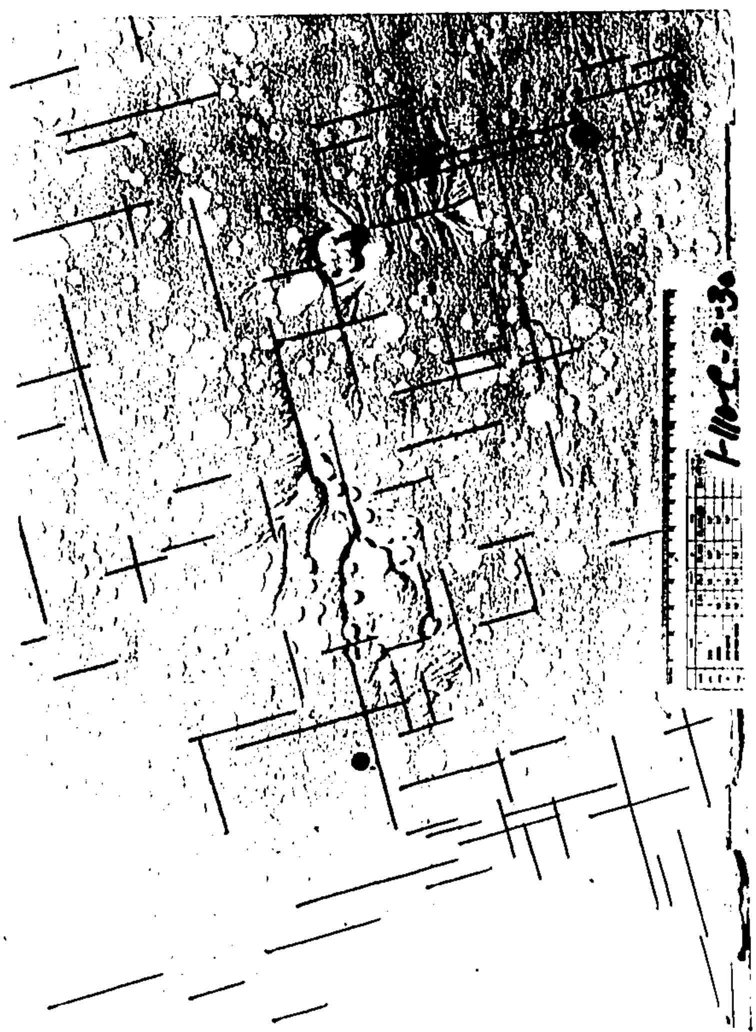

Figure 10.3
Conduit pattern developed in solution experiment 1-110-C-2-30 with the "C" surface. Headloss is identical to figure 10.1.

morphology of caves developed by phreatic dissolution should be the network or maze. Maze caves are those which posess a freely interconnecting network pattern; they occur in both bedding plane and joint determined caves. Second, the primary speleogenetic problem is not why maze caves form, but why dominant conduits develop. Tributary conduit systems are in the overwhelming majority, more than 75 percent according to Palmer (1975).

Curl (1974) correctly pointed out a significant problem. His analysis focused on a situation where the change in saturation of the bulk of the solvent flow in the tubes was small over the tube length under consideration. Therefore, the saturation change normal to the flow was of primary consideration. This analysis is not trivial or unimportant, but it does not address the most fundamental question of why tributary systems evolve. The problem of tributary caves is not one of diametrical growth of tubes, but one of longitudinal propagation in the direction of flow. In Chapter 3.5.3 the contrast between the case where significant change in saturation occurs over the length of the evolving network, and where it does not, is shown to be quite profound.

Thus, in his approach to the maze cave problem, Curl uses a deterministic approach. He assumes that a preferred conduit already exists, with dimensions such that the penetration distance to 90% saturation is long, in relation to the conduit under consideration. If an array of such conductive elements exists in a soluble rock unit, a maze cave should develop as Curl suggests. If, on the other hand, the conductive elements are of proportions such that the penetration distance to 90% saturation is very small relative to their length, a competition will ensue. The outcome of this competition should be a dominant conduit, tributary network. Maze caves do indeed exist. Anvil cave in Alabama, Breathing Cave in Virginia, and Carlsbad Caverns in New Mexico are some of the best known examples (Palmer, 1975). These caves tend to be located in situations of highly fractured (Anvil and Breathing Caves), reefal, or very young limestones (Carlsbad Caverns), conditions which are likely to provide highly permeable regions within the rock mass, where the penetration distance to 90% saturation is likely to be long. In addition to this kinetic/hydraulic control, Palmer (1975) demonstrated several structural and stratigraphic situations where the tendency toward dominant conduit development may be further suppressed.

10.5 THE PROBLEM OF WATER-TABLE CAVES

Ford (1971, 1974) and Ford and Ewers (1978) analysed the evidence for water-table caves, those which form along or at shallow depth beneath an hydraulic potential surface, and showed that their formation was related to the frequency of penetrable fissures in the limestone mass. While the field evidence for this assertion is convincing, the elucidation of the processes by which such conduits are differentiated was somewhat less than satisfactory. Ford and Ewers' argument was essentially this: after being subjected to groundwater circulation, the fissure frequency of a limestone mass significantly penetrable to groundwater can be expected to increase with time. Where sucessive levels of conduit development occur in a given limestone mass, the deeper flow systems, which formed after the longest exposure of the limestone, most closely approximate an ideal water-table profile. Shallower systems, formed early when fissure frequency was less, exhibit a wide range of elevations between the input and output points. Moreover, highly tectonized limestones, with very closely spaced fissures, exhibit water-table caves, while massive reef limestones with sparse but pervasive jointing may show deep phreatic circulation.

It seems self evident, as pointed out above, that the possibilty of selecting a straight line course from input to output increases with increasing fissure frequency. This does not, however, explain why the route closest to an as yet nonexistant water-table or hydraulic potential surface should be selected from a very large number of possibilities. Thrailkill (1968) demonstrated that in many situations the competing flow routes are of rather similar proportions and possess very similar groundwater flows. In a widely reproduced figure (Fig. 3.1) depicting a set of hypothetical pipes, he showed that there is "no hydrologic reason for the flow in shallow conduits to be significantly greater than in deep ones." However, in the situation of very high fissure frequency, State 4 in the Ford-Ewers (1978) classification, a carbonate aquifer may approach the three dimensional resistance medium state of a granular aquifer. In such a case, the competition rules developed in the present research would apply. The minor flow differences between the various paths would be greatly accentuated by the distortions of the pressure field engendered by conduit growth. This effect was shown in the dissolution experiments (Chapters 4 & 7). The pressure field distortions in this case, however, are transmitted to the deeper regions by the numerous vertical elements in the high fissure frequency situation. Several adjustments from the initial water table to a lower more mature one may be required, but the shortest, shallowest path remaining in a phreatic condition would be the clear winner, as Swinnerton (1932) suggested, but for different reasons.

In the absence of high fissure frequency, there is no apparent reason why conduit growth should not proceed along all available avenues. Furthermore, there is no _a priori_ reason why any particular horizon should win in such a competition. Therefore, a limestone mass should contain networks of proto-caves at several levels. Sediment blockage or other secondary controls must be invoked to explain how enlargement processes produce any water table caves in low fissure frequency situations.

10.6 THE ROLE OF MISCHUNGSKORROSION

Where flow envelopes of effectively saturated water deriving from separate inputs impinge upon one another, there exists the possibility for renewed aggressivity by mixing effects (Bogli, 1964). The magnitude of this saturation decrease is directly proportional to the difference in the carbon dioxide partial pressure with which the waters were equilibrated. The amount of calcium carbonate dissolved is directly proportional to the undersaturation and the quantities which are mixed. In a thin planar parting such as a bedding plane, the efficiency of mixing due to hydrodynamic dispersion is probably small. In addition, the waters entering at groundwater inputs to a parting during the period of network propagation are likely to be quite similar, since the quantity of water flowing is quite small. For these reasons, it appears unlikely that the potential for michungskorrosion is large. A quantitative answer to this question is not presently possible because we do not posess reliable information concerning the size, distribution, or conductivity of typical bedding plane porosity.

It is interesting to note that the most recent, comprehensive analysis of the solution kinetics problem by a non-speleologist chemist arrives at precisely the opposit conclusion (Dreybrodt, 1981): limestone cave genesis is impossible without mischungskorrosion! [with all that that must imply with respect to flow across lines of zero pressure differential, as defined in the analysis in Chapter 7.2.3.1 of this thesis]. Dreybrodt (1981) concludes his analysis by citing Ford and Ewers (1978) in support of his findings. It is suggested here that this is an instance of the laboratory analyist quite failing to appreciate the magnitude of geologic time that is available for the slow process of cave initiation.

1Ø.7 THE GRADIENT - Q PROBLEM

In the electric analog experiments and in their subsequent use in constructing the linking models, the input Q has been equated with network propagation rate. In some cases, this may not be strictly true. For instance, it was shown that individual input Q is reduced as density is increased. However, if the rank distance remains constant, the gradient along the principal flow vector from each input remains the same, no matter what the density. This means that the discharge along that vector remains constant, indicating that input Q is a poor predictor of network propagation rate. Initially this may be true, but as soon as the first flow channelization has occurred, the potential for enlargement of the developing tube is increased by the ability to discharge through a greater proportion of the bedding plane. Table 7.4 indicates that the time to breakthrough for a dominant network is inversely proportional to network density, and therefore, proportional to the throughput at a specific input.

10.8 FUTURE RESEARCH NEEDS

A recurrent theme throughout this work has been the inability to produce quantitative results in a real-world setting through lack of knowledge of the precise nature of a penetrable bedding plane. During the course of the research, a computer simulation was prepared, in collaboration with William James and J. J. Drake of McMaster University. In theory, this program was capable of accepting information on bedding plane characteristics and algorithms for the solution kinetics of limestone, to produce real-world simulations of conduit propagation. The incentive to complete the simulation was reduced by three factors: a difficulty with convergence of a head calculation routine, confusion about a suitable algorithm for the solution kinetics, and the lack of data on the nature of bedding planes in limestone. The first item was considered readily tractable but the others presented fundamental difficulties. With the combined work of Berner and Morse (1974), Plummer and Wigly (1976), Curl (1965), and White

(1977) the first of these fundamental problems seems largely resolved. There remains the final difficulty, which has no ready solution by inexpensive means. As of the date of this writing, it is the largest obstacle to the verification of much of this work and it's technological usefulness.

10.9 CONCLUSION

The masters degree thesis (Ewers 1972) which formed the point of departure for this work concluded with a hopeful statement which is repeated here.

> The bedding plane tube formation processes discussed above provide a framework for understanding the patterns and interrelationships of existing karst drainage. ...This analysis promises to be of practical value to hydrologists studying groundwater supply and pollution problems... Finally, it is a step in the direction of understanding the origin of caves - features which have stirred the curiosity of men since remotest antiquity.

A FINAL NOTE

As the writing of this chapter was in progress, word arrived from Colorado that a major lead-zinc mining firm was sucessfully using the high dip model presented here in interpreting the paleohydrology of a carbonate sequence, where ore bodies consist of mineralized cave fills (Rick Tschauder, personal communication, Nov. 30 1981).

BIBLIOGRAPHY

Adams, W.C., 1875. On the forms of equipotential curves and surfaces and lines of electric force. Proc. Roy. Soc. (London), 23, pp. 280-284.

Adams, C.S., and Swinnerton, A.C., 1937. Solubility of limestone. Amer. Geophys. Union Trans., 18, pp. 504-508.

Arnberger, E., 1955. Höhlen und Niveaus. Die Hohle, 6(1), pp. 1-4.

Bear, J., 1972. Dynamics of fluids in porous media Elsevier, New York, 764 pp.

Bedinger, M.S., 1966. Electric-analog study of cave formation. Bull. Natl. Speleol. Soc., 28, pp. 127-136.

Berner, R.A., and Morse, J.W., 1974. Dissolution kinetics of calcium carbonate in sea water: IV. Theory of calcite dissolution. Amer. Jour. Sci. 274, pp. 108-134.

Bleahu, M.D., 1974. Morfologia Carstica. Editura Stiintifica, Bucharest, Rumania, 590 pp.

Blumburg, P.N., and Curl, R.L., 1974. Experimental and theoretical studies of dissolution roughness. Jour. Fluid Mechanics 65, p. 735.

Bögli, A., 1964. Die Kalkkorrosion, das zentrale Problem der Unterirdischen Verkarstung. Steirische Beitrage Zur Hydrogeologie, pp. 75-90.

Bögli, A., 1966. Karstwasserfläche und unterirdische Karstniveaus. Erdkunde, 20, pp. 11-19.

Bögli, A., 1968. Präglazial und präglaziale Verkarstung im hinteren Muotatal. Regio Basiliensis, Basel, pp. 135-153.

Bögli, A., 1970. Le Hölloch et son karst. Baconniere, Neuchatel, Switzerland, 109 pp.

Bohr, C. 1899. Definition und Methode zur Bestimmung der Invasions und Evasionscoefficienten bei der Auflosung von Gasen in Flussigkeiten. Werthe der genannter Constanten sowie der Absorptionscoefficienten der Kohlensaure bei Auflosung in Wasser und in Chlornatium-losungen. Ann. Phys. Lpz., 304(68), pp. 500-525.

Bretz, J.H., 1942. Vadose and phreatic features of limestone caves. Jour. Geol., 50, pp. 675-811.

Brucker R.W., Hess J.W., and White, W.B., 1972. Role of vertical shafts in the movement of ground water in cabonate aquifers. Ground Water, 10(6), pp. 5-13.

Chabot, G., 1927. Les plateaux du Jura central: étude morphogénique. Publ. Fac. Lett. Univ. Strasbourg.

Charity, R.A.P., and Christopher, N.S.J., 1977a. The stratigraphy and structure of the Ogof Ffynnon Ddu area. Trans. British Cave Research Assoc., 4(2), pp. 403-416.

Charity, R.A.P., and Christopher, N.S.J., 1977b. The Ogof Ffynnon Ddu cave system related to geological structure. Proc. 7th Internat. Congress Speleol., Sheffield, England, pp. 108-110.

Choquett, P.W., and Prey, L.C., 1970. Geologic nomenclature and classification of porosity in sedimentary carbonates. The Amer. Asso. of Petroleum Geologists Bull., 54(2), pp. 207-250.

Cloos, H., 1930. Zur Experimentellen Tektonik. Die Naturwissenschaften, Jhg. 18, pp. 714-747.

Cogley, J.G., 1972. Processes of solution in the Arctic limestone terraine. Inst. Brit. Geographers, Spec. Publ. No. 4.

Corbel, J., 1959. Erosion en terrain calcaire. Ann. Geogr., 68, pp. 97-116.

Cullingford, C.H.D., 1962. British Caving. 2nd ed., London.

Curl, R.L., 1968. Solution kinetics of calcite. Proc. 4th Internat. Congress Speleol., Ljubljana, Yugosl., pp. 61-66.

Curl, R.L., 1974. Cave conduit competition: Nonautonomous systems. Fourth Conference on Karst Geology and Hydrology Proceedings, West Virginia Geological and Economic Survey, Rauch, H.W., and Werner, E., eds., 187 pp.

Cvijic, J., 1893. Das Karstphänomen. Geogr. Abh., pp. 215-319.

Cvijic, J., 1918. Hydrogralphie souterraine et évolution morphologique du karst. Recueil des travaux de l'Institut de géographie alpine, 6(4), pp. 1-56.

Davies, W.E., 1960. Origin of caves in folded limestone. Bull. Natl. Speleol. Soc., 22, pp. 5-18.

Davis, W.M., 1930. Origin of limestone caverns. Geol. Soc. Amer. Bull., 41, pp. 475-628.

Davis, S.N., and DeWiest, R.J.M., 1966. Hydrogeology. John Wiley and Sons, New York, 463 pp.

Deike, G.H., 1967. The Development of Caverns of the Mammoth Cave Region. Unpublished Ph.D dissertation, Pennsylvania State University, University Park, Penn., 235 pp.

Drake, J.J., and Harmon, R.S., 1973. Hydrochemical environments of carbonate terrains. Water Resources Research, 9(4), pp. 949-957.

Drake, J.J., 1974. Hydrology and Karst Solution in the Southern Canadian Rockies. Ph.D. dissertation, McMaster Univ,. Hamiltion, Ontario, 222 pp.

Dreybrodt, W., 1981. Kinnetics of the dissolution of calcite and its applications to karstification. Chem. Geol., 31(3), pp. 245-269.

Eddington, A., 1934. New Pathways in Science. University of Michigan Press, Ann Arbor, Mich., 333 pp.

Embleton, C., and King, C.A.M., 1971. Glacial and Periglacial Geomorphology. Macmillan of Canada, Toronto, 608 pp.

Erga, O., and Terjesen, S.G., 1956. Kinetics of the heterogeneous reaction of calcium bicarbonate formation, with special reference to copper ion inhibition. Acta Chem. Scand., 10, pp. 872-875.

Ewers, R.O., 1964. Application of experimental geology to problems in cavern development. Abstract only, Bull. Natl. Speleol. Soc., 26(1), pp. 65-66.

-------- 1966. Bedding-plain anastomoses and their relation to cavern passages. Bull. Natl. Speleol. Soc.., 28(3), pp. 133-140.

-------- 1972. A model for the development of subsurface drainage routes along bedding planes. Unpublished M.S. Thesis, University of Cincinnati, Cincinnati, Ohio, 84 pp.

-------- 1974. The patterns of speleogenesis in the midwestern United States karst. Fourth Conference on Karst Geology and Hydrology Proceedings, West Virginia Geological and Economic Survey, Rauch, H.W., and Werner, E., eds., pp. 139-143.

-------- 1976. A model for the development of subsurface drainage routes along bedding planes. Proceedings, 6th Internat. Congress Speleol., Olomouc, Czechoslovakia, pp. 79-82.

-------- 1977. A model for the development of broad scale networks of groundwater flow in carbonate aquifers. Karst Hydrogeology Tolson, J.S., and Doyle, F.L., eds., Memoirs Vol. XII, UAH Press, Huntsville, Alabama, pp. 503-517.

Ewers, R.O. and Quinlan, J.F., 1981. Cavern porosity development in limestone: A low dip model from Mammoth Cave, Kentucky. Proc. 8th Internat. Congress Speleol., Bowling Green, Kentucky, USA., pp. 727-731.

Fenneman, N.M., 1938. Physiography of Eastern United States. McGraw-Hill Book Co., New York, 714 pp.

Ford, D.C., 1965. The origin of limestone caverns: a model from the central Mendip Hills, England. Bull. Natl. Speleol. Soc., 27(4) pp. 109-132.

-------- 1968. Features of cavern development in central Mendip. Trans. of the Cave Research Group of Great Britain, 10, pp. 11-25.

-------- 1968a. Stalactite and stalagmite. In: The Encyclopedia of Geomorphology, Fairbridge, R.W., ed., Reinhold Book Corporation, New York, pp. 1048-1051.

-------- 1971. Geologic structure and a new explanation of limestone cavern genesis. Trans. of the Cave Research Group of Great Britain, 13, pp. 81-94.

-------- 1971a. Characteristics of limestone solution in the southern Rocky Mountains and Selkirk Mountains, Alberta and British Columbia. Can. Jour. Earth Sci., 8(6), pp. 585-690.

Ford, D.C., Brown, M.C., and Quinlan, J.F., 1972. Guidebook to sumposium SA6. Karst Geomorphology of the Canadian Rockies, 22nd Internat. Geogr. Congress, Canada, 84 pp.

Ford, D.C., and Ewers, R.O., 1978. The development of limestone cave systems in the dimensions of length and depth. Can. Jour. Earth Sci., 15(11), pp. 1783-1798.

Frear, G.L., and Johnston, J., 1929. Solubilities of calcium carbonate (calcite) in certain aqueous solutions at 25 C. Jour. Amer. Chem. Soc., 51, pp. 2082-2093

Freeze, R.A., and Cherry, J.A., 1979. Groundwater. Prentice-Hall, Inc., Englewood Cliffs, New Jersey, 604 pp.

Garrels, R.M., 1960. Mineral equilibria at low temperature and pressure. Harper and Bros., New York, 254 pp.

Garrels R.M., and Christ, C.L., 1965. Solutions, Minerals and Equilibria. Freeman, Cooper and Co., San Francisco, Calif., 450 pp.

Gams, I. 1965. La Grotte de Postojna. Guide-book of the Congress Excursion through the Dinaric Karst, 4th Internat. Congress Speleol., Ljubljana, Yugoslavia.

Gams, I. 1968. Versuch einer Klassifikation der Tropfsteinformen in der Grotte von Postjna. Proc. 4th Internatl. Congress Speleol., Ljubljana, Yugoslavia, 3, pp. 117-126.

Glennie, E.A., 1948. Some points relating to Ogof Ffynnon Ddu. Trans. Cave Research Group of Great Britain, 1(1), pp. 13-25.

Glew, J.R., 1976. The Simulation of Rillenkarren. Unpublished M.S. thesis, McMaster University, Hamilton, Ontario, 116 pp.

Glew, J.R., and Ford,D.C., 1980. A simulation study of the development of rillenkarren. Earth Surface Processes, 5, pp. 25-36.

Goodchild , M., and Ford, D.C., 1971. An analysis of scallop patterns by simulation under controlled conditions. Jour. Geol. 79(1), pp. 52-62.

Gortikov, V.M. 1937. Jour. Gen. Chem. USSR, See Curl (1968).

Groom, G.E., and Williams, V., 1965. The solution of limestone in South Wales. Geog. Jour. 131, pp. 37-41.

Grund, A., 1914. Der geographische Zyklus im Karst. Z. Ges. Erdk. Berl., 1914, pp. 23-29.

Halliday, W.R., 1960. Changing concepts of speleogenesis. Bull. Natl. Speleol. Soc. 22(1) pp. 23-28.

Harmon, R.S., Hess, J.S., Jacobson, R.W., Schuster, E.T., Haygood, C., et al, lWhite, W.B., 1972. Chemistry of carbonate denudation in North America. Trans. Cave Research Group of Great Britain, 14(2), pp. 96-103.

Hatch, N.L.,Jr., 1964. Geology of the Shopville Quadrangle, Kentucky. U.S. Geol. Surv., Geologic Quadrangle Map CQ-282.

Haynes, D.C., 1964. Geology of the Mammoth cave quadrangle, Kentucky. U.S. Geol. Surv. Geologic Quadrangle Map GQ-351.

Hess, J.W., Jr., 1974. Hydrochemical Investigations of the Central Kentucky Karst Aquifer System. Unpublished Ph.D. dissertation, Pennsylvania State University, University Park, Penn., 219 p.

Holland, H.D., Kirsipu, T.V., Huebner, J.S., and Oxburgh, U. M., 1964. On some aspects of the chemical evolution of cave waters. Jour. Geol., 72, pp. 36-67.

Hooke, R.L., 1968. Model geology: Prototype and laboratory streams: Discussion. Geol. Soc. Am. Bull., 79, pp. 391-393.

Howard, A.D., 1963. The development of karst features. Bull. Natl. Speleol. Soc., 25(1), pp. 45-65.

Howard, A.D., and Howard, B.Y., 1967. Solution of limestone under laminar flow between parallel boundaries. Caves and Karst, 9(4), pp. 25-38.

Hubbert, M.K., 1937. Theory of scale models as applied to the study of geologic structures. Bull. Geol. Soc. Amer., 48, pp. 1459-1520.

Hubbert, M.K., 1940. The theory of ground-water motion. Jour. Geol., 48(8), pp., 785-944.

Hutchinson, G.E., 1957. A Treatise on Limnology. Vol.1, John Wiley and Sons, Inc., New York, 1015 pp.

Jennings, J.N., 1971. Karst. M.I.T. Press, Cambridge, Mass., 252 pp.

Johnson, A.M., 1970. Physical Processes in Geology. Freeman, Cooper and Co., San Francisco, Calif., 577 pp.

Karplus, W.J., 1958. Analog Simulation. McGraw-Hill, New York.

Katzer, F. von, 1909. Karst un Karsthydrographie. Zeitschrift Kunde der Balkanhalbinsel, 8, p. 94.

Kay, C.A., 1957. The effects of solvent motion on limestone solution. Jour. Geol. 65, pp. 35-46.

King, C.V., and Liu, C.L., 1933. The rate of solution of marble in dilute acids. Jour. Amer. Chem. Soc., 55, pp. 1928-1940.

Krausse, H.F., and Treworgy, C.G., 1979. Major structures of the southern part of the Illinois Basin. In: Depositional and structural history of the Pennsylvanian System of the Illinois Basin, Part 2, Palmer, J.E., and Dutcher, R.R., eds., Ill. State Geol. Surv., Guideb. Ser., no. 15a. pp. 115-120.

Krieg, W., 1954. Höhlen und Niveaus. Die Hohle, 5(1), pp. 1-4.

Krieg, W., 1955. Höhlen und Niveaus. Die Hohle, 6, pp. 74-77.

Kunsky, J., 1958. Karst et grottes. Heintz, Paris.

Lamb, H., 1945. Hydrodynamics. 6th ed., Dover Publications, New York, pp. 581-586.

Lange, A.L., 1960. Geometrical basis for cave interpretation. Bull. Natl. Speleol. Soc., 22(1), pp. 45-65.

Langmuir, D., 1971. The geochemistry of some carbonate ground waters in central Pennsylvania. Geochim. Cosmochim. Acta, 35, pp. 1023-1045.

Lavalle, P., 1967. Some aspects of linear karst depression development in south central Kentucky. Ann. Asso. Amer. Geogr., 57, pp. 49-71.

Lewis, R.Q., Sr., 1971. The Monteagle Limestone of south-central Kentucky. U.S. Geol. Surv. Bull. 1324.E, 10 pp.

Lindquist, E., 1935. On the flow of water through porous soil. Premier Congres des Grands Barrages, pp. 81-101.

Malott, C.A., 1937. The invasion theory of cavern development. Abstract only. Proc. Geol. Soc. Amer., p. 323.

Martell, E.A., 1921. Nouveau traité des eaux souterraines. Editions Doin, Paris, France, 840 pp.

Mayfield, S.M., and Withers, S., 1929. Map of areal and structural geology of Pulaski County, Kentucky. Kentucky Geol. Surv., Lexington, Kentucky.

McFarlan, A.C., 1943. Geology of Kentucky. Kentucky Geol. Surv., reprinted 1961, 531 pp.

McFarlan, A.C., and Walker, F.H., 1956. Some Old Chester problems - Correlation along the eastern belt of outcrop. Kentucky Geol. Surv., Ser. 9, Bull. 16, 37 pp.

Meunier, S., 1899. Histoire experimentale des eaux d'infiltration superficielle. La Geologie Experimentale, Felix Alcan, Paris, pp. 172-204.

Miotke, F.D., 1974. Carbon Dioxide and the Soil Atmosphere. Abhandlungen zur Karst -und Hohlenkunde, Reihe A, Heft 9, 49 pp.

Miotke, F.D., and Papenberg, H., 1972. Geomorphology and hydrology of the Sinkhole Plain and Glasgow Upland, Central Kentucky Karst: Preliminary report. Caves and Karst, 14, pp. 25-32.

Moore, G.W., 1964. Abrupt change in cave history when ventilation begins. Abstract only, Bull. Natl. Speleol. Soc., 26, p. 76.

Moore, G.W., 1966. Introduction to limestone hydrology. Bull. Natl. Speleol. Soc., 28, pp. 109-111.

Morehouse, D.F., 1968. Cave development via the sulfuric acid reaction. Bull. Natl. Speleol. Soc., 30, pp. 1-10.

Morgan, M.A., 1967. Hardware models in geography. Models in Geography, Chorley, R.J., and Haggett, P., eds., Methuen and Co., London.

Morris, F.R., 1981. Karst Hydrogeology of Cedar Creek and Adjacent Basins in East-central Pulaski County, Kentucky. Unpublished Ph.D. thesis, Eastern Kentucky Univ., Richmond, Kentucky, in progress.

Morse, J.W., 1974. Dissolution kinetics of calcium carbonate in sea water: V. Effects of natural inhibitors and position of the chemical lysocline. Amer. Jour. Sci., 274(2), pp. 97-107.

Morse, J.W., and Berner, R.A., 1972. Dissolution kinetics of calcium carbonate in sea water: II. A kinetic origin for the lysocline. Amer. Jour. Sci., 272, pp. 840-851.

Mowat, G.D., 1962. Progressive changes of shapes by solution in the laboratory. Cave Notes, 4, pp. 45-59.

Nestas, I., and Terjesen, S.G., 1969. The inhibiting effect of scandium ions upon the dissolution of calcium carbonate. Acta Chem. Scand., 23, pp. 2519-2531.

O'Reilly, P.M., 1973. Morphology and hydrology of the Ogof Ffynnon Ddu karst area. Proc. 6th Internatl. Congress Speleol., Olomouc, Czech., 3, pp. 235-242.

Palmer, A.N., 1975. The origin of maze caves. Bull. Natl. Speleol. Soc., 37(3), pp. 57-76.

Passini, G., 1967. Nota preliminare sul ruolo speleogenetico dell'erosione "antigravitativa". Estratto da Le Grotte D'Italia, Serie IV, 1, pp. 75-88.

-------- 1973. Sull'importanza speleogenetica dell' "erosione antigravitativa". Estratto da Le Grotte D'Italia, Serie 4, Vol. IV, pp. 297-322.

Patterson, K., 1972. Responses in the chemistry of spring waters in the Oxford region to some climatic variables. Trans. Cave Research Group of Great Britain, 14(2), pp. 132-140.

Pavlovsky, N.N., 1918. Motion of water under large dams. In: Collected Works, Akad. Nauk, USSR, Leningrad, 1956.

Pesret, F., 1972. Kinetics of Carbonate-Seawater Reactions. Unpublished M.S. thesis, Univ. Hawaii, 49 pp.

Picknett, R.G., 1964. A study of calcite solutions at 10 C. Trans. Cave Research Group of Great Britain, 7(1), pp. 41-62.

Pitty, A.F., 1966. An approach to the study of karst water. Occasional Papers in Geogr., no. 5, Univ. of Hull, Hull, Eng.

Plummer, L.N., 1972. Rates of Mineral-Aqueous Solution Reactions. Unpublished Ph.D. dissertation, Northwestern Univ., Evanston, Ill., 144 pp.

Plummer, L.N., and Wigley, T.M.L., 1976. The dissolution of calcite in CO2-saturated solutions at 25 C and 1 atmosphere total pressure. Geochim. Cosmochim. Acta, 40, pp. 191-202.

Plummer, L.N., and Wigley, T.M.L., and Parkhurst, D.L., 1978. The kinetics of calcite dissolution in CO2-water systems at 5 C to 60 C and 0.0 to 1.0 atm. CO 2. Amer. Jour. Sci., 278, pp. 179-216.

Pohl, E.R., 1970. Upper Mississippiian deposits of south-central Kentucky, a project report. Ky. Acad. Sci., Trans., 31, pp. 1-15.

Pulina, M., 1971. Observations on the chemical denudation of some karst areas of Europe and Asia. Studia Geomorph. Carpatho-Balcanica, 5, pp. 79-91.

Quinlan, J.F., 1970. Central Kentucky Karst. Reunion Internationale karstologie en Languedoc-Provence,1968, Actes: Mediteranee, Etudés et Travaus, 7, pp. 235-253.

Quinlan, J.F., 1981. Hydrologic research techniques and instrumentation used in the Mammoth Cave Region, Kentucky. In: Roberts, T.G., ed., GSA Cincinnati '81 Field Trip Guidebooks. American Geological Institute, Washington, D.C., 3, pp. 457-506.

Quinlan, J.F., and Ewers, R.O., 1981a. Hydrogeology of the Mammoth Cave region, Kentucky. In: Roberts, T.G., ed., GSA Cincinnati '81 Field Trip Guidebooks. American Geological Institute, Washington, D.C., 3, pp. 457-506.

Quinlan, J.F., and Ewers, R.O., 1981b. Preliminary speculations on the evolution of groundwater basins in the Mammoth Cave Region, Kentucky. In: Roberts, T.G., ed., GSA Cincinnati '81 Field Trip Guidebooks. American Geological Institute, Washington, D.C., 3, pp. 457-506.

Quinlan J.F., and Ray, J.A., 1981. Groundwater basins in the Mammoth Cave region, Kentucky, showing springs, major caves, flow routes, and potentiometric surface. Friends of the Karst Occasional Publication no. 1.

Quinlan, J.F., and Rowe, D.R., 1977. Hydrology and water quality in the Central Kentucky Karst: Phase I. Ky. Univ. Water Resour. Res. Rep. no. 109, 93 pp. (Reprinted, National Park Service Uplands Field Research Laboratory Management Report 12.).

Quinlan, J.F., and Rowe, D.R., 1978. Hydrology and water quality in the Central Kentucky Karst: Phase I. Univ. Ky. Water Resources Research Inst., no. 101, 93 pp.

Quinlan, J.F., McCann, M.R., Andrews, W.M., and Branstetter, J.A., 1977. Heavy metals and optical brighteners as ground-water tracers in the Central Kentucky Karst: Implications concerning regional hydrology. In: Tolson, J.S., and Doyle, F.L., ed., Karst Hydrogeology., Int. Assoc. Hydrogeol., Int. Cong., 12th, Huntsville, Ala., 12, pp. 535-536.

Rauch, H.W., and White, W.B., 1970. Lithologic controls on the development of solution porosity in carbonate aquifers. Water Resources Research, 6(4), pp. 1175-1192.

Reams, M.W., 1965. Laboratory and field evidence for a vadose origin of foibe (dome pits). Int. Jour. Speleol., 1, pp. 373-389.

Renault, P., 1967. Le probleme de la spéléogenèse. Annales de Spéléologie, 22, pp. 5-21, 209-267.

Rhoades, R., and Sinacori, N.M., 1941. Patterns of groundwater flow and solution. Jour. Geol., 49, pp. 785-794.

Rice, C.L., 1979. The Mississippian and Pennsylvanian (Carboniferous) Systems in the United States - Kentucky. U.S. Geol. Surv. Prof. Pap., no. 1110-F, 32 p.

Romanik, P.B., 1981. Delineation of a Karst Groundwater Basin in Sinking Valley, Pulaski County, Kentucky. Unpublished M.S. Thesis, Eastern Kentucky University, Richmond, Kentucky, In progress.

Roques, H., 1969. A review of present-day problems in the physical chemistry of carbonates in solution. Trans. Cave Research Group of Great Britian, 11(2), pp. 139-163.

Sawicki, L., 1909. Beitrage zum geographischen Zyklus im Karst. Zeitschrift Geographische, 15 pp. 185-281.

Schmidt, V., 1981. Personal communication.

Schumm, S.A., and Khan, H.R., 1972. Experimental study of channel patterns. Geol. Soc. Amer. Bull., 83, pp. 1755-1770.

Shauberger, O., 1955. Uber die vertikale Verteilung der nordalpinen Karsthohlen. Mitt. Hohlenkomm., 1, pp. 21-28.

Smith, D.I., and Mead, D.G., 1962. The solution of limestone with special reference to Mendip. Proc. Univ. Bristol Speleol. Soc., 9(3), pp. 188-211.

Smith, J.H., Pomerene, J.B., and Ping, R.G., 1973. Geologic map of the Hail Quadrangle, McCreary and Pulaski Counties, Kentucky. U.S. Geol. Surv., Geologic Quadrangle Map GQ-1058.

Stumm, W., and Morgan, J.J., 1970. Aquatic Chemistry. Wiley-Interscience, New York, 583 pp.

Swann, D.H., 1963. Classification of Genevievian and Chesterian (Later Mississippian) rocks of Illinois. Ill. State Geol. Surv., Rep. Invest., no. 216, 91pp.

Sweeting, M.M., 1950. Erosion cycles and limestone caverns in the Ingleborough District of Yorkshire. Geogrl. Jour., 115, pp. 63-78.

Sweeting, M.M., 1966. The weathering of limestones with particular reference to the carboniferous limestones of northern England. Essays in Geomorphology, Dury, G.H., ed., Heinemann, London, pp. 177-210.

Sweeting, M.M., 1972. Karst Landforms. Macmillan Press Ltd., New York, 362 pp.

Swinnerton, A.C., 1932. Origin of limestone caverns. Geol. Soc. Am. Bull., 43, pp. 662-693.

Terjesen, S.G., Erga, O., Thorsen, G., and Ve, A., 1961. Phase boundary processes as rate determining steps in reactions between solids and liquids: The inhibitory action of metal ions on the formation of calcium bicarbonate by the reaction of calcite with aqueous carbon dioxide. Chem. Eng. Sci., 14, pp. 277-289.

Thrailkill, J., 1968. Chemical and hydrologic factors in the excavation of limestone caves. Geol. Soc. Am. Bull., 79, pp. 19-46.

Tillmans, J., 1932. Die chemische Untersuchung von Wasser und Abwasser. 2nd ed., Knappe, Halle.

Todd, D.K., 1959. Ground Water Hydrology. John Wiley and Sons, Inc., New York, 336 pp.

Tominaga, H., Adzumi, H., and Isobe, T., 1939. Viscosity effect on the rate of solution of calcium carbonate in hydrochloric acid. Bull. Chem. Soc. Japan, 14, pp. 348-352.

Trimmel, H., 1955. Hohlen und Niveaus. Die Hohle, 6(1), pp. 5-9.

Trombe, F., 1952. Traité de Spéléologie. Payot, Paris.

Tschauder, R., Personal communication. Nov. 30, 1981.

Vreedenburg, C.G.J., and Stephens, O., 1936. Electric investigation of underground water flow nets. Proc. Intl. Conf. Soil Mech. and Foundation Eng., Harvard Univ., Cambridge, Mass., 1, pp. 219-222.

Waltham, A.C., 1971. Controlling factors in the development of caves. Trans. Cave Research Group of Great Britain, 13, pp. 73-80.

Waterman, S.E., 1975. Simulation of Conduit Network Development on Bedding Planes. Unpublished M.S. thesis, McMaster University, Hamilton, Ontario, 116 pp.

Watson, R.A., 1965. Similitude in direct and thought experiments in cave geology. Bull. Natl. Speleol. Soc., 27(3), pp. 65-76.

Weaver, J.D., 1971. The Swansea Valley Disturbance. Unpublished Ph.D. dissertation, University of Wales.

Wells, S.G., 1973. Geomorphology of the Sinkhole Plain in the Pennyroyal Plateau of the Central Kentucky Karst. Unpublished M.S. thesis, Univ. Cincinnati, Cincinnati, Ohio, 115 pp.

Weyl, P.K., 1958. The solution kinetics of calcite. Jour. Geol., 66, pp. 163-176.

White, W.B., 1969. Conceptual models for carbonate aquifers. Ground Water, 7, pp. 15-21.

White, W.B., 1977. Role of solution kinetics in the development of karst aquifers. Karst Hydrogeology, Tolson, J.S., and Doyle, F.L., eds., UAH Press, Huntsville, Alabama, pp. 503-517.

White, W.B., and Longyear, J., 1962. Some limitations on speleogenetic speculation imposed by the hydraulics of groundwater flow in limestone. Nittany Grotto Newsletter, 10(9), pp. 155-167.

White, W.B., and Stellmack, J.A., 1968. Seasonal fluctuations in the chemistry of karst groundwater. Proc. 4th Internat. Congress Speleol., Ljubljana, Yugoslavia, 3, pp. 261-267.

White, W.B., Watson, R.A., Pohl, E.R., and Brucker, R., 1970. The central Kentucky karst. Geogr. Rev., 60, pp. 88-115.

Williams, P.W., 1969. The geomorphic effects of ground water. Water, Earth and Man, Chorley, R.J. ed., pp. 269-294.

Wigley, T.M.L., 1971. Solution of pipes by turbulent fluids. Caves and Karst, 13(5), p. 50.

Wigley, T.M.L., 1973. Computer program for chemical analysis of water sampling. Unpublished, Dept. Mechanical Engineering, University of Waterloo, London, Ontario.

Woodson, F., 1981. Lithologic and Structural Controls on Karst Landforms of the Mitchell Plain, Indiana, and of the Pennyroyal Plateau, Kentucky Unpublished M.S. thesis, Indiana State Univ., Terre haute, Ind., 132 pp.

Yalin, M., 1971. Theory of Hydraulic Models. MacMillan, London.

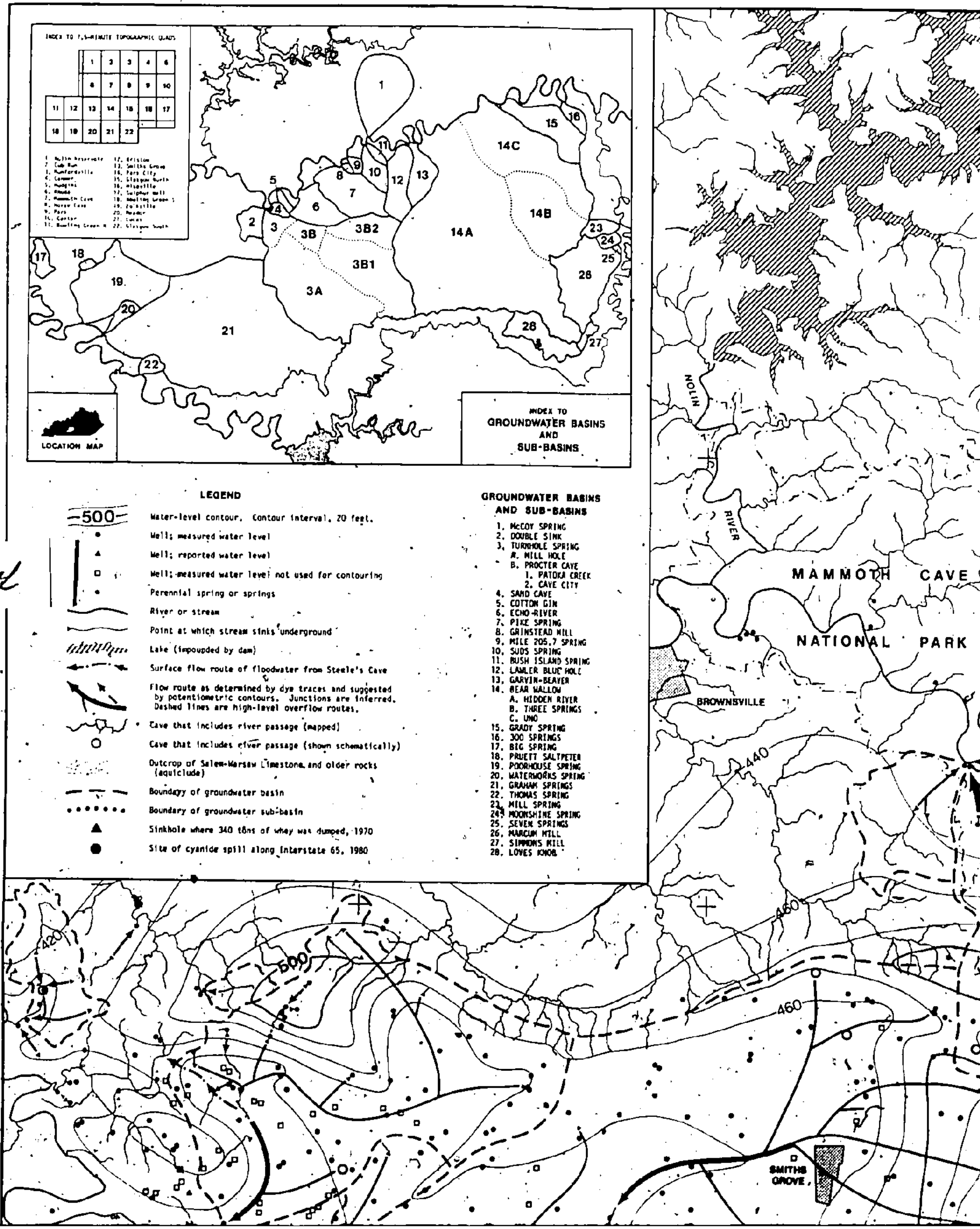

INDEX TO GROUNDWATER BASINS AND SUB-BASINS
LOCATION MAP
LEGEND
500
Water-level contour. Contour interval, 20 feet.
Well; measured water level
Well; reported water level
Well; measured water level not used for contouring
Perennial spring or springs
River or stream
Point at which stream sinks underground
Lake (impounded by dam)
Surface flow route of floodwater from Steele's Cave
Flow route as determined by dye traces and suggested by potentiometric contours. Junctions are inferred. Dashed lines are high-level overflow routes.
Cave that includes river passage (mapped)
Cave that includes river passage (shown schematically)
Outcrop of Salem-Warsaw Limestone and older rocks (aquiclude)
Boundary of groundwater basin
Boundary of groundwater sub-basin
Sinkhole where 340 tons of whey was dumped, 1970
Site of cyanide spill along Interstate 65, 1980
GROUNDWATER BASINS AND SUB-BASINS
1. McCOY SPRING
2. DOUBLE SINK
3. TURNHOLE SPRING
A. MILL HOLE
B. PROCTER CAVE
1. PATOKA CREEK
2. CAVE CITY
4. SAND CAVE
5. COTTON GIN
6. ECHO RIVER
7. PIKE SPRING
8. GRINSTEAD MILL
9. MILE 205.7 SPRING
10. SUDS SPRING
11. BUSH ISLAND SPRING
12. LAWLER BLUE HOLE
13. GARVIN-BEAVER
14. BEAR WALLOW
A. HIDDEN RIVER
B. THREE SPRINGS
C. UNO
15. GRADY SPRING
16. 300 SPRINGS
17. BIG SPRING
18. PRUETT SALTPETER
19. POORHOUSE SPRING
20. WATERWORKS SPRING
21. GRAHAM SPRINGS
22. THOMAS SPRING
23. MILL SPRING
24. MOONSHINE SPRING
25. SEVEN SPRINGS
26. MARCUM MILL
27. SIMMONS MILL
28. LOVES KNOB
NOLIN
RIVER
MAMMOTH CAVE
NATIONAL PARK
BROWNSVILLE
440
460
500
420
SMITHS GROVE

2 of

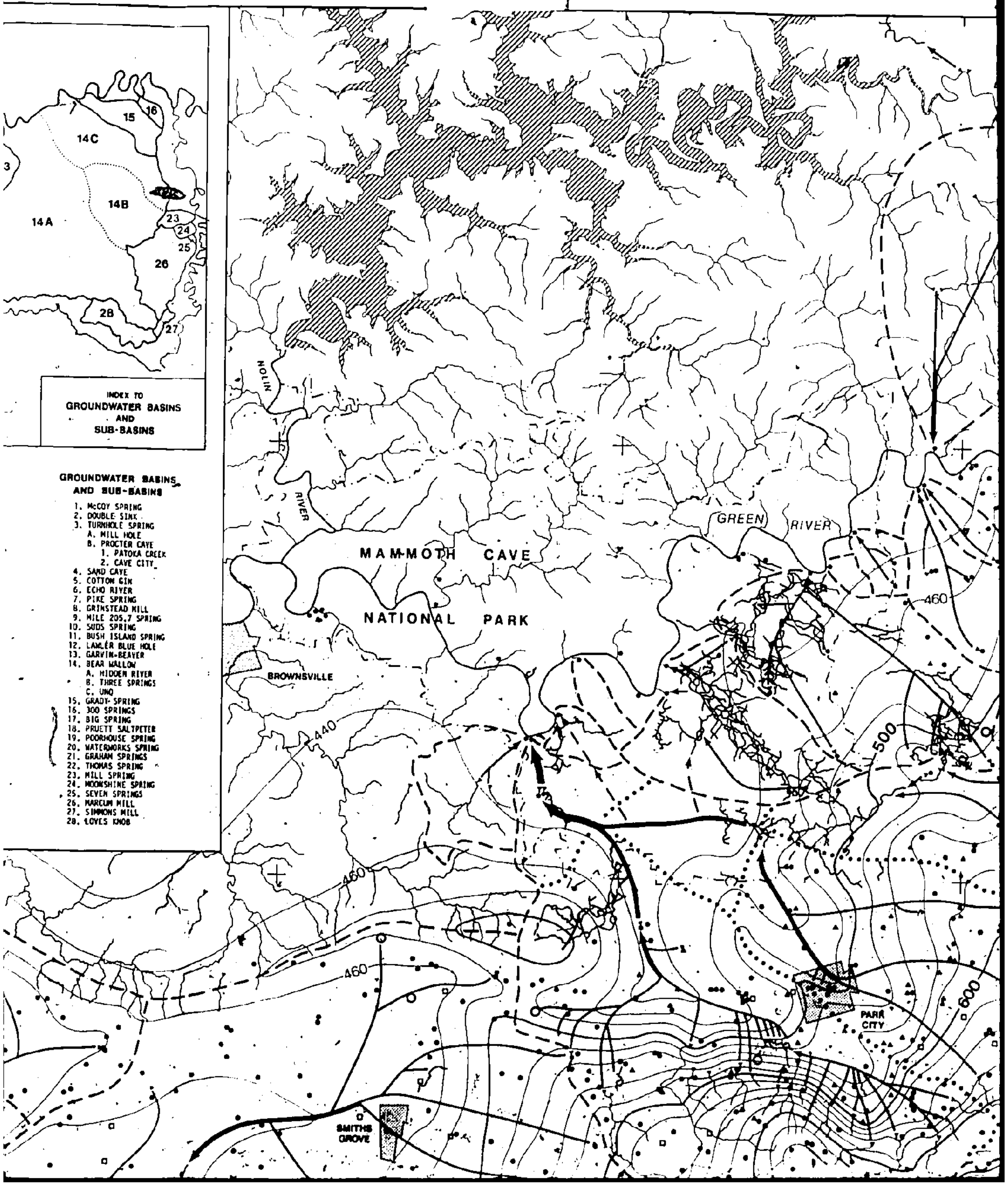
14C
15
16
14B
14A
23
24
25
26
28
27
INDEX TO
GROUNDWATER BASINS
AND
SUB-BASINS
GROUNDWATER BASINS
AND SUB-BASINS
1. McCOY SPRING
2. DOUBLE SINK
3. TURNHOLE SPRING
A. MILL HOLE
B. PROCTER CAVE
1. PATOKA CREEK
2. CAVE CITY
4. SAND CAVE
5. COTTON GIN
6. ECHO RIVER
7. PIKE SPRING
8. GRINSTEAD MILL
9. MILE 205.7 SPRING
10. SUDS SPRING
11. BUSH ISLAND SPRING
12. LAWLER BLUE HOLE
13. GARVIN-BEAVER
14. BEAR WALLOW
A. HIDDEN RIVER
B. THREE SPRINGS
C. UNQ
15. GRADY SPRING
16. 300 SPRINGS
17. BIG SPRING
18. PRUETT SALTPETER
19. POORHOUSE SPRING
20. WATERWORKS SPRING
21. GRAHAM SPRINGS
22. THOMAS SPRING
23. MILL SPRING
24. MOONSHINE SPRING
25. SEVEN SPRINGS
26. MARCUM MILL
27. SIMMONS MILL
28. LOVES KNOB
NOLIN
RIVER
GREEN
RIVER
MAMMOTH CAVE
NATIONAL PARK
BROWNSVILLE
440
460
460
460
500
600
PARK
CITY
SMITHS
GROVE

3 of

BACON CREEK
MUNFORDVILLE
GREEN RIVER
460
500
500
HORSE CAVE
560
CAVE CITY
HISEVILLE
600
PARK CITY
700
740

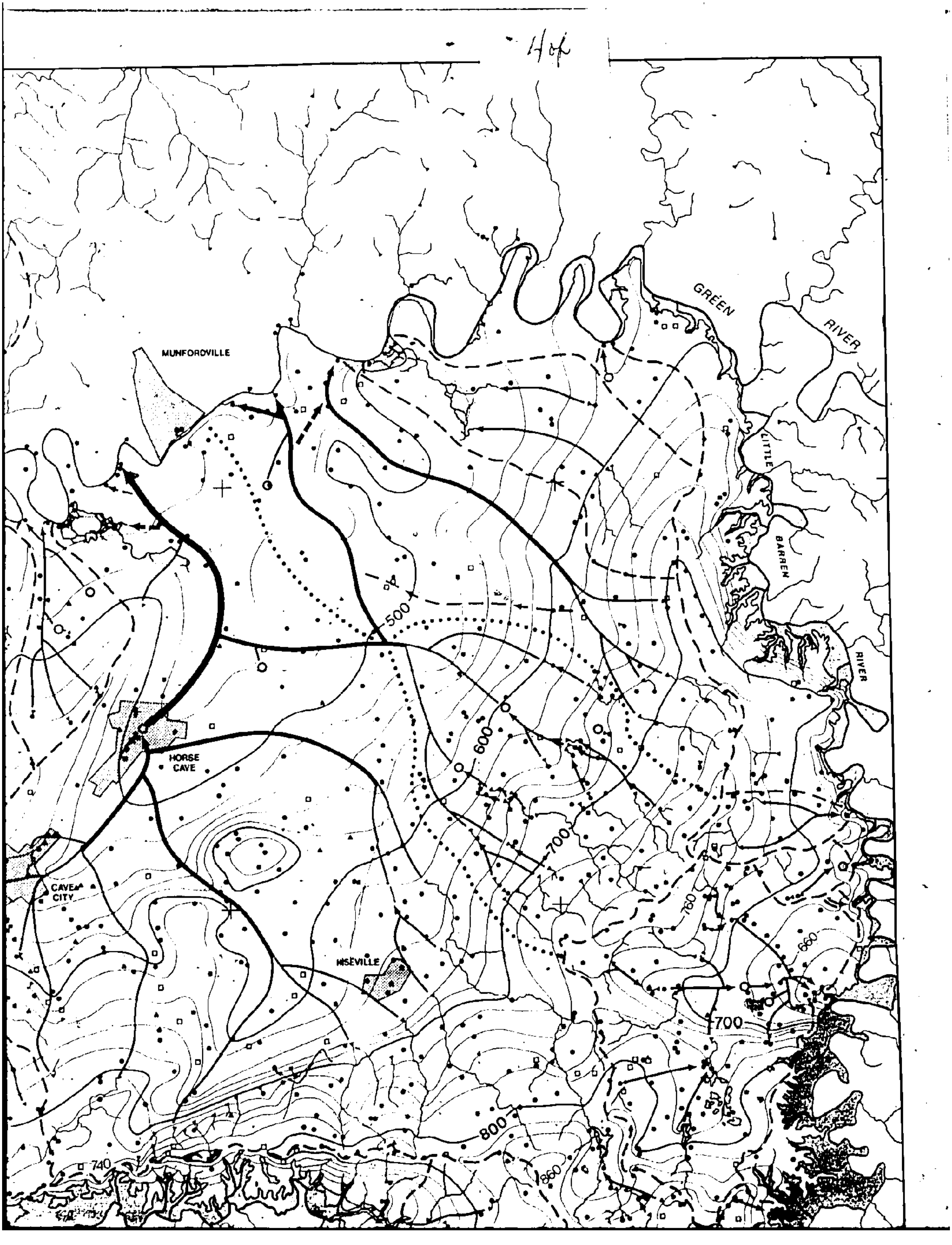

Hof
GREEN RIVER
MUNFORDVILLE
LITTLE BARREN RIVER
500
600
700
HORSE CAVE
CAVE CITY
HISEVILLE
760
660
700
800
740
860

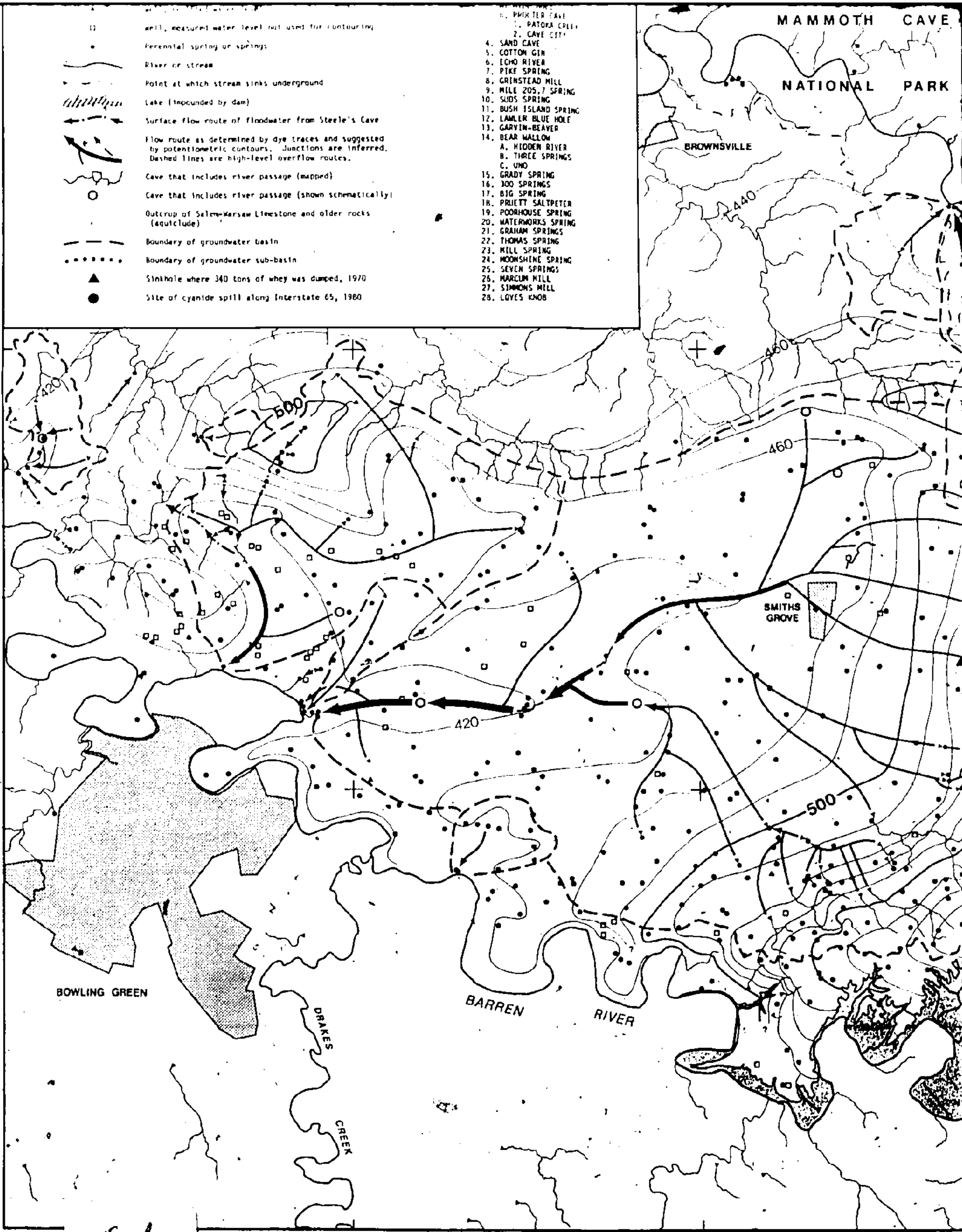
Well, measured water level not used for contouring
Perennial spring or springs
River or stream
Point at which stream sinks underground
Lake (impounded by dam)
Surface flow route of floodwater from Steele's Cave
Flow route as determined by dye traces and suggested by potentiometric contours. Junctions are inferred. Dashed lines are high-level overflow routes.
Cave that includes river passage (mapped)
Cave that includes river passage (shown schematically)
Outcrop of Salem-Warsaw Limestone and older rocks (aquiclude)
Boundary of groundwater basin
Boundary of groundwater sub-basin
Sinkhole where 340 tons of whey was dumped, 1970
Site of cyanide spill along Interstate 65, 1980
2. CAVE CITY
4. SAND CAVE
5. COTTON GIN
6. ECHO RIVER
7. PIKE SPRING
8. GRINSTEAD MILL
9. MILE 205.7 SPRING
10. SUDS SPRING
11. BUSH ISLAND SPRING
12. LAWLER BLUE HOLE
13. GARVIN-BEAVER
14. BEAR WALLOW
A. HIDDEN RIVER
B. THREE SPRINGS
C. UNO
15. GRADY SPRING
16. 300 SPRINGS
17. BIG SPRING
18. PRUETT SALTPETER
19. POORHOUSE SPRING
20. WATERWORKS SPRING
21. GRAHAM SPRINGS
22. THOMAS SPRING
23. MILL SPRING
24. MOONSHINE SPRING
25. SEVEN SPRINGS
26. MARCUM MILL
27. SIMMONS MILL
28. LOVES KNOB
MAMMOTH CAVE NATIONAL PARK
BROWNSVILLE
SMITHS GROVE
BOWLING GREEN
BARREN RIVER
DRAKES CREEK
440
460
500
420

5 of

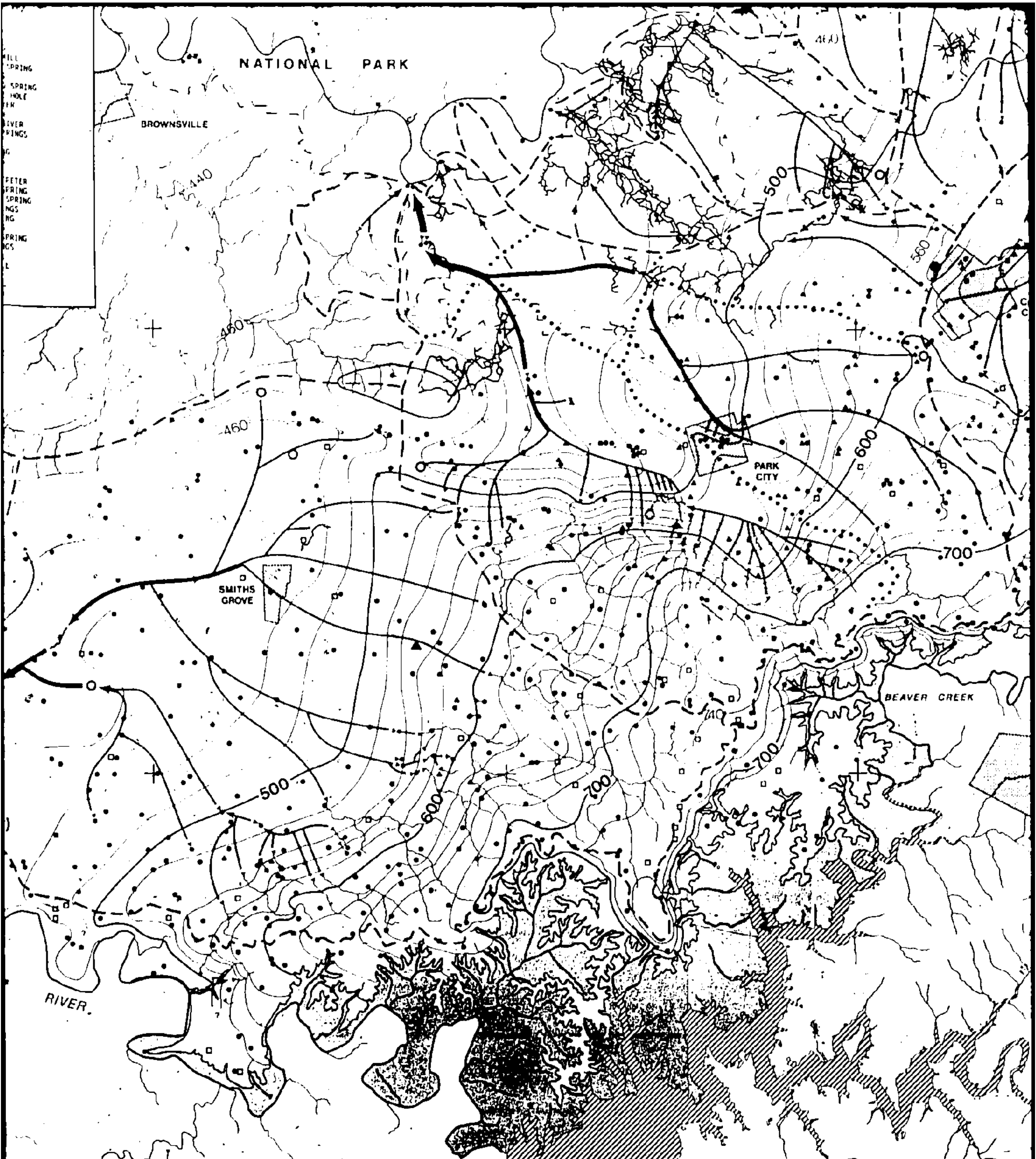
NATIONAL PARK
BROWNSVILLE
440
460
460
500
560
600
700
500
600
700
700
PARK CITY
SMITHS GROVE
BEAVER CREEK
RIVER

lo. of

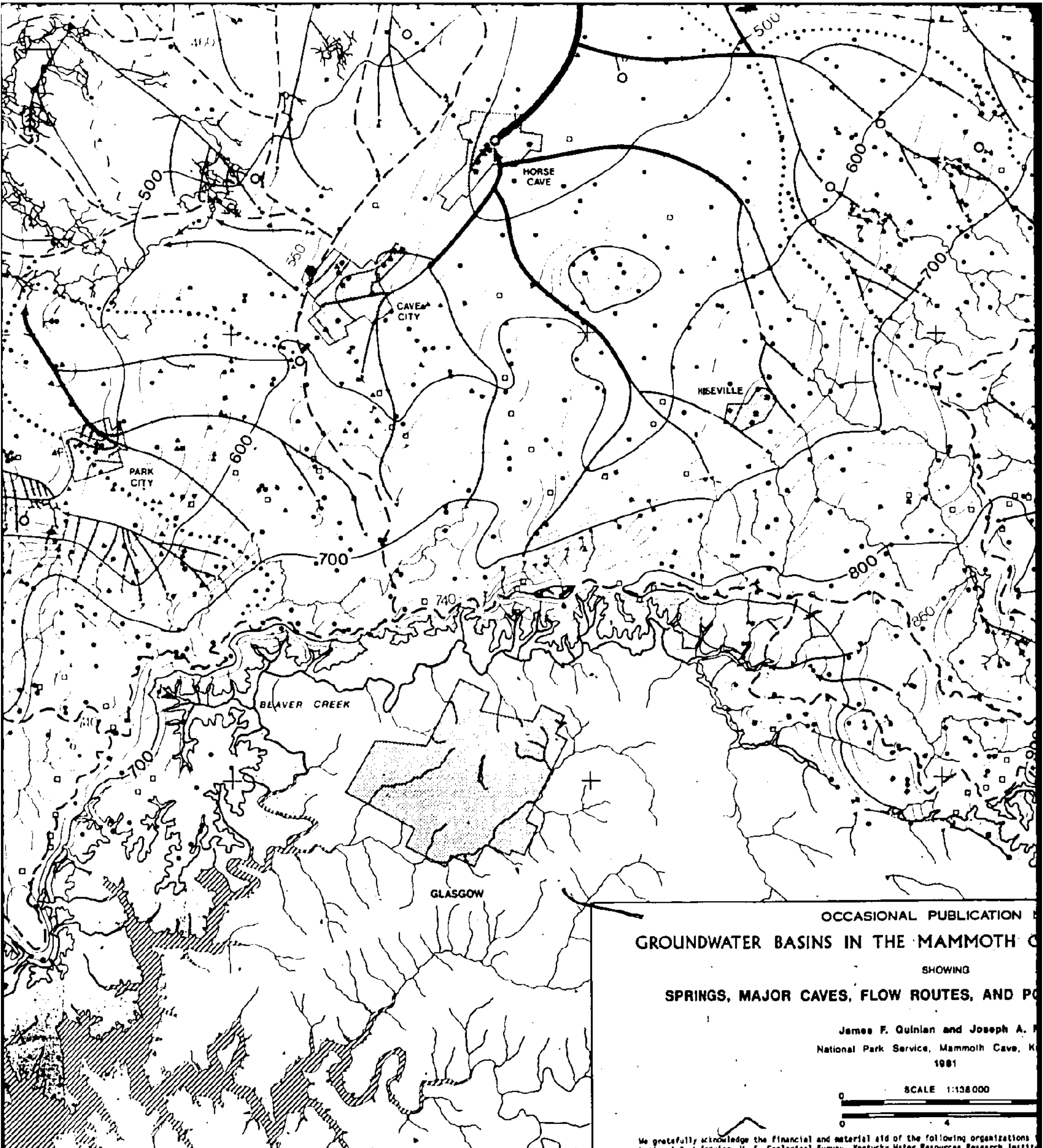

OCCASIONAL PUBLICATION N

GROUNDWATER BASINS IN THE MAMMOTH C

SHOWING

SPRINGS, MAJOR CAVES, FLOW ROUTES, AND PO

James F. Quinlan and Joseph A. R

National Park Service, Mammoth Cave, K

1981

SCALE 1:138 000

0

0 4

We gratefully acknowledge the financial and material aid of the following organizations National Park Service, U. S. Geological Survey, Kentucky Water Resources Research Instit Cumberland Karst Research Lab, Gannett Fleming Corddry and Carpenter, Inc., Internationa banks and companies that demonstrated that they were interested in helping the people of Trust Co., Citizens Bank and Trust Co., Horse Cave State Bank, The People's Bank, Dart I Quarry. Perhaps most of all, we are deeply appreciative to the numerous property owners to gather data and to make tests.

Published by: Friends of the Karst, Box 8, Mammoth Ca

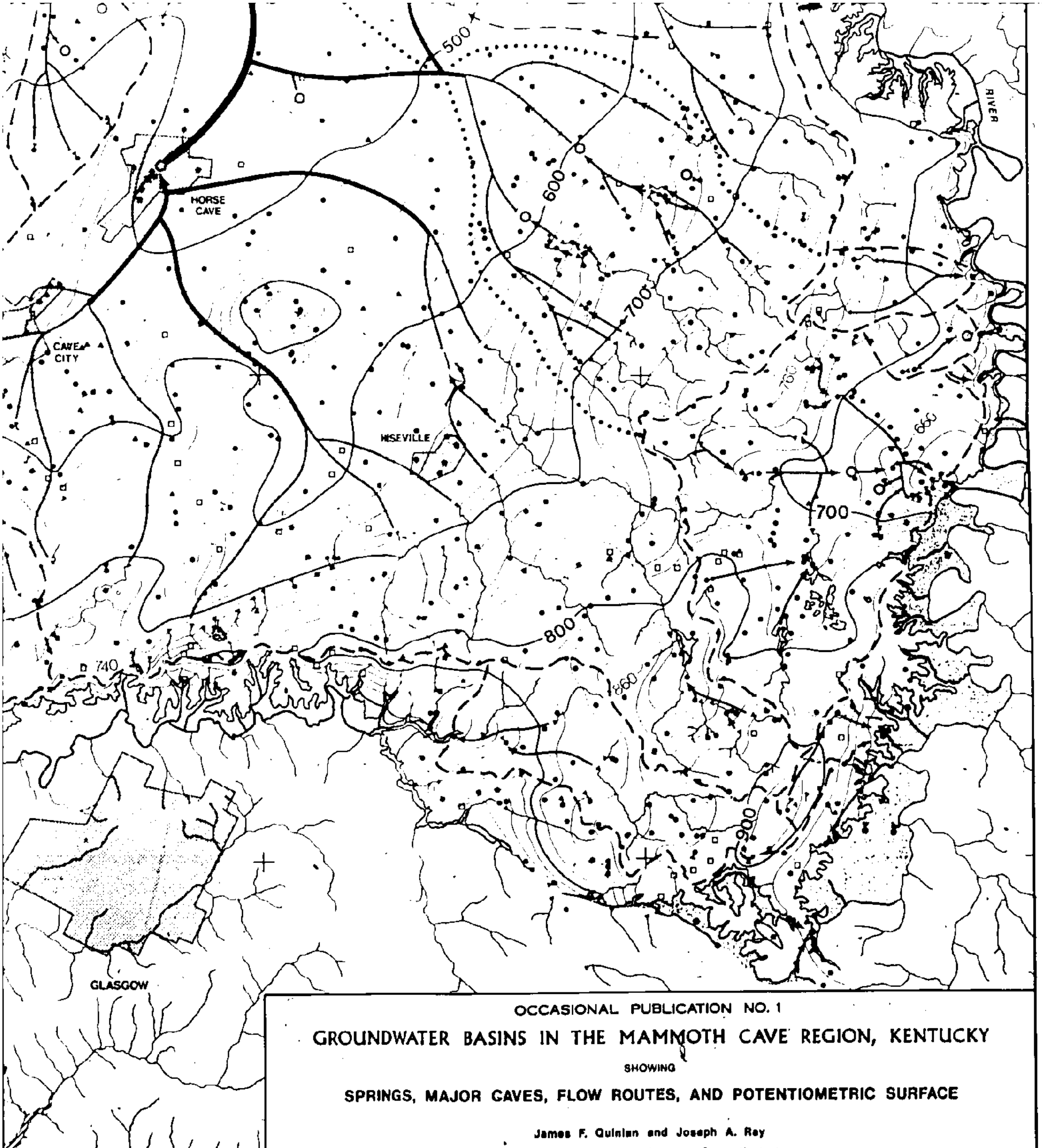

OCCASIONAL PUBLICATION NO. 1

GROUNDWATER BASINS IN THE MAMMOTH CAVE REGION, KENTUCKY

SHOWING

SPRINGS, MAJOR CAVES, FLOW ROUTES, AND POTENTIOMETRIC SURFACE

James F. Quinlan and Joseph A. Ray

National Park Service, Mammoth Cave, Kentucky

1981

SCALE 1:138 000

0 — 5 MILES

0 — 4 — 8 KILOMETERS

We gratefully acknowledge the financial and material aid of the following organizations that supported the research summarized on this map: National Park Service, U. S. Geological Survey, Kentucky Water Resources Research Institute, Barren River Area Development District, Cumberland Karst Research Lab, Gannett Fleming Corddry and Carpenter, Inc., International Business Machines Corporation, and the following banks and companies that demonstrated that they were interested in helping the people of the area they serve: American National Bank and Trust Co., Citizens Bank and Trust Co., Horse Cave State Bank, The People's Bank, Dart Industries, Hart Stone Co., and J. F. Pace Stone Quarry. Perhaps most of all, we are deeply appreciative to the numerous property owners who gave us access to their land and permission to gather data and to make tests.

Published by: Friends of the Karst, Box 8, Mammoth Cave, Kentucky 42259

8 of 8

Unteres Stockwerk
1 [illegible]
2 [illegible]
3 [illegible]
4 [illegible]
5 [illegible]
6 [illegible]
7 [illegible]
8 [illegible]

HAUPTGANG
9 [illegible]
10 Rittersaal
11 Kapelle
12 Kanzel
13 Zimmermanns [illegible]
14 Holzweg
15 Böse Wand
16 [illegible]
17 [illegible]
18 Funkengang
19 Aquarium
20 Fuchsloch
21 [illegible]
22 Nordgang

Seengang
23 [illegible]
24 [illegible]
25 [illegible]
26 [illegible]
27 Schlossgang

DOMGANG
28 [illegible]
29 [illegible]
30 SSS Camp
31 Katakomben [illegible]
32 [illegible]
33 [illegible]
34 [illegible]

Styx
35 Jochgang
36 Styxsee
37 [illegible]
38 Sisyphus
39 Tantalusschacht

40 Bogentunnel
41 [illegible]
42 Hallengang
43 Kletterstollen
44 [illegible]
45 Geistersee
46 Schlitzgang

HIMMELSGANG
47 [illegible]
48 [illegible]
49 Salle [illegible]
50 Couloir Oranges
51 Surprise
52 Galerie Mitta
53 Pas de l'Echelle

TITANENGANG
54 [illegible]
55 [illegible]
56 [illegible]
57 [illegible]
58 [illegible]
59 [illegible]
60 [illegible]

RABENGANG
61 Ratsaal
62 Sternsaal, Knochenkammer
63 [illegible]
64 [illegible]
65 [illegible]

SCHUTTUNNEL
66 [illegible]
67 [illegible]
68 [illegible]
69 [illegible]
70 [illegible]
71 [illegible]
72 [illegible]
73 [illegible]
74 [illegible]
75 [illegible]
76 [illegible]

H = Beginn Hochsystem
G = Beginn Guttergangsystem

SAC GANG
77 [illegible]
78 [illegible]
79 [illegible]
80 [illegible]
81 [illegible]
82 Hochburg
83 [illegible]
84 [illegible]
85 Faule Wand
86 [illegible]
87 Pfeiler

PAGODENGANG
88 [illegible]
89 Pagodensee
90 Pagode
91 [illegible]
92 [illegible]
93 Andreasstollen

HOFFNUNGSGANG
94 [illegible]
95 [illegible]
96 Stich
97 [illegible]

SCHLUCHTGANG
98 [illegible]
99 Lehmdom
100 [illegible]

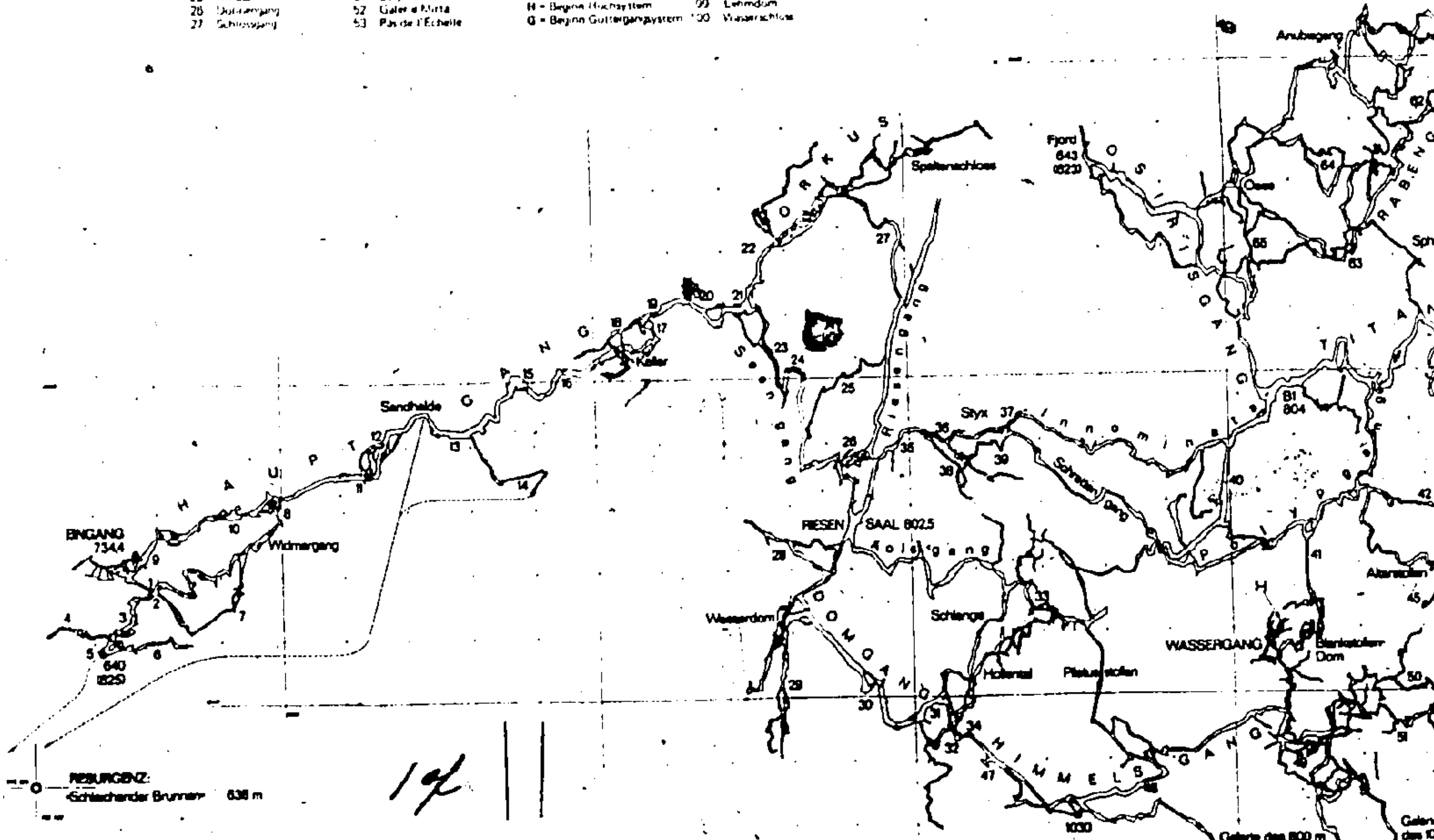

14

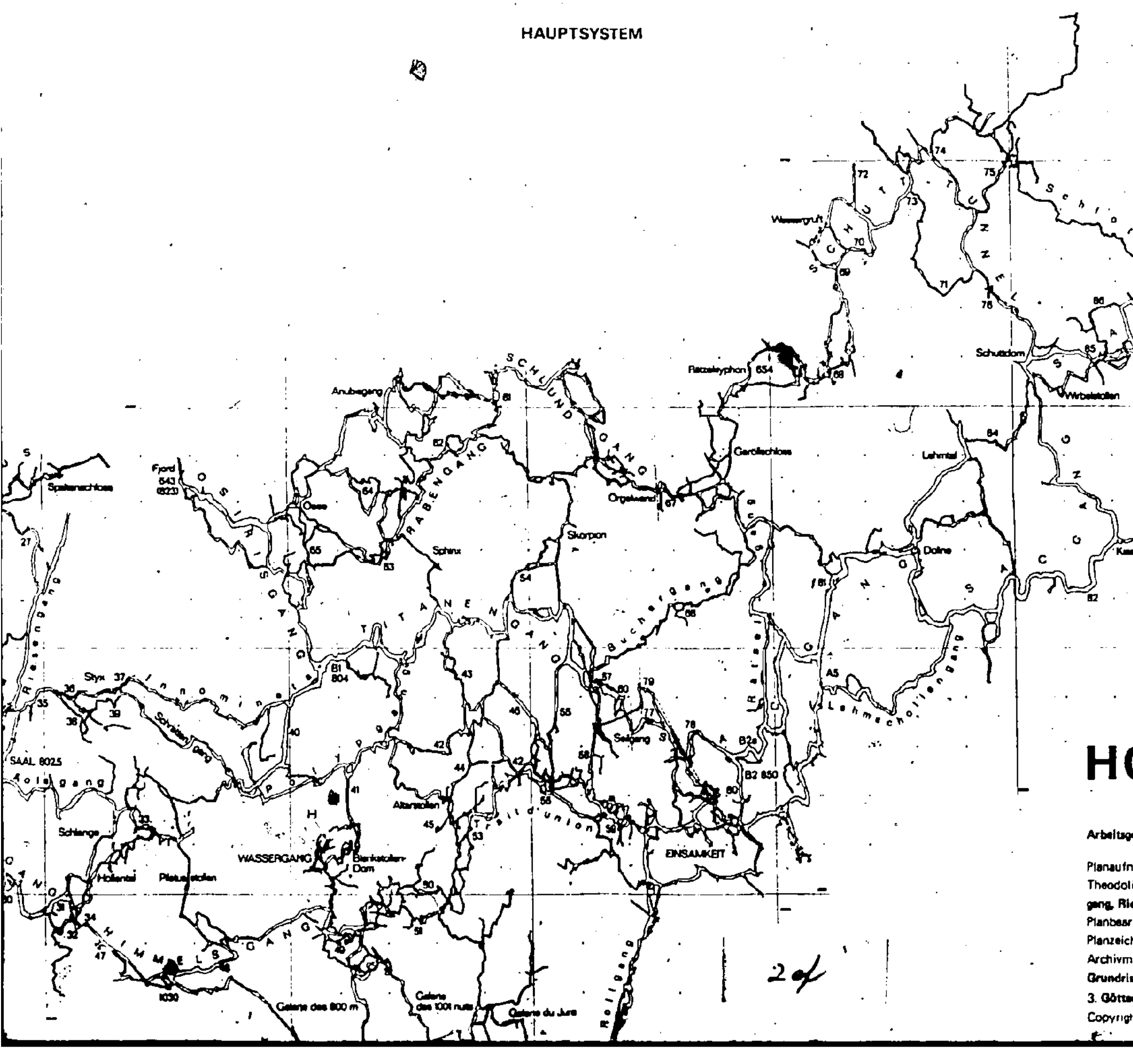

HÖ

Arbeitsge

Planaufn
Theodoli
gang, Rie
Planbear
Planzeich
Archivma
Grundris
3. Götter
Copyrigh

2 of

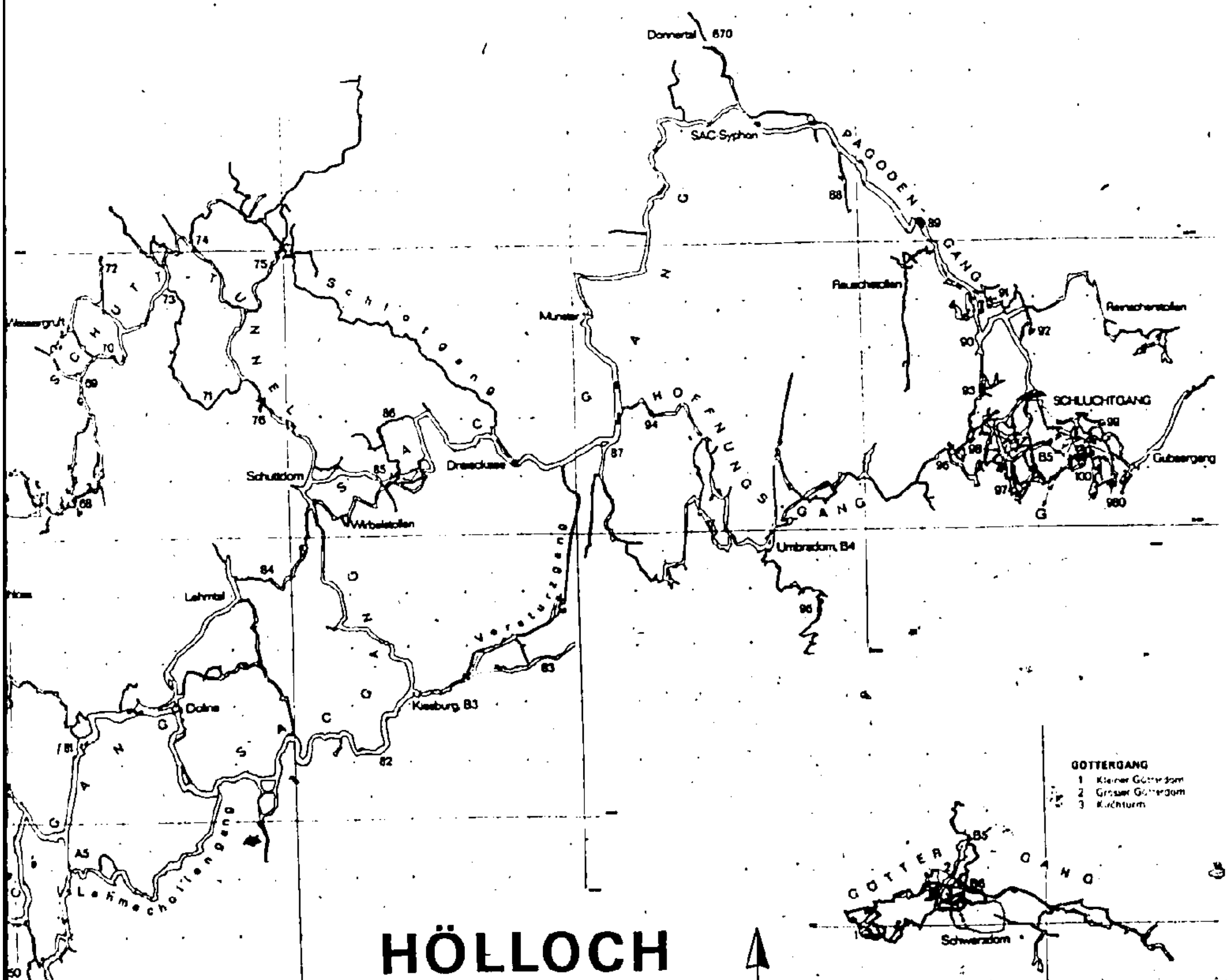

HÖLLOCH

1970

Arbeitsgemeinschaft Höllochforschung AGH

Planaufnahme AGH
Theodolitische Vermessung Eingang, Hauptgang, Riesensaal, Titanengang, S A C - Gang
Planbearbeitung Prof. Dr. A. Bögli
Planzeichnung P. Berg
Archivmaßstab 1 : 1000
Grundriss. 1. Hauptsystem 2. Hochsystem
3. Göttergangsystem

3¼

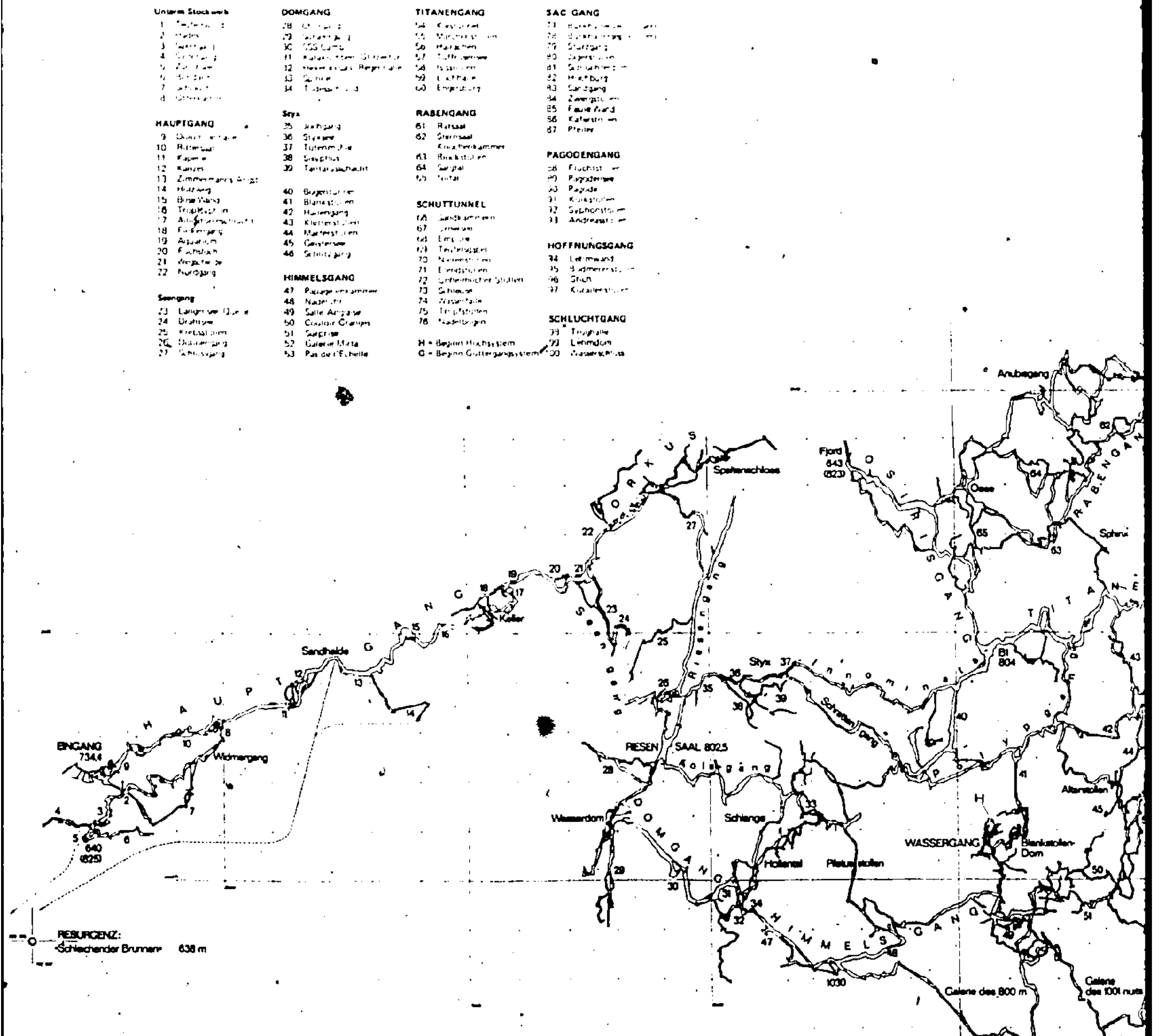
Unterm Stockwerk
HAUPTGANG
9
10 Rittersaal
11 Kapelle
12 Kanzel
13 Zimmermanns Angst
14 Holzweg
15 Böse Wand
17
18
19 Aquarium
20 Fuchsloch
22 Nordgang
Seengang
24 Drahtsee
DOMGANG
30 SSS Camp
33 Schlange
Styx
36 Stygsee
37 Totenmühle
38 Sisyphus
39 Tantalusschacht
40 Bogenstollen
41 Blankstollen
42 Hallengang
43 Kletterstollen
44 Marterstollen
45 Geistersee
46 Schlotgang
HIMMELSGANG
47
48 Nadelöhr
49 Salle Angoisse
50 Couloir Crampes
51 Surprise
52 Galerie Mista
53 Pas de l'Echelle
TITANENGANG
56 Hallachen
60 Engeburg
RABENGANG
61 Ratsaal
62 Sternsaal
Knochenkammer
64 Sargtal
SCHUTTUNNEL
71 Elendstollen
72 Unheimlicher Stollen
75 Tropfstollen
76 Nadelbogen
H = Beginn Hochsystem
G = Beginn Guttergangsystem
SAC GANG
79 Stuttgang
82 Hochburg
83 Sandgang
84 Zwergstollen
85 Faule Wand
86 Käferstollen
87 Pfeiler
PAGODENGANG
89 Pagodensee
90 Pagode
93 Andreasstollen
HOFFNUNGSGANG
94 Lehmwand
96 Stich
SCHLUCHTGANG
99 Lehmdom
Anubisgang
ORKUS
Spatenschloss
Fjord
643
(623)
OSIRISGANG
Oase
RABENGANG
Sphinx
TITANE
HAUPTGANG
Sandheide
Keller
Seengang
Riesengang
Styx
Innominata
Schwitzengang
Bl
804
PAGODENGANG
EINGANG
734,4
Widmergang
RIESENSAAL 802,5
Folgegang
Wasserdom
DOMGANG
Schlange
Höllental
Plateaustollen
WASSERGANG
Blankstollen-Dom
Altarstollen
HIMMELSGANG
1030
Galerie des 800 m
Galerie des 1001 nuits
640
(625)
RESURGENZ:
»Schleichender Brunnen« 638 m

4of

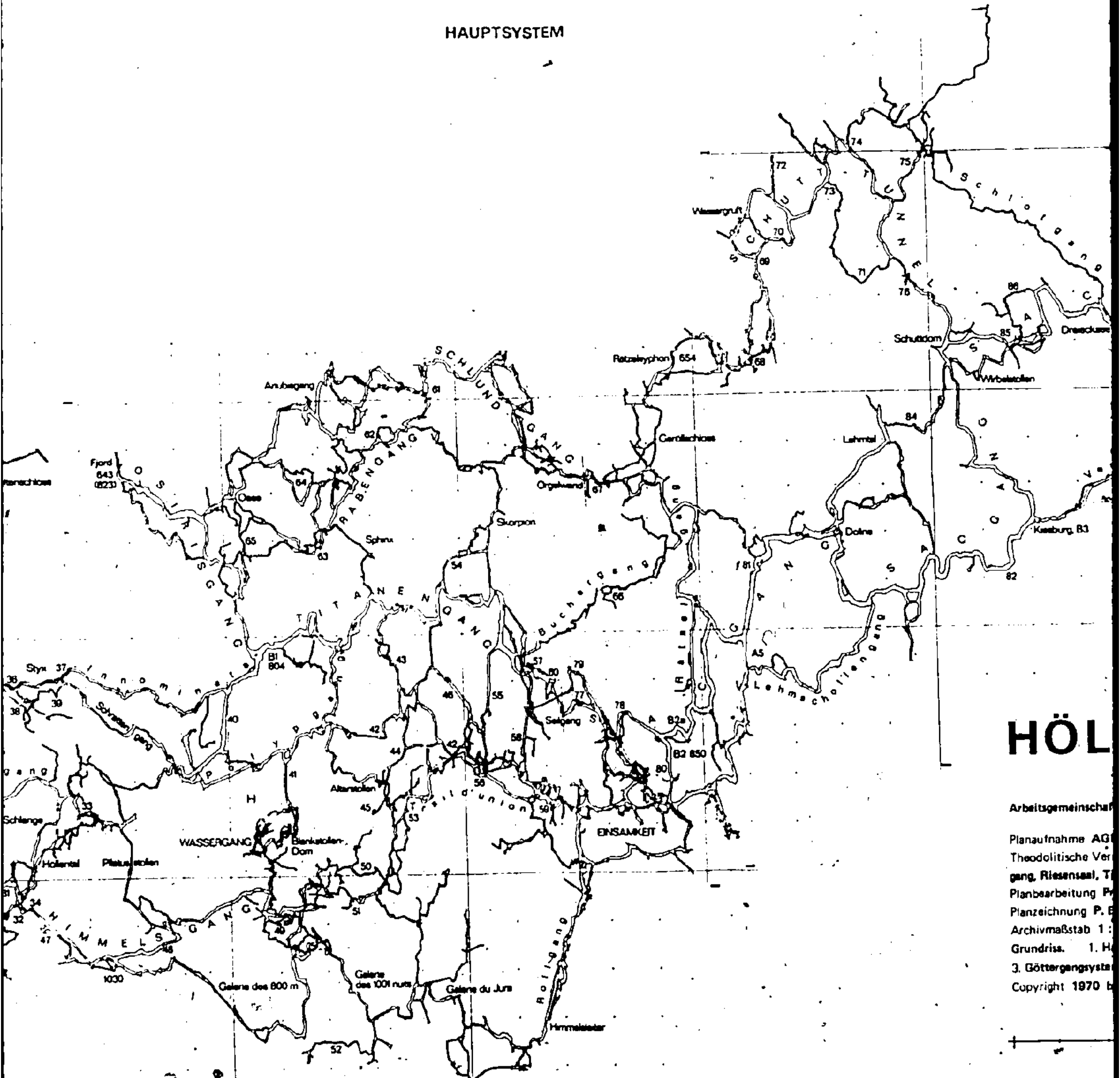
HAUPTSYSTEM
Schlotgang
Wassergruft
Schutzdom
Wirbelstollen
Dreieckuss
Rätselsyphon 654
Schlundgang
Anubisgang
Rabengang
Geröllschloss
Lehmtal
Fjord
643
(823)
Osirisgang
Oase
Sphinx
Skorpion
Orgelwand
Titanengang
Bucherigang
Doline
Kaseburg B3
Ratneigang
Lehmschollengang
Styx
Innominata
Schrattengang
B1
804
Polypgang
Seilgang
B2 850
B2a
Altarstollen
Traitd'union
EINSAMKEIT
WASSERGANG
Blankstollen-
Dom
Schlange
Höllental
Plattenstollen
Himmelsgang
Galerie des 800 m
Galerie des 1001 nuits
Galerie du Jura
Rollgang
Himmelsleiter
HÖL
Arbeitsgemeinschaf
Planaufnahme AG
Theodolitische Ver
gang, Riesensaal, T
Planbearbeitung P
Planzeichnung P. E
Archivmaßstab 1 :
Grundriss. 1. H
3. Göttergangsyste
Copyright 1970 b

5 of

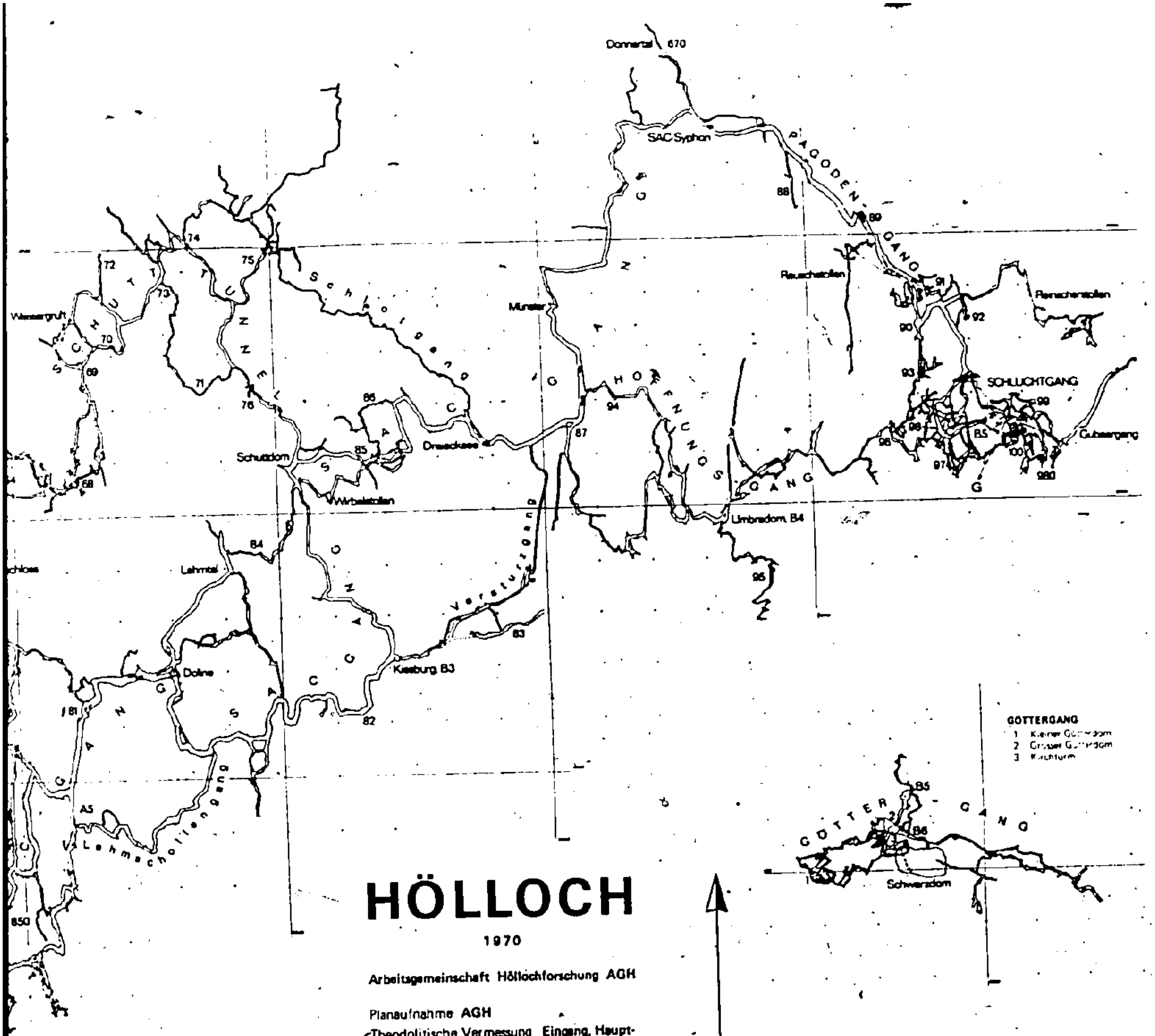

HÖLLOCH

1970

Arbeitsgemeinschaft Höllochforschung AGH

Planaufnahme **AGH**
Theodolitische Vermessung **Eingang, Hauptgang, Riesensaal, Titanengang, S A C - Gang**
Planbearbeitung **Prof. Dr. A. Bögli**
Planzeichnung **P. Berg**
Archivmaßstab **1 : 1000**
Grundriss. **1. Hauptsystem 2. Hochsystem 3. Göttergangsystem**
Copyright 1970 by AGH

676